3.3.2 Number of research papers per teachers in the Journals notified on UGC website during the year

List of research papers per teachers in the Journals notified on UGC website during the year

RAMANANDA COLLEGE

BISHNUPUR * BANKURA
Pin - 722122, West Bengal

Mob:- 6297976619
e-mail : principalramananda@gmail.com
Website : www.ramanandacollege.org

Estd.: 1945

UGC Recognized & State Government Aided Constituent College
Under the Bankura University (dt.-01.01.2017)
(Re-Accredited by NAAC 3rd Cycle at B++ Level)

Ref. No..... Date.....

From : Principal
Secretary, G.B.

Number of research papers per teachers in the Journals notified on UGC website during the year 2022-23

Title of paper	Name of the author/s	Department of the teacher	Name of journal	Year of publication	ISSN number	Link to the recognition in UGC enlistment of the Journal
Dibit-based OR and NOR gates using reflectivesemiconductor optical amplifier	Baibaswata Bhattacharjee and Surajit Bosu	Physics	Journal of Nonlinear Optical Physics & Materials	2023	ISSN (print): 0218-8635 ISSN(online): 1793-6624	https://www.scopus.com/sourceid/12183
A design of all-optical read-only memory using reflective semiconductor optical amplifier	Surajit Bosu, Baibaswata Bhattacharjee	Physics	Journal of Optics, Springer, (Scopus), (Web of Science)	2022	Electronic ISSN-0974-6900 Print ISSN-0972-8821	https://www.scopus.com/sourceid/19700189500
All-optical dibit based Feynman gate using reflective semiconductor optical amplifier with frequency encoding scheme	Surajit Bosu, Baibaswata Bhattacharjee	Physics	Journal of Optics, Springer, (Scopus), (Web of Science)	2022	Electronic ISSN-0974-6900 Print ISSN-0972-8821	https://www.scopus.com/sourceid/19700189500

Principal
Ramananda College

RAMANANDA COLLEGE

BISHNUPUR * BANKURA
Pin - 722122, West Bengal

Mob:- 6297976619
e-mail : principalramananda@gmail.com
Website : www.ramanandacollege.org

Estd.: 1945

UGC Recognized & State Government Aided Constituent College
Under the Bankura University (dt.-01.01.2017)
(Re-Accredited by NAAC 3rd Cycle at B ++ Level)

Ref. No..... Date.....

From : Principal
Secretary, G.B.

An Alternative Approach to Design an Inhibitor Logic Gate Using Reflective Semiconductor Optical Amplifier	Surajit Bosu, Baibaswata Bhattacharjee	Physics	Journal of Active and Passive Electronic Devices (Web of Science)	2023	ISSN: 1555-0281 (print) ISSN: 1555-029X (online)	https://mjl.clarivate.com:/search-results?issn=1555-0281&hide_exact_match_fl=true&utm_source=mjl&utm_medium=share-by-link&utm_campaign=search-results-share-this-journal
Dibit-based frequency encoded binary-to-gray code converter	Surajit Bosu, Baibaswata Bhattacharjee	Physics	Old City Publication (USA) Journal of Optics, Springer, (Scopus),(Web of Science)	2023	ISSN online 1753-2515 ISSN print 1753-2507	https://www.scopus.com/sourceid/19700189500
A novel approach of developing all-optical frequency encoded dibit-based Peres gate using reflective semiconductor optical amplifier	Surajit Bosu, Baibaswata Bhattacharjee	Physics	Journal of Nonlinear Optical Physics & Materials, World Scientific	2022	ISSN(print): 0218-8635 ISSN(online): 1793-6624	https://www.scopus.com/sourceid/12183

Principal
Ramananda College

RAMANANDA COLLEGE

BISHNUPUR * BANKURA
Pin - 722122, West Bengal

Mob:- 6297976619
e-mail : principalramananda@gmail.com
Website : www.ramanandacollege.org

Estd.: 1945

UGC Recognized & State Government Aided Constituent College
Under the Bankura University (dt.-01.01.2017)
(Re-Accredited by NAAC 3rd Cycle at B ++ Level)

Ref. No..... Date.....

From : Principal
Secretary, G.B.

Localization and delocalization in networks with varied connectivity	Tamoghna Ray, Amit Dey, and Manas Kulkarni	Physics	Physical Review A	2022	ISSN 2469-9934 (online), 2469-9926 (print).	https://www.scopus.com/sourceid/21100855841
Effects Of Various Gymnastic Exercises on Selected Motor Fitness Components of School Students	**Dr. Deepaak Kumar Singh**	Physical Education	International Journal For Multidisciplinary Research	2023	2582-2160	https://www.ijfmr.com/research-paper.php?id=3420
Comparison Of Endurance Running Performance Of Varsity Males With And Without Face Mask-A Field Based Analysis.	**Dr. Deepaak Kumar Singh**	Physical Education	Journal of Advanced Zoology	2023	0253-7214	http://dx.doi.org/10.53555/jaz.v45i2.4316
Spatiotemporal Synchronization of Diffusively Coupled Modified Logistic Map Under Complex Network	Mohammad Ali Khan, Debjani Maity, and Syeda Darakhshan Jabeen	Mathematics	Proceedings of the National Academy of Sciences	2022	2250-1762	https://link.springer.com/article/10.1007/s40010-020-00726-5

ESTD-1945 (BANKURA) RAMANANDA COLLEGE BISHNUPUR

Principal
Ramananda College
Bishnupur, Bankura

RAMANANDA COLLEGE

BISHNUPUR * BANKURA
Pin - 722122, West Bengal

Mob:- 6297976619
e-mail : principalramananda@gmail.com
Website : www.ramanandacollege.org

Estd.: 1945

UGC Recognized & State Government Aided Constituent College
Under the Bankura University (dt.-01.01.2017)
(Re-Accredited by NAAC 3rd Cycle at B ++ Level)

Ref. No..... Date.....

From : Principal
Secretary, G.B.

Design of multistable system of coupled different lorenz and nuclear spin generator systems	Jayanta Kumar Sarkar, Mohammad Ali Khan and Gour Chand Mahata	Mathematics	Advances in Mathematics Scientific Journal	2022	1857-8365	https://scopus.com/sourceid/21100913565
A mathematical model for fluxes associated with internal gravity waves excited by a corner mountain	Prasanta Das and Somnath Dutta	Mathematics	MAUSAM	2022	2529416	https://www.scopus.com/sourceid/13430
Numerical solution for a 3-D lee wave associated with barotropic mean flow across the Assam-Burma hills	Prasanta Das	Mathematics	MAUSAM	2023	2529416	https://www.scopus.com/sourceid/13430
Emergence of Englishes and the Issues of Teaching English Pronunciation to Indian Learners	Dr.Narendra Ranjan Malas	English	LANGUAGE IN INDIA (EBSCHost database)	2023	1930-2940	http://www.languageinindia.com/

Principal
Ramananda College
Bishnupur, Bankura

RAMANANDA COLLEGE

BISHNUPUR * BANKURA
Pin - 722122, West Bengal

Mob:- 6297976619
e-mail : principalramananda@gmail.com
Website : www.ramanandacollege.org

Estd. : 1945

UGC Recognized & State Government Aided Constituent College
Under the Bankura University (dt.-01.01.2017)
(Re-Accredited by NAAC 3rd Cycle at B ++ Level)

Ref. No.....

Date.....

From : Principal
Secretary, G.B.

Effect of Substitution of methanatoboron difluoride derivatives on non-covalent interaction with tetraphenyl porphyrin	Dr. Chiranjit Pal	Chemistry	Bangladesh Journal of Scientific and Industrial Research	2022	0304-9809	https://doi.org/10.3329/bjsir.v57i3.62018
Out-of-equilibrium chemical logic systems: Light- and sound-controlled programmable spatiotemporal patterns and mechanical functions	S.Choi, R.D.Mukhopadhyay, S.K.Sen, I.Hwang, K.Kim	Chemistry		2022	2451-9294 (online)	https://www.scopus.com/sourceid/21100788876
Spatiotemporal segregation of chiral supramolecular polymers	S.K.Sen, R.D.Mukhopadhyay*, S.Choi, I.Hwang*, K.Kim*	Chemistry	Chem	2023	2451-9294 (online)	https://www.scopus.com/sourceid/21100788876
Cucurbituril curiosities	R. D. mukhopadhyay, K. Kim*	Chemistry	Nature Chemistry	2023	1755-4330 (print); 1755-4349 (web)	https://www.scopus.com/sourceid/18100156701

Principal
Ramananda College

RAMANANDA COLLEGE

BISHNUPUR * BANKURA
Pin - 722122, West Bengal

Mob:- 6297976619
e-mail : principalramananda@gmail.com
Website : www.ramanandacollege.org

Estd.: 1945

UGC Recognized & State Government Aided Constituent College
Under the Bankura University (dt.-01.01.2017)
(Re-Accredited by NAAC 3rd Cycle at B ++ Level)

Ref. No..... Date.....

From : Principal
Secretary, G.B.

The pangenome structure of human pathogen Mycobacterium kansasii.	Saubashya Sur	Botany	Acta Biologica Szegediensis	2022	1588-4082	https://www.scopus.com/sourceid/87723
Mycobacterium abscessus: insights from a bioinformatic perspective	Saubashya Sur, Tanushree Patra, Mistu Karmakar, Anindita Banerjee	Botany	Critical Reviews in Microbiology	2023	1549-7828	https://www.scopus.com/sourceid/19662
In silico immunoinformatics based prediction and designing of multi-epitope construct against human rhinovirus C	Saubashya Sur, Mrityunjoy Ghosh, Ritu Rai	Botany	Acta Biologica Szegediensis	2023 (Accepted)	1588-4082	https://www.scopus.com/sourceid/87723

Principal
Ramananda College
Bishnupur, Bankura

Supporting Document

Baibaswata Bhattacharjee

SPRINGER LINK

Log in

Menu Search Cart

Home > Journal of Optics > Article

A design of all-optical read-only memory using reflective semiconductor optical amplifier

| Research Article | Published: 29 August 2022

| Volume 52, pages 1083–1093, (2023) Cite this article

Journal of Optics

Aims and scope →

Submit manuscript →

Surajit Bosu & Baibaswata Bhattacharjee

145 Accesses 6 Citations Explore all metrics →

Abstract

In recent times, any device should be designed with taken care of power consumption as well as speed. Photon has super-fast speed so it is very preferable to the researcher rather than the electron. So the researchers focus on the development of low-power-consuming devices. The reflective semiconductor optical amplifier (RSOA) is a suitable candidate for that purpose. It has a versatile gain medium and also it has huge application in passive optical networks. In this article, we have proposed a design of read-only memory using RSOA. To verify the practical feasibility, we have used MATLAB software to simulate the design. For all the memory outputs, the quality factor (Q), extinction ratio, contrast ratio, and also bit error rate have been calculated.

This is a preview of subscription content, log in via an institution to check access.

Access this article

Log in via an institution →

Buy article PDF 39,95 €

Price includes VAT (India)

Instant access to the full article PDF.

Rent this article via DeepDyve

Institutional subscriptions →

Similar content being viewed by others

Resistive Random Access Memory (RRAM): an Overview of Materials, Switching...

Article | Open access

22 April 2020

Resistive random access memory: introduction to device mechanism, materials and...

Article | Open access

09 March 2023

Recent Advances in In-Memory Computing: Exploring Memristor and Memtransistor...

Article | Open access

19 February 2024

References

| Research Paper No Access

A novel approach of developing all-optical frequency encoded dibit-based Peres gate using reflective semiconductor optical amplifier

Baibaswata Bhattacharjee and Surajit Bosu

https://doi.org/10.1142/S0218863523500224 | **Cited by:** 3 **(Source: Crossref)**

< Previous Next >

Abstract

In recent trends, digital systems in the light of power dissipation are a crucial issue. In computing, the computational process of reversible logic is bijective and can decrease the rising issue of power dissipation. In reversible circuit design, Peres gate considered as one of the fundamental reversible gate. Therefore, a Peres gate using Add/Drop Multiplexer (ADM) and Reflective Semiconductor Optical Amplifier (RSOA) is proposed in this paper. Frequency encoding scheme and dibit-based logic are incorporated here. In long range transmission, frequency encoding bears huge benefits in respect with the other encoding techniques. This encoding technique may decrease the probability of bit error. Due to the high gain and low noise property of RSOA, the proposed design can perform operations like computation, data processing, etc. at ultra-high speed with low noise. MATLAB Simulink (R2018a) software has been used to verify the operation of the proposed design.

Keywords: Frequency encoding ▪ dibit-based logic ▪ Peres gate ▪ reflective semiconductor optical amplifier (RSOA) ▪ add/drop multiplexer (ADM)

World Scientific
Connecting Great Minds

back

Privacy policy

© 2024 World Scientific Publishing Co Pte Ltd

Powered by Atypon® Literatum

SPRINGER LINK

Log in

Menu Search Cart

Home > Journal of Optics > Article

All-optical dibit-based Feynman gate using reflective semiconductor optical amplifier with frequency encoding scheme

| Research Article | Published: 16 May 2022

| Volume 52, pages 33–41, (2023) Cite this article

Journal of Optics

Aims and scope →

Submit manuscript →

Surajit Bosu & Baibaswata Bhattacharjee

162 Accesses 7 Citations Explore all metrics →

Abstract

In recent years, reversible gates have a great impact on optical nanotechnology, quantum and DNA computing. In the optical field, reversible gates like the Fredkin gate, Feynman gate, Toffoli gate, and Peres gate are very demanding due to their low power consumption. In this article, a novel design of Feynman gate using Add/Drop Multiplexer and Reflective Semiconductor Optical Amplifier (RSOA) is proposed. Frequency encoding scheme and dibit-based logic are incorporated in the proposed design. The Frequency encoding technique decreases the probability of bit error in long-range transmission. Due to the high gain and low noise property of RSOA, the proposed design can perform operations like computation and data processing at ultra-high speed with low noise. To verify the operation of the proposed design, we have used MATLAB Simulink (R2018a) software.

This is a preview of subscription content, log in via an institution to check access.

Access this article

Log in via an institution →

Buy article PDF 39,95 €

Price includes VAT (India)

Instant access to the full article PDF.

Rent this article via DeepDyve

Institutional subscriptions →

Similar content being viewed by others

All-Optical Feynman Gate Using Frequency Encoding Scheme, Add/Drop Multiplexer…

Chapter | © 2023

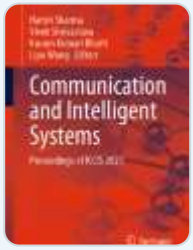

A Design of Frequency Encoded Dibit-Based Inhibitor Logic Using Reflective…

Chapter | © 2022

All-Optical Frequency Encoded Dibit-Based Half Subtractor Using Reflective…

Chapter | © 2022

References

Baibaswata Bhattacharjee

SPRINGER LINK

Log in

Menu Search Cart

Dibit-based frequency encoded binary-to-gray code converter

| Research Article | Published: 13 May 2023

| Volume 53, pages 315–327, (2024) Cite this article

Journal of Optics

Aims and scope →

Submit manuscript →

Surajit Bosu & Baibaswata Bhattacharjee

We're sorry, something doesn't seem to be working properly.
Please try refreshing the page. If that doesn't work, please contact support so we can address the problem.

Abstract

In the all-optical domain, the reflective semiconductor optical amplifier (RSOA) creates due attention in the research community because the RSOA has high gain, low power consumption, high-speed signal processing ability. In this work, we have proposed Binary-to-Gray code converter using RSOA, and Add/drop multiplexer. We have also implemented dibit-based logic and frequency encoding technique in this design to get the reduced bit-error problems and high degree of parallelism. We utilized the MATLAB Simulink software to confirm that the aforementioned design worked as desired.

This is a preview of subscription content, log in via an institution to check access.

Access this article

Log in via an institution →

Buy article PDF 39,95 €

Price includes VAT (India)

Instant access to the full article PDF.

Rent this article via DeepDyve

Institutional subscriptions →

Similar content being viewed by others

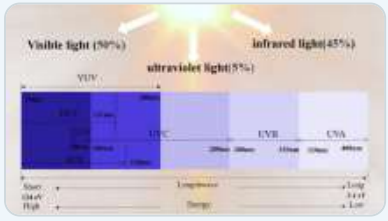

Ultraviolet photodetectors based on wide bandgap semiconductor: a...

Article | 29 April 2024

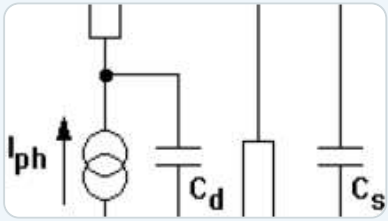

Adaptive composite bandwidth and automatic gain control receiver for 6G wireles...

Article | Open access

26 April 2024

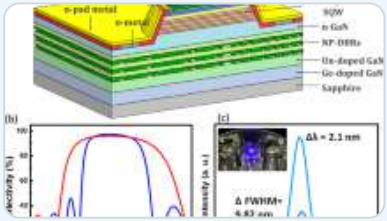

InGaN blue resonant cavity micro-LED with RGY quantum dot layer for broad gamut,...

Article | Open access

30 April 2024

References

Dibit-based OR and NOR gates using reflective semiconductor optical amplifier

Surajit Bosu and Baibaswata Bhattacharjee

https://doi.org/10.1142/S0218863523500467 | **Cited by:** 2 **(Source: Crossref)**

Previous Next

Abstract

In the all-optical domain, the reflective semiconductor optical amplifier (RSOA) creates due attention in the research community because the RSOA has high gain, low-power consumption, high-speed signal processing ability as well as low noise performance. In this work, we have proposed dibit-based OR and NOR gates using RSOA. Dibit-based logic is utilized in this design to get the reduced bit-error problems and high degree of parallelism. To verify the functionality of the aforementioned designs, we have used MATLAB software and also the quality factor (Q), extinction ratio (ER), contrast ratio (CR), and bit-error-rate (BER) have been calculated.

Keywords: Dibit-based logic ▪ reflective semiconductor optical amplifier ▪ soliton ▪ OR and NOR gate

World Scientific
Connecting Great Minds

Privacy policy

© 2024 World Scientific Publishing Co Pte Ltd

Powered by Atypon® Literatum

Amit Dey

Localization and delocalization in networks with varied connectivity

Tamoghna Ray, Amit Dey, and Manas Kulkarni
Phys. Rev. A **106**, 042610 – Published 17 October 2022

1 (https://www.altmetric.com/details.php?domain=journals.aps.org&citation_id=123624037)

More

Article

PDF (/pra/pdf/10.1103/PhysRevA.106.042610)

HTML (/pra/abstract/10.1103/PhysRevA.106.042610#fulltext)

Export Citation (/pra/export/10.1103/PhysRevA.106.042610)

This site uses cookies. To find out more, read our Privacy Policy (https://www.aps.org/about/privacy.cfm).

I Agree ()

REFERENCES

ABSTRACT

We study the phenomenon of localization and delocalization in a circuit-QED network with connectivity varying from finite-range coupling to all-to-all coupling. We find a fascinating interplay between interactions and connectivity. In particular, we consider (i) harmonic, (ii) Jaynes-Cummings, and (iii) Bose-Hubbard networks. We start with the initial condition where one of the nodes in the network is populated and then let it evolve in time. The time dynamics and steady state characterize the features of localization (self-trapping) in these large-scale networks. For the case of harmonic networks, exact analytical results are obtained, and we demonstrate that all-to-all connection shows self-trapping whereas the finite-ranged connectivity shows delocalization. The interacting cases (Jaynes-Cummings and Bose-Hubbard networks) are investigated both via exact quantum dynamics and via a semiclassical approach. We obtain an interesting phase diagram when one varies the range of connectivity and the strength of the interaction. We investigate the consequence of imperfections in the cavity or qubit and the role of inevitable disorder. Our results are relevant especially given recent experimental progress in engineering systems with long-range connectivity.

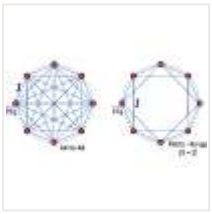
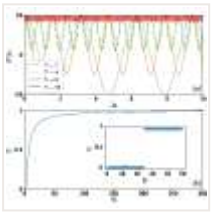
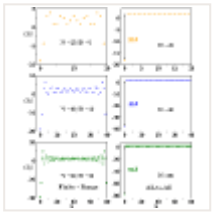
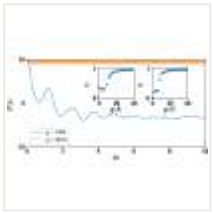
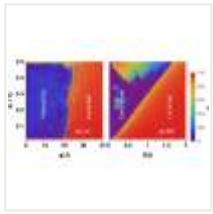
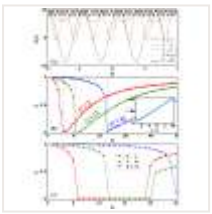
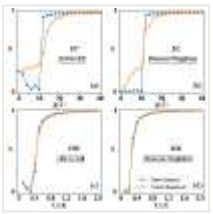

4 More

Received 6 April 2022 Accepted 26 September 2022

DOI: https://doi.org/10.1103/PhysRevA.106.042610

©2022 American Physical Society

Physics Subject Headings (PhySH)

Research Areas

Cavity quantum electrodynamics (/search/results?clauses=%5B%7B%22field%22%3A%22physh%22%2C%22value%22%3A
c24fba575e45%5C%22%2C%5C%22label%5C%22%3A%5C%22Cavity%20quantum%20electrodynamics%5C%22%2C%5

Circuit quantum electrodynamics (/search/results?clauses=%5B%7B%22field%22%3A%22physh%22%2C%22value%22%3A
508852ef3d9d%5C%22%2C%5C%22label%5C%22%3A%5C%22Circuit%20quantum%20electrodynamics%5C%22%2C%5

This site uses cookies. To find out more, read our Privacy Policy (https://www.aps.org/about/privacy.cfm).

I Agree ()

Dr. Deepaak Kumar Singh

International Journal for Multidisciplinary Research (IJFMR)
E-ISSN: 2582-2160 ● Website: www.ijfmr.com ● Email: editor@ijfmr.com

Effects Of Various Gymnastic Exercises on Selected Motor Fitness Components of School Students

Pradip Saini[1], Dr. Deepak Kumar Singh[2], Dr.T. Onima Reddy[3], Dr. Vikram Singh[4]

[1]Ph.D. Scholar, Department of physical Education, Banaras Hindu University, India
[2]Assistance Professor, Department of Physical Education, Ramananda College, India
[3,4]Professor, Department of Physical Education, Banaras Hindu University, India

Abstract

Purpose: The study was to clarify the influence of six-week various gymnastic exercises on selected motor fitness components of school going students. **Materials and Methods:** Thirty boys students (age = 14 to 16 years) were randomly assigned to the experimental group (n=30) and control group (n=30). All student was selected from The Jain International School, Bilaspur, Chhattisgarh. Various gymnastic exercises were included in the experimental group training session 6 times (each session 60 minutes) per week over 6 weeks as part of their usual weekly training regime. Both groups of gymnasts were tested selected motor fitness components before and after training. Motor fitness components performance were tested and measured through standard procedure with the help of expert and under the direct supervision of the experimenter. For the analysis of data statistical mean, standard deviation and 'T'-test was used. The level of significance was set at 0.05 ($p \leq 0.05$). **Conclusion:** In conclusion, there was a significant effect of various gymnastic exercises on selected motor fitness components of experimental group.

Keyword: Gymnastic exercise, motor fitness, muscular strength, agility, cardio-vascular endurance.

1. Introduction

Modern gymnastics welcomes creative quest and self-expression. It reveals that the human body possesses practically limitless opportunities and is also a means of moral education and importantly, gymnastics has a great appeal for the young. Gymnastics is an activity involving performance of exercises requiring strength, flexibility, agility, coordination, balance and grace. Internationally, all of the gymnastics sports. Gymnastics is divided into several different and distinct forms and these are all gaining in popularity. The types of gymnastics are A. Modern Artistic gymnastics. Modern Rhythmic gymnastics. Trampoline and Tumbling. Floor Gymnastic exercise [4]. There has been a clear tendency toward younger gymnasts executing increasingly challenging exercises in artistic gymnastics, one of the most well-liked and quickly expanding sports for young females [5]. Muscular strength in boys increases fairly linearly with chronological age, from early childhood until approximately 13 or 14 years of age (mid-puberty). In girls, strength improves linearly up until about 15 years of age, but there is no clear

evidence of an adolescent spurt [9]. compared the isokinetic muscle performance of the scapular muscles in elite adolescent gymnasts and non-athletic adolescents to find out if there were any differences in strength, endurance, and muscle balance based on high-level sport participation. It was discovered that elite gymnasts showed higher values for the protraction peak force/body mass [3]. The effects of a 6-week combined electro myo stimulation (EMS) and gymnastics training program on muscle strength and vertical jump performance in 16 prepubescent gymnasts and found that improvement was found after three weeks of EMS training in the maximal voluntary torque (MVT) [7]. Isokinetic training of knee extensors and flexor muscles increases functional correlation between speed and strength leading to improved performance of acrobatic elements in floor exercises[13].Effect of plyometric training when added to habitual gymnastic training on handspring vault performance variables on twenty youth female competitive gymnasts and found significant improvements for run-up velocity, take-off velocity, hurdle to board distance, board contact time, table contact time and post-flight time. However, there were no significant improvements on pre-flight time, shoulder angle or hip angle on the vault for the plyometric training group [11].The 10-week isokinetic training that was added to the traditional training improved the knee strength, which consequently improved aspects of the vault, but did not affect other technical aspects of the handspring performance[6].The findings of this study show that older persons who were living independently experienced significant gains in gait performance, muscle power, and ETGUG following a typical training regimen. However, after performing foot gymnastics exercises, there is no further impact on physical performance. [10].Water gymnastics helps improve the aerobic exercise capacity, to superior indices compared to the activity on the ground, being directly influenced by materials used through the size of water surface contact and complexity of movements[1].High-intensity circuit training using sport-specific exercises, increased HR to levels above 80% and 90% HR_{max} for extended time periods, and thus may be considered as an appropriate stimulus, in terms of intensity, for improving aerobic fitness in child female gymnasts [12].

1.1 Objective of the study

To find-out effect of various gymnastic exercise on motor fitness components of secondary school students.

1.2 Hypothesis

H0-There would be no significance change of various gymnastic Exercises on Selected motor fitness components of school students.

2. Methodology

Selection of the subject, Sampling technique, Selection of the variable, Design of the study, Training Schedule, Collection of data.

2.1 Population and Sampling technique

For this study the subjects was selected from The Jain International School, Bilaspur, Chhattisgarh, India. Total of sixty (60) subjects was randomly selected out of which thirty (30) were experimental group and other thirty (30) were control group. The age of the subjects was ranged between 14-16 years.

2.2 Selection of variables & Criterion measuring tools

For the present study the researcher used to measure the following motor fitness variables through the AAHPER test.

A) Muscular Strength: To measure the muscular strength (Arm and Shoulder) Pull-ups (for boys) used from AAHPER test and it was measured in number.

B) Agility: To measure the agility Shuttle run used from AAHPER test and it was measured in second.

C) Cardio-vascular Endurance: To measure the cardio-vascular endurance six hundred yard run-walk from AAHPER test and it was measure in minute and second.

2.3 Administration of the test:

After the selection of this subject from The Jain International School, Bilaspur, Chhattisgarh, the researcher administered motor fitness tests to measure the motor fitness components before and after the gymnastic exercise training program of six weeks. The motor fitness components were tested and measure through AAHPER & Bass Stick Test with the help of expert and under the direct supervision of the experimenter. Research scholar administrated the following tests given below.

i) Pull-ups (for boys)

Purpose: To measure the arm and shoulder strength.

Equipment: A wooden or metal bar approximately 1.5’ in diameter a piece of pipe or the runs of a ladder may also be used and stopwatch (only for girls).

Procedure: The height of the bar should be such that when the subject hangs from it with fully extended arms, his feet do not touch the ground. The subject is asked to use an overhand grasp with the palms facing away from the body. From the hanging position, the pupil raises the body by the arms until the chin can be placed over the bar and then lowers the body to a full extension hang and repeats the pull ups as many times as possible. Only one trial is given unless it is obvious that the pupil has not had a fair chance. Neither swinging, nor kicking the legs nor knee-raising is allowed.

Scoring: - The maximum number of completed pull ups is the score which may be evaluated with the help of local norms (if available) or by comparison with other subjects tested.

ii) Shuttle Run:

Purpose: To measure the speed and agility.

Equipment: Two blocks of wood (2”x2”x4”), a stopwatch and marking power. The subject should wear spikes or run bare foot.

Procedure: Two parallel lines are marked on the floor 10 yards apart or the width of the regular volleyball court may be used for the test. The two wooden blocks are placed behind one of the lines. The subject is asked to start from behind the other line. On the signal ready? Go, the time starts the watch and the subject runs towards the blocks, picks-up one block, runs back to the starting line, places the block behind the starting line, runs back and picks-up the second block to be carried back across the starting line. As soon as the second block is placed on the ground the timer stops the watch and records the time.

Scoring: Two trials are allowed to each subject with some rest in between. The time of the better of the two trials is recorded to the nearest 10^{th} of a second as the score of the test item.

iii) Six hundred Run-Walk:

Purpose: To measure the cardio-vascular endurance.

Equipment: Track or marked area and stopwatch.

Procedure: The subject is asked to take a standing start. At the signal Ready? Go!, the subject starts running the 600 yard distance. The test is usually performed on 10-12 subjects together by pairing off before the start of the event. Walking is permitted but the performer is to cover the distance in the shortest period of time.

Scoring: - The time taken to run 600 yards recorded in minutes and seconds is the score of this test item.

2.4 Design of the study

For the present study sixty (60) male subjects were selected randomly from The Jain International School, Bilaspur, Chhattisgarh, India.Their age ranged from 14-16 years. The subject divided into two equal groups of 30 (thirty) subjects in each. One is treated as experimental (practice gymnastic exercise) group, the second one is control (without practice) group. The experimental group will practice gymnastics exercise, for six (6) days a week for 1hours (60) minutes each day, for the period of six weeks under direct supervision of the experimenter. The control group did not practice any special training during the period of six weeks.

2.5 Training Schedule

Table-1: Six weeks Training Schedule

Sr. No.	Gymnastic-Exercises	Week (1-2)	Week (3-4)	Week (5-6)
1	Forward roll, jump with half turn (180 degree)	4 repetitions 2 set	6 repetitions 3 set	8 repetitions 4 set
2	Backward roll and jump with half turn (180 degree)	4 repetitions 2 set	6 repetitions 3 set	8 repetitions 4 set
3	Handstand	4 repetitions 2 set	6 repetitions 3 set	8 repetitions 4 set
4	Cartwheel	4 repetitions 2 set	6 repetitions 3 set	8 repetitions 4 set
5	Leg Split	5 repetitions 2 set	7 repetitions 3 set	9 repetitions 4 set
6	Leaps and jumps	4 repetitions 2 set	6 repetitions 3 set	8 repetitions 4 set
7	Illusion turn	4 repetitions 2 set	6 repetitions 3 set	8 repetitions 4 set

Note: Relaxation 10-15 seconds after each exercise

2.6 Collection of the Data:

To find out the Effects of gymnastic exercises on selected motor fitness components of school students, the data were collected through the administration of "AAHPER test" before and after the gymnastic exercises program of six weeks. To see any significant deferent 'T' test was used for farther statistical analysis.

3. Results

All the data pertaining to the present study were examined by employing 't' test to find out whether any significance difference between the means of motor fitness component of school students. The following notations were used for all the subsequent tables for elaborations.

E.G.- Experimental group, C.G.- Control group, N- Number of subjects in group, M- Mean score of the group, S.D.- Standard deviation of 't' – 't' value, 'P'- P value.

Table-2: Mean, Standard Deviation, Men difference, and 't' ratio of the pre and post test of experimental and control groups on muscular strength (Pull-ups in numbers)

Sl.no.	Group	Test	N	M	SD	MD	't' value	P- value
1	E.G	Pre test	30	5.33	0.95	0.06	0.13	.448508
2	C.G	Pre test	30	5.27	1.57			
1	E.G	Post test	30	7.6	1.35	2.2	4.33	.00003
2	C.G	Post test	30	5.4	1.43			

Level of Significance was at .05 (2,58) =2.00

Table- 2 reveals that the pre test mean of experimental and control groups muscular strength are 5.33 and 5.27 and their calculated 't' value is 0.13 which is lesser than of tabulated value 2.00 at 0.05(58) level of confidence. There is no significance difference found between the experimental and control groups of pre test on muscular strength. Whereas the mean of post test experimental and control groups are 7.6 and 5.4 and their calculated 't' value is 4.33 which is greater than that of the tabulated value 2.00 at 0.05 level of confidence. It was indicated that there is significance difference between the experimental and control groups of post test on muscular strength. It can be said that six weeks gymnastic exercises training effect on muscular strength of muscular group. Hence, the null hypothesis is rejected.

Figure-1: Graphical presentation of mean difference between the experimental and control groups on muscular strength

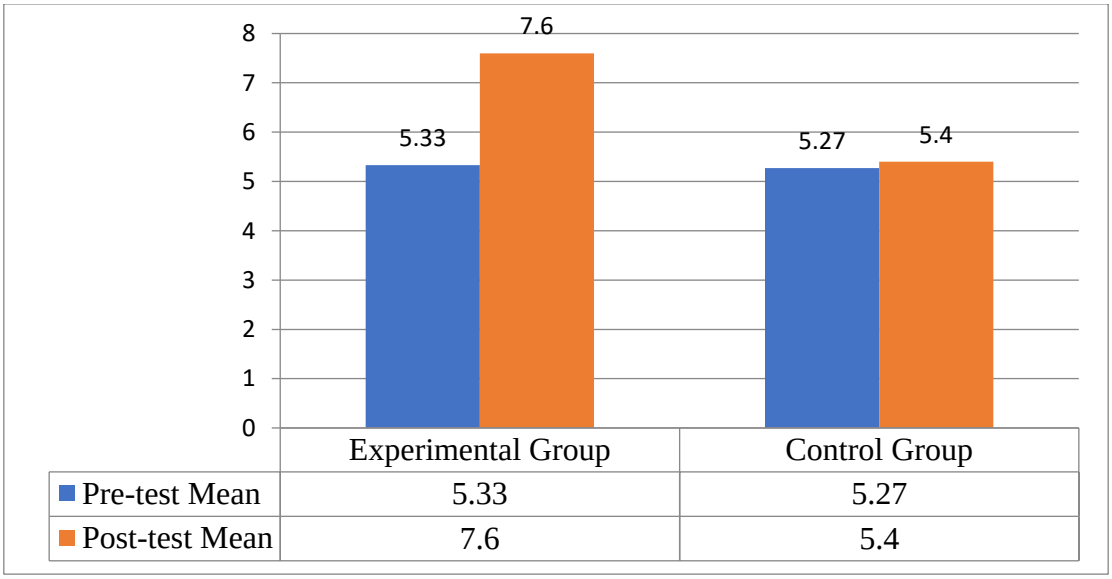

Table-3: Mean, Standard Deviation, Men difference, and 't' ratio of the pre and post test of experimental and control groups on agility (shuttle run in seconds)

Sl.no.	Group	Test	N	M	SD	MD	't' value	P- value
1	E.G	Pre test	30	7.16	0.68	0.04	0.14	.444573
2	C.G	Pre test	30	7.20	0.84			
1	E.G	Post test	30	6.13	0.05	1.03	4.62	.000011
2	C.G	Post test	30	7.16	0.78			

Level of Significance was at .05 (2,58) =2.00

Table-3 show that the pre test mean of experimental and control groups on muscular power are 7.16 and 7.20 and their calculated 't' value is 0.14 which is lesser than that of tabulated value 2.00 at 0.05(58) level of confidence. There is no significance difference found between the experimental and control groups of pre test on agility. Whereas the mean of post test experimental and control groups are 6.13 and 7.16 and their calculated 't' value is 4.62 which is greater than that of tabulated value 2.00 at 0.05(58) level of confidence. It was indicated that there is significance difference between the experimental and control groups of post test on agility. It can be said that six weeks gymnastic exercises training effect on agility of experimental groups. Hence, the null hypothesis is rejected.

Figure-2: Graphical presentation of mean difference between the experimental and control groups on agility

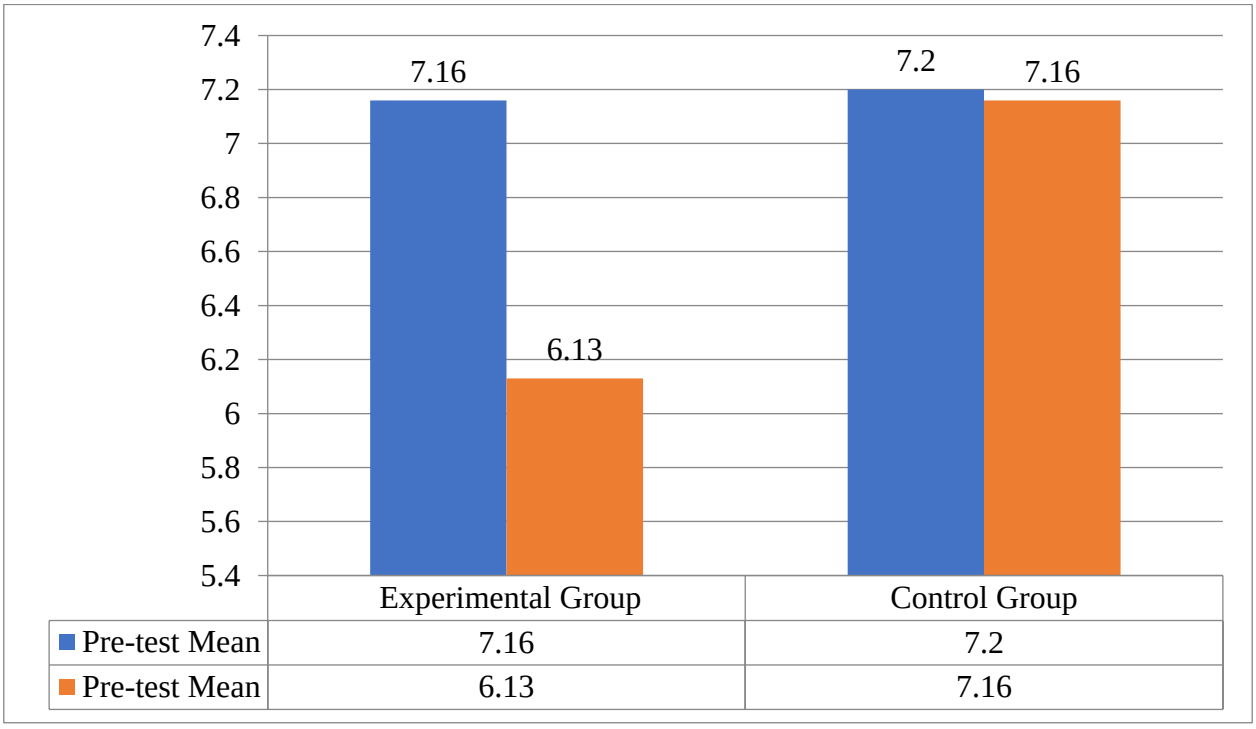

Table-4: Mean, Standard Deviation, Men difference, and 't' ratio of the pre and post test of experimental and control groups on cardio vascular endurance (six hundred run-walk in minutes & seconds)

Sl.no.	Group	Test	N	M	SD	MD	't' value	P- value
1	E.G	Pre test	30	140.47	6.57	1.8	0.82	.207787
2	C.G	Pre test	30	138.67	5.24			
1	E.G	Post test	30	119.73	9.22	14.67	3.15	.001291
2	C.G	Post test	30	134.40	7.94			

Level of Significance was at .05 (2,58) =2.00

Table-4 show that the pre-test mean of experimental and control groups on cardio-vascular endurance are 140.47 and 138.67 and their calculated 't' value is 0.82 which is lesser than that of tabulated value 2.00 at 0.05(58) level of confidence. There is no significance difference found between the experimental and control groups of pre test on cardio-vascular endurance. Whereas the mean of post test experimental and control groups are 119.73 and 134.4 and their calculated 't' value is 3.15 which is greater than that of tabulated value 2.00 at 0.05(58) level of confidence. It was indicated that there is significance difference between the experimental and control groups of post test on cardio-vascular endurance. It can be said that six weeks gymnastic exercises training effect on cardio-vascular endurance of experimental groups. Hence, the null hypothesis is rejected.

Fig-3: Graphical presentation of mean between the experimental and control groups on cardio-vascular endurance

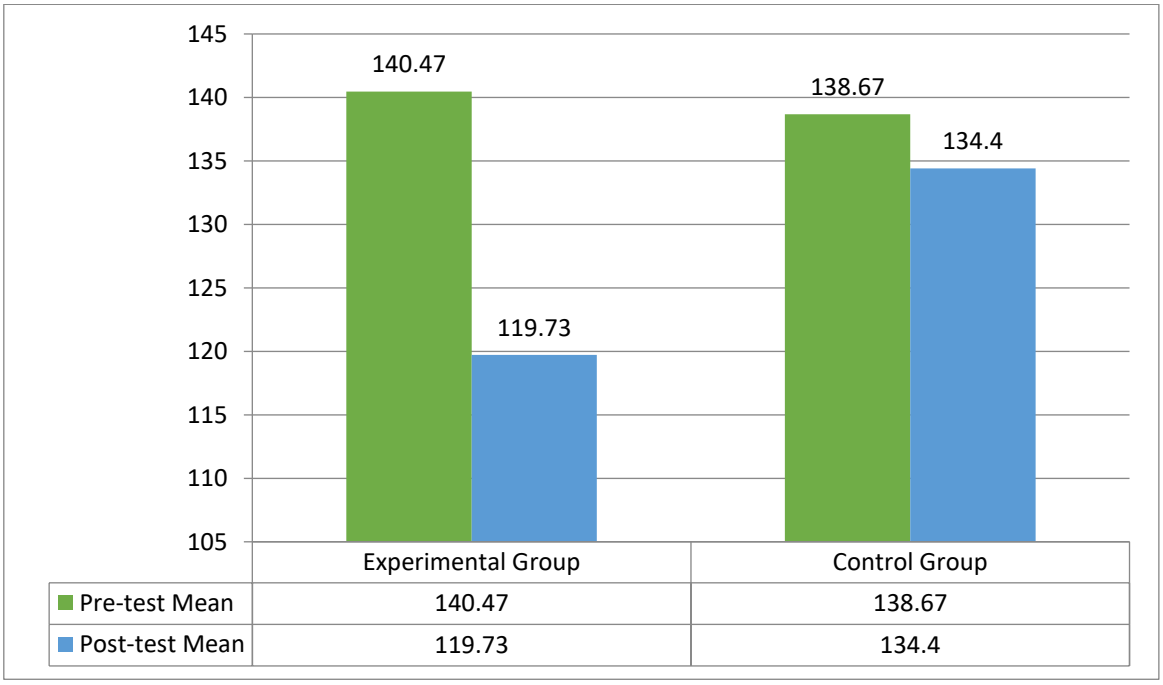

4. Discussion of the Findings

On the basis of the results and findings it was concluded that there are significance differences in motor fitness variable between the experimental and control groups. It was found that experimental group is highly muscular strength, agility and cardio-vascular endurance then that of control group. It may be attributed to the fact that six weeks gymnastic exercises training may be improve the muscular strength, agility, cardio-vascular endurance of experimental group.

5.Testing of Hypothesis

According to the hypothesis of the study, the observed result was confirming that there was significant difference of various gymnastic Exercises on Selected motor fitness components of students, so, as per the assessment of significance, the null hypothesis was rejected.

6.Conclusion

Six weeks various gymnastic exercises training significantly improved on selected motor fitness components of school students. The muscular strength, agility and cardio-vascular endurance of the students in experimental group has improved significantly in comparison with the control group due to the effect of six weeks gymnastic exercise training.

References

1. Badau, D. & Badau, A. (2015). The Influence of Various Types of Water Gymnastics Upon the Exercise Capacity. International Journal of Sport Culture and Science, 3 (4), 94-102. Retrieved from https://dergipark.org.tr/en/pub/intjscs/issue/28297/300631
2. Cabrejas, C., Solana-Tramunt, M., Morales, J., Nieto, A., Bofill, A., Carballeira, E., & Pierantozzi, E. (2023). The Effects of an Eight-Week Integrated Functional Core and Plyometric Training Program on Young Rhythmic Gymnasts' Explosive Strength. International journal of environmental research and public health, 20(2), 1041. https://doi.org/10.3390/ijerph20021041
3. Cools, A.M., Geerooms, E., Van den Verghe, D.F.M., Cambier, D.C., Witrvouw, E.E. (2007). Isokinetic scapular muscle performance in young elite gymnasts. Journal of Athletic Training, 42(4), 458-463.
4. Chacraborty Samiran. (1998). “Women’s Gymnastics Fundamentals and Applications”, Friends Publications (India) Delhi, P-1 to 27.
5. Cote, J., Salmela, J., and Russel, S. (1995). The knowledge of high performance gymnastic coaches: Competition and training considerations. The Sport Psychologist, 9, 76-95.
6. Dallas, G. C., Dallas, C., & Maridaki M. (2021). The effect of 10-week isokinetic training on muscle strength and gymnastic performance in preadolescent female gymnast. Science of Gymnastics Journal, 13(3), 399–409.https://doi.org/10.52165/sgj.13.3.399-409

7. Deley, G., Cometti, C., Fatnassi, A., Paizis, C., and Babault, N. (2011). Effects of Combined Electromyo stimulation and Gymnastics Training in Prepubertal Girls. Journal of Strength and Conditioning Research, 25(2), 520-526.
8. Douda, H., Tokmakidis, S., and Tsiggilis, N. (1997). The effect of training during growth of rhythmic sports gymnastics development. The Third Annual Congress of the European College of Sport Science. Manchester, England, p. 676.
9. Erlandson, M. C., Sherar, L. B., Mirwald, R. L., Maffulli, N., & Baxter-Jones, A. D. (2008). Growth and maturation of adolescent female gymnasts, swimmers, and tennis players. Medicine & Science in Sports & Exercise, 40(1), 34-42.
10. Hartmann, A., Murer, K., de Bie, R.A. (2009). The effect of a foot gymnastic exercise programme on gait performance in older adults: a randomized controlled trial. Disability and rehabilitation, 31(25),2101–2110. https://doi.org/10.3109/09638280902927010
11. Hall, E., Bishop, D.C., and Gee, T.I. (2016). Effect of Plyometric Training on Handspring Vault Performance and Functional Power in Youth Female Gymnasts. PLoS ONE. 11(2): e0148790. doi:10.1371/journal.pone.0148790.
12. Salagas, A., Donti, O., Katsikas, C., & Bogdanis, G. C. (2020). Heart Rate Responses during Sport-Specific High-Intensity Circuit Exercise in Child Female Gymnasts. Sports (Basel, Switzerland), 8(5), 68. https://doi.org/10.3390/sports8050068
13. Tabakovic, M., Atikovic, A., Kazazović, E., and Turkovic, S. (2016). Effects of isokinetic resistance training on strength knee stabilizers and performance efficiency of acrobatic elements in artistic gymnasts. Science of Gymnastic Journal, 8(2), 135-148.

Journal of Advanced Zoology

ISSN: 0253-7214

*Volume **44** Issue **2 Year 2023** Page 1493-**1496***

Comparison Of Endurance Running Performance Of Varsity Males With And Without Face Mask-A Field Based Analysis.

Dr. Saikot Chatterjee[1*], Uttam Roy[2], Deepak Kumar Singh[3], Asoke Banerjee[4]

[1]Assoc. Professor Department of Physical Education University of Kalyani*
[2]Research Scholar Department of Physical Education University of Kalyani
[3]Asst. Professor Ramananda College Bishnupur West Bengal
[4]State Aided College Teacher Srikrishna College Bagula. West Bengal

***Corresponding Author:** Dr. Saikot Chatterjee*
[*]Assoc. Professor Department of Physical Education University of Kalyani

Abstract

Research in Physical Education and Sports is going on since centuries back. Scientists are engaged in unveiling various facets of sports training. Apart from biomechanics, sports psychology, sports training and many others exercise physiology occupies a significant position. Research related to various bodily organs and systems and their relationship with physical activities has been attracting the researchers continuously. So far, the recent studies in the field of Physical Education and Sports Science are concerned a good number of scholars are focusing towards the area of pollution and their impact on the health and fitness of athletes. Some are suggesting for use of face mask during sports training, particularly when the athletes are getting much more exposed to areas with higher air pollution. The use of mask became more prevalent and crucial during the 2020 pandemic. Men started thinking more about the use of face masks, their positive as well as ill effects as a whole. At this juncture the scholar being an athlete by passion and physical educationist by profession settled with the topic comparison of endurance running of varsity males with and without mask. Purpose: The key purpose of the study was to locate the difference on endurance performance running of varsity male with and without face mask. Methodology: To accomplish the study the scholar selected 30 varsity males between the age group 20 to 25. So far, the design of the study it was experimental in nature composed of a pretest followed by a post one. The scholar incorporated Cooper Test i.e. 12 mins run and walk to assess the endurance performance of the subjects. As an ethical part the scholar also prepared a consent form and got filled by the subjects prior to their taking part in the experimentation. Conclusion: From data analysis it was revealed that the average distance covered by the varsity males wearing mask was 2223.30 mts. and the average distance covered by them without mask was 2366.63 mts respectively. The scholar further computed inferential statistics and from which it was discovered that the performance of the boys was significantly better without mask.

CC License
CC-BY-NC-SA 4.0

Keywords: Endurance, Face Mask

Introduction:

Research in the field of Physical Education and Sports Science is one of the most prominent areas so far explorations and inventions in the areas of science. Technology, social science and humanities are concerned. It is also worth mentioning that sphere of research in the territory of Physical Education and Sports Science is vivid and widely spread encompassing number of interdisciplinary subjects. Among the subjects Exercise Physiology or Sports Physiology is one of the most common. Relationship between Human Physiology and human physical abilities is mostly experimented. Keeping in view the area of experimentation and at the same time to look into something new the scholar planned to conduct the study entitled: Comparison of endurance running performance of varsity males with and without mask.

Running with mask the physiology behind:
When you wear a mask, it acts as a barrier to help prevent respiratory droplets from traveling into the air and onto other people. These droplets go airborne when you sneeze, talk, cough, or raise your voice, which we all do at some point during the day.
And since most cloth masks are breathable, Dr. Joshua Scott, primary care sports medicine physician at Cedars-Sinai Kerlan-Jobe Institute in Los Angeles, says it should not limit oxygen intake or cause a buildup of carbon dioxide.
To keep the likelihood of transmission low, Scott says running in crowded areas is not wise without a mask. He also points out that running in groups or drafting off of other runners can increase the likelihood of more virus exposure. In those situations, runners need to wear a mask in order to minimize the risk.
As with any barrier that may make it harder to breathe, Scott says a mask may make your workout harder than usual. “Like running on an incline or at increased altitude, most healthy people will adapt to this over time,” he said. However, you may fatigue more quickly while wearing the mask.
Scott points out that properly fitting face masks can increase the work of breathing.
s aerobic activity increases, he says wearing a mask while running can affect airflow and may increase your perceived workload and heart rate.

Some literature: Nonetheless, as of March 2021, the World Health Organization (WHO) recommended that individuals not wear masks while exercising as it may limit the ability to breathe.
Face masks have been recommended for preventing the spread of viruses (Chu et al., 2020; Hendrix et al. 2020).
The potential for spread of infections may be exacerbated during exercise due to heavy breathing, especially indoors such as in fitness (Jang et al., 2020; Lendacki et al., 2021) and sport centres (Atrubin et al., 2020).
While some propose the use of a mask may increase carbon dioxide rebreathing, leading to hypercapnic hypoxia and subsequently decreased tissue oxygenation (Chandrasekaran & Fernandes, 2020), others suggest no impact on exercise (Shaw et al., 2020).
An expert narrative review recently concluded wearing face masks had minimal impact on physiological function during exercise (Hopkins et al., 2021).

Purpose: The key purpose of the study was to compare endurance running performance of varsity males with and without mask.
Significance: The author is of the view that the outcomes of the study will be able to establish a knowledge base regarding use of mask during endurance running performance. It will help the coaches to acquire understanding related to use of mask by the athletes its advantages and disadvantages.

Methodology: With respect to methodology at the very outset the scholar randomly selected 30 varsity males as subjects of his study with an average age of 26.6 yrs. After recording the age of the subjects, the scholar estimated the height and body weight of them as personal data with the help of standard equipment. So far, the design of the study it is experimental in nature composed of a pretest followed by a post one. As an ethical part the scholar also prepared a consent form and got filled by the subjects prior to their taking part in the experimentation.
Result and discussion: In this part of the monograph the scholar tried to depict the results derived from the statistical analysis.

Table 1. Descriptive statistics of age height and weight of the subjects.

	N	Minimum	Maximum	Mean	Std. Deviation
AGE yrs	30	22	35	26.60	3.450
HEIGHT(CM)	30	152	183	168.27	6.721
WEIGHT(KG)	30	50	82	62.33	8.172
Valid N (listwise)	30				

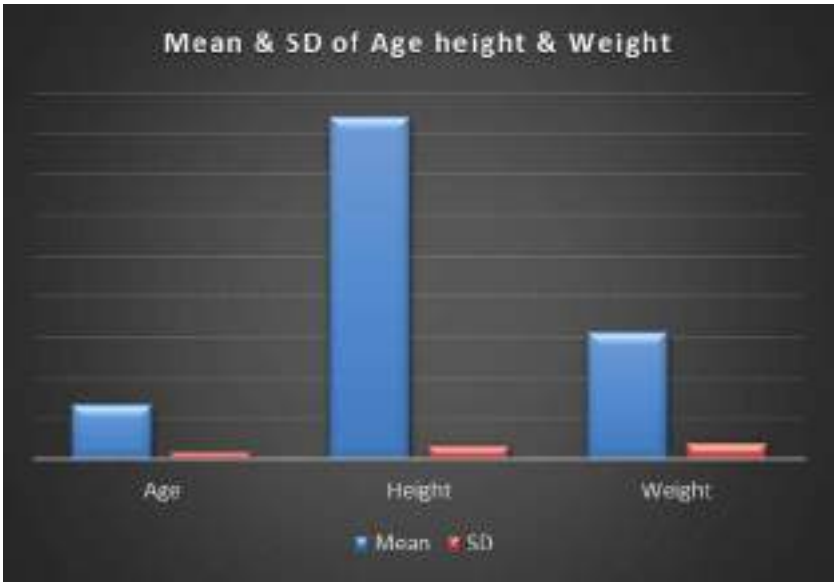

Fig. No. 1 Column chart showing the Mean and SD of Age Height and weight

The results of descriptive statistics related to personal data i.e. age height and weight of the subjects have been presented in table No. 1 and the bar diagram showing the vertical spread of the same values are presented in fig. No.1.

Table No. 2 descriptive statistics of endurance running performance with and without mask

	N	Minimum	Maximum	Mean	Std. Deviation
12 MINUTES RUN AND WALK WITHOUT MASK(METER)	30	1700	2950	2366.63	335.729
12 MINUTES RUN AND WALK WITH MASK(METER)	30	1570	2940	2223.30	328.765
Valid N (listwise)	30				

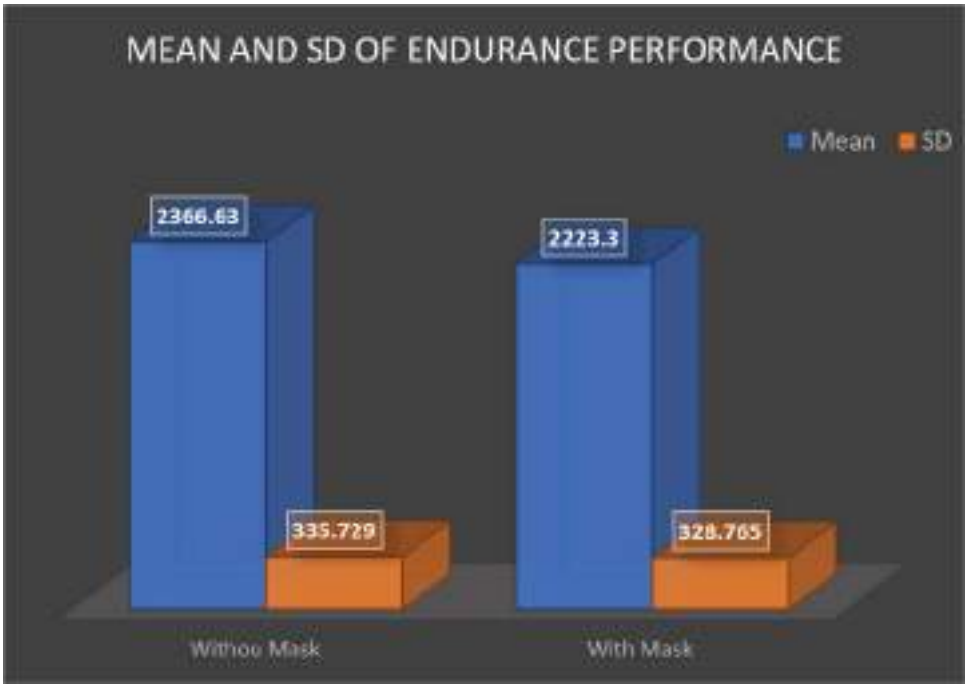

Fig. 3. Mean and SD of endurance performance

From table 2 and the bar diagram presented in fig. no. 2 it is somehow clear that the performance of the subjects vary while running with and without mask. It is also clear that the performance is better without mask. To prove the degree of difference between the means to determine whether the difference is significant or not the scholar further computed paired samples T test.

Table No. 3 Paired Samples Test Result

		Paired Differences					T	df	Sig. (2-tailed)
		Mean	Std. Deviation	Std. Error Mean	95% Confidence Interval of the Difference				
					Lower	Upper			
Pair 1	12 MINUTES R AND W W/M (mts) - 12 MINUTES R AND W WO/M (mts)	-143.333	128.257	23.416	-191.225	-95.441	-6.121	29	.000

From the results of paired samples test it is evident that the endurance performance of the subjects without mask is significantly better than that of with mask.

Conclusion:

From the findings of likeminded scholars, it is somehow clear that individuals feel some sort of uneasiness due to the additional mask fitted on the face which probably leads to some physiological as well as psychological changes. WHO also recommends use of mask during exercise is not suitable. Some of the physiological like restricted pulmonary ventilation, carbon dioxide rebreathing, may be hindering performance as well as ease to exercise. From the above discussion it is clear that use of mask though help in protecting athletes from unwarranted pollution and some other biological factors it is better to avoid mask during sports training or performance except in some special cases like epidemic pandemic or environmental conditions.

References:

1. World Health Organization (2020). https://www.who.int/emergencies/diseases/novel-coronavirus-2019/advice-for-public/myth-busters.
2. Atrubin D, Wiese M, Bohinc B. An Outbreak of COVID-19 Associated with a Recreational Hockey Game - Florida, June 2020. MMWR Morb Mortal Wkly Rep. 2020 Oct 16;69(41):1492-1493. doi: 10.15585/mmwr.mm6941a4. PMID: 33056952; PMCID: PMC7561093
3. Chandrasekaran B, Fernandes S. "Exercise with facemask; Are we handling a devil's sword?" - A physiological hypothesis. Med Hypotheses. 2020 Nov;144:110002. doi: 10.1016/j.mehy.2020.110002. Epub 2020 Jun 22. PMID: 32590322; PMCID: PMC7306735.
4. Chu DK, Akl EA, Duda S, Solo K, Yaacoub S, Schünemann HJ; COVID-19 Systematic Urgent Review Group Effort (SURGE) study authors. Physical distancing, face masks, and eye protection to prevent person-to-person transmission of SARS-CoV-2 and COVID-19: a systematic review and meta-analysis. Lancet. 2020 Jun 27;395(10242):1973-1987. doi: 10.1016/S0140-6736(20)31142-9. Epub 2020 Jun 1. PMID: 32497510; PMCID: PMC7263814.
5. Douglas M, Katikireddi SV, Taulbut M, McKee M, McCartney G. Mitigating the wider health effects of covid-19 pandemic response. BMJ. 2020 Apr 27;369:m1557. doi: 10.1136/bmj.m1557. PMID: 32341002; PMCID: PMC7184317.
6. Hendrix MJ, Walde C, Findley K, Trotman R. Absence of Apparent Transmission of SARS-CoV-2 from Two Stylists After Exposure at a Hair Salon with a Universal Face Covering Policy - Springfield, Missouri, May 2020. MMWR Morb Mortal Wkly Rep. 2020 Jul 17;69(28):930-932. doi: 10.15585/mmwr.mm6928e2. PMID: 32673300.
7. Jang S, Han SH, Rhee JY. Cluster of Coronavirus Disease Associated with Fitness Dance Classes, South Korea. Emerg Infect Dis. 2020 Aug;26(8):1917-1920. doi: 10.3201/eid2608.200633. Epub 2020 May 15. PMID: 32412896; PMCID: PMC7392463.

Mohammad Ali Khan

ResearchGate

See discussions, stats, and author profiles for this publication at: https://www.researchgate.net/publication/348798013

Spatiotemporal Synchronization of Diffusively Coupled Modified Logistic Map Under Complex Network

Article *in* Proceedings of the National Academy of Sciences, India - Section A · January 2021

DOI: 10.1007/s40010-020-00726-5

CITATION
1

READS
113

3 authors, including:

Syeda DARAKHSHAN Jabeen

20 PUBLICATIONS **41** CITATIONS

SEE PROFILE

All content following this page was uploaded by Syeda DARAKHSHAN Jabeen on 27 October 2021.

The user has requested enhancement of the downloaded file.

Proc. Natl. Acad. Sci., India, Sect. A Phys. Sci.
https://doi.org/10.1007/s40010-020-00726-5

RESEARCH ARTICLE

Spatiotemporal Synchronization of Diffusively Coupled Modified Logistic Map Under Complex Network

Mohammad Ali Khan[1] · Debjani Maity[2] · Syeda Darakhshan Jabeen[3]

Received: 2 August 2017 / Revised: 2 February 2019 / Accepted: 2 December 2020
© The National Academy of Sciences, India 2021

Abstract We study spatiotemporal synchronization under complex network of diffusively coupled chaotic modified logistic map. In modified logistic map a new parameter is introduced such that nonlinear term is in fractional power. The complex network is dynamic whose coupling connections change stochastically in time. Here we investigate the spatiotemporal dynamics of coupled modified logistic maps whose coupling connections are rewired randomly, and we determine (1) the effects of variation of newly induced parameter β, (2) the effects of variation of low and high rewiring probability, (3) the effects of variation of growth rate r and (4) the effects of variation of different randomness and linear stability analysis of the synchronized steady-state solution. We have calculated analytically the critical coupling coefficient for the transition to spatiotemporal regularity of the lattice. The analytical results match well with the numerical simulation results. The variation of the basin size with respect to coupling strength and rewiring probability with various randomness and coupling is plotted. The simulation results do not change significantly with the variation of lattice sizes.

Keywords Modified logistic map (MLM) · Coupled map lattice (CML) · Spatiotemporal synchronization (SS)

✉ Mohammad Ali Khan
mdmaths@gmail.com

Debjani Maity
debjanisamanta01@gmail.com

Syeda Darakhshan Jabeen
jabeen@bitmesra.ac.in

[1] Department of UG and PG Mathematics, Ramananda College, Bankura University, Bishnupur, Bankura, West Bengal, India

[2] Department of Mathematics, Bankura University, Bankura, West Bengal, India

[3] Department of Mathematics, Birla Institute of Technology, Mesra, Ranchi, India

1 Introduction

Since the synchronization of dynamical systems observed by Pecora and Carroll [1], chaos has become a topic of great interest of science and engineering. Different types of synchronization have been proposed. Shooshtari et al. [2] discussed identical synchronization of nonautonomous unified chaotic system with continuous periodic switch. Generalized synchronization for delay and nondelay chaotic systems discussed by Tarai et al. [3, 4]. Phase synchronization control of complex networks of Lagrangian system on adaptic digraphs has been observed by Chung et al. [5]. Wang et al. [6] also analysed module-phase synchronization in hyperchaotic complex Lorenz system after modified complex projection. Khan and Poria [7] and Bao and Cao [8] described projective synchronization of bidirectional coupled chaotic systems and fractional-order memristor-based neural networks. Anti-synchronization of different types of chaotic systems is discussed by Al-Sawalha and Noorani [9] and Sing et al. [10], respectively. Adaptive lag synchronization for uncertain complex dynamical network observed by Ji et al. [11] and also Hung et al. [12] discussed finite-time lag synchronization of delayed neural network. Synchronization of coupled map lattice (CML) of chaotic maps has been hellaciously examined. CMLs were introduced in a simple model holding the essential features of nonlinear dynamics of extended systems involving many individual units [13].

Published online: 26 January 2021

The spatiotemporal dynamics in turbulence in fluids and optics [14], solid-state physics [15], chemistry [16] and even evolutionary biology [17] have been studied. Sinha [18] discussed the spatiotemporal dynamics of network of diffusively coupled chaotic logistic map with varying degrees of randomness in coupling connections. Poria et al. [19] studied spatiotemporal synchronization (SS) behaviour of coupled Ricker maps over a complex network. Here complex network is dynamic as at every update, connect a fraction of randomly chosen sites to a node instead of their nearest neighbours. Nag and Poria [20] investigated the SS behaviour of delay coupled chaotic smooth unimodal maps over a ring network with stochastic switching of links at every time step. We have observed SS behaviour of a complex network of coupled logistic map with varying degrees of randomness in coupling [21]. Here we have calculated analytically the critical coupling coefficient for the transition to spatiotemporal regularity of the lattice and checked that our analytical result matches well with the numerical simulation results. Our new motivation is to introduce the modified logistic map (MLM) of extended dynamical systems that have received the CML's considered as spatiotemporal synchronization. The well-known logistic map is of the form $x_{n+1} = rx_n(1 - x_n)$, where r is the growth rate of the population. Noymanee and San-Um [22] used MLM in the form of $x_{n+1} = rx_n^{\alpha}(1 - x_n^{\beta})$, where α and β are the arbitrary power of the variable x_n. But we consider the MLM inducing a single parameter β in the nonlinear term of the logistic map, as

$$x_{n+1} = rx_n(1 - x_n^{\beta-1}), \tag{1}$$

where $0 < r \leq 4$ and $2 \leq \beta < 3$. The main difference of this model to logistic map is that the nonlinear term is in fractional power instead of integer power.

2 Model

We have studied the circle lattice of MLM under diffusive coupling. The map corresponding to this is written as

$$x_{n+1}(i) = \epsilon' f(x_n(i)) + \epsilon/2\{x_n(i+1) + x_n(i-1)\}, \tag{2}$$

where $\epsilon' = 1 - \epsilon$. The sites are denoted by integers $i = 1, 2, ..., N$; N is the linear size of the lattice, where $x_n(i)$ is defined as population size of ith node at time n and ϵ is the strength of coupling. Now we consider a model where diffusion takes place randomly in varying degrees and try to determine what dynamical properties are significantly affected by the way connections are made between elements with its coupling connections rewired randomly with probability p. Namely, at every update we will connect a site with probability p to randomly chosen sites and with probability $p'(= 1 - p)$ to nearest neighbour, i.e. at every instant, a fraction p of randomly chosen nearest neighbour links is replaced by random links

$$x_{n+1} = \epsilon' f(x_n(i)) + \epsilon/2\{x_n(\xi_1) + x_n(\xi_2)\}, \tag{3}$$

where ξ_1 and ξ_2 both are random integers uniformly distributed in $\{1, 2, 3, ..., N\}$ and with probability p' the dynamical equation of the system are governed by

$$x_{n+1}(i) = \epsilon' f(x_n(i)) + \epsilon/2\{x_n(i+1) + x_n(i-1)\}. \tag{4}$$

The case of $p = 0$ corresponds to the regular diffusion, while $p = 1$ corresponds to completely random diffusion. For any value of p between 0 and 1 $(0 < p < 1)$ corresponds to small world diffusion.

For MLM function Eq. (1) holds. Here $x_n \geq 0$ is a dimensionless measure of the population in the nth generation, $r \geq 0$ is the intrinsic growth rate, and β is the newly induced parameter. This type of connectivity has been observed in a range of natural and human engineered system.

3 Stability Analysis of MLM

MLM Eq. (1) has two fixed points $x^* = 0$ and $x^* = (\frac{r-1}{r})^{\frac{1}{\beta-1}}$. The fixed point 0 is stable for $0 < r < 1$ and unstable for $r \geq 1$, and the other nontrivial fixed point $(\frac{r-1}{r})^{\frac{1}{\beta-1}}$ is stable for $1 < r < \frac{\beta+1}{\beta-1}$ and unstable for $r \geq \frac{\beta+1}{\beta-1}$. Now we show by analytical method that the unstable point $(\frac{r-1}{r})^{\frac{1}{\beta-1}}$ is stabilized in the range $\frac{\beta+1}{\beta-1} \leq r \leq 4$ under the effect of randomness and impossible for nearest neighbour coupling. We assume that the total contribution due to k randomly chosen neighbour is $k\langle x(t)\rangle$. The averaged out evolution equation can be written as

$$x_{n+1}(i) = \epsilon' f(x_n(i)) + p'\epsilon/2\{x_n(i+1) + x_n(i-1)\} + \frac{p\epsilon}{N}\sum_{i=1}^{N} x_n(i), \tag{5}$$

where p is the probability of being coupled to random sites.

Any random process can be classified into two parts: first part is the mean, and another part is fluctuating part. If the fluctuation is uniformly distributed with mean zero, then we can neglect the contribution due to fluctuating part and use the mean evolution for analytical result. Since the random network is dynamic and the average connectivity of each node is greater than 1, long time evolution of the system would be equivalent to a globally coupled map lattice. In MLM, each node in the ring network diffuses certain fraction of material to the nodes which are connected to it and receives certain fraction of material from the nodes to which it is connected. A complete spatiotemporal synchronization occurs when the state variables of each node adopt the same for all the coupled maps

at all time n greater than transient time, i.e. $x_n(1) = x_n(2) = \cdots = x_n(N)$.

4 Stability Conditions for Fixed Points of MLM

The Jacobian matrix for system (5) is given by

$$J = \begin{pmatrix} \epsilon' a + \frac{\epsilon p}{N} & \epsilon\left(\frac{p'}{2} + \frac{p}{N}\right) & \frac{\epsilon p}{N} & \ldots & \epsilon\left(\frac{p'}{2} + \frac{p}{N}\right) \\ \epsilon\left(\frac{p'}{2} + \frac{p}{N}\right) & \epsilon' a + \frac{\epsilon p}{N} & \epsilon\left(\frac{p'}{2} + \frac{p}{N}\right) & \ldots. & \frac{\epsilon p}{N} \\ \vdots & \vdots & \vdots & \vdots & \vdots \\ \epsilon\left(\frac{p'}{2} + \frac{p}{N}\right) & \ldots & \frac{\epsilon p}{N} & \ldots & \epsilon' a + \frac{\epsilon p}{N} \end{pmatrix} \tag{6}$$

where $a = \frac{df(x)}{dx}|_{x=x^*}$, x^* is the spatiotemporal fixed point of the MLM. Now, a Toeplitz matrix C is a circulant matrix having the form

$$C = \begin{pmatrix} c_0 & c_1 & c_2 & \ldots & c_{n-1} \\ c_{n-1} & c_0 & c_1 & \ldots. & c_{n-2} \\ \vdots & \vdots & \vdots & \vdots & \vdots \\ c_1 & c_2 & c_3 & \ldots & c_0 \end{pmatrix}, \tag{7}$$

where each row is a cyclic shift of the row above it. Above circulant matrix (7) can also be characterized in the form $c_{k,j} = c_{(j-k) \bmod (n)}$. Let the eigenvalues ψ_k and the eigenvectors $y^{(k)}$ of C are solutions of $Cy = \psi y$ or equivalently expressed as

$$\sum_{k=0}^{m-1} c_{n-m+k}\, y_k + \sum_{k=m}^{n-m} c_{k-m}\, y_k = \psi y_m. \tag{8}$$

Changing the dummy, Eq. (8) becomes

$$\sum_{k=0}^{n-1-m} c_k y_{k+m} + \sum_{k=n-m}^{n-1} c_k y_{k-(n-m)} = \psi y_m. \tag{9}$$

Let $y_k = \rho_n^k$, where $\rho_n = e^{\frac{2\pi i}{n}}$, $i = \sqrt{-1}$ be the initial solution of Eq. (9); therefore, from Eq. (9) we get $\sum_{k=0}^{n-1-m} c_k \rho_n^k + \rho_n^{-n} \sum_{k=n-m}^{n-1} c_k \rho_n^k = \psi$. Let $\psi_m = \sum_{k=0}^{n-1} c_k \rho_n^{mk}$ with the corresponding eigenvector $[1\ \rho_n{}^m\ \rho_n{}^{2m} \ldots \rho_n{}^{(n-1)m}]^T$, i.e.

$$\begin{aligned} \psi_m &= c_0 + c_1 \rho_n^m + c_2 \rho_n^{2m} + \cdots + c_{n-1} \rho_n^{(n-1)m} \\ &= c_0 + c_1 e^{\frac{2\pi i m}{n}} + c_2 e^{\frac{4\pi i m}{n}} + \cdots + c_{n-1} e^{\frac{2(n-1)\pi i m}{n}} \\ &= \left[\epsilon' a + \frac{\epsilon p}{N}\right] + \left[\epsilon\left(\frac{p'}{2} + \frac{p}{N}\right)\right] e^{\frac{2\pi i m}{n}} + \frac{\epsilon p}{N} e^{\frac{4\pi i m}{n}} \\ &\quad + \cdots + \left[\epsilon\left(\frac{p'}{2} + \frac{p}{N}\right)\right] e^{\frac{2(n-1)\pi i m}{n}} \\ &= \epsilon' a + \epsilon p' \cos\frac{2\pi m}{n}. \end{aligned} \tag{10}$$

The synchronized spatiotemporal fixed point will be stable if all the eigenvalues of J lie inside the unit circle (centred at origin). Therefore the stability condition is given by $|\epsilon' a + p' \epsilon \cos\frac{2\pi m}{n}| \le 1$ for all m and n. This condition holds if $|\epsilon' a + p'\epsilon| \le 1$ and $|\epsilon' a - p'\epsilon| \le 1$ hold simultaneously. After simplification the synchronized fixed point $x^* = (\frac{r-1}{r})^{\frac{1}{\beta-1}}$ of the dynamic random network is stable if

$$\text{Max}\left\{\frac{\gamma}{\delta + p}, \frac{\gamma}{\gamma - p}\right\} \le \epsilon \le \text{Min}\left\{\frac{\delta}{\delta + p}, \frac{\delta}{\gamma - p}, 1\right\}, \tag{11}$$

where $\gamma = \beta(1-r) + (1+r)$, $\delta = (\beta - 1)(1 - r)$ Therefore the synchronized fixed point $x^* = (\frac{r-1}{r})^{\frac{1}{\beta-1}}$ of the dynamic random network is stable if

$$\frac{\gamma}{\gamma - p} \le \epsilon \le 1, \tag{12}$$

for $\frac{\beta+1}{\beta-1} \le r \le 4$ and $2 \le \beta < 3$. Therefore qualitative change of the dynamics occurred at the coupling strength $\epsilon_{BIFUR} = \frac{\gamma}{\gamma - p}$. Here stability range

$$R = 1 - \frac{\gamma}{\gamma - p} = \frac{p}{p - \gamma}. \tag{13}$$

Surprisingly, we notice that stability range does not depend on the lattice size. Therefore for regular nearest neighbour coupling $p = 0$ gives the null range of stability of the synchronized fixed point $x^* = (\frac{r-1}{r})^{\frac{1}{\beta-1}}$ for any $\frac{\beta+1}{\beta-1} \le r \le 4$ and $2 \le \beta < 3$.

5 Numerical Simulation Results

The bifurcation diagram of MLM with respect to r is plotted in Fig. 1, which propagates the well-known bifurcation scenario of MLM. Now we show numerically that the unstable point $x^* = (\frac{r-1}{r})^{\frac{1}{\beta-1}}$ is stabilized in the range $\frac{\beta+1}{\beta-1} \le r \le 4$ and $2 \le \beta < 3$ under random rewiring. We have chosen the lattice size $N = 100$ for all numerical simulations.

5.1 Variation of the Newly Induced Parameter β

Case I In the 1st case we fixed the randomness at $p = 0$ and growth rate $r = 3.5$; then, the bifurcation diagram showing the state of the lattices $x_n(i), i = 1, 2, 3, \ldots, 100$ with respect to coupling strength ϵ is drawn for $\beta = 2.09, \beta = 2.13, \beta = 2.2$ and $\beta = 2.43$ in Fig. 2a–d. From figures it is clear that no synchronized periodic behaviour is observed.

Case II Here we draw the bifurcation diagram of the lattices $x_n(i), i = 1, 2, 3, \ldots, 100$ with respect to ϵ for different values of induced parameter $\beta = 2.09, \beta = 2.13, \beta = 2.135$ and $\beta = 2.2$ in Fig. 3a–d fixing the randomness at $p = 0.5$ and growth rate at $r = 3.5$. From figures, we obtain the different stability ranges for different

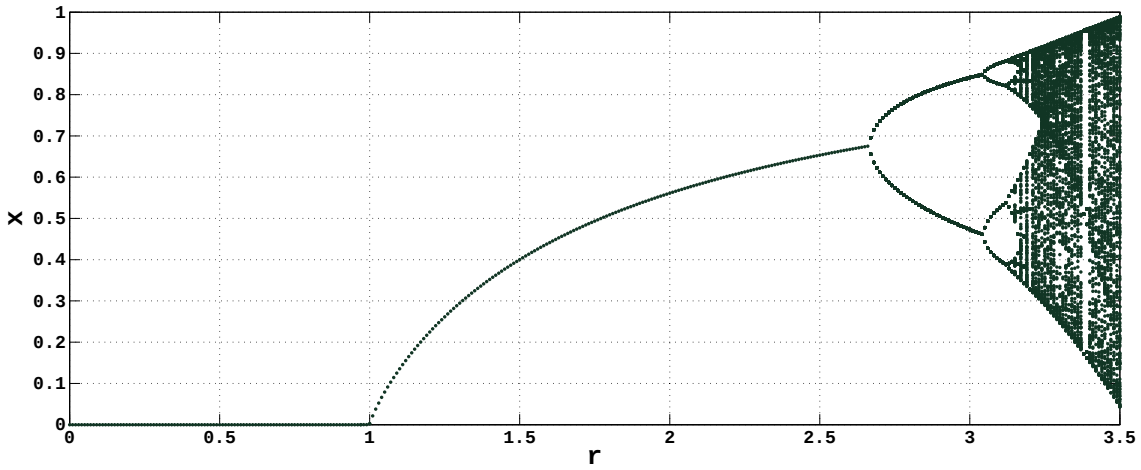

Fig. 1 Bifurcation diagram with respect to population growth rate r of modified logistic map

values of parameter β, which matches very well of our analytically estimated ranges $0.5918 \leq \epsilon \leq 1$ for $\beta = 2.09$, $0.6226 \leq \epsilon \leq 1$ for $\beta = 2.13$, $0.6262 \leq \epsilon \leq 1$ for $\beta = 2.135$ and $0.6667 \leq \epsilon \leq 1$ for $\beta = 2.2$. Therefore we observed that with the increase of the newly induced parameter β, the stability ranges are decreased. We observed from Fig. 3b, c that periodic orbit is observed for $\beta = 2.13$ and for $\beta = 2.135$ for complex network $(p = 0.5)$ when $r = 3.5$. But for lower values of $\beta = 2.13$ and higher values of $\beta = 2.135$, this type of behaviour is not observed for complex network $(p = 0.5)$ which is established by our Fig. 3a, d, respectively.

Case III In this case we draw the bifurcation diagram of the lattices $x_n(i), i = 1, 2, 3, ..., 100$ with respect to ϵ, fixing the randomness at $p = 1$ and growth rate at $r = 3.5$, for different values of induced parameter $\beta = 2.09, \beta = 2.13, \beta = 2.135$ and $\beta = 2.2$ in Fig. 4a–d. The stability ranges, obtained in Fig. 4a–d, map very well in our analytical estimated ranges $0.4203 \leq \epsilon \leq 1$ for $\beta = 2.09$, $0.4520 \leq \epsilon \leq 1$ for $\beta = 2.13$, $0.4558 \leq \epsilon \leq 1$ for $\beta = 2.135$ and $0.5 \leq \epsilon \leq 1$ for $\beta = 2.2$. Interestingly, we noticed that synchronized periodic behaviour is observed only for $\beta = 2.13$ with $r = 3.5$ for completely random coupling, but for lower and higher values of $\beta = 2.13$, there is no synchronized periodic state observed which are established by our Fig. 4a–d. Here we notice that with the increase in the newly induced parameter β, the stability ranges decrease.

5.2 Variation for Low and High Rewiring Probability

Case I

In the 1st case, we draw the bifurcation diagram of the lattices $x_n(i), i = 1, 2, 3, ..., 100$ with respect to coupling

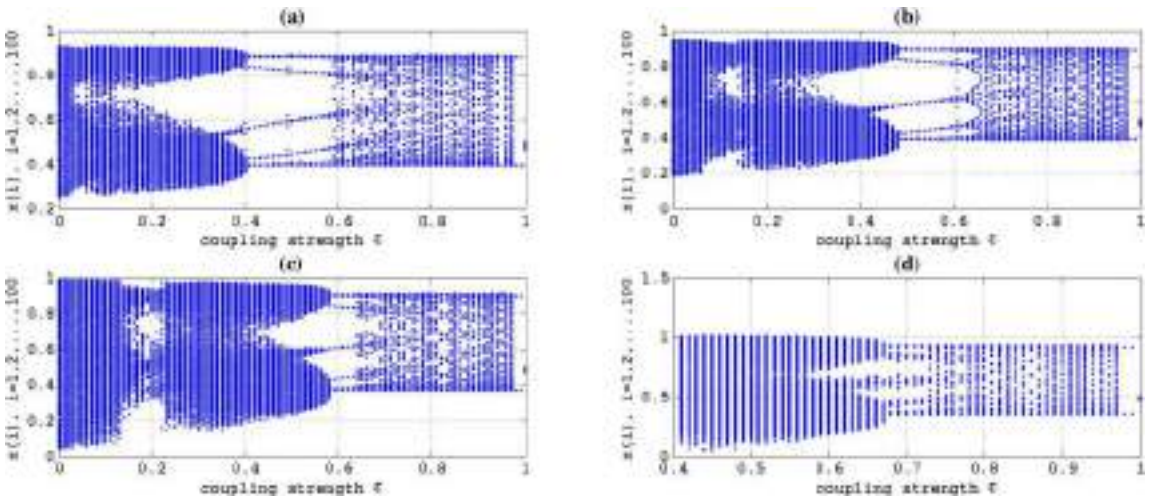

Fig. 2 Bifurcation diagram showing values of $x_n(i), i = 1, 2, ..., 100$, with respect to coupling strength ϵ, for coupled modified logistic maps with strictly regular nearest neighbour connections for **a** $\beta = 2.09, r = 3.5$, **b** $\beta = 2.13, r = 3.5$, **c** $\beta = 2.2, r = 3.5$ and **d** $\beta = 2.43, r = 3.5$

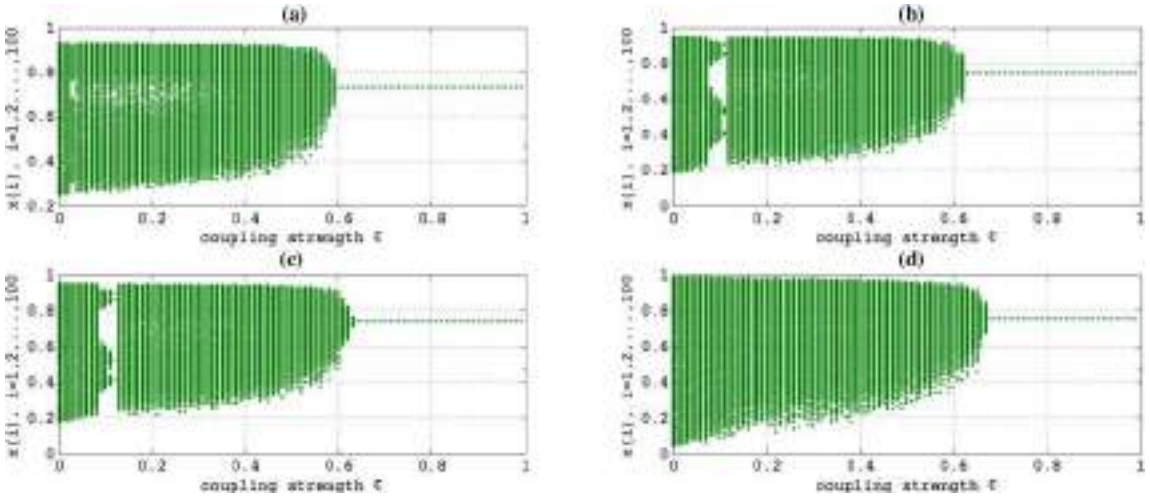

Fig. 3 Bifurcation diagram showing values of $x_n(i), i = 1, 2, ..., 100$, with respect to coupling strength ϵ, for coupled modified logistic maps with $p = 0.5$ for **a** $\beta = 2.09, r = 3.5$, **b** $\beta = 2.13, r = 3.5$, **c** $\beta = 2.135, r = 3.5$ and **d** $\beta = 2.2, r = 3.5$

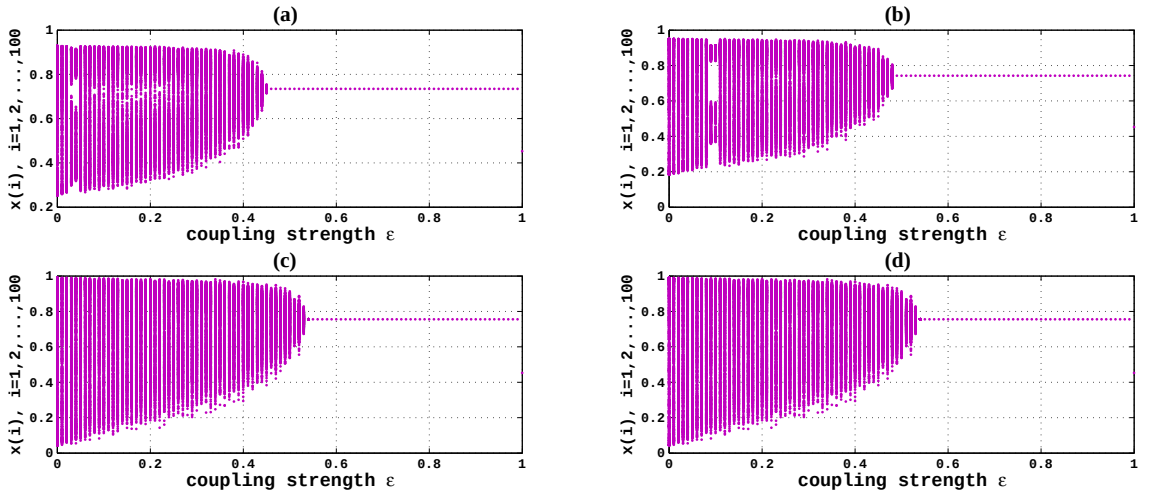

Fig. 4 Bifurcation diagram showing values of $x_n(i), i = 1, 2, ..., 100$, with respect to coupling strength ϵ, for coupled modified logistic maps with completely random connections for **a** $\beta = 2.09, r = 3.5$, **b** $\beta = 2.13, r = 3.5$, **c** $\beta = 2.135, r = 3.5$ and **d** $\beta = 2.2, r = 3.5$

strength ϵ for low and high rewiring probability for $\beta = 2.09$ and $r = 3$ in Fig. 5a, b and same for $\beta = 2.09$ and $r = 3.5$ in Fig. 5c, d. From Fig. 5a, c, we observe that no synchronized fixed point is observed in low rewiring probability, but synchronized fixed point is observed for high rewiring probability in Fig. 5b, d, whose stability ranges match very well with our analytical estimated ranges obtained from Eq. (12).

Case II

In case II, the bifurcation diagram of the CML for $\beta = 2.09$ and $r = 3.5$ with respect to coupling strength ϵ for low and high rewiring probability are shown in Fig. 6a, b, respectively, and same for $\beta = 2.139$ and $r = 3.5$ in Fig. 6c, d, respectively. In Fig. 6a, c, no synchronized fixed point is observed in low rewiring probability, but for high rewiring probability synchronized fixed point observed in Fig. 6b, d, whose stability ranges match very well with our analytical estimated ranges obtained from Eq. (12).

5.3 Variation of Growth Rate *r*

Case I

In this case, we fixed the randomness at $p = 0$ and newly induced parameter β at $\beta = 2.135$; then, the bifurcation diagram of CML is drawn in Fig. 7a–d for different $r(= 3.0, 3.2, 3.4, 3.5)$. Here we notice that no synchronized fixed point arises.

Case II

In case II, we fixed the randomness at $p = 0.5$ and $\beta = 2.135$; then, the bifurcation diagram of CML is drawn in Fig. 8a–d for different $r(= 3.0, 3.2, 3.4, 3.5)$. Here we achieve the stability ranges for synchronized fixed point.

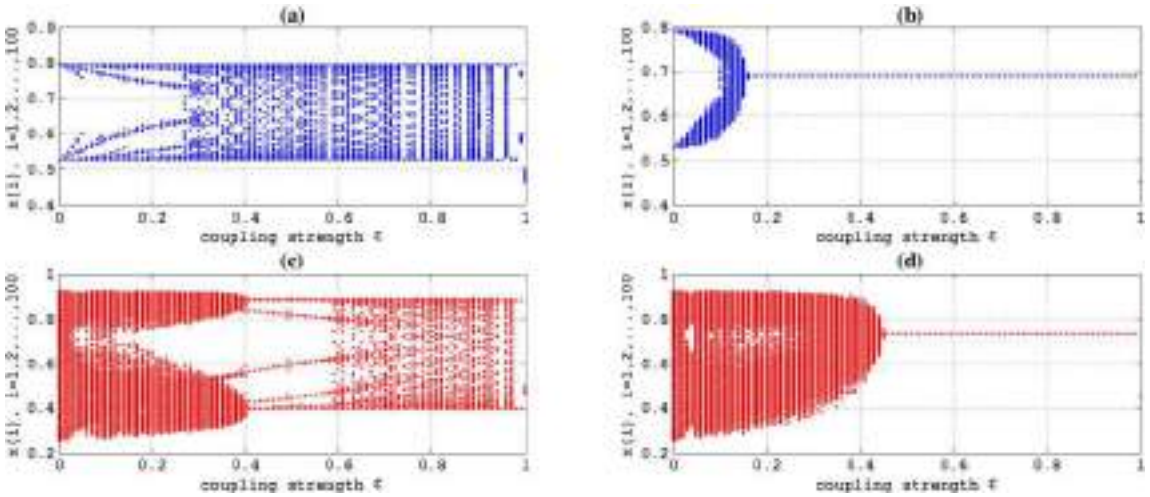

Fig. 5 Bifurcation diagram showing the state of the lattice $x_n(i), i = 1, 2, ..., 100$, with respect to coupling strength ϵ, with $\beta = 2.09$, for **a** $r = 3.0, p = 0$, **b** $r = 3.0, p = 1$, **c** $r = 3.5, p = 0$ and **d** $r = 3.5, p = 1.0$

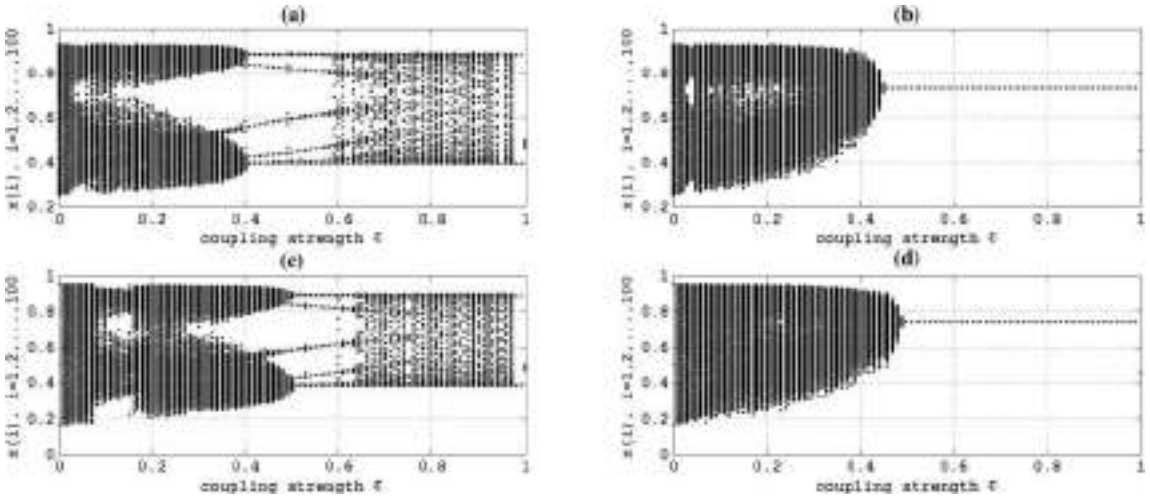

Fig. 6 Bifurcation diagram showing the state of the lattice $x_n(i), i = 1, 2, ..., 100$, with respect to coupling strength ϵ, with $r = 3.5$, for **a** $\beta = 2.09, p = 0$, **b** $\beta = 2.09, p = 1$, **c** $\beta = 2.139, p = 0$ and **d** $\beta = 2.139, p = 1.0$

Figures establish that for increase of growth rate, stability ranges also increase, which supports Eq. (12). In Fig. 8d we observe that synchronized periodic behaviour is observed for complex network ($p = 0.5$) with $\beta = 2.135$ for $r = 3.5$ in low coupling strength, but for $r < 3.5$, there is no synchronized periodic behaviour which is establish in Fig. 8a–c.

Case III

In case III, we fixed the randomness at $p = 1$ and $\beta = 2.135$, the bifurcation diagram of CML is drawn in Fig. 9a–d for different $r(= 3.0, 3.2, 3.4, 3.5)$. Here stability ranges increase with the increase of the growth rate r and also support our analytical estimated range from Eq. (12).

5.4 Variation of Randomness from $p = 0$ to $p = 1$

We draw the bifurcation diagram of the lattices $x_n(i), i = 1, 2, 3, ..., 100$ with respect to coupling strength ϵ for different randomness $p = 0, 0.01, 0.05, 0.10, 0.45, 0.75, 0.90$ and $p = 1.0$ fixing the growth rate $r = 3.5$ and parameter $\beta = 2.135$ as shown in Fig. 10a–g. Figure 10a shows no stability range, as established from analytical range of Eq. (13), and from Fig. 10b–g, we observe that the stability ranges increase with increase of randomness. Synchronized periodic behaviour is observed in low coupling strength with $r = 3.5$, $\beta = 2.135$ for $p \geq 0.05$, but for $p < 0.05$, there is no synchronized periodic behaviour.

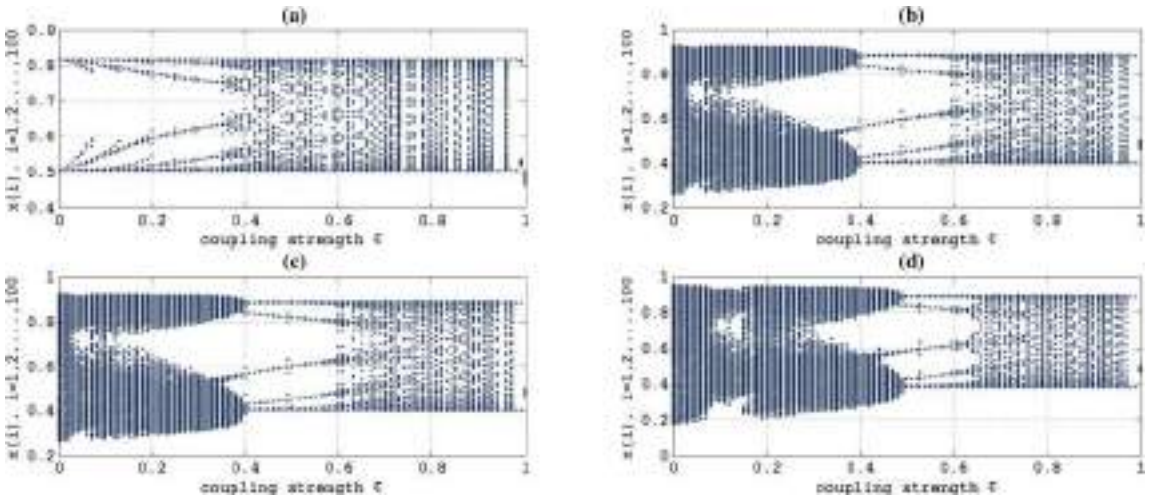

Fig. 7 Bifurcation diagram showing values of $x_n(i), i = 1, 2, ..., 100$, with respect to coupling strength ϵ, for coupled modified logistic maps with strictly regular nearest neighbour connections with $\beta = 2.135$ for **a** $r = 3.0$, **b** $r = 3.2$, **c** $r = 3.4$ and **d** $r = 3.5$

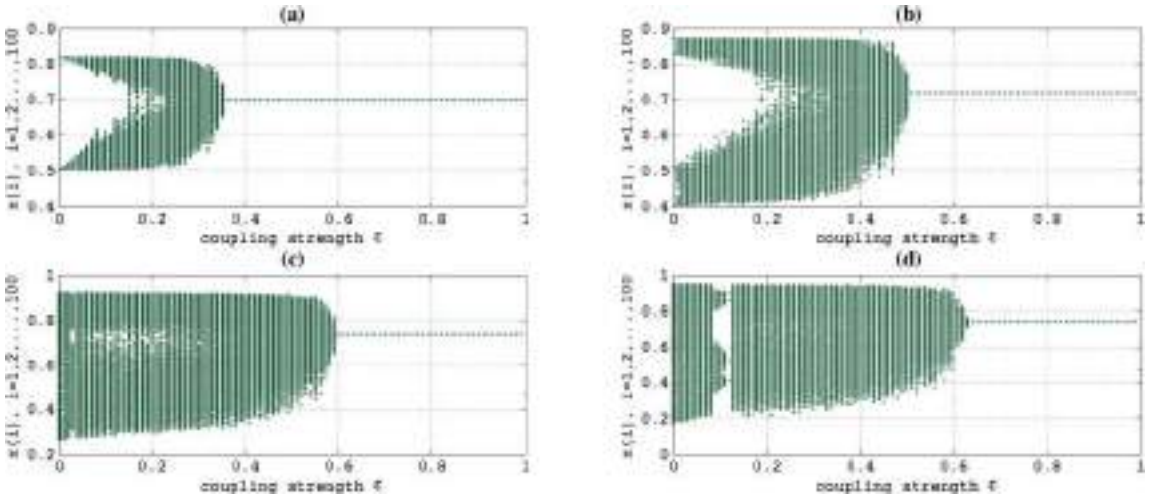

Fig. 8 Bifurcation diagram showing values of $x_n(i), i = 1, 2, ..., 100$, with respect to coupling strength ϵ, for coupled modified logistic maps with $p = 0.5, \beta = 2.135$ for **a** $r = 3.0$, **b** $r = 3.2$, **c** $r = 3.4$ and **d** $r = 3.5$

6 Variation of Basin Size of the Synchronized State

If out of n random initial conditions, synchronization is obtained in m cases; then, the basin size is equal to $\frac{m}{n}$. It is clear that basin size lies between the values 0 and 1. To compute basin size we have taken 100 random initial conditions. If $m = 0$, then no synchronization occurs and the values of basin size are equal to 0, and if $m = n$, then the synchronization is observed in all cases and the values of basin size become 1. We have plotted variation of basin sizes with respect to coupling strength ϵ for different connectivity and basin sizes with respect to rewiring probability p for different coupling strengths. In Fig. 11a we plot the size of the basin of attraction with respect to rewiring probability p for $r = 3.5$ with different $\epsilon(= 0.20, 0.40, 0.75, 1)$, and in Fig. 11b, variation of the size of basin of attraction of the synchronized state with respect to coupling strength for $r = 3.5$ with $p = 0.50, 0.75, 0.85$ and $p = 1$ is drawn. Here we observe that the range of synchronization increases with the increase of p. In Fig. 12 we plot the variation of the size of basin of attraction of the synchronized state with respect to coupling strength for various newly induced parameter $\beta(= 2.00, 2.02, 2.04, 2.10)$ for $(a)\, p = 0$, $(b)\, p = 0.50$, $(c)\, p = 0.75$ and $(d)\, p = 1$ and same for different values of growth rate $r(= 3.2, 3.5, 3.8, 4.0)$ in Fig. 13.

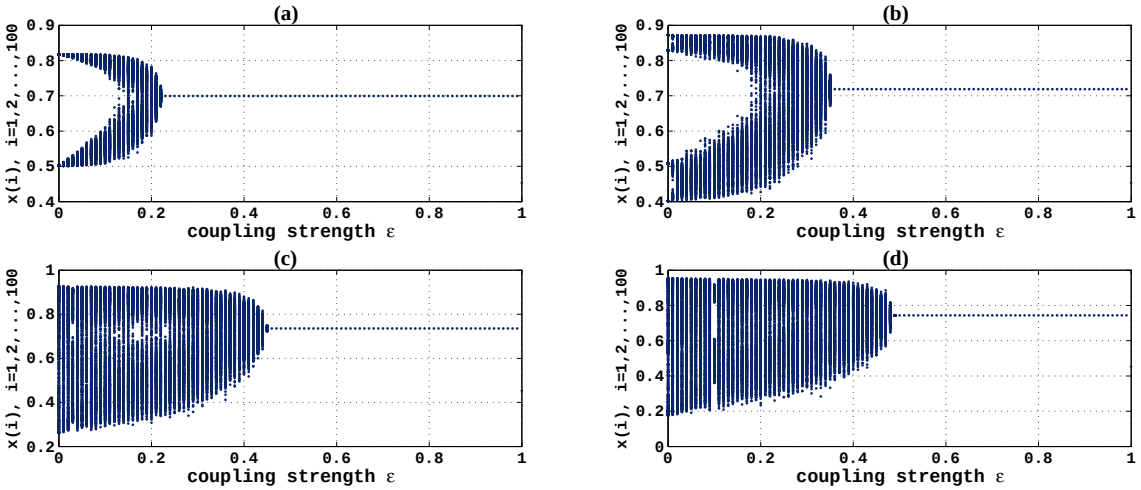

Fig. 9 Bifurcation diagram showing values of $x_n(i), i = 1, 2, ..., 100$, with respect to coupling strength ϵ, for coupled modified logistic maps with completely random connections with $\beta = 2.135$ for **a** $r = 3.0$, **b** $r = 3.2$, **c** $r = 3.4$ and **d** $r = 3.5$

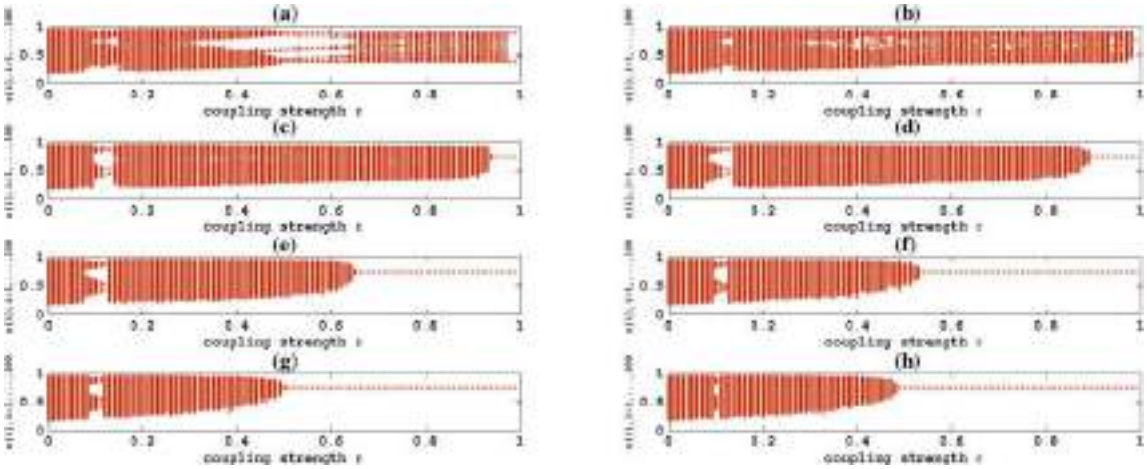

Fig. 10 Bifurcation diagram showing values of $x_n(i), i = 1, 2, ..., 100$, with respect to coupling strength ϵ, for coupled modified logistic maps with $r = 3.5, \beta = 2.135$ for different randomness **a** $p = 0$, **b** $p = 0.01$, **c** $p = 0.05$, **d** $p = 0.10$, **e** $p = 0.45$, **f** $p = 0.75$, **g** $p = 0.90$ and **h** $p = 1.0$

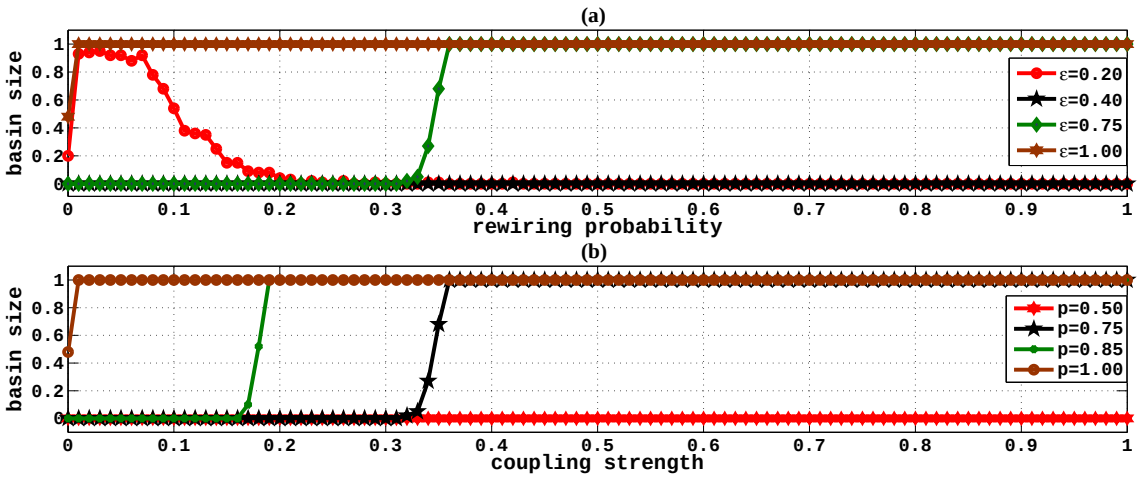

Fig. 11 **a** Size of the basin of attraction with respect to rewiring probability p for $r = 3.5$ with different $\epsilon(= 0.20, 0.40, 0.75, 1)$. **b** Variation of the size of basin of attraction of the synchronized state with respect to coupling strength for $r = 3.5$ with $p = 0.50, 0.75, 0.85$ and $p = 1$

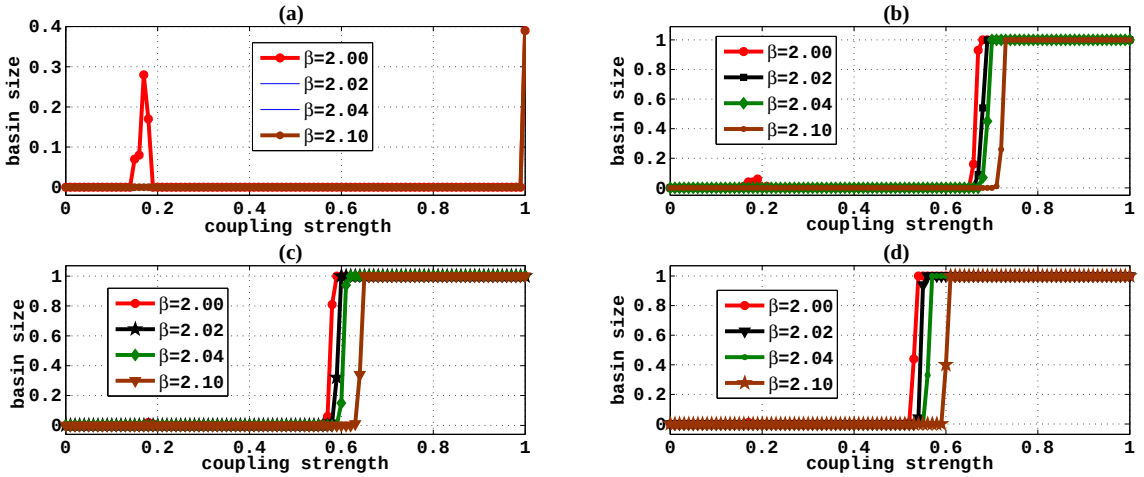

Fig. 12 Variation of the size of basin of attraction of the synchronized state with respect to coupling strength for various newly induced parameter $\beta(= 2.00, 2.02, 2.04, 2.10)$ for **a** $p = 0$, **b** $p = 0.50$, **c** $p = 0.75$ and **d** $p = 1$

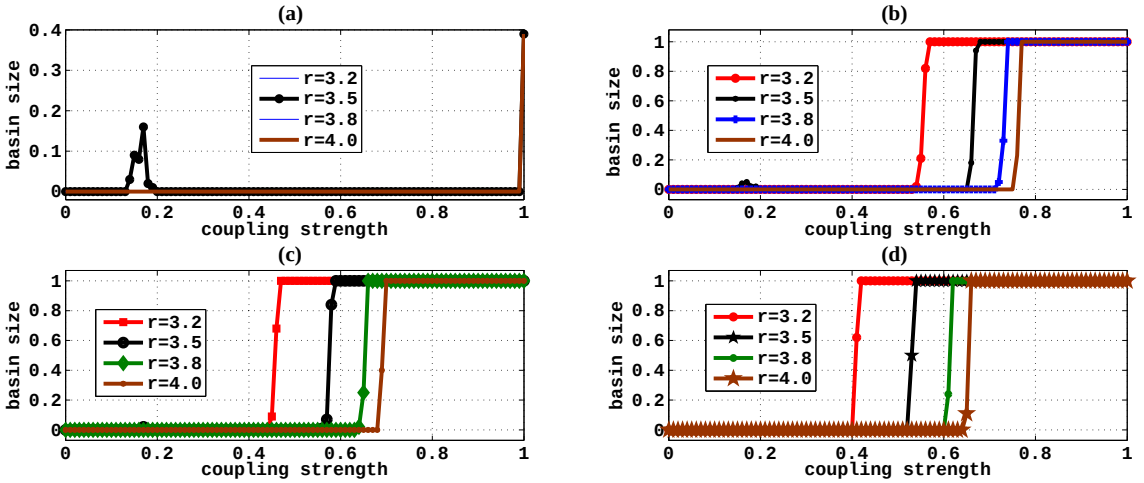

Fig. 13 Variation of the size of basin of attraction of the synchronized state with respect to coupling strength for different values of growth rate $r(= 3.2, 3.5, 3.8, 4.0)$ for **a** $p = 0$, **b** $p = 0.50$, **c** $p = 0.75$ and **d** $p = 1$

7 Conclusions

We have reported the SS behaviour of MLM in presence of stochastically switching of links. The analytical derivation of the stability range of the synchronized steady state of CML, matches very well with the numerical simulation results with respect to coupling strength and randomness for different values of rewiring probability and couplings. We observe that range of synchronization increases with increasing p and also with increasing ϵ.

References

1. Pecora LM, Carroll TL (1990) Synchronization in chaotic systems. Phys Rev Lett 64:821–824
2. Shooshtari BK, Forouzanfar AM, Molai MR (2016) Identical synchronization of a non-autonomous unified chaotic system with continuous periodic switch. Springer Plus. https://doi.org/10.1186/s40064-016-3299-6
3. Tarai A, Poria S, Chatterjee P (2009) Generalized synchronization of unified chaotic system. Chaos Solitions Fractals 40:885–892
4. Tarai A, Poria S, Chatterjee P (2009) Synchronization of bidirectionally of coupled chaotic Chen's system with delay. Chaos Solitions Fractals 41:190–197
5. Chung SJ, Bandyopadhyay S, Chang I, Hadaegh FY (2003) Phase synchronization control of complex networks of Lagrangian systems on adaptive digraphs. Automatica 49:1148–1161

6. Wang X, Zhang H, Lin X (2014) Module-phase synchronization in hyperchaotic complex Lorenz system after modified complex projection. Appl Math Comput 232:91–96
7. Khan MA, Poria S (2013) Projective synchronization of chaotic systems with bidirectional nonlinear coupling. Pramana J Phys 81:395–406
8. Bao HB, Cao JD (2015) Projective synchronization of fractional order memristor based neural networks. Neural Netw 63:1–9
9. Al-Sawalha M, Noorani M (2009) Anti-synchronization of two hyperchaotic systems via nonlinear control. Commun Nonlinear Sci Numer Simul 14:3402–3411
10. Sing PP, Sing JP, Roy BK (2014) Synchronization and anti-synchronization of Lu and Bhalekar–Gejji chaotic systems using nonlinear active control. Chaos Solitions Fractals 69:31–39
11. Ji DH, Jeong SE, Park JH, Lee SM, Won SC (2012) Adaptive lag synchronization for uncertain complex dynamical network with delayed coupling. Appl Math Comput 218:4872–4880
12. Huang J, Li C, Huang T, He X (2014) Finite time lag synchronization of delayed neural networks. Neurocomputing 139:145–149
13. Kaneko K (1993) Theory and application of coupled map lattices. Wiley, Hoboken
14. Casagrande V, Mikhailov AS (2005) Birhythmicity, synchronization and turbulence in an oscillatory system with nonlocal inertial coupling. Phys D Nonlinear Phenom 205:154–169
15. Oppo GL, Yao AM, Prati F, Valcarcel GJ (2009) Long term spatiotemporal dynamics of solid state lasers and vertical cavity surface emitting lasers. Phys Rev A 79:033824
16. Kastrup CJ, Kastrup CJ, Runyon MK, Shen F, Ismagilov RF (2006) Modular chemical mechanism predicts spatiotemporal dynamics of initiation in the complex network of hemostasis. Proc Natl Acad Sci USA 103:15747–15752
17. Bascompte J, Sole RV (1995) Rethinking complexity: modelling spatiotemporal dynamics in ecology. Trends Ecol Evol 10:361–366
18. Sinha S (2005) Spatiotemporal consequence of random coupling. Proc Indian Natl Sci Acad 71:97–111
19. Poria S, Khan MA, Nag M (2013) Spatiotemporal synchronization of coupled Ricker maps over a complex network. Phys Scr 88:015004
20. Nag M, Poria S (2015) Synchronization in a network of delay coupled maps with stochastically switching topologies. Chaos Solitions Fractals. https://doi.org/10.1016/j.chos.2016.04.022
21. Khan MA, Sahoo B (2016) Temporospatial synchronization of discrete logistic map through complex network. Optik 127:1526–1531
22. Noymanee J, San-Um W (2015) A modified simple logistic chaotic map through exponential controller in nonlinear term. In: Science and information conference 2015, London UK, 28–30 July

Publisher's Note Springer Nature remains neutral with regard to jurisdictional claims in published maps and institutional affiliations.

View publication stats

Mohammad Ali Khan

ResearchGate

See discussions, stats, and author profiles for this publication at: https://www.researchgate.net/publication/361493543

DESIGN OF MULTISTABLE SYSTEM OF COUPLED DIFFERENT LORENZ AND NUCLEAR SPIN GENERATOR SYSTEMS

Article *in* Advances in Mathematics Scientific Journal · June 2022

DOI: 10.37418/amsj.11.6.3.

CITATIONS
0

READS
92

3 authors, including:

Gour Chandra Mahata
Sidho Kanho Birsha University
93 PUBLICATIONS **1,457** CITATIONS

SEE PROFILE

All content following this page was uploaded by Gour Chandra Mahata on 23 June 2022.

The user has requested enhancement of the downloaded file.

Advances in Mathematics: Scientific Journal **11** (2022), no.6, 539–556
ISSN: 1857-8365 (printed); 1857-8438 (electronic)
https://doi.org/10.37418/amsj.11.6.3

DESIGN OF MULTISTABLE SYSTEM OF COUPLED DIFFERENT LORENZ AND NUCLEAR SPIN GENERATOR SYSTEMS

Jayanta Kumar Sarkar, Mohammad Ali Khan[1], and Gour Chandra Mahata

ABSTRACT. In this paper, we propose a new theoretical scheme design of multistable system of coupled Nuclear spin generator and Lorenz systems. In the system coupled Nuclear spin generator and Lorenz systems reduces to a single modified Lorenz system. We derive the existence conditions of fixed points and the conditions of local stability of the modified system is also derived. To obtain multistable behaviour maximum lyapunov exponent of the system and bifurcation analysis are analyzed. Dynamical behaviour with respect to multistable parameter using MATCONT software are also analyzed. The main observation is that: In coupling two m-dimensional dynamical systems multistable behaviour can be obtained if i number of variables of the two systems are completely synchronized and j number of variables keep a constant difference between them, where $i + j = m$ and $1 \leq i, j \leq m-1$. Numerical simulation results are presented to verify the proposed schemes.

1. INTRODUCTION

Multistability is the property whereby the solutions of a dynamical system can alternate between two or more exclusive lyapunov stable and convergent equilibrium states under asymptotically slowly changing inputs or system parameters.

[1]*corresponding author*
2020 *Mathematics Subject Classification.* 37 Dynamical systems and ergodic theory, 58 Global analysis, analysis on manifolds, 97 Mathematics education.
Key words and phrases. Multistability, Lorenz system, Nuclear spin generator system and Bifurcation analysis.
Submitted: 21.05.2022; *Accepted:* 05.06.2022; *Published:* 13.06.2022.

Multistable systems are observed in laser physics [1], condensed matter physics [2] and electronic oscillators [3] etc. and biological system namely population dynamics [4], neuroscience [5] and climate dynamics [6]. The dynamics of multistable systems are extremely sensitive to the initial state due to the coexistence of different attractors and as a result very small perturbations of the initial state might cause a large change in the final state. The mechanisms behind multistable behaviour of many natural system's are not completely known. Understanding the rules behind multistability behaviour of a dynamical system remains one of the fundamental problem of dynamical systems theory. In extreme multistability the number of coexisting attractors is infinite. Techniques for designing extreme multistable systems had been reported by Sun et.al. [7]. In their technique the choice of coupling plays the vital role. Synchronization of two or more coupled nonlinear systems are fundamental concept of nonlinear dynamics. Many synchronization techniques were proposed since the pioneer work of Pecora and Carroll [8]. In 1997, Feudel et.al.[9] have studied the behaviour of multistable systems that one obtained from conservative ones by adding a small amount of damping. Layton et.al. [10] have studied multistability in tubuloglomerular feedback and spectral complexity in spontaneously hypertensive rats in 2006. In 2011, Geltrude et.al.[11] have discussed multistability of chaotic systems to explore a complexity deterministic closed loop mechanism to control bursting phenomenon. In 2015, Li et.al. [12] have studied multistability in symmetric chaotic systems using amplitude control techniques. Since multistability and amplitude control sometimes involved in dynamical systems with involutional symmetry. Hens et.al.[13] have shown that the coexistence of infinitely many attractors in two coupled m dimensional systems will be possible if $m-1$ of the variable of the two systems are completely synchronized and one of them keeps a constant difference between them and Pal et.al.[14] observed the coupling two $m-$ dimensional dynamical systems in multistable nature by obtaining i number of variables of the two systems are completely synchronized and j number of variables keep a constant difference between them, where $i+j=m$ and $1 \leq i,j \leq m-1$. Very recently, in 2017, Bao et.al.[15] have illustrated that the long term dynamical behaviour closely depends on memristor initial conditions, thus leading to the immergence of hidden extreme multistability in the memristive hyper chaotic systems. In the same year

2017, Khan et. al.[16] have introduced a generalized scheme for designing multistable systems by coupling two different dynamical systems. The basic idea of the scheme is to design partial synchronization of states between the coupled systems and finding some completely initial condition-dependent constants of motion.

The basic idea of the scheme is to design multistability of states between the coupled systems and finding some completely initial condition-dependent constants of motion. We discuss our scheme coupling two different Lorenz and Nuclear spin generator systems. The bifurcation diagrams of the system with respect to multistability parameters are shown here.

The paper is organized as follows: In Section 2, a generalized scheme for designing multistability system is proposed and discussed taking two coupled Lorenz system and Nuclear spin generator system. The existence conditions of local stability is discussed in Section 3. Numerical simulation results are presented in Section 4. Finally, a conclusion is drawn in Section 5.

2. Generalised scheme for designing multistable systems

Consider the coupled two dynamical systems in the following way

$$\begin{aligned}
\dot{x_1} &= f_1(x_1, x_2, x_3, \ldots, x_n) + u_1(x_1, x_2, x_3, \ldots, x_n; y_1, y_2, y_3, \ldots, y_n) \\
\dot{x_2} &= f_2(x_1, x_2, x_3, \ldots, x_n) + u_2(x_1, x_3, x_3, \ldots, x_n; y_1, y_2, y_3, \ldots, y_n) \\
\dot{x_3} &= f_3(x_1, x_2, x_3, \ldots, x_n) + u_3(x_1, x_2, x_3, \ldots, x_n; y_1, y_2, y_3, \ldots, y_n) \\
&\ldots \\
\dot{x_n} &= f_n(x_1, x_2, x_3, \ldots, x_n) + u_n(x_1, x_2, x_3, \ldots, x_n; y_1, y_2, y_3, \ldots, y_n)
\end{aligned} \tag{2.1}$$

and

$$\begin{aligned}
\dot{y_1} &= g_1(y_1, y_2, y_3, \ldots, y_n) + v_1(x_1, x_2, x_3, \ldots, x_n; y_1, y_2, y_3, \ldots, y_n) \\
\dot{y_2} &= g_2(y_1, y_2, y_3, \ldots, y_n) + v_2(x_1, x_2, x_3, \ldots, x_n; y_1, y_2, y_3, \ldots, y_n) \\
\dot{y_3} &= g_3(y_1, y_2, y_3, \ldots, y_n) + v_3(x_1, x_2, x_3, \ldots, x_n; y_1, y_2, y_3, \ldots, y_n) \\
&\ldots \\
\dot{y_n} &= g_n(y_1, y_2, y_3, \ldots, y_n) + v_n(x_1, x_2, x_3, \ldots, x_n; y_1, y_2, y_3, \ldots, y_n)
\end{aligned} \tag{2.2}$$

where $u_1, u_2, u_3, \ldots, u_n$ and $v_1, v_2, v_3, \ldots, v_n$ are the controllers. We define the error as $e_i = y_i - x_i, i = 1, 2, \ldots, n$. Now we obtain the error dynamical system

$$
\begin{aligned}
\dot{e_1} &= g_1(y_1, y_2, y_3, \ldots, y_n) - f_1(x_1, x_2, x_3, \ldots, x_n) + v_1 - u_1 \\
\dot{e_2} &= g_2(y_1, y_2, y_3, \ldots, y_n) - f_2(x_1, x_2, x_3, \ldots, x_n) + v_2 - u_2 \\
\dot{e_3} &= g_3(y_1, y_2, y_3, \ldots, y_n) - f_3(x_1, x_2, x_3, \ldots, x_n) + v_3 - u_3 \\
&\ldots \\
\dot{e_n} &= g_n(y_1, y_2, y_3, \ldots, y_n) - f_n(x_1, x_2, x_3, \ldots, x_n) + v_n - u_n
\end{aligned} \tag{2.3}
$$

We choose the controllers $u_1, u_2, u_3, \ldots, u_n$ and $v_1, v_2, v_3, \ldots, v_n$ suitable such that the above system become multistable. Hens et al.[13] propose that the coupled systems (1)and (2) have multistable behaviour if $(n-1)$ states of the two systems synchronize and one state variable keeps constant difference with corresponding state variable of the other system. They choose controllers $u_1, u_2, u_3, \ldots, u_n$ and $v_1, v_2, v_3, \ldots, v_n$ in such way that

$$
\begin{aligned}
\dot{e_1} &= 0 \\
\dot{e_2} &= -e_2 \\
\dot{e_3} &= -e_3 \\
&\ldots \\
\dot{e_n} &= -e_n
\end{aligned} \tag{2.4}
$$

Here, we generalize the results of Hens et al.[13] and conjecture that "multistable systems can be designed choosing $u_1, u_2, u_3, \ldots, u_n$ and $v_1, v_2, v_3, \ldots, v_n$ in such way that i $(1 \leq i \leq n-1)$ number of state variables synchronize and $(n-i)$ number of state variables keeps constant difference". Therefore according to our scheme we choose $u_1, u_2, u_3, \ldots, u_n$ and $v_1, v_2, v_3, \ldots, v_n$ in such way that

$$
\begin{aligned}
\dot{e_1} &= 0 \\
\dot{e_2} &= 0 \\
\dot{e_3} &= 0 \\
&\ldots \\
\dot{e_i} &= 0 \\
\dot{e_{i+1}} &= -e_{i+1}
\end{aligned} \tag{2.5}
$$

$$\begin{aligned} \dot{e_{i+2}} &= -e_{i+2} \\ &\dots \\ \dot{e_n} &= -e_n \end{aligned}$$

where $1 \leq i \leq n-1$. Then for such choice the system formed by coupling (1) and (2) may show multistability.

Now we choose the function $L = (e_{i+1}^2 + e_{i+2}^2 + e_{i+3}^2 + \ldots + e_n^2)/2$ is a lyapunov function for the above system because

$$\begin{aligned} \dot{V} &= e_{i+2}\dot{e_{i+2}} + e_{i+3}\dot{e_{i+3}} + \ldots + e_n\dot{e_n} \\ &= -e_{i+1}^2 - e_{i+2}^2 - e_{i+3}^2 - \ldots - e_n^2. \end{aligned}$$

Hence the errors $e_{i+1}, e_{i+2}, e_{i+3}, \ldots, e_n$ must tend to zero i.e., $y_{i+1} = x_{i+1}$, $y_{i+2} = x_{i+2}$,...,$y_n = x_n$, as t tends to $\to \infty$ and $e_1, e_2, e_3, \ldots, e_i$ remains constant in time.

Therefore $y_1 = x_1 + c_1, y_2 = x_2 + c_2, y_3 = x_3 + c_3, \ldots, y_i = x_i + c_i$ and $y_{i+1} = x_{i+1}$, $y_{i+2} = x_{i+2}$,...,$y_n = x_n$.

Now the dynamics of the coupled system(1) and (2) is equivalent to the following system:

$$\begin{aligned} \dot{x_1} &= f_1(x_1, \ldots, x_n) + u_1(x_1, \ldots, x_n; x_1 + c_1, \ldots, x_i + c_i, x_{i+1} \ldots, x_n) \\ \dot{x_2} &= f_2(x_1, \ldots, x_n) + u_2(x_1, \ldots, x_n; x_1 + c_1, \ldots, x_i + c_i, x_{i+1} \ldots, x_n) \\ \dot{x_3} &= f_3(x_1, \ldots, x_n) + u_3(x_1, \ldots, x_n; x_1 + c_1, \ldots, x_i + c_i, x_{i+1} \ldots, x_n) \\ &\dots \\ \dot{x_n} &= f_n(x_1, \ldots, x_n) + u_n(x_1, \ldots, x_n; x_1 + c_1, \ldots x_i + c_i, x_{i+1} \ldots, x_n) \end{aligned} \tag{2.6}$$

where $c_1, c_2, c_3, \ldots, c_i's$ are initial condition dependent constants. The system (6) shows multistable behaviour if its dynamics changes qualitatively with varition of $c_1, c_2, c_3, \ldots, c_i's$. Notice that we have chosen $\dot{e_1} = \dot{e_2} = \cdots = \dot{e_i} = 0$ in general $\dot{e_1}, \dot{e_2}, \ldots \dot{e_i}$ may be chosen as any polynomial functions of $e_{i+1}, e_{i+2}, e_{i+3}, \ldots, e_n$.

In the following section, we shall discuss our scheme coupling two different Lorenz and Nuclear spin generator systems. Example of a proposition.

3. Construction of multistable systems using Lorenz and Nuclear spin generator systems

We consider the coupled Lorenz system [17] and Nuclear spin generator system [18] in the following form:

$$\begin{aligned} \dot{x_1} &= \sigma(x_2 - x_1) + u_1 \\ \dot{x_2} &= rx_1 - x_2 - x_1x_3 + u_2 \\ \dot{x_3} &= x_1x_2 - bx_3 + u_3 \\ \dot{y_1} &= -\beta y_1 + y_2 + v_1 \\ \dot{y_2} &= -y_1 - \beta y_2(1 - \kappa y_3) + v_2 \\ \dot{y_3} &= \beta[\alpha(1 - y_3) - \kappa y_2^2] + v_3 \end{aligned} \tag{3.1}$$

where $u_1, u_2, u_3, v_1, v_2, v_3$ are controllars and we choose $u_1 = \sigma(x_1 - y_1)$, $u_2 = x_2 - y_2$, $u_3 = 0$ and $v_1 = (\sigma - 1)y_2 + \beta y_1$, $v_2 = y_1 + (\beta - 1)y_2 + rx_1 - y_2 - y_3(\beta\kappa y_2 + x_1)$, $v_3 = \beta\kappa y_2^2 + x_1x_2 - \beta\alpha(1 - y_3) - by_3$ in such way that the above system reduces to

$$\begin{aligned} \dot{x_1} &= \sigma(x_2 - y_1) \\ \dot{x_2} &= rx_1 - y_2 - x_1x_3 \\ \dot{x_3} &= x_1x_2 - bx_3 \\ \dot{y_1} &= \sigma y_1 \\ \dot{y_2} &= rx_1 - y_2 - x_1y_3 \\ \dot{y_3} &= x_1x_2 - by_3 \end{aligned} \tag{3.2}$$

We now show that the six dimensional dynamical system is a multistable system. Following Sun et al.[19] we construct the governing equations for the synchronization errors $e_1 = y_1 - x_1$, $e_2 = y_2 - x_2$ and $e_3 = y_3 - x_3$ as

$$\begin{aligned} \dot{e_1} &= \sigma e_2 \\ \dot{e_2} &= -x_1e_3 \\ \dot{e_3} &= -be_3 \end{aligned} \tag{3.3}$$

It follows that e_3 must tend to zero with time i.e., $y_3 = x_3$. Since x_1 is a bounded physical quantity therefore

$$\begin{aligned} \dot{e_1} &= 0 \\ \dot{e_2} &= 0 \end{aligned} \tag{3.4}$$

which implies e_1= constant=c_1 and e_2= constant=c_2. Hence, $y_1 = x_1 + c_1$ and $y_2 = x_2 + c_2$ where c_1, c_2 are some constants (dependent on the initial condition of the full system). Each new set of initial conditions gives rise to different value of c_1 and c_2. Therefore, the dynamics of the system of equations (7) is equivalent to following three dimensional system

$$\begin{aligned} \dot{x_1} &= \sigma(x_2 - x_1 - c_1) \\ \dot{x_2} &= rx_1 - x_2 - c_2 - x_1x_3 \\ \dot{x_3} &= x_1x_2 - bx_3. \end{aligned} \tag{3.5}$$

The system (7) is a multistable system if the dynamical behaviour of the system (11) varies with the variation of the value of c_1 and c_2.

4. PRELIMINARIES

4.1. **Dissipativity and existence of attractor.** For the above system(11), we observe that $\nabla V = \frac{\partial \dot{x_1}}{\partial x_1} + \frac{\partial \dot{x_2}}{\partial x_2} + \frac{\partial \dot{x_3}}{\partial x_3} = -(\sigma + b + 1) < 0$, as $\sigma > 0$ and $b > 0$. So, the above system is dissipative, with an exponential contraction rate $\frac{dV}{dt} = -(\sigma + b + 1)V$. That is, a volume element V_0 is contracted by the flow into a volume element $V_0 e^{-(\sigma+b+1)t}$ in time t. This means that each volume containing the system trajectory shrinks to zero as $t \to +\infty$ at an exponential rate,$-(\sigma + b + 1)$. Therefore, system orbits are ultimately confined to a specific subset of zero volume, and the asymptotic motion settles onto an attractor.

4.2. **Equilibrium Points.** We first study the nature of equilibrium points of the system (11). An equilibrium point (x_1, x_2, x_3) is such that the solution of a system does not change in time. The equilibrium point of the system (11) is the point $E^* \equiv (x_1^*, x_2^*, x_3^*)$, where $x_2^* = x_1^* + c_1$, $x_3^* = b(rx_1^* - x_1^* - c_1 - c_2)/x_1^*(x_1^* + c_1)$ and x_1^* is the real root of the cubic equation $x_1^3 + c_1x_1^2 + b(1-r)x_1 + b(c_1 + c_2) = 0$. Therefore, existence of non-trivial equilibrium points depend on the parameter value c_1 and

c_2. E^* exist when $\triangle = 19b^2c_1^2 + 18b^2c_1c_2(1-r) + 4b^3r^3 + r^2b^2c_1^2 - 4b^3 + 12b^3r(1-r) - 27b(c_1+c_2) - 18b^2c_1r - 4bc_1^4 - 4bc_1^3c_2 - 2rb^2c_1^2 > 0$.

The Jacobian matrix of the system (11) at the equilibrium point $E^* = (x_1^*, x_2^*, x_3^*)$ is given by

$$J(E^*) = \begin{pmatrix} -\sigma & \sigma & 0 \\ r - x_3^* & -1 & -x_1^* \\ x_2^* & x_1^* & -b \end{pmatrix}. \tag{4.1}$$

The eigenvalues of the Jacobian matrix are the roots of the following equation

$$\lambda^3 + a_1\lambda^2 + a_2\lambda + a_3 = 0.$$

where, $a_1 = \sigma(x_1^*x_2^* + bx_3^* - br) + \sigma(x_1^{*2} + b)$, $a_2 = x_1^{*2} + b + b\sigma + \sigma x_3^* + \sigma - \sigma r$, $a_3 = b + 1 + \sigma$.

The equilibrium point $E^* = (x_1^*, x_2^*, x_3^*)$ is stable if $a_1 > 0$, $a_3 > 0$ and $a_1a_2 - a_3 > 0$, otherwise E^* is unstable.

5. Numerical results

We perform the dynamical behaviours of the system (11) through numerical analysis with the parameter values which are taken form Lorenz system [17]. We have varied the vital parameters c_1 and c_2 throughout the whole numerical simulations.

First, we discuss the simulation results of the system (11) with bifurcation and maximum lyapunov exponent. The bifurcation and maximum lyapunov exponent of the system(11) for different values of c_1 and c_2 are plotted for fixed $\sigma = 10$, $r = 28$ and $b = 8/3$. The bifurcation and maximum lyapunov exponent diagram with respect to c_1 of the system(11) are plotted in figures 1(a),(b) to 4(a),(b) for $c_2 = -2$, $c_2 = -1$, $c_2 = 1$ and $c_2 = 2$ respectively. Also the bifurcation and maximum lyapunov exponent diagrams with respect to c_2 of the system(11) are plotted in figures 5(a),(b) to 7(a),(b) for $c_1 = -1$, $c_1 = 1$ and $c_1 = 2$ respectively. The multistable behaviour of the system(11) is established from these diagrams. In figure 8 extinction region of c_1 and c_2 of the system (11) are plotted for $\sigma = 10$, $r = 28$ and $b = 8/3$. Figure 8 depicts regions of stable state, unstable state and stable state. Notice that in Figure 8 the boundaries between the different dynamical regions are not perfectly distinct. Because, in Figure 8 that the high

periodic oscillations and chaotic region there are small areas. This occurs because there is some degree of sensitivity to small changes in parameter values resulting in sharp transitions between different dynamical outcomes. For internal bifurcation scenarios of the system (11), we study a pattern of bifurcation sequences in next Section.

6. HOPF BIFURCATION AND CONTINUATION

Our main aim of this section is to investigate the bifurcation scenarios of the system(11) with respect to the parameter c_1 and c_2. These are done by studying the change in the eigenvalues of the Jacobian matrix and following the continuation algorithm. We choose initial points $x_{10} = 9.5043676$, $x_{20} = 15.565189$, $x_{30} = 18.166588$ fixing the parameter values $\sigma = 10$, $r = 28$ and $b = 8/3$. The characteristics of Hopf point, limit cycle and the general bifurcation nature are explored using the software package MATCONT2.5.1. In this package we use prediction-correction continuation algorithm based on the Moore-Penrose matrix pseudo inverse for computing the curves of equilibria, limit point (LP) and its continuation curves.

The continuation curves from the equilibrium point of x_3 with respect to c_1 for $c_2 = -5$(Red line), $c_2 = 0$(Blue line) and $c_2 = 5$(Magenta line) for the fixed parameter values $\sigma = 10,\ r = 28,\ b = 8/3$ are presented in figure 9. Existence of two Hopf points (H_1, H_2), two limit points (LP_1, LP_2) are observed in figure 9 for all those cases. The Hopf points H_1 and H_2 for $c_2 = -5$ are located at $(x_1, x_2, x_3, c_1, c_2)$ $\equiv$(9.5043676,15.565189,18.166588,-0.022349081,-5.0) and $(x_1, x_2, x_3, c_1, c_2) \equiv$(9.5043676,15.565189,18.166588,2.293176,-5.000) with first Lyapunov coefficient is to be 0.002076872, indicating a sub critical Hopf bifurcation. Therefore, there are two complex eigenvalues of the equilibrium with real $\lambda_{2,3} \approx 0$ at the parameter. First Lyapunov coefficient is positive implies that a unstable limit cycle appears from the equilibrium point. The limit points LP_1 and LP_2 occur at $(x_1, x_2, x_3, c_1, c_2) \equiv$ (9.5043676,15.565189,18.166588,18.741569, -5.00) with normal form of coefficient $a = -0.2615149$ and $(x_1, x_2, x_3, c_1, c_2) \equiv$ (9.5043676, 15.565189,18.166588,-24.076094,-5.00) with normal form of coefficient $a = -0.2585899$. The Hopf points H_1 and H_2 for $c_2 = 0$ are located at $(x_1, x_2, x_3, c_1,$ $c_2) \equiv$ (9.5043676,15.565189,18.166588,-1.2610557,0.000) and (x_1,x_2, x_3, c_1,c_2)$\equiv$

(9.5043676,15.565189,18.166588,1.2610557,0.000) with first Lyapunov coefficient is to be 0.002029014, indicating a sub critical Hopf bifurcation. Therefore, there are two complex eigenvalues of the equilibrium with real $\lambda_{2,3} \approx 0$ at the parameter. First Lyapunov coefficient is positive implies that a unstable limit cycle appears from the equilibrium point. The limit points LP_1 and LP_2 occur at (x_1, x_2, x_3, c_1,c_2)≡(9.5043676, 15.565189,18.166588,-21.280859,0.00) with normal form of coefficient $a = -0.2599334$ and (x_1, x_2, x_3,c_1,c_2)≡ (9.5043676, 15.565189, 21.28085918.166588,21.280859,0.00) with normal form of coefficient $a = -0.2599334$. The Hopf points H_1 and H_2 for $c_2 = 5$ are located at (x_1, x_2, x_3, c_1, c_2)≡ (9.5043676,15.565189,18.166588,-2.293173,5.00) with first Lyapunov coefficient is to be 0.002076873 and (x_1, x_2,x_3, c_1,c_2) ≡ (9.5043676, 15.565189, 18.166588, 0.022354, 5.0) with first Lyapunov coefficient is to be 0.001964840, indicating a sub critical Hopf bifurcation. Therefore, there are two complex eigenvalues of the equilibrium with real $\lambda_{2,3} \approx 0$ at the parameter. First Lyapunov coefficient is positive implies that a unstable limit cycle appears from the equilibrium point. The limit points LP_1 and LP_2 occur at (x_1, x_2, x_3, c_1,c_2)≡ (9.5043676, 15.565189, 18.166588, -24.076094, 5.0) with normal form of coefficient $a = -0.2585901$ and (x_1, x_2, x_1,c_1,c_2)≡(9.5043676, 15.565189, 18.166588, 18.741569, 5.0) with normal form of coefficient $a = 0.2615148$. The bifurcation results together with normal coefficients with respect to c_1 are listed in Table 1.

The continuation curves from the equilibrium point of x_3 with respect to c_2 for $c_1 = -5$ (Red line), $c_1 = 0$ (Blue line) and $c_1 = 5$ (Magenta line) for the fixed parameter values $\sigma = 10$, $r = 28$, $b = 8/3$ are also presented in figure 10. Existence of two Hopf points (H_1, H_2), two limit points (LP_1, LP_2) are also observed in figure 10 for all these cases. The bifurcation results together with normal coefficients with respect to c_2 are also listed in Table 2.

Table 1: Bifurcation points of the system(11) in figure 9, together with first Lyapunov coefficients, normal form coefficients and eigenvalues for parameters $\sigma = 10$, r=28 $b = 8/3$. H_1, H_2- Hopf points; LP_1, LP_2-Limit Points.

c_2	c_1	Label	First Lyapunov coefficients/ Normal	Eigenvalues

			form coefficient	
-5.0000	-0.022349081	H_1	$l_1 = 0.002076872$	$-13.666,\ \pm i10.43590$
-5.0000	2.293176	H_2	$l_1 = 0.002076872$	$-13.666,\ \pm i10.9509$
-5.000	-18.741569	LP_1	$a = -0.2615149$	$-19.2776, 0.0000, 5.61162$
-5.0000	24.076094	LP_2	$a = -0.2585899$	$-19.2436, -0.000001148, 5.57762$
0.0000	-1.2610557	H_1	$l_1 = 0.002029014$	$-13.666,\ \pm i10.7053$
0.0000	1.2610557	H_2	$l_1 = 0.002029013$	$-13.666,\ \pm i10.7053$
0.0000	-21.280859	LP_1	$a = -0.2599334$	$-19.259, 0.0000, 5.59298$
0.0000	21.280859	LP_2	$a = -0.2599334$	$-19.259, 0.0000, 5.59298$
5.0000	-2.293173	H_1	$l_1 = 0.002076873$	$-13.666,\ \pm i10.8509$
5.0000	0.022354	H_2	$l_1 = 0.001964840$	$-13.666,\ \pm i10.4359$
5.0000	-24.076094	LP_1	$a = -0.2585901$	$-19.2436, 0.0000, 5.57761$
5.0000	18.741569	LP_2	$a = 0.2615148$	$-19.2776, 0.0000, 5.61162$

TABLE 2. Bifurcation points of the system(11) in figure 10, togather with first Lyapunov coefficients, normal form coefficients and eigenvalues for parameters $\sigma = 10$, r=28 $b = 8/3$. H_1, H_2- Hopf points; LP_1, LP_2-Limit Points.

c_2	c_1	Label	First Lyapunov coefficients/ Normal form coefficient	Eigenvalues
-5.0000	-17.569229	H_1	$l_1 = 0.001737604$	$-13.666,\ \pm i9.60221$
-5.0000	22.684046	H_2	$l_1 = 0.002156435$	$-13.666,\ \pm i11.6893$
-5.000	-50.443686	LP_1	$a = 0.2822183$	$-19.6054, 0.00000, 5.9394$
-5.0000	157.38987	LP_2	$a = 0.2981529$	$-20.7374, -0.00000, 7.07142$
0.0000	-5.0813	H_1	$l_1 = 0.001963648$	$-13.666,\ \pm i10.4313$
0.0000	5.0813	H_2	$l_1 = 0.001963647$	$-13.666,\ \pm i10.434$
0.0000	-88.170607	LP_1	$a = 0.2946126$	$-20.00, 0.0000, 6.334$
0.0000	88.170607	LP_2	$a = -0.2946126$	$-20., 0.00000, 6.334$
5.0000	-17.569224	H_1	$l_1 = 0.001737605$	$-13.666,\ \pm i9.60221$
5.0000	-22.684046	H_2	$l_1 = 0.002156435$	$-13.666,\ \pm i11.6893$
5.0000	-50.443686	LP_1	$a = 0.2822182$	$-19.6054, 0.0000, 5.9394$
5.0000	157.38987	LP_2	$a = -0.2981532$	$-20.7374, -0.00000, 7.07142$

7. CONCLUSION

We introduce a generalised scheme for designing multistable coupling Lorenz system. In this scheme the two state variables of the coupled systems synchronize and other state variables keep constant difference. In this scheme the coupled Lorenz system reduces to a single modified Lorenz system. Equilibrium points of the proposed system are determined and the local stability criteria is derived. Multistable nature of the coupled Lorenz system is described through bifurcation and maximum lyapunov exponent diagrams. One and two parameter bifurcation analysis is done using MATCONT software. Our investigation and predictions may be very useful for designing multistable systems in different branches such as biology, physics and engineering sciences.

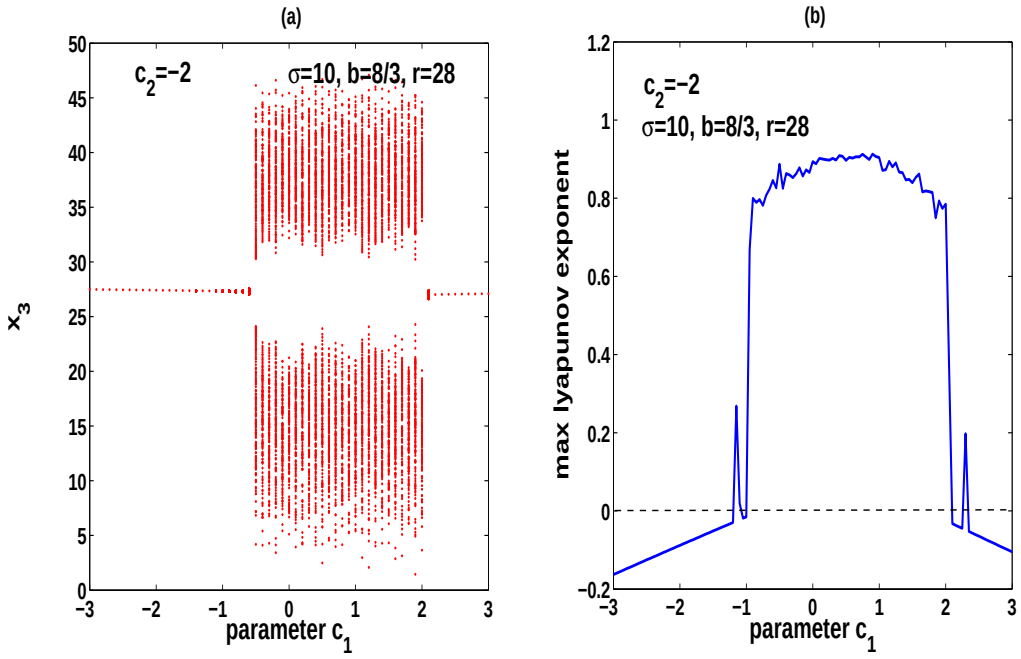

FIGURE 1. Figure depicts in(a)Bifurcation of x_3 with respect to c_1 and in (b) Maximu lyapunov exponent with respect to c_1 for fixed $c_2 = -2$ and $\sigma = 10, r = 28, b = 8/3$

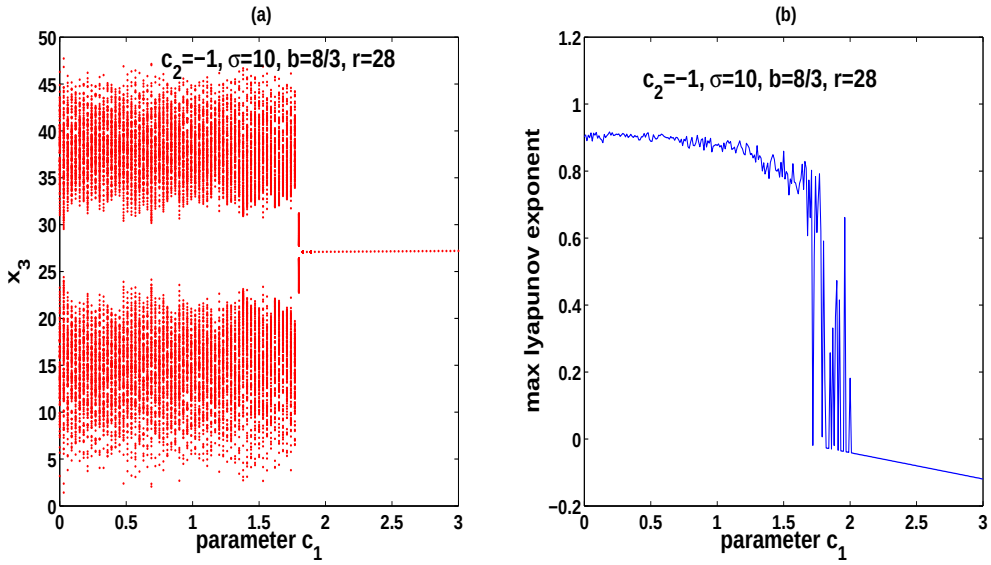

FIGURE 2. Figure depicts in(a)Bifurcation of x_3 with respect to c_1 and in (b) Maximu lyapunov exponent with respect to c_1 for fixed $c_2 = -1$ and $\sigma = 10, r = 28, b = 8/3$

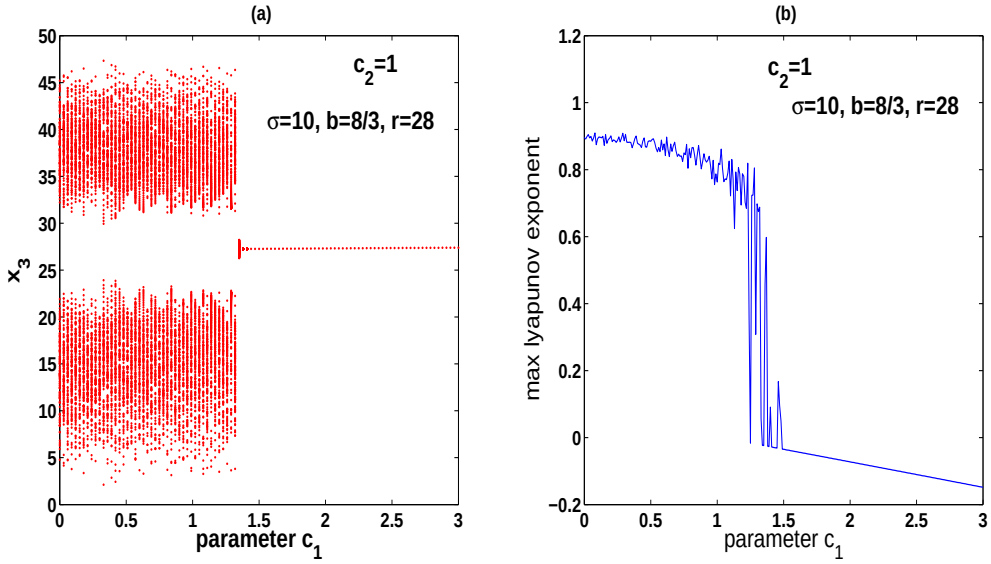

FIGURE 3. Figure depicts in(a)Bifurcation of x_3 with respect to c_1 and in (b) Maximu lyapunov exponent with respect to c_1 for fixed $c_2 = 1$ and $\sigma = 10, r = 28, b = 8/3$

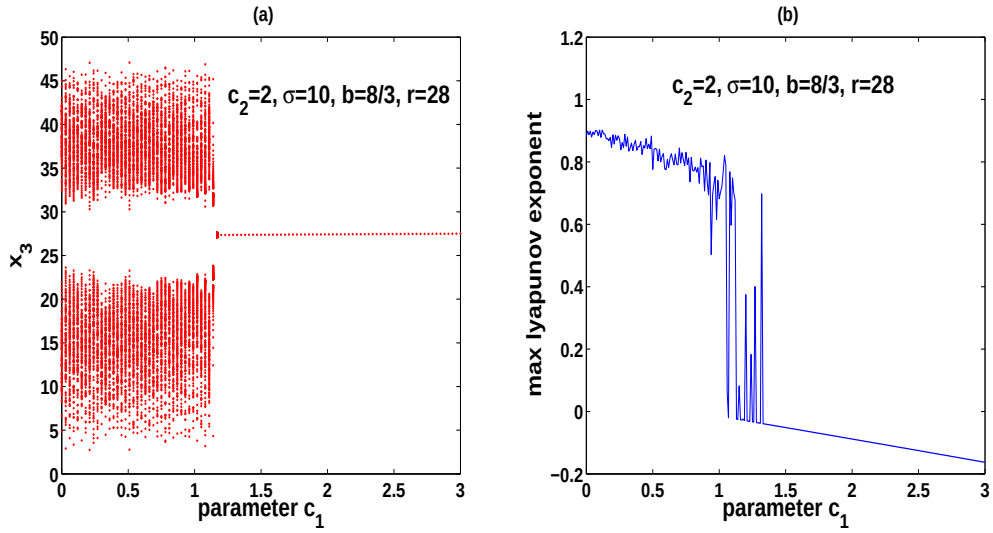

FIGURE 4. Figure depicts in(a)Bifurcation of x_3 with respect to c_1 and in (b) Maximu lyapunov exponent with respect to c_1 for fixed $c_2 = 2$ and $\sigma = 10, r = 28, b = 8/3$

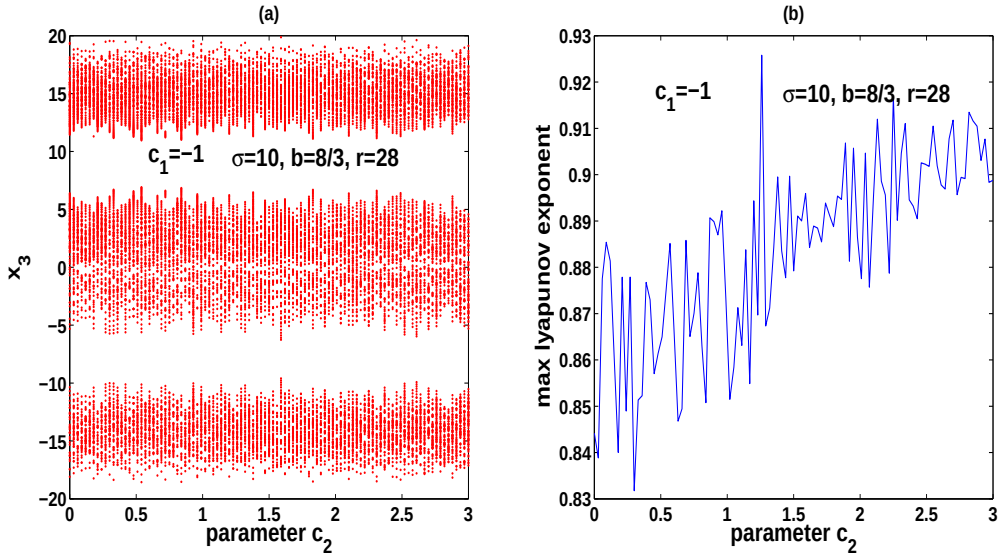

FIGURE 5. Figure depicts in(a)Bifurcation of x_3 with respect to c_2 and in (b) Maximu lyapunov exponent with respect to c_2 for fixed $c_1 = -1$ and $\sigma = 10, r = 28, b = 8/3$

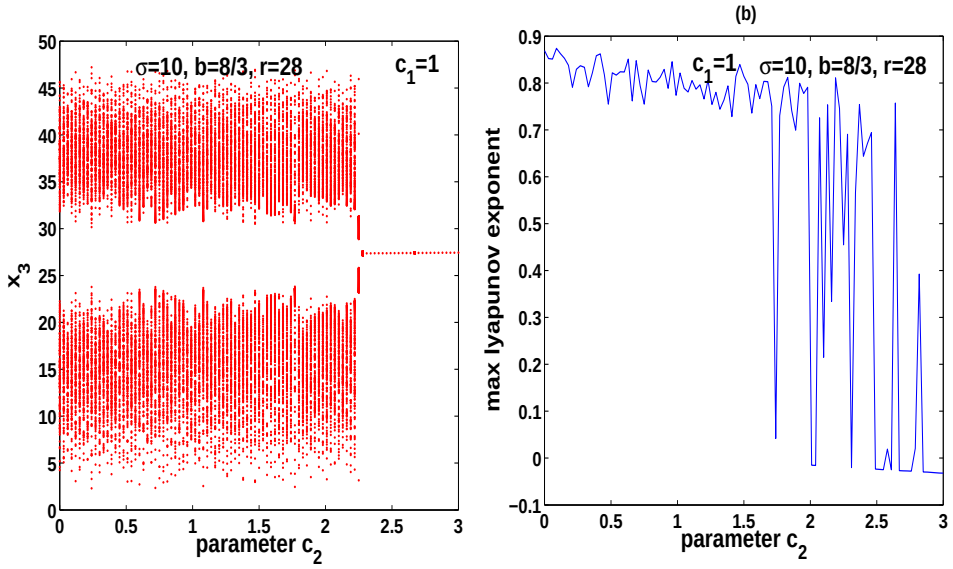

FIGURE 6. Figure depicts in(a)Bifurcation of x_3 with respect to c_2 and in (b) Maximu lyapunov exponent with respect to c_2 for fixed $c_1 = 1$ and $\sigma = 10, r = 28, b = 8/3$

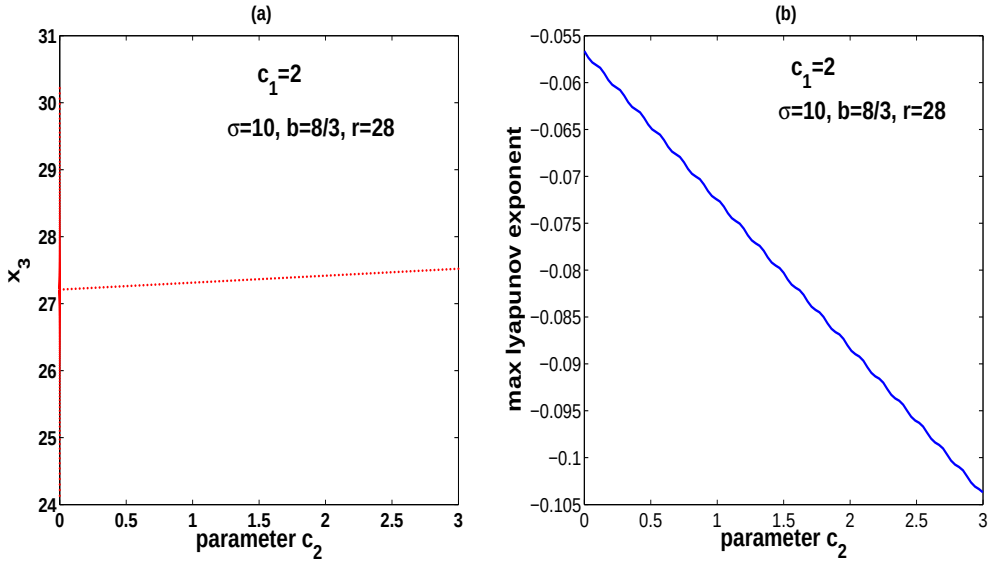

FIGURE 7. Figure depicts in(a)Bifurcation of x_3 with respect to c_2 and in (b) Maximu lyapunov exponent with respect to c_2 for fixed $c_1 = 2$ and $\sigma = 10, r = 28, b = 8/3$

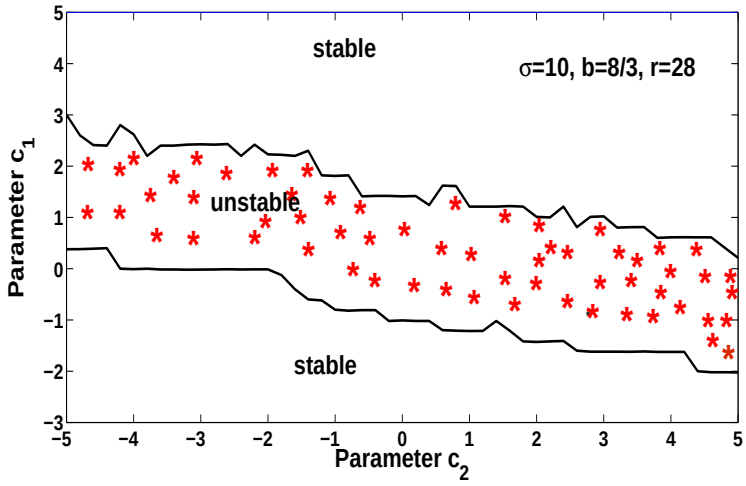

FIGURE 8. Dynamics of the system with respect to c_2 as a function of c_1. It divides the plane as the stable and unstable region for $\sigma = 10, r = 28, b = 8/3$.

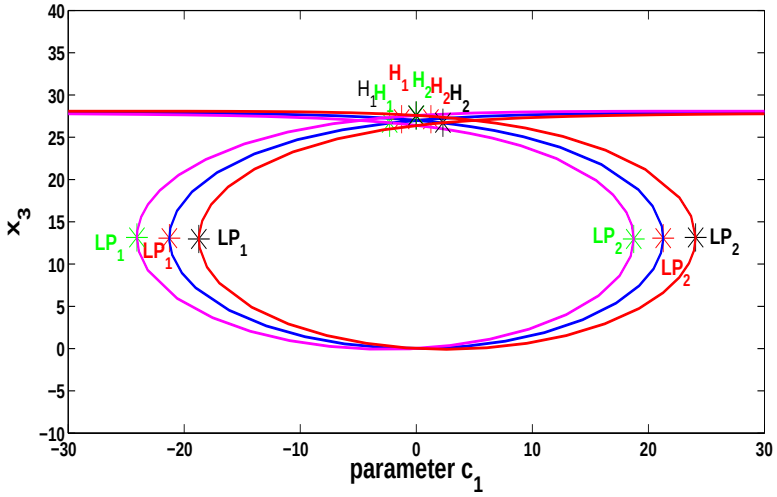

FIGURE 9. Continuation curves of equilibrium with the variation of the parameter c_1 for c_2= -5(red line), 0 (blue line), 5 (magenta line) of the system (11) for $\sigma = 10.0, r = 28, b = 8/3$: $H_1,\ H_2$-Hopf point, $LP_1,\ LP_2$-limit point.

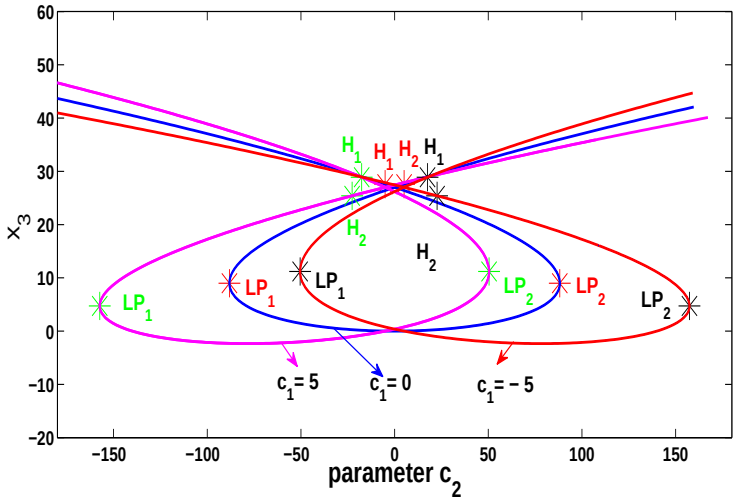

FIGURE 10. Continuation curves of equilibrium with the variation of the parameter c_2 for c_1 = -5(red line), 0 (blue line), 5 (magenta line) of the system (11) for $\sigma = 10.0, r = 28, b = 8/3$: $H_1,\ H_2$-Hopf point, $LP_1,\ LP_2$-limit point.

REFERENCES

[1] F.T. ARECCHI, R. MEUCC, G. PUCCIONI, J. TREDICCE: *Experimental evidence of subharmonic bifurcations, multistability and turbulence in Q-switched gas laser*, Phys. Rev. Lett., **49** (1982), 1217-1220.

[2] S.A. BEZNOSYUK, B.F. MINAEV, Z.M. MULDAKHMETOV: *Informative energetic structure and electronic multistability of condensed state*, Journal of Molecular Structure: THEOCHEM, **227** (1991), 125-129.

[3] M.S. PATEL, U. PATEL, A. SEN, G.C. SETHIA, C. HENS, S.K. DANA, R.E> AMRITKAR: *Experimental observation of extreme multistability in an electronic system of two coupled Rossler oscillators*, Physical Review E, **89**(2) (2014), 022918.

[4] E. ULLNER, A. ZAIKIN, E.I. VOLKOV, J. GARCIA-OJALVO: *Multistability and clustering in a population of synthetic genetic oscillators via phase-repulsive cell-to-cell communication*, Physical review letters, **99**(14) (2007), 148103.

[5] M.I. RABINOVICH, P. VARONA, A.I. SELVERSTON, H.D. ABARBANEL: *Dynamical principles in neuroscience*, Reviews of modern physics, **78**(4) (2006), 1213.

[6] R. CALOV, A. GANOPOLSKI: *Multistability and hysteresis in the climate cryosphere system under orbital forcing*, Geophysical research letters, **32**(21) (2003), L21717.

[7] H. SUN, S.K. SCOTT, K. SHOWALTER: *Uncertain destination dynamics*, Phys. Rev. E, **60** (1999), 3876-3880.

[8] L.M. PECORA, T.L. CARROL: *Synchronization in chaotic systems*, Phys. Rev. Lett., **64** (1990), 821-824.

[9] U. FEUDEL, C. GREBOGI: *Multistability and the control of complexity*, Chaos: An Interdisciplinary Journal of Nonlinear Science, **7**(4) (1997), 597-604.

[10] A.T. LAYTON, L.C. MOORE, H.E. LAYTON: *Multistability in tubuloglomerular feedback and spectral complexity in spontaneously hypertensive rats*, American Journal of Physiology-Renal Physiology, **291**(1) (2006), F79-F97.

[11] A. GELTRUDE, K. AL NAIMEE, S. EUZZOR, R. MEUCCI, F.T. ARECCHI, B.K. GOSWAMI: *Feedback control of bursting and multistability in chaotic systems*, Communications in Nonlinear Science and Numerical Simulation, **17**(7) (2012), 3031-3039.

[12] C. LI, W. HU, J.C. SPROTT, X. WANG: *Multistability in symmetric chaotic systems*, The European Physical Journal Special Topics, **224**(8) (2015), 1493-1506.

[13] C. HENS, S.K. DANA, U. FEUDEL: *Extreme multistability: Attractor manipulation and robustness*, Chaos: An Interdisciplinary Journal of Nonlinear Science, **25**(5) (2015), 053112.

[14] S. PAL, B. SAHOO, S. PORIA: *Multistable behaviour of coupled Lorenz-Stenflo systems*, Phys. Scr. **89** (2014), 045202.

[15] B.C. BAO, H. BAO, N. WANG, M. CHEN, Q. XU: *Hidden extreme multistability in memristive hyperchaotic system*, Chaos, Solitons and Fractals, **94** (2017), 102-111.

[16] M.A. KHAN, M. NAG, S. PORIA: *Design of multistable systems via partial synchronization*, Pramana, **89**(2) (2017), 19.

[17] E. LORENZ: *Deterministic non-periodic flow*, J. Atmospheric Science. **20** (1963), 130-141.

[18] P.L. SACHDEV, R. SARTHY: *Periodic and chaotic solutions for a non-linear system arising from a nuclear spin generator*, Chaos, solitons and Fractals. **4**(11) (1994), 2015-2041.

[19] H. SUN, S.K. SCOTT, K. SHOWALTER: *Uncertain destination dynamics*, Phys. Rev. E, **60** (1990), 3876-3880.

DEPARTMENT OF MATHEMATICS, RAJA N.L.KHAN WOMEN'S COLLEGE, MIDNAPORE, WEST BENGAL, INDIA.

Email address: jayantasarkar68@rediffmail.com

DEPARTMENT OF MATHEMATICS, RAMANANDA COLLEGE, BISHNUPUR, BANKURA, INDIA.

Email address: mdmaths@gmail.com

DEPARTMENT OF MATHEMATICS, SIDHO-KANHO-BIRSHA UNIVERSITY, PURULIA, WEST BENGAL, INDIA.

Email address: gourmahata@yahoo.co.in

View publication stats

Prasanta Das

ResearchGate

See discussions, stats, and author profiles for this publication at: https://www.researchgate.net/publication/362715662

A mathematical model for fluxes associated with internal gravity waves excited by a corner mountain

Article *in* MAUSAM · January 2022

DOI: 10.54302/mausam.v73i1.5091

CITATIONS
0

READS
18

3 authors:

Prasanta Das
Ramananda College, Bishnupur, Bankura, WB, India
9 PUBLICATIONS **16** CITATIONS
SEE PROFILE

Somenath Dutta
India Meteorological Department
44 PUBLICATIONS **151** CITATIONS
SEE PROFILE

Mausam IMD
India Meteorological Department
174 PUBLICATIONS **171** CITATIONS
SEE PROFILE

All content following this page was uploaded by Prasanta Das on 17 January 2022.

The user has requested enhancement of the downloaded file.

MAUSAM, **73**, 1 (January 2022), 181-188

551.34.01

A mathematical model for fluxes associated with internal gravity waves excited by a corner mountain

PRASANTA DAS and SOMENATH DUTTA*

Department of Mathematics, Ramananda College, Bishnupur, Bankura – 722 122, West Bengal, India

**India Meteorological Department (IMD), MoES, Pune – 411 005, India*

(*Received 1 June 2020, Accepted 20 September 2021*)

e mails : pdas.math1986@gmail.com

सार – इस मॉडल में एक बैरोक्लिनिक माध्य प्रवाह में कॉर्नर माउंटेन हिल्स (CMH) द्वारा उत्तेजित आंतरिक गुरुत्वाकर्षण तरंगों (IGW) से जुड़े ऊर्ध्वाधर ऊर्जा प्रवाह (E_z) और गति प्रवाह (τ_{zx} और τ_{zy}) के क्षैतिज घटकों को मानकीकृत करने का प्रयास किया गया है। भारत के उत्तर-पूर्वी क्षेत्र में, खासी-जयंतिया हिल्स (KJH) मोटे तौर पर पूर्व-पश्चिम उन्मुख हैं जबकि असम-बर्मा हिल्स (ABH) मोटे तौर पर उत्तर-दक्षिण उन्मुख हैं और वे लगभग समकोण पर मिलते हैं जिससे एक CMH बनता है। इस अध्ययन में, उछाल आवृत्ति (N) के यथार्थवादी ऊर्ध्वाधर भिन्नता और मूल प्रवाह के दो घटकों यू, वी पर विचार किया गया है। सर्दी के मौसम के दौरान दो चुनिंदा मामले हैं और बरसात के मौसम पर चर्चा की गई है। दो मामलों का अध्ययन किया गया है और सभी मामलों में विभिन्न स्तरों पर ऊर्जा प्रवाह और गति प्रवाह की गणना की गई है और पहले के जांचकर्ताओं द्वारा प्राप्त परिणामों के साथ तुलना की गई है।

ABSTRACT. In this model an attempt has been made to parameterize the vertical energy flux (E_z) and the horizontal components of momentum flux (τ_{zx} and τ_{zy}) associated with internal gravity waves (IGW) excited by the Corner Mountain Hills (CMH) in a baroclinic mean flow. In the north-eastern region of India, the Khasi-Jayantia Hills (KJH) is broadly east-west oriented whereas the Assam-Burma Hills (ABH) is broadly north-south oriented and they meet approximately at right angle forming a CMH. In this study, realistic vertical variation of the Buoyancy frequency (N) and two components U, V of the basic flow have been considered. There are two selective cases during winter season and rainy season have been discussed. Two cases have been studied and in all cases the energy flux and momentum fluxes at different levels have been computed and compared with the results obtained by earlier investigators.

Key words – Corner mountain hills, Energy flux, Momentum flux.

1. Introduction

It is a well-established fact that, when a stably stratified air-stream flows across an orographic barrier, gravity waves are excited to propagate upward direction under certain conditions of thermal stability and airflow stratification. Now, these gravity waves are known as internal gravity waves (IGW). These IGW can propagate vertically to a great distance carrying energy and momentum to higher levels in the atmosphere. Sometimes, they are associated with the formation of clear air turbulence (CAT). The information about standing waves, which under favourable meteorological conditions form on the lee side of the mountain barrier, is very important for the safety of aviation. Many aircraft accidents reported in mountainous areas are often attributed to the vertical velocities of large magnitude associated with the lee waves. Hence the studies on lee waves associated with air flow across an orographic barrier have an important bearing on the safety of aviation.

Sawyer (1959) first pointed out the relative importance of this momentum loss in the mean flow due to continuous extraction of momentum by the orographic gravity waves. He considered a 2-D bell-shaped obstacle with half with (a = 2 km) and height (b = 300 m) and determined the typical value of wave momentum flux of the order 1-10 dynes/cm^2. Eliassen and Palm (1961) showed that in case of 2-D linear gravity waves, the vertical flux of horizontal momentum due to gravity waves is independent of height when the waves are steady and non-dissipative. Blumen (1965) showed that the magnitude of the waves drag is sensible to the vertical wavelength. He also noted that the maximum value of the drag is attained when the vertical wavelength is twice the maximum height of the momentum. Bertherton (1969) reviewed the theories concerning the propagation of internal gravity waves (IGW) in a horizontal uniform shear flow. His computations showed that for a 19 m/s gradient wind over hilly terrain in north Welsh, the wave drag amounted to 4 dyne/cm^2 of which 3 dyne/cm^2

probably acted on the atmosphere above 20 km. Lilly (1972) reported that a conclusive evidence of the importance of the wave drag obtained from the data collected over the Front Range of the Colorado Rockies by instrumented aircraft during field experiments.

Smith (1978) computed the pressure drag on the Blue-ridge Mountain in the Central Appalachains. During the first two weeks of January 1974, he observed several periods with significant wave drag with pressure differences typically of the order of 50 N/m^2 across the ridge. Blumen and Dietze (1981) considered a 3-D linear hydrostatic model of stationary mountain wave in a stably stratified air-stream. They took both the incoming basic flow buoyancy frequency to be independent of height, but lateral variation of incoming flow was incorporated by assuming a hyperbolic secant profile (U = *sechy*). Somieski (1981) considered a 3-D circular mountain for the stratified hydrostatic flow. He derived a second order wave equation from the primitive equation including constant rotation and vertical shear of the mean flow. He solved the equation numerically and showed that in case of non-shear and constant static stability, the nodal lines are parabolic for circular mountain of diameter 50 km. Palmer *et al*. (1986) addressed the general westerly bias of the global general circulation models (GCM). They showed that one way to reduce this general westerly bias is to incorporate the gravity wave drag parameterization scheme in the GCM. Gravity waves drag parameterization scheme proposed by Palmer *et al*. (1986) and McFarlane (1987) reduced the westerly bias mainly in stratosphere. Iwasaki *et al*. (1989) addressed a new type of gravity wave drag parameterization scheme to improve the tropospheric westerly bias by including the effects of these tropospheric-trapped lee waves.

Dutta (2001) studied the momentum and energy fluxes associated mountain wave across Mumbai-Pune section of the Western Ghats in an idealized air-stream. He showed that the momentum and energy flux both were independent of height and half width of the bell-shaped part of the barrier. Dutta and Naresh Kumar (2005) considered a 2-D mathematical model for an idealistic air-stream across the Assam-Burma Hills (ABH). They showed that fluxes were independent of height and also dependent the length of valley of ABH. Dutta (2007) addressed a linear dynamical model for air flow across the Western Ghats and Khasi-Jayantia Hills in a realistic air-stream. He also showed that the variation of momentum and energy flux both were not uniform with height. Das *et al.* (2016) developed a 3-D mathematical model for parameterization of momentum and energy flux for an realistic air flow across the Assam-Burma Hills (ABH). They showed that both momentum and energy fluxes vary in the vertical.

Das *et al.* (2017) used a mathematical model for the 3-D dynamics of lee wave across a meso-scale mountain corner. They studied the relation between the possible transverse and divergent lee wave numbers (k, l) and also discussed and mapped the updraft/downdraft regions associated with lee waves at different heights.

In some of the above studies, wind and stability were assumed to be either invariant with height or assumed to have some analytical behaviour with height. Solutions for such studies were essentially obtained by analytical method. In other studies, realistic vertical variation of wind and stability were considered and the solution obtained using quasi numerical or numerical method. In all the studies the barrier (2-D) or the major ridge axis (3-D) of the barrier has been assumed to be extended broadly either in the East-West (EW) direction or in North-South (NS) direction.

In India in the northeast region, the Khasi-Jayantia Hills (KJH) is broadly East-West oriented whereas the Assam-Burma Hills (ABH) is broadly North-South oriented and they meet at almost right angle forming a mountain corner to the northeast. It is believed that weather and climate in that region are neither controlled by KJH alone nor it is controlled by ABH alone, rather they may be controlled by their combined effect. To address the problem of this combined effect, one has to investigate the effect of the above mountain corner on airflow and rainfall in that region.

The objective of the present study is to propose a 3-D dynamical model for parameterizing energy flux and momentum flux associated with IGW across Corner Mountain Hills, which has not been addressed so far.

2. Data

Guwahati (26.19° N Latitude and 91.73° E Longitude) is the only Radio-Sonde station to the upstream of ABH. Accordingly, for the present study we have used the average of 0000 UTC and 1200 UTC RS/RW data of Guwahati for 8th January, 1967 and 18th July, 2004, have been obtained from Archive of India Meteorological Department (IMD), Pune, India.

3. Methodology

The mathematical model has been used in this study for lee wave across a meso-scale mountain corner. The proposed model considers a steady state, adiabatic, inviscid, non-rotating and Boussines q mean flow across a meso-scale mountain corner. The realistic vertical variation of mean flow has been considered here. The basic flow consists of two components U and V along x

and *y* axis respectively. Under these assumptions the linearized governing equations are simplified to:

$$U\frac{\partial u'}{\partial x}+V\frac{\partial u'}{\partial y}+w'\frac{dU}{dz}=-\frac{1}{\rho_0}\frac{\partial p'}{\partial x} \tag{1}$$

$$U\frac{\partial v'}{\partial x}+V\frac{\partial v'}{\partial y}+w'\frac{dU}{dz}=-\frac{1}{\rho_0}\frac{\partial p'}{\partial y} \tag{2}$$

$$U\frac{\partial w'}{\partial x}+V\frac{\partial w'}{\partial y}=-\frac{1}{\rho_0}\frac{\partial p'}{\partial z}+g\frac{\theta'}{\theta_0} \tag{3}$$

$$\frac{\partial u'}{\partial x}+\frac{\partial v'}{\partial y}+\frac{\partial w'}{\partial z}=0 \tag{4}$$

$$U\frac{\partial \theta'}{\partial x}+V\frac{\partial \theta'}{\partial y}+w'\frac{d\theta_0}{dz}=0 \tag{5}$$

where, U, V, ρ_0, θ_0 are respectively zonal component, meridional component, density and potential temperature of basic flow and u', v', w', p', θ' are respectively the perturbation part of zonal wind, meridional wind, vertical wind, pressure, density and potential temperature. Since the perturbation quantities, u', v', w', p', θ' etc are all continuous functions of x, y, z hence their horizontal variation may be represented by a double Fourier integral, such as,

$$u'(x,y,z)=\frac{1}{4\pi^2}\int_{-\infty}^{\infty}\int_{-\infty}^{\infty}\hat{u}(k,l,z)e^{i(kx+ly)}dkdl$$

where, $\hat{u}(k,l,z)=\int_{-\infty}^{\infty}\int_{-\infty}^{\infty}u'(x,y,z)e^{-i(kx+ly)}dxdy$ is the double Fourier transform of u' (x, y, z). Performing double Fourier transform from (1) to (5) we get

$$i(kU+lV)\hat{u}+\hat{w}\frac{dU}{dz}=-ik\frac{\hat{p}}{\rho_0} \tag{6}$$

$$i(kU+lV)\hat{v}+\hat{w}\frac{dV}{dz}=-il\frac{\hat{p}}{\rho_0} \tag{7}$$

$$i(kU+lV)\hat{w}=-\frac{1}{\rho_0}\frac{\partial \hat{p}}{\partial z}+g\frac{\hat{\theta}}{\theta_0} \tag{8}$$

$$ik\hat{u}+il\hat{v}+\frac{\partial \hat{w}}{\partial z}=0 \tag{9}$$

$$i(kU+lV)\hat{\theta}+\hat{w}\frac{d\theta_0}{dz}=0 \tag{10}$$

where, $\hat{u},\hat{v},\hat{w},\hat{p},\hat{\theta}$ are double Fourier transformation of u',v',w',p',θ.

Eliminating $\hat{u},\hat{v},\hat{p},\hat{\theta}$ from the equations (6) to (10) we get

$$\frac{\partial^2\hat{w}}{\partial z^2}+\frac{1}{\rho_0}\frac{d\rho_0}{dz}\frac{\partial\hat{w}}{\partial z}+\left\{\frac{N^2(k^2+l^2)}{(kU+lV)^2}-\left(\frac{k\frac{dU}{dz}+l\frac{dV}{dz}}{kU+lV}\right)\frac{1}{\rho_0}\frac{d\rho_0}{dz}-\left(\frac{k\frac{d^2U}{dz^2}+l\frac{d^2V}{dz^2}}{kU+lV}\right)-(k^2+l^2)\right\}\hat{w}=0 \tag{11}$$

where, $N=\sqrt{\frac{g}{\theta_0}\frac{d\theta_0}{dz}}$ is the Brunt-Vaisala frequency.

Now putting $\hat{w}(k,l,z)=\sqrt{\frac{\rho_0(0)}{\rho_0(z)}}\hat{w}_1(k,l,z)$ in equation (11), we get vertical structure equation

$$\frac{\partial^2\hat{w}_1}{\partial z^2}+\left[f(k,l,z)-K^2\right]\hat{w}_1=0 \tag{12}$$

where,

$$f(k,l,z)=\frac{N^2(k^2+l^2)}{(kU+lV)^2}-\left[\frac{k\frac{dU}{dz}+l\frac{dV}{dz}}{kU+lV}\right]\frac{1}{\rho_0}\frac{d\rho_0}{dz}-\left[\frac{k\frac{d^2U}{dz^2}+l\frac{d^2V}{dz^2}}{kU+lV}\right]+\frac{1}{4\rho_0^2}\left(\frac{d\rho_0}{dz}\right)^2-\frac{1}{2\rho_0}\frac{d^2\rho_0}{dz^2}$$

and $K^2=k^2+l^2$

It is very complicated to solve the equation (12) analytically. So, the equation (12) is solved quasi-numerically for the given wave number vectors (k, l) of all vertical levels. The direction of the zonal wind changes

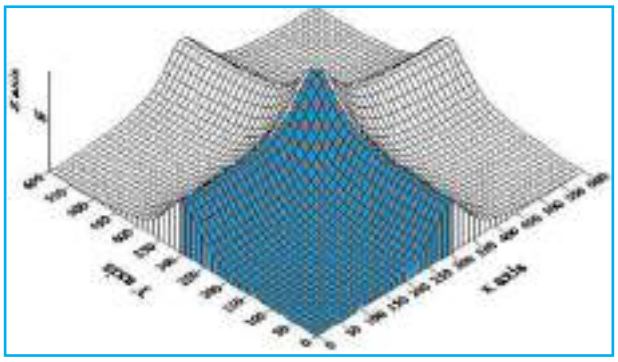

Fig. 1. The profile of Corner Mountain Hills

from north to south during winter season at all levels (De, 1973). The solution of (12) is strictly indeterminate unless the values of *f*(*k*, *l*, *z*) is specified at great height. Therefore it is assumed that above the upper boundary *f*(*k*, *l*, *z*) is constant. For simplicity, it is also assumed that above the upper boundary *f*(*k*, *l*, *z*) = 0, which is similar to Sarker (1967), Dutta (2005, 2007), Das *et al*. (2016) etc.

Therefore the approximate solution of the equation (12) in the region *f*(*k*, *l*, *z*) = 0 is of the form

$$\hat{w}_1(k,l,z) = Ce^{-Kz} \tag{13}$$

where, 'C' is an arbitrary constant. Since the pressure and vertical velocity are continuous function of *z*. So, $\hat{w}_1, \frac{\partial^2 \hat{w}_1}{\partial z^2}$ are also continuous function of *z* in the region *f*(*k*, *l*, *z*) = 0. Hence

$$\frac{\partial \hat{w}_1}{\partial z} = -K\hat{w}_1 \tag{14}$$

here, the equations (13) and (14) are the upper boundary condition of the equation (12). Now at the surface the airflow follows the contour of the corner mountain, the profile is given by :

$$h(x,y) = \frac{H}{2}\left[\frac{a^2}{a^2+(x-x_0)^2} + \frac{b^2}{b^2+(y-y_0)^2}\right] \tag{15}$$

Profile of (15) is given by Fig. 1**.** The chess colour of this figure is the corner mountain, which we are interested to study. Now the double Fourier transform of (15) is given by :

$$\hat{h}(k,l) = -\frac{iH}{2}\left[\frac{a}{l}e^{-ak-ikx_0} + \frac{b}{k}e^{-bk-ily_0}\right] \tag{16}$$

Now the linearized lower boundary condition (at *z* = 0) for w_1' is given by

$$w'_1(x,y,0) = w'(x,y,0) = U(0)\frac{\partial h(x,y,0)}{\partial x} + V(0)\frac{\partial h(x,y,0)}{\partial y}$$

Therefore,

$$\hat{w}_1(k,l,z) = i[kU(0)+lV(0)]\hat{h}(k,l) \tag{17}$$

Using the above boundary conditions and following Das *et al.* (2016) the equation (12) has been solved quasi-numerically. Therefore the solution for $\hat{w}_1(k,l,z)$ is given by :

$$\hat{w}_1(k,l,z) = i[kU(0)+lV(0)]\hat{h}(k,l)\frac{\Psi(k,l,z)}{\Psi(k,l,0)} \tag{18}$$

Hence,

$$\hat{w}(k,l,z) = \sqrt{\frac{\rho_0(0)}{\rho_0(z)}}i\left[kU(0)+lV(0)\right]\hat{h}(k,l)\frac{\Psi(k,l,z)}{\Psi(k,l,0)} \tag{19}$$

where, $\Psi(k,l,z)$ is an arbitrary function, which satisfying equations (12), (13) and (14) and its value at above the upper boundary is 1. Following Das *et al.* (2016) $\Psi(k,l,z)$ has been computed numerically at different vertical levels and different vertical grid points, at intervals of *d* = 0.25 km, for a given wave number vector (*k*, *l*). Now we obtain $\hat{p}, \hat{u}$ and $\hat{v}$ from equations (6), (7), (8) and (10) by following Das *et al*. (2016).

$$\hat{p}(k,l,z) = \frac{i\left[\left(k\frac{dU}{dz}+l\frac{dV}{dz}\right)\hat{w}(k,l,z) - (kU+lV)\frac{\partial \hat{w}}{\partial z}\right]\rho_0(z)}{K^2} \tag{20}$$

$$\hat{u}(k,l,z) = \frac{i\left[\hat{w}(k,l,z)\frac{dU}{dz} + \frac{k}{K^2}\left\{\left(k\frac{dU}{dz}+l\frac{dV}{dz}\right)\hat{w}(k,l,z) - (kU+lV)\frac{\partial \hat{w}}{\partial z}\right\}\right]}{(kU+lV)} \tag{21}$$

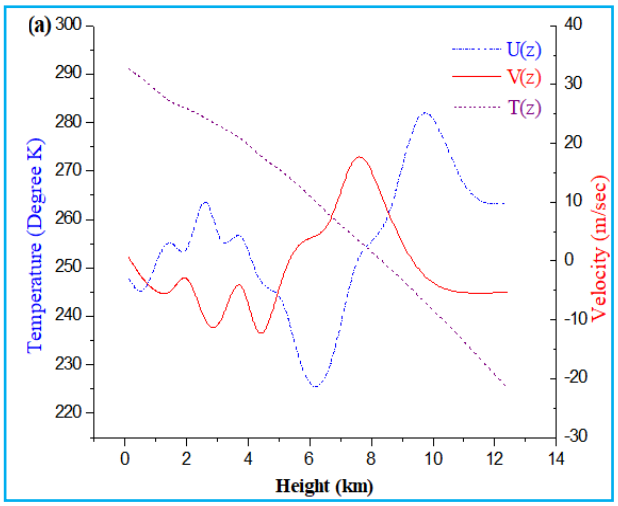

Figs. 2(a&b). (a) Vertical profile of $U(z)$, $V(z)$, $T(z)$ and (b) Vertical profile of energy flux, on 8th January, 1967

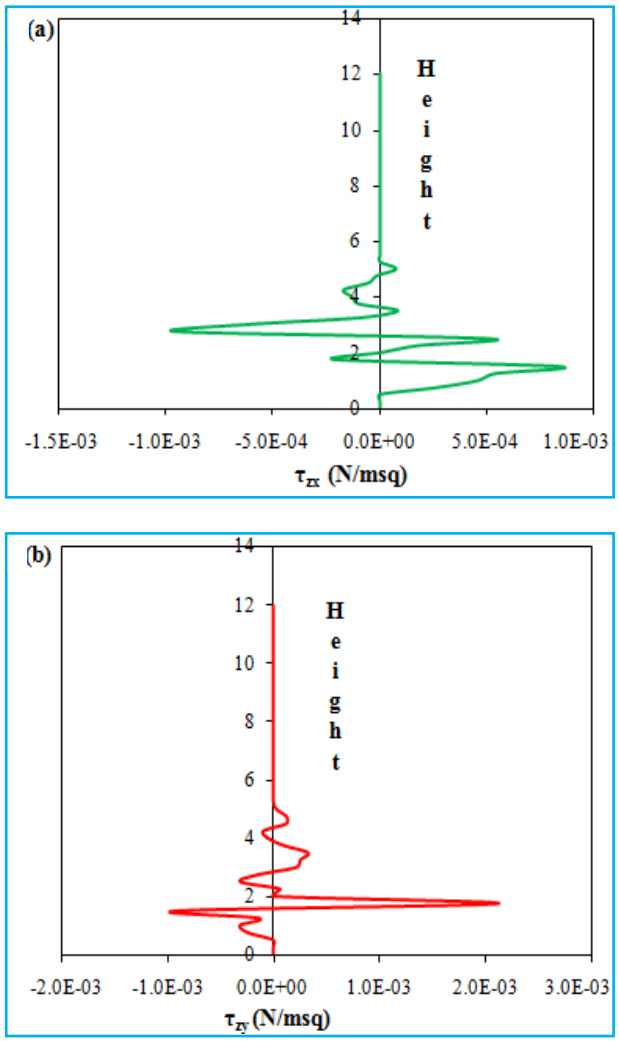

Figs. 3(a&b). (a) Vertical profile of momentum flux (τ_{zx}) along x-axis and (b) Vertical profile of momentum flux (τ_{zy}) along y-axis on 8th January, 1967

$$\hat{v}(k,l,z)=\frac{i\left[\hat{w}(k,l,z)\frac{dV}{dz}+\frac{k}{K^2}\left\{\left(k\frac{dU}{dz}+l\frac{dV}{dz}\right)\hat{w}(k,l,z)-(kU+lV)\frac{\partial\hat{w}}{\partial z}\right\}\right]}{(kU+lV)} \tag{22}$$

Using Eqn. (19), $\hat{w}$ can be found out at each level for a given wave number vector (k, l) and also using Eqn. (19) and vertical profile of basic state wind and temperature field, $\hat{p},\hat{u},\hat{v}$ can be found out. By performing inverse double Fourier transformation on equations (19)-(22) numerically, we obtain w', p', u', v' at each horizontal grid point (5 km apart) at each vertical level. Following Das *et al.* (2016), then the two horizontal components of the momentum flux vector, *viz.*, $\tau_{zx}=\overline{\overline{\hat{u}\hat{w}}}$, $\tau_{zy}=\overline{\overline{\hat{v}\hat{w}}}$ and energy flux $E_z=\overline{\overline{\hat{p}\hat{w}}}$ at any vertical level and any horizontal grid point have been computed, where $\overline{\overline{()}}$ indicates the average surface area 'S' of the orographic barrier, where $S=\frac{H}{2}\left[y_0\tan^{-1}\left(\frac{x_0}{a}\right)+x_0\tan^{-1}\left(\frac{y_0}{b}\right)\right]$.

4. Results and discussion

Using the equations (19)-(22) we have computed the energy flux and the components of horizontal flux for two selected cases when air stream characteristics where favourable for occurrence of the mountain wave.

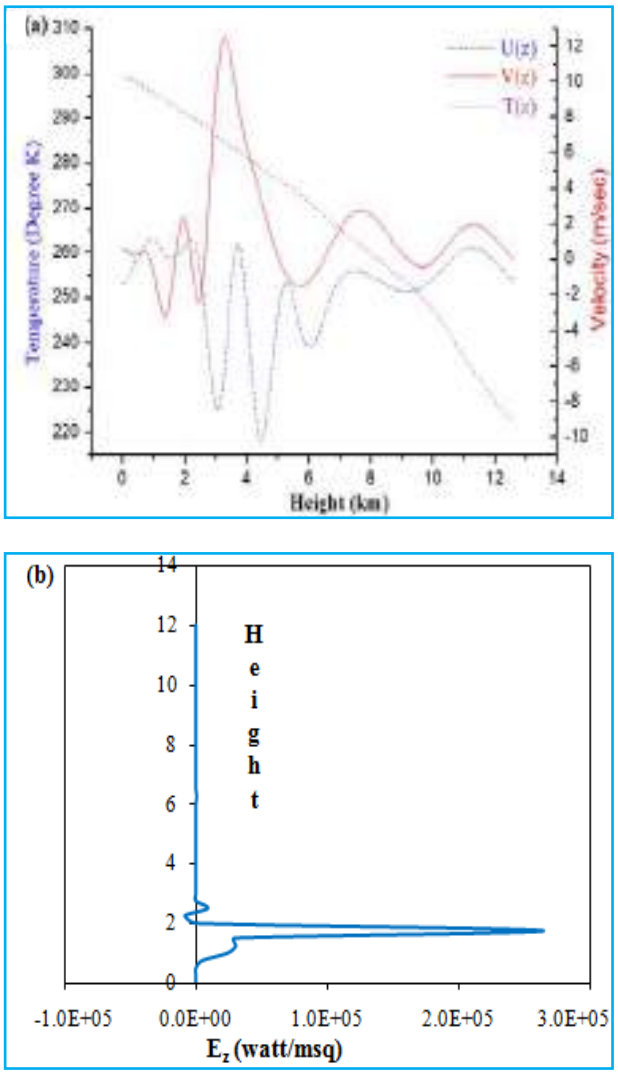

Figs. 4(a&b). (a) Vertical profile of $U(z)$, $V(z)$, $T(z)$ and (b) Vertical profile of energy flux (E_z), on 18th July, 2004

Computations are made allowing realistic vertical variation of wind and static stability.

Case 1 : *8th January, 1967 (Winter season)*

The vertical profiles of two components of basic flow $U(z)$, $V(z)$ and temperature $T(z)$ in the undisturbed flow shown in Fig. 2(a), which are based on the average of 0000 UTC and 1200 UTC RS/RW data of Guwahati for that date during winter season. This figure shows that the profile of temperature $T(z)$ is constant lapse rate with vertical. Using this profile the vertical energy flux (E_z) and two horizontal components of momentum flux τ_{zx} along x-axis and τ_{zy} along y-axis are computed at different levels.

The energy flux (E_z) is shown in Fig. 2(b). The figure shows that energy flux is invariant in the vertical above z = 3 km. It is seen that at the lower levels up to z = 1.2 km E_z is invariant and in the layer from z = 1.2 km to z = 2 km E_z is vertically upward and in the layer from z = 2 km to z = 3 km E_z is vertically alternatively downward and upward. Hence Fig. 2(b) also shows that the divergence/convergence of E_z in the layer up to z = 3 km.

The vertical profile of momentum flux (τ_{zx}) along x-axis is shown in Fig. 3(a). It is seen that the momentum flux τ_{zx} is invariant in the vertical above z = 5.3 km. It is seen that at the layer from z = 0.4 km to z = 1.7 km and from z = 2.1 km to z = 2.6 km the flux τ_{zx} is vertically upward. In the layer from z = 2.6 km to z = 3.4 km τ_{zx} is vertically downward.

The vertical profile of momentum flux (τ_{zy}) along y-axis is shown in Fig. 3(b). From this figure, it is seen that, the momentum flux (τ_{zy}) is invariant in the vertical above z = 5 km. It is also seen that at the layer from z = 1.7 km to z = 2 km τ_{zx} is vertically upward and in the layer from z = 0.5 km to z = 1.7 km the momentum flux (τ_{zy}) is vertically downward.

Case 2 : *18th July, 2004 (Rainy season)*

The vertical profiles of $U(z)$, $V(z)$ and $T(z)$ in the undisturbed flow are shown in Fig. 4 (a), which are based on the average of 0000 UTC and 1200 UTC RS/RW data of Guwahati of 18th July, 2004 during rainy season. The figure shows that the profile of temperature $T(z)$ is constant moist adiabatic lapse rate with vertical and hence following Sarker (1967) and De (1971), $T(z)$ is approximated by the pseudo-adiabatic line through the surface dry bulb temperature. Using this profile, the vertical energy flux (E_z) and the two horizontal components of the momentum flux τ_{zx} and τ_{zy} at different levels have been computed.

The vertical profile of the energy flux (E_z) has been shown in Fig. 4(b). It is seen that the energy flux (E_z) is invariant in vertical above z = 2.6 km. It is also shown that from z = 0.5 km to z = 2 km the energy flux (E_z) is upward.

The vertical profile of momentum flux (τ_{zx}) along x-axis has been shown in Fig. 5(a). It is seen that τ_{zx} is vertically upward in the layer from z = 1.7 km to z = 2.8 km and it is also invariant in vertical above z = 2.8 km.

The momentum flux (τ_{zy}) along y-axis is invariant with vertical above z = 2.8 km, which is shown in

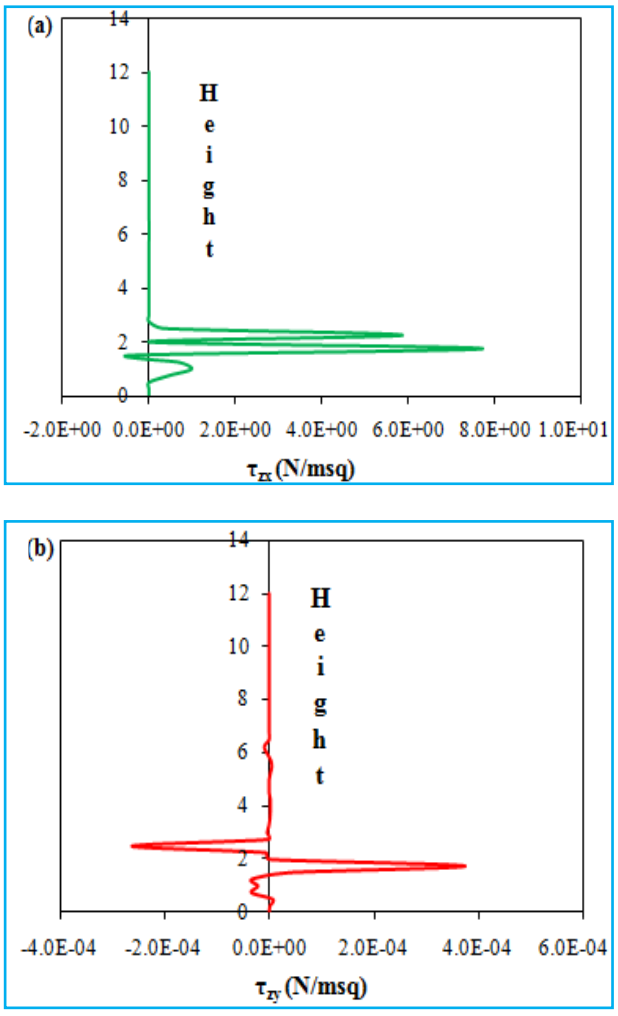

Figs. 5(a&b). (a) Vertical profile of momentum flux (τ_{zx}) along x axis and (b) Vertical profile of momentum flux (τ_{zy}) along y axis on 18th July, 2004

Fig. 5(b). The Fig. 5(b) also shows that τ_{zy} is vertically upward in the layer from z = 1.6 km to z = 2 km and vertically downward in the layer from z = 2 km to z = 2.8 km. Dutta (2001) considered the profile of Mumbai-Pune section of Western-Ghats (WG) and there was only one ridge and a plateau. He showed that the plateau portion does not contribute to the fluxes of energy or momentum. In the present study, corner of the CMH has contributed to the fluxes of energy and momentum.

5. Conclusions

In this investigation, we have presented the wave momentum flux and energy flux for 3-D meso-scale lee wave across the CMH following a quasi-numerical approach. In the sequel, we have made some interesting observation. Moreover,

(*i*) From the study of above two cases, it is found that the fluxes vary in the vertical but the vertical variation is not uniform with height. In the some layers, fluxes are upward and somewhere fluxes are downward.

(*ii*) In the both cases, the effects of corner of the CMH have been observed. This makes the energy flux (E_z) or momentum fluxes (τ_{zx}, τ_{zy}) divergent / convergent in the vertical.

(*iii*) The above model may be used for any 3-D mountain profile to compute the energy flux (E_z) and two horizontal components of the momentum fluxes (τ_{zx} and τ_{zy}) at different levels.

(*iv*) Information revealed from this study about vertically upward fluxes of energy and momentum at lower levels appears to be important for aircraft operation.

Acknowledgements

Authors are grateful to Dr. U. S. De, Former Addl. Director General of Meteorology of India Meteorological department and Prof. M. Maiti, Retd. professor, Deptt. of Applied Mathematics, Vidyasagar University, Midnapore, West Bengal for their kind valuable suggestions and guidance. Second author is thankful to all personnel at Meteorological Training Institute, IMD, Pune for their valuable supports.

Disclaimer : The contents and views expressed in this study are the views of the authors and do not necessarily reflect the views of the organizations they belong to.

References

Bluemen, W. and Dietze, S. C., 1981, "An analysis of three-dimensional mountain lee waves in a stratified shear flow", *J. Atmos. Sci.*, **38**, 1949-1963.

Blumen, W., 1965, "Momentum flux by mountain waves in a stratified rotating atmosphere", *Journal of the Atmospheric Sciences*, **22**, 5, 529-534.

Bretherton, F. P., 1969, "Momentum transport by gravity waves", *Quart. J. Roy. Meteor. Soc.*, **95**, 213-243.

Das, P., Dutta, S. and Mondal, S. K., 2017, "A mathematical model for the 3-D dynamics of lee wave across a meso-scale mountain corner", *MAUSAM*, **68**, 2, 195-204.

Das, P., Dutta, S., Mondal, S. K. and Khan, A., 2016, "Momentum flux and energy flux associated with internal gravity waves excited by the Assam-Burma hills in India", *Modeling Earth Systems and Environment*, **2**, 2, 1-9.

De, U. S. (1973). Some studies of mountain waves (Doctoral dissertation, Ph. D. Thesis, Banaras Hindu University, Varnasi (India).

Dutta, S. and Kumar, N., 2005, "Parameterization of momentum and energy flux associated with mountain wave across the Assam-Burma hills", *MAUSAM*, **56**, 3, 527.

Dutta, S., 2001, "Momentum flux, energy flux and pressure drag associated with mountain wave across western ghat", *MAUSAM*, **52**, 2, 325-332.

Dutta, S., 2005, "Effect of static stability on the pattern of 3-D baroclinic lee wave across a meso-scale elliptical barrier", *Meteorol. Atmos. Phys.*, **90**, 139-152.

Dutta, S., 2007, "Parameterization of momentum flux and energy flux associated with orographically excited internal gravity waves in a baroclinic background flow", *MAUSAM*, **58**, 4, 459-470.

Eliassen, A. and Palm, E., 1961, "On the transfer of energy in stationary mountain waves", *Geophys. Publ.*, **22**, 3, 1-23.

Iwasaki, T., Yamada, S. and Tada, K., 1989, "A parameterization scheme of orographic gravity wave drag with two different vertical partitioning", *Journal of the Meteorological Society of Japan, Ser. II*, **67**, 1, 11-27.

Lilly, D. K., 1972, "Wave momentum flux-A GARP problem", *Bull. Amer. Met. Soc*., **53**, 17-23.

McFarlane, N. A., 1987, "The effect of orographically excited gravity wave drag on the general circulation of the lower stratosphere and troposphere", *Journal of the atmospheric sciences*, **44**, 14, 1775-1800.

Palmer, T. N., Shutts, G. J. and Swinbank, R., 1986, "Alleviation of a systematic westerly bias in general circulation and numerical weather prediction models through an orographic gravity wave drag parametrization", *Quarterly Journal of the Royal Meteorological Society*, **112**, 474, 1001-1039.

Sarker, R. P., 1967, "Some modifications in a Dynamical model of orographic rainfall", *Mon. Wea. Rev*., **95**, 673-684.

Sawyer, J. S., 1959, "The introduction of the effects of topography into methods of numerical forecasting", *Quarterly Journal of the Royal Meteorological Society*, **85**, 363, 31-43.

Smith, R. B., 1978, "A measurement of mountain drag", *J. Atmos. Sci*., **35**, 1644-1654.

Somieski, F., 1981, "Linear theory of three-dimensional flow over mesoscale mountains", *Beitr. Phys. Atmosph*., **54**, 3, 315-334.

View publication stats

Prasanta Das

MAUSAM, **74**, 1 (January, 2023), 1-10

MAUSAM

DOI : https://doi.org/10.54302/mausam.v74i1.3220
Homepage: https://mausamjournal.imd.gov.in/index.php/MAUSAM

UDC No. 551.509.333 : 551.511.3 (541)

Numerical Solution for 3-D lee wave associated with barotropic mean flow across the Assam-Burma hills

PRASANTA DAS

Department of Mathematics, Ramananda College, Bishnupur, West Bengal – 722 122, India

(*Received 7 October 2021, Accepted 28 September 2022*)

e mail : pdas.math1986@gmail.com

सार – भारत में, उत्तर-पूर्व क्षेत्र में, असम-बर्मा हिल्स (ABH) को दो त्रि-आयामी अण्डाकार बाधाओं द्वारा संश्लेषित किया गया है, वे कुछ परिमित दूरी की घाटी द्वारा अलग किए गए हैं। इस पेपर में एबीएच में मेसो-स्केल ड्राई मीन फ्लो से जुड़े 3-डी ली वेव न्यूमेरिकल सॉल्यूशन को प्राप्त करने का प्रयास किया गया है। जहां प्रवाह एक एडियाबेटिक, इनविसिड, लामिनार, स्थिर, बूसिनस्क, गैर-घूर्णी है और मूल प्रवाह में जोनल घटक (यू) और मेरिडियनल घटक (वी) होते हैं, वे अंडाकार के प्रमुख धुरी के सामान्य और समानांतर होते हैं बाधा क्रमशः। सादगी के लिए, मूल प्रवाह के दो घटकों (यू, वी) और उत्प्लावकता आवृत्ति (एन) को ऊंचाई के साथ एक समान माना जाता है और गवर्निंग समीकरणों के लिए गड़बड़ी तकनीक भी लागू की गई है। पर्टर्बेशन वर्टिकल वेलोसिटी (w') और स्ट्रीम लाइन विस्थापन (η') को डबल इंटीग्रल के रूप में व्यक्त किया जाता है, जिसका मूल्यांकन संख्यात्मक विस्तार के रूप में अनुमानित किया गया है। अंत में, गणना किए गए परिणामों की तुलना पहले के जांचकर्ताओं द्वारा प्राप्त किए गए स्पर्शोन्मुख परिणामों से की गई है।

ABSTRACT. In India, in the North-East region, the Assam-Burma Hills (ABH) has been synthesized by two three-dimensional elliptical barriers, they are separated by a valley of some finite distance. In this paper, an attempt has been made to obtain a 3-D lee wave numerical solution associated with a meso-scale dry mean flow across the ABH. Where the flow is an adiabatic, inviscid, laminar, steady, Boussinesq, non-rotational and the basic flow consists of the zonal component (U) and the meridional component (V), they are normal and parallel to the major axis of the elliptical barrier respectively. For simplicity, the two components (U, V) of the basic flow and Buoyancy frequency (N) are assumed to be uniform with height and also the perturbation technique has been applied to the governing equations. The perturbation vertical velocity (w') and stream line displacement (η') are expressed as a double integral, which have been evaluated to approximate as the numerical expansion. Finally, the computed results have compared with the asymptotic results obtained by earlier investigators.

Key words – ABH, Perturbation vertical velocity (w'), Streamline displacement (η').

1. Introduction

Orography is the study of the formation and relief of mountains and can more broadly include hills and any part of a region's elevated terrain. The climate and weather of a place are strongly influenced by the orography. In the past, many aircraft accidents reported in mountainous areas are often attributed to the vertical velocities of large magnitude associated with the lee waves. Hence, the studies on the lee waves are associated with air flow across an orographic barrier, have an important bearing to the safety of aviation.

Theoretical studies on this field can widely be divided by two categories. In one category, the mountain barrier has been assumed the two-dimensional. The two-dimensional mountain wave problem was first addressed by Lyra (1943) and subsequently by Queney (1947); Scorer (1949); Sawyer (1960); Sarker (1965, 1966); De (1973); Sinha Ray (1988); Kumar *et al*. (1998) etc. In another category of theoretical studies on the three-dimensional mountain wave problem was first addressed by Scorer and Wilkinson (1956) and subsequently by Wurtele (1957); Crapper (1959); Sawyer (1962); Das (1964); Smith (1979); Dutta *et al*. (2002); Dutta (2005, 2007); Das *et al*. (2013, 2016) etc.

In India, studies on the effects of an orographic barrier on airflow have been addressed by Das (1964); Sarker (1965, 1966); Sarker *et al.* (1978); De (1973);

Sinha Ray (1988); Dutta *et al*. (2002); Dutta (2005); Dutta and Kumar (2005) etc. In other countries, studies on the orographic effects are associated with airflow have been addressed by Abbs & Pielke (1987); Bischoff-Gauss *et al*. (1989); Leung and Ghan (1995); Lin and Chen (2002); Li *et al*. (2007); Xu *et al.* (2008); Jourdain & Gallee (2010) etc.

In some of the above studies, the wind and stability were assumed to be either constant with height or assumed to be variant with height. Solutions for these studies were essentially obtained by an analytical method or the numerical method. Das *et al*. (2013) developed a three-dimensional mountain waves problem over the Assam-Burma hills (ABH) are associated with idealistic basic flow. They obtained the asymptotic solutions using the perturbation approach and compared with the two-dimensional waves problem of the earlier authors.

To develop this model, here consider the same mountain profile the Assam-Burma Hills (ABH) and obtain the numerical solutions for the perturbation vertical velocity (w') and stream line displacement (η') are associated with 3-D lee wave using the perturbation approach and the computed results have compared with the earlier investigators Das *et al*. (2013).

2. Database

As the Assam-Burma Hills are situated in North-East position of India, the only station to the upstream side is Guwahati (26.19° N Latitude and 91.73° E Longitude). The average of 0000 UTC and 1200 UTC RS/RW data of Guwahati for those dates, which corresponds to the observed lee waves across ABH, as reported by De (1970, 1971); Farooqui and De (1974) and Das *et al*. (2013), has been obtained from the Archive of India Meteorological Department (IMD), Pune.

3. Methodology

In this model, an adiabatic, steady, laminar, inviscid, non-rotating flow of a vertical unbounded, a stratified and Boussinesq fluid across 3-D meso-scale elliptical orographic barrier has been considered. Here, this model has applied on the Assam-Burma Hills. The profile of the Assam-Burma Hills (Fig. 1) is analytically expressed as:

$$h(x,y)=\frac{h_1}{1+\frac{x^2}{a^2}+\frac{y^2}{b^2}}+\frac{h_2}{1+\frac{(x-d)^2}{a^2}+\frac{y^2}{b^2}} \tag{1}$$

where, a and b are the half width of the barrier along the zonal wind component (U) and along the meridional component (V) respectively, h_1 and h_2 are the height of the two ridges of the mountain and d be the distance of the valley between two ridges.

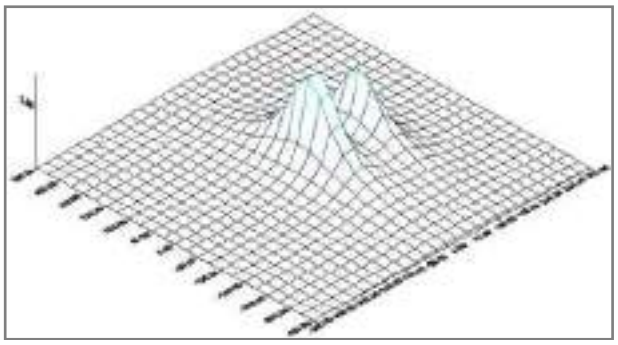

Fig. 1. The profile of the Assam-Burma hills

We consider a co-ordinate system in which the x-axis and the y-axis are perpendicular and parallel to the axis of the major ridge of the barrier and the z-axis is vertically upwards. The two components U and V of the basic flow, are normal and parallel to the major ridge of the barrier respectively. It is again simplified by assuming U, V and the Buoyancy frequency (N), to be invariant with height. Under the above assumptions, the linearized governing equations can be written as:

$$U\frac{\partial u'}{\partial x}+V\frac{\partial u'}{\partial y}=-\frac{1}{\rho_0}\frac{\partial p'}{\partial x} \tag{2}$$

$$U\frac{\partial v'}{\partial x}+V\frac{\partial v'}{\partial y}=-\frac{1}{\rho_0}\frac{\partial p'}{\partial y} \tag{3}$$

$$U\frac{\partial w'}{\partial x}+V\frac{\partial w'}{\partial y}=-\frac{1}{\rho_0}\frac{\partial p'}{\partial z}+\frac{g\theta'}{\theta_0} \tag{4}$$

$$\frac{\partial u'}{\partial x}+\frac{\partial v'}{\partial y}+\frac{\partial w'}{\partial z}=0 \tag{5}$$

$$U\frac{\partial \theta'}{\partial x}+V\frac{\partial \theta'}{\partial y}+w'\frac{d\theta_0}{dz}=0 \tag{6}$$

where, $\rho_0=\rho_0(z)$, $\theta_0=\theta_0(z)$ are respectively density and potential temperature of the basic flow and u', v', w', p', θ' are respectively the perturbation part of the zonal wind, the meridional wind, the vertical wind, pressure and potential temperature. Since the perturbation quantities u', v', w', p', θ' are all continuous functions of x, y, z. Hence, the double Fourier integral is :

$$u'(x,y,z)=\frac{1}{4\pi^2}\int_{-\infty}^{\infty}\int_{-\infty}^{\infty}\hat{u}(k,l,z)e^{i(kx+ly)}dkdl$$

where, $u'(k,l,z)=\int_{-\infty}^{\infty}\int_{-\infty}^{\infty}u'(x,y,z)e^{-i(kx+ly)}dxdy$ is the double Fourier transformation of u' (x, y, z). Using 2-D Fourier transformation in the equations (2)-(6) and they are transformed to :

$$i(kU+lV)\hat{u}=-ik\frac{\hat{p}}{\rho_0} \tag{7}$$

$$i(kU+lV)\hat{v}=-il\frac{\hat{p}}{\rho_0} \tag{8}$$

$$i(kU+lV)\hat{w}=-\frac{1}{\rho_0}\frac{\partial\hat{p}}{\partial z}+g\frac{\hat{\theta}}{\theta_0} \tag{9}$$

$$i(k\hat{u}+l\hat{v})+\frac{\partial\hat{w}}{\partial z}=0 \tag{10}$$

$$i(kU+lV)\hat{\theta}+\hat{w}\frac{d\theta_0}{dz}=0 \tag{11}$$

where, $\hat{u},\hat{v},\hat{w},\hat{p},\hat{\theta}$ are respectively double Fourier transformations of u', v', w', p', θ'. Now, eliminating $\hat{u},\hat{v},\ \hat{p},\hat{\theta}$ from the equations (7) - (11) we have :

$$\frac{\partial^2\hat{w}}{\partial z^2}+\frac{1}{\rho_0}\frac{d\rho_0}{dz}\frac{\partial\hat{w}}{\partial z}+\left(k^2+l^2\right)\left[\frac{N^2}{(Uk+Vl)^2}-1\right]\hat{w}=0 \tag{12}$$

where, $N=\sqrt{\frac{g}{\theta_0}\frac{d\theta_0}{dz}}$ is the Buoyancy frequency.

Now, by the substitution $\hat{w}(k,l,z)=\left[\frac{\rho_0(0)}{\rho_0(z)}\right]^{1/2}\hat{w}_1(k,l,z)$, the equation (12) is further simplified to :

$$\frac{\partial^2\hat{w}_1}{\partial z^2}+\left[\frac{N^2\left(k^2+l^2\right)}{(Uk+Vl)^2}-\frac{1}{2\rho_0}\frac{d^2\rho_0}{dz^2}+\frac{1}{4\rho_0^2}\left(\frac{d\rho_0}{dz}\right)^2-\left(k^2+l^2\right)\right]\hat{w}_1=0 \tag{13}$$

where, the terms $\left(-\frac{1}{2\rho_0}\frac{d^2\rho_0}{dz^2}\right)$ and $\frac{1}{4\rho_0^2}\left(\frac{d\rho_0}{dz}\right)^2$ in equation (13) are smaller in their magnitude than other terms in the square bracket. So, the equation (13) reduces to :

$$\frac{\partial^2\hat{w}_1}{\partial z^2}+\left(k^2+l^2\right)\left[\frac{N^2}{(Uk+Vl)^2}-1\right]\hat{w}_1=0 \tag{14}$$

If η' (x, y, z) be the perturbation streamline displacement, then we can write :

$$w'(x,y,z)=U\frac{\partial\eta'}{\partial x}+V\frac{\partial\eta'}{\partial y} \tag{15}$$

Using 2-D Fourier transformation in the above equation, then it becomes :

$$\hat{w}(k,l,z)=i(kU+lV)\hat{\eta}$$

Clearly seen that, $\hat{\eta}$ satisfies equation (14). Now, by the substitution $\hat{\eta}(k,l,z)=\sqrt{\frac{\rho_0(0)}{\rho_0(z)}}\hat{\eta}_1(k,l,z)$ we obtain :

$$\frac{\partial^2\hat{\eta}_1}{\partial z^2}+\left(k^2+l^2\right)\left[\frac{N^2}{(Uk+Vl)^2}-1\right]\hat{\eta}_1=0 \tag{16}$$

The equations (14) and (16) will be solved using the following boundary conditions:

(a) At the surface, that is lower boundary streamline pattern follows the contour of the terrine.

(b) At the upper boundary, the mountain waves are permitted to propagate vertically.

The general integral of the equations (14) and (16) are [using boundary condition (b)] :

$$\hat{w}_1(k,l,z)=\mathrm{A}e^{imz} \tag{17}$$

and

$$\hat{\eta}_1(k,l,z)=\mathrm{B}e^{imz} \tag{18}$$

where, A and B are arbitrary constants and m is given:

$$m^2=\left[\frac{N^2}{(kU+lV)^2}-1\right]\left(k^2+l^2\right)$$

Clearly m may be recognized as the vertical wave number of the vertically propagating mountain waves. Now, at the lower boundary, that is, at the surface, the airflow follows the contour of the mountain profile which is given in Eqn. (1).

In the present study, the values of a, d, h_1 and h_2 are the same as those in De (1971) and $b = 2.5a$ as in Dutta (2005), as in Das *et al*. (2013, 2016). Therefore, we take a = 20 km, b = 2.5a, d = 45 km, h_1 = 0.9 km and h_2 = 0.7 km. Now, the 2-D Fourier transformation of the mountain profile (1) is :

$$\hat{h}(k,l) = 2\pi ab\left(h_1 + h_2 e^{-ikd}\right)K_0\left(\sqrt{a^2k^2 + b^2l^2}\right)$$

[See Appendix] (19)

where, $K_0\left(\sqrt{a^2k^2 + b^2l^2}\right)$ is the zero-order second kind Bessel function. Using lower boundary condition, we have :

$$\eta'(x,y,0) = h(x,y)$$

Using double Fourier transformation in the above equation, we get :

$$\hat{\eta}(k,l,0) = \hat{h}(k,l)$$

Hence,

$$B = 2\pi ab\left(h_1 + h_2 e^{-ikd}\right)K_0\left(\sqrt{a^2k^2 + b^2l^2}\right)$$

Again, the linearized lower boundary condition for w', the equation (15) becomes :

$$w'(x,y,0) = U\frac{\partial \eta'(x,y,0)}{\partial x} + V\frac{\partial \eta'(x,y,0)}{\partial y}$$

Using double Fourier transformation in the above equation, we have :

$$\hat{w}(k,l,0) = i(kU + lV)\hat{\eta}(k,l,0) \qquad (20)$$

Hence,

$$A = 2\pi iab\left(h_1 + h_2 e^{-ikd}\right)K_0\left(\sqrt{a^2k^2 + b^2l^2}\right)$$

Thus, the solutions of (14) and (16) are obtained by putting the values of A and B respectively, we get :

$$\hat{w}_1(k,l,z) = 2\pi iab\left(h_1 + h_2 e^{-ikd}\right)K_0\left(\sqrt{a^2k^2 + b^2l^2}\right)e^{imz} \qquad (21)$$

$$\hat{\eta}_1(k,l,z) = 2\pi ab\left(h_1 + h_2 e^{-ikd}\right)K_0\left(\sqrt{a^2k^2 + b^2l^2}\right)e^{imz} \qquad (22)$$

Using inverse Fourier transformation $w_1'(x,y,z)$ can be expressed as :

$$w_1'(x,y,z) = \mathrm{Re}\frac{1}{4\pi^2}\int_{-\infty}^{\infty}\int_{-\infty}^{\infty}\hat{w}_1(k,l,z)e^{-i(kx+ly)}dkdl$$

$$= \frac{ab}{2\pi}\mathrm{Re}\int_{-\infty}^{\infty}\int_{-\infty}^{\infty} i(kU + lV)\left(h_1 + h_2 e^{-ikd}\right) K_0\left(\sqrt{a^2k^2 + b^2l^2}\right)e^{i(kx+ly+mz)}\,dkdl \qquad (23)$$

Similarly, $\eta_1'(x,y,z)$ can also be expressed as :

$$\eta_1'(x,y,z) = \mathrm{Re}\frac{1}{4\pi^2}\int_{-\infty}^{\infty}\int_{-\infty}^{\infty}\hat{\eta}_1(k,l,z)e^{i(kx+ly)}dkdl$$

$$= \frac{ab}{2\pi}\mathrm{Re}\int_{-\infty}^{\infty}\int_{-\infty}^{\infty}\left(h_1 + h_2 e^{-ikd}\right)K_0\left(\sqrt{a^2k^2 + b^2l^2}\right) e^{-i(kx+ly+mz)}dkdl \qquad (24)$$

The above two equations (23) and (24) reduce to :

$$w'(x,y,z) = \sqrt{\frac{\rho_0(0)}{\rho_0(z)}}w_1'(x,y,z) = c \times \mathrm{Re}(I_1) \qquad (25)$$

and

$$\eta'(x,y,z) = \sqrt{\frac{\rho_0(0)}{\rho_0(z)}}\eta_1'(x,y,z) = c \times \mathrm{Re}(I_2) \qquad (26)$$

where, $c = \frac{ab}{2\pi}\sqrt{\frac{\rho_0(0)}{\rho_0(z)}}$

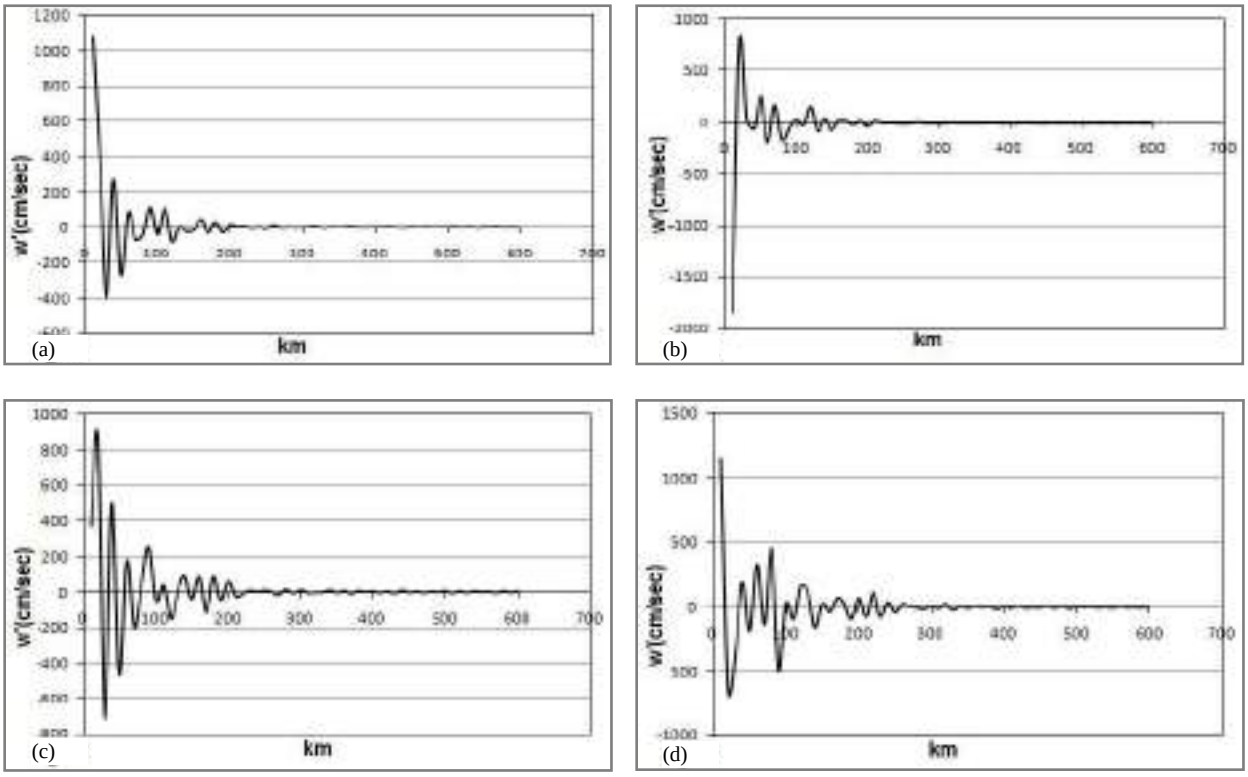

Figs. 2(a-d). Down-stream variation of *w*' along the line *Uy* – *Vx* = 0, at 1.5 km, 3 km, 6 km and 9 km above the mean sea level respectively

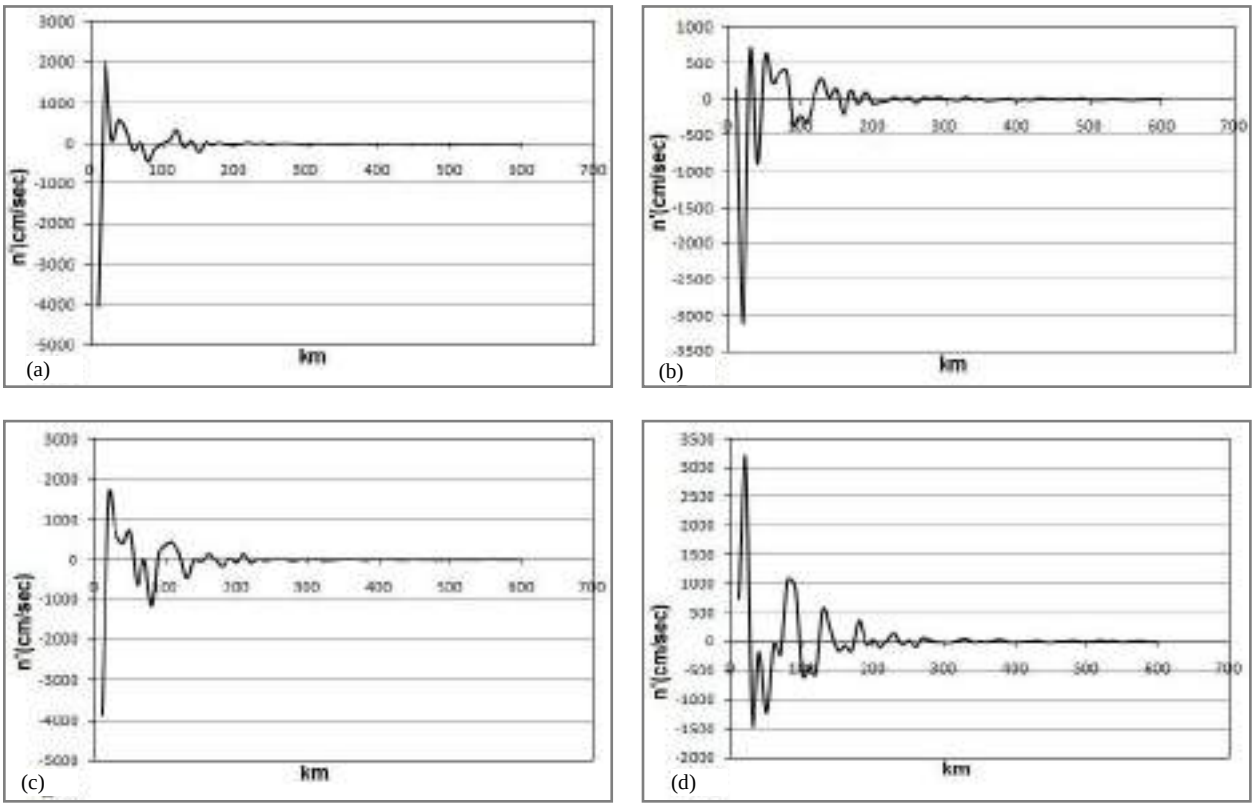

Figs. 3(a-d). Down-stream variation of η' along the line *Uy* – *Vx* = 0, at 1.5 km, 3 km, 6 km and 9 km above the mean sea level respectively

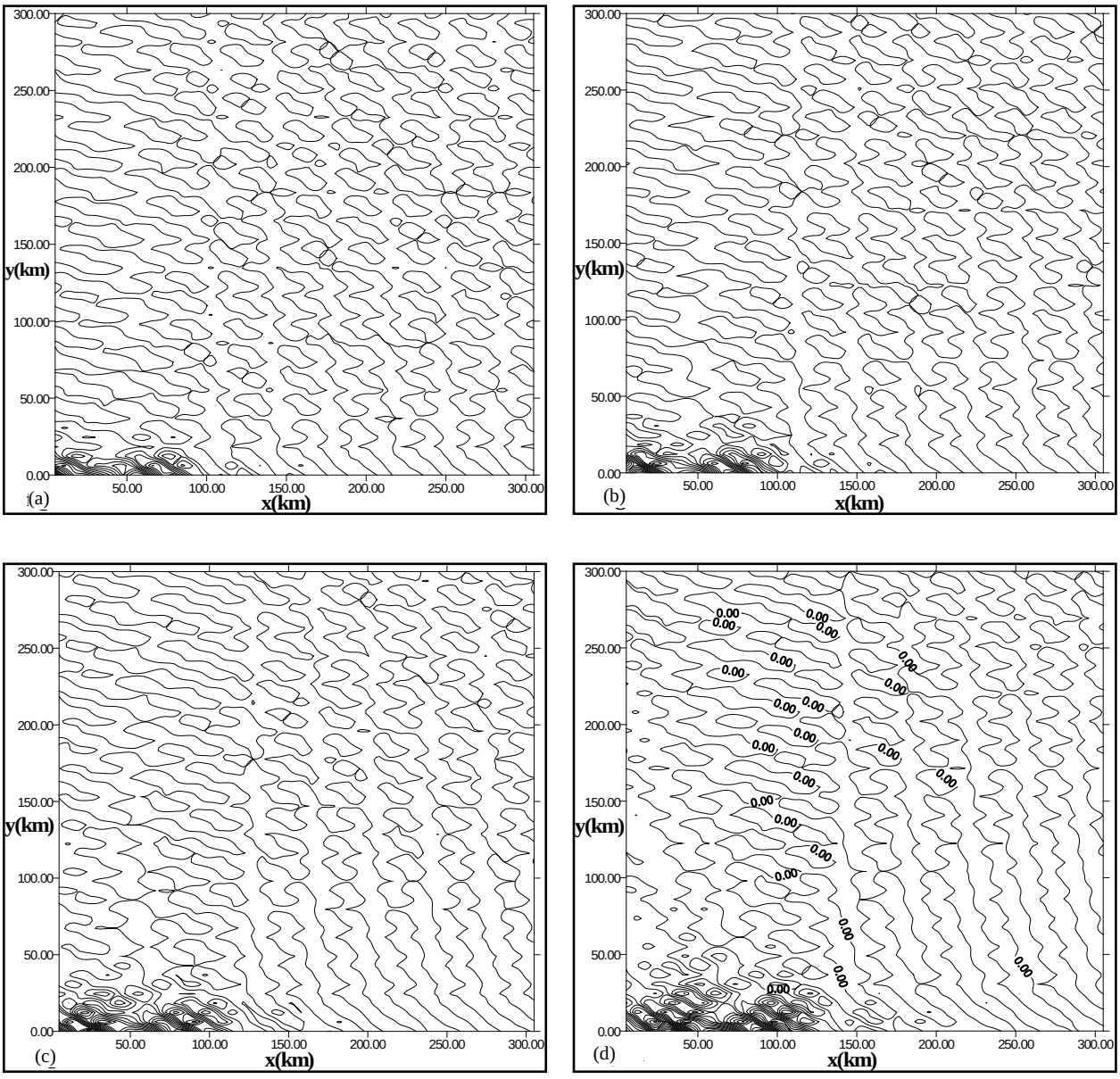

Figs. 4(a-d). Contours of the perturbation vertical velocity (*w*') at 1.5 km, 3 km, 6 km and 9 km above the mean sea level respectively

$$I_1 = \int_{-\infty}^{\infty}\int_{-\infty}^{\infty} i(kU+lV)\left(h_1 + h_2 e^{-ikd}\right) K_0\left(\sqrt{a^2k^2+b^2l^2}\right) e^{i(kx+ly+mz)}dkdl$$

$$I_2 = \int_{-\infty}^{\infty}\int_{-\infty}^{\infty} i\left(h_1 + h_2 e^{-ikd}\right)K_0\left(\sqrt{a^2k^2+b^2l^2}\right) e^{i(kx+ly+mz)}dkdl$$

The integrals (25) and (26) are evaluated numerically, we get :

$$w'(x,y,z) = -c\sum\sum (kU+lV)K_0\left(\sqrt{a^2k^2+b^2l^2}\right) \{h_1\sin(kx+ly+mz) + h_2\sin(kx+ly+mz-kd)\}\delta k\delta l \quad (27)$$

$$\eta'(x,y,z) = c\sum\sum K_0\left(\sqrt{a^2k^2+b^2l^2}\right) \{h_1\sin(kx+ly+mz) + h_2\sin(kx+ly+mz-kd)\}\delta k\delta l \quad (28)$$

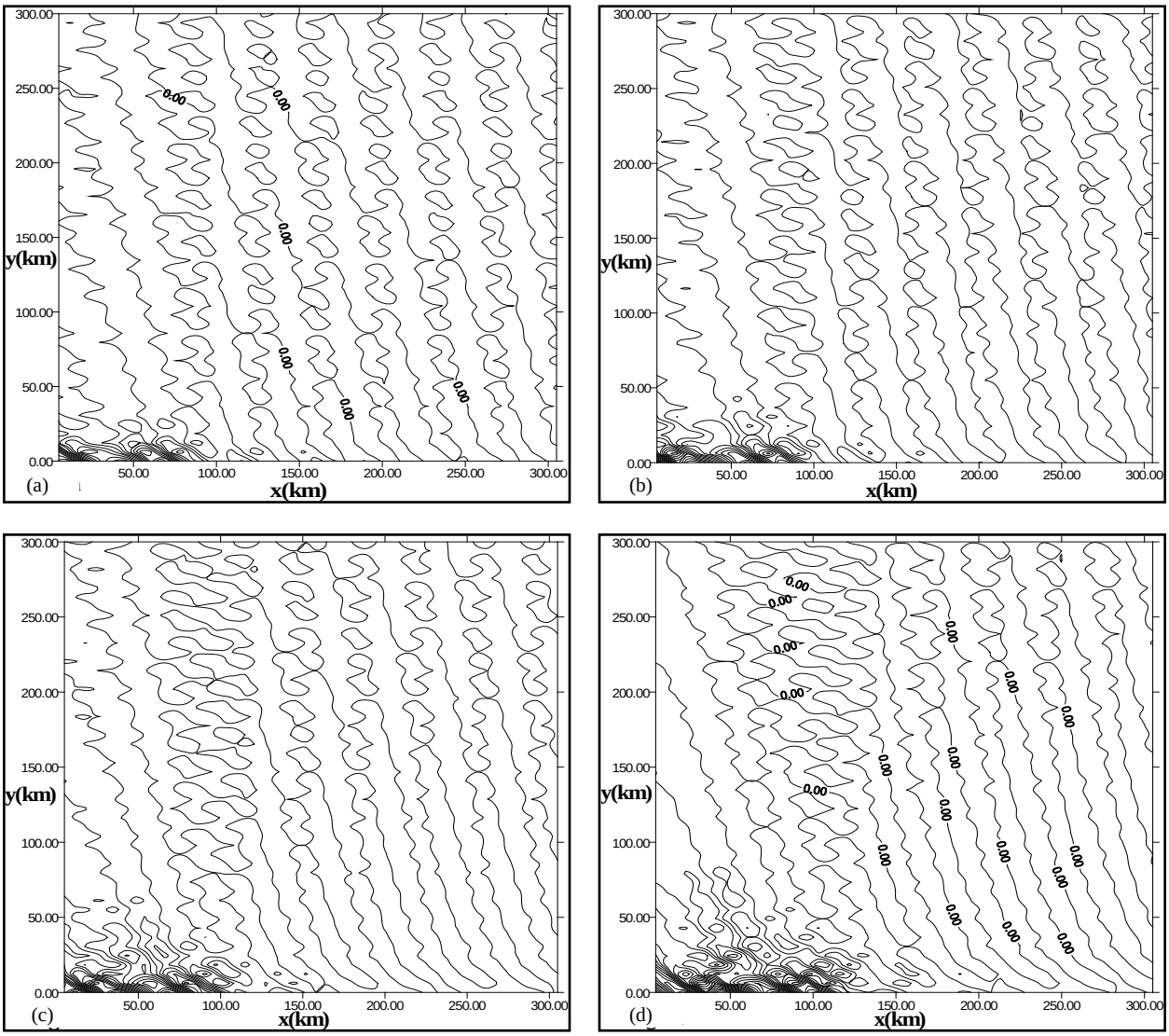

Figs. 5(a-d). Contours of stream line displacement (η') at 1.5 km, 3 km, 6 km and 9 km above the mean see level respectively

where, the above summations are extended between those wave numbers determined by the maximum wave length and the minimum wave length of the disturbance and $\delta k = \delta l = \frac{2\pi}{4L_{\max}}$, where L_{max} is the maximum wave length.

4. Results and discussion

The numerical computation for both the vertical velocity (w') and streamline displacement (η') are made using equations (27) and (28) respectively, for all those waves for which $\left(k^2 + l^2\right) < \frac{N^2\left(k^2 + l^2\right)}{\left(Uk + Vl\right)^2}$. Scale analysis by Sarker (1965), Dutta *et al*. (2002) and Das *et al*. (2013) exhibited that, by ignore the effects of earth's rotation for the basic flow consists of both the zonal wind (U) and the meridional component (V), scale of the disturbance should not exceed 150 km. Since the horizontal grid size in the present study, has been taken to be 5 km. Hence, the minimum wave length should not be less than 30 km. In the equations (27) and (28) the summations k ranges from 4δk to 20δk and l ranges from $-20\delta k$ to $-4\delta k$ and $4\delta k$ to $20\delta k$. Where, we have been taken to avoid all those wave number vectors (k, l), which are inclined with the basic flow vectors (U, V) at an angle of $90°$ or more, to eliminate the critical level effect.

The down-stream variation of both w' and η' on a horizontal plane along the line $Uy - Vx = 0$ have been shown in Figs. 2(a-d) and Figs. 3(a-d) respectively, at

1.5 km, 3 km, 6 km and 9 km above the mean sea level, which is approximately resemble to 850 hPa, 700 hPa, 500 hPa and 300 hPa respectively.

From these figures, we see that both w' and η' decay downwind of the barrier, in qualitative conformity with the asymptotic solutions of Das *et al*. (2013, 2016). But, is no such specific rate of decay like as in the case of the asymptotic solution [Das *et al*. (2013)] could be found in the numerical case. From the expressions (27) and (28) of w' and η' respectively, we see that there are only one damping factor Bessel function is present, whereas in Das *et al*. (2013) found two damping factors in the asymptotic solution across the ABH.

The contours of the perturbation vertical velocity w' and streamline displacement η' at different horizontal planes above the mean sea level have been shown in Figs. 4(a-d) and Figs. 5(a-d) respectively. These figures show that, the vertical tilt of the wave field is insignificant and the maximum updraft/downdraft regions are no specific shaped, whereas, Das *et al*. (2013) have shown that, the maximum updraft/downdraft regions are crescent shaped in the asymptotic case across the same mountain barrier ABH.

Das *et al*. (2013) found the vertical velocity (w') and streamline displacement (η') tilt upstream and spread laterally with the vertical across the ABH. But, in the numerical case, the spreading rate of both w' and η' are almost the same at every level, *i.e*., is no spreading laterally with the vertical across the same barrier ABH. The dynamical cause of this situation may be due to the presence of a divergent part in the asymptotic case and the absence of a divergent part in the numerical case.

5. Conclusions

In this model, we have presented the numerical solution of 3-D meso-scale lee wave across the 3-D elliptical mountain barrier following the numerical approach. In the sequel, we have furnished some remarkable results. Moreover,

(*i*) The numerical solution for the vertical velocity (w') and streamline displacement (η') along the line $Uy - Vx = 0$ both decay down wind of the barrier. But, is no such specific rate of decay has found across the barrier.

(*ii*) In the horizontal plane, the contours of the vertical velocity (w') and streamline displacement (η') have not been seen any specific shaped across the barrier.

(*iii*) Both the vertical velocity (w') and streamline displacement (η') across the 3-D mountain barrier are upwind tilt along the line $Uy - Vx = 0$ and not spread laterally with height. The spreading rate almost the same for both w' and η' on every level across the barrier.

Acknowledgement

The author is thankful to Dr. U. S. De, Former Addl. Director General of Meteorology of India Meteorological Department and to Dr. S. N. Dutta, Scientist-E, India Meteorological Department (IMD), Pune, India and to Prof. M. Maiti, Retd. Professor and Prof. S. K. M, Deptt of Applied Mathematics, Vidyasagar University, Midnapore, West Bengal for their kind valuable insinuation and trips.

Disclaimer : The contents and views expressed in this research paper/article are the views of the authors and do not necessarily reflect the views of the organizations they belong to.

References

Abbs, D. J. and Pielke, R. A., 1987, "Numerical simulations of orographic effects on NE Colorado snowstorms", *Meteorology and Atmospheric Physics*, **37**, 1, 1-10.

Bischoff-Gauss, I., Gross, G. and Wippermann, F., 1989, "Numerical studies on cold fronts Part II : Orographic effects on gravity flows", *Meteorology and Atmospheric Physics*, **40**, 4, 159-169.

Crapper, G. D., 1959, "A three-dimensional solution for waves in the lee of mountains", *Journal of Fluid Mechanics*, **6**, 01, 51-76.

Das, P. K., 1964, "Lee waves associated with a large circular mountain", *Indian J. Meteorol. Geophys.*, **15**, 547-554.

Das, P., Mondal, S. K. and Dutta, S., 2013, "Asymptotic solution for 3-D Lee waves across Assam-Burma hills", *MAUSAM*, **64**, 3, 501-516.

Das, P., Mondal, S. K. and Dutta, S., 2016, "Orographic effect of the Assam-Burma hills in India on a barotropic air-stream", *IRJNAS*, **1**, 3, 46-65.

De, U. S., 1970, "Lee waves as evidenced by satellite cloud pictures", *I.J.Met. Geophy.*, **21**, 637-647.

De, U. S., 1971, "Mountain waves over northeast India and neighbouring regions", *Indian J. Meteorol. Geophys.*, **22**, 361-364.

De, U. S., 1973, "Some studies of mountain waves", Doctoral dissertation, Ph. D. Thesis, Banaras Hindu University, Varnasi (India).

Dutta, S. N. and Kumar, N., 2005, "Parameterization of momentum and energy flux associated with mountain wave across the Assam-Burma hills", *MAUSAM*, **52**, 2, 325-332.

Dutta, S., 2005, "Effect of static stability on the pattern of three-dimensional baroclinic lee wave across a meso-scale elliptical barrier", *Meteorology and Atmospheric Physics*, **90**, 3-4, 139-152.

Dutta, S., 2007, "Parameterization of momentum flux and energy flux associated with orographically excited internal gravity waves in a baroclinic background flow", *MAUSAM*, **58**, 4, 459-470.

Dutta, S., Maiti, M. and De, U. S., 2002, "Waves to the lee of a meso-scale elliptic orographic barrier", *Meteorology and Atmospheric Physics*, **81**, 3-4, 219-235.

Farooqui, S. M. T. and De, U. S., 1974, "A numerical study of the mountain wave problem", *Pure and Applied Geophysics*, **112**, 2, 289-300.

Jourdain, N. C. and Gallée, H., 2010, "Influence of the orographic roughness of glacier valleys across the Transantarctic Mountains in an atmospheric regional model", *Clim. Dyn. Climate Dynamics*, **36**, 5-6, 1067-1081.

Kumar, P., Singh, M. P., Padmanabhan, N. and Natarajan, N., 1998, "An analytical model for mountain waves in stratified atmosphere", *MAUSAM*, **49**, 4, 433-438.

Leung, L. R. and Ghan, S. J., 1995, "A subgrid parameterization of orographic precipitation", *Theoretical and Applied Climatology*, **52**, 1-2, 95-118.

Li, Y., Huang, W. and Zhao, J., 2007, "Roles of mesoscale terrain and latent heat release in typhoon precipitation : A numerical case study", *Advances in Atmospheric Sciences*, **24**, 1, 35-43.

Lin, C. Y. and Chen, C. S., 2002, "A study of orographic effects on mountain-generated precipitation systems under weak synoptic forcing", *Meteorology and Atmospheric Physics*, **81**, 1-2, 1-25.

Lyra, G., 1943, "Theorie der stationären Leewellenströmung in freier Atmosphäre", *Zeitschriftfür Angewandte Mathematik und Mechanik*, **23**, 1, 1-28.

Queney, P., 1947, "Theory of perturbations in stratified currents with applications to air flow over mountain barriers", University of Chicago Press.

Sarker, R. P., 1965, "A curvilinear study of yield with reference to weather-sugar cane", *Indian J. Met. and Geoph*., **16**, 103-110.

Sarker, R. P., 1966, "A dynamical model of orographic rainfall", *Mon. Wea. Rev*., **94**, 555-572.

Sarker, R. P., Sinha Ray, K. C. and De, U. S., 1978, "Dynamics of orographic rainfall", *Indian journal of meteorology and geophysics*, **29**, 335-348.

Sawyar, J. S., 1962, "Gravity waves in the atmosphere as a 3-D problem", *Quart. J. R. Met. Soc.*, **88**, 412-425.

Sawyer, J. S., 1960, "Numerical calculation of the displacements of a stratified airstream crossing a ridge of small height", *Quart. J. R. Met. Soc*., **86**, 326-345.

Scorer, R. S. and Wilkinson, M., 1956, "Waves in the lee of an isolated hill", *Quarterly Journal of the Royal Meteorological Society*, **82**, 354, 419-427.

Scorer, R. S., 1949, "Theory of waves in the lee of mountain", *Quart .J. R. Met. Soc*., **45**, 41-56.

Sinha Ray, K. C., 1988, "Some studies on effects of orography on airflow and rainfall (Doctoral dissertation", Ph. D. thesis, University of Pune, India).

Smith, R. B., 1979, "The influence of mountains on the atmosphere", *Adv. Geophys.*, **21**, 87-230.

Wurtele, M. G., 1957, "The three-dimensional lee wave", *Beitr. Phys. Atmos*., **29**, 242-252.

Xu, H., Xie, S., Wang, Y., Zhuang, W. and Wang, D., 2008, "Orographic effects on South China Sea summer climate", *Meteorology and Atmospheric Physics*, **100**, 1-4, 275-289.

Appendix

The Fourier Transform of the function $h(x,y)=\dfrac{h_1}{1+\dfrac{x^2}{a^2}+\dfrac{y^2}{b^2}}+\dfrac{h_2}{1+\dfrac{(x-d)^2}{a^2}+\dfrac{y^2}{b^2}}$ is

$$F[h(x,y)]=\int_{-\infty}^{\infty}\int_{-\infty}^{\infty}h(x,y)e^{-i(kx+ly)}dxdy$$

$$\hat{h}(k,l)=\int_{-\infty}^{\infty}\int_{-\infty}^{\infty}\left[\frac{h_1}{1+\dfrac{x^2}{a^2}+\dfrac{y^2}{b^2}}+\frac{h_2}{1+\dfrac{(x-d)^2}{a^2}+\dfrac{y^2}{b^2}}\right]e^{-i(kx+ly)}dxdy$$

$$\hat{h}(k,l)=ab\int_{-\infty}^{\infty}\int_{-\infty}^{\infty}\left[\frac{h_1e^{-i(kx+ly)}}{1+\dfrac{x^2}{a^2}+\dfrac{y^2}{b^2}}dxdy+\int_{-\infty}^{\infty}\int_{-\infty}^{\infty}\frac{h_2e^{-i(kx+ly)}}{1+\dfrac{(x-d)^2}{a^2}+\dfrac{y^2}{b^2}}\right]dxdy$$

Putting $x = aX$, $y = bY$ for the first term and $x - d = aX$, $y = bY$ for the second term

and use $k = \frac{k'}{a}, l = \frac{l'}{b}$ for the both terms, we have

$$\hat{h}(k,l) = ab\int_{-\infty}^{\infty}\int_{-\infty}^{\infty}\frac{h_1 e^{-i(k'X+l'Y)}}{1+X^2+Y^2}dXdY + abe^{-i\frac{k'd}{a}}\int_{-\infty}^{\infty}\int_{-\infty}^{\infty}\frac{h_2 e^{-i(k''X+l'Y)}}{1+X^2+Y^2}dXdY$$

$$\hat{h}(k,l) = ab\left(h_1 + h_2 e^{-ikd}\right)\int_{-\infty}^{\infty}\int_{-\infty}^{\infty}\frac{e^{-i(k'X+l'Y)}}{1+X^2+Y^2}dXdY$$

Putting $X = r\cos\theta$, $Y = r\sin\theta$ and $k' = \kappa\cos\alpha$, $l' = \kappa\sin\alpha$ we get

$$\hat{h}(k,l) = ab\left(h_1 + h_2 e^{-ikd}\right)\int_{0}^{\infty}\int_{0}^{2\pi}\frac{e^{-ir\kappa\cos(\theta-\alpha)}}{1+r^2}rdrd\theta$$

Now, $\int_0^{2\pi} e^{-ir\kappa\cos(\theta-\alpha)}d\theta = 2\pi J_0[r\kappa]$ [Dutta *et al*. (2002)]

and $\int_0^{\infty}\frac{J_0(r\kappa)}{1+r^2}rdr = K_0(\kappa)$ [Dutta *et al*. (2002)]

where $J_0(r\kappa)$ and $K_0(\kappa)$ are Bessel function of 1st and 2nd kind of order zero respectively.

Hence, $\hat{h}(k,l) = 2\pi a\left(h_1 + h_2 e^{-ikd}\right)K_0(\kappa)$, where $\kappa = \sqrt{a^2k^2 + b^2l^2}$

Therefore, $\hat{h}(k,l) = 2\pi a\left(h_1 + h_2 e^{-ikd}\right)K_0\left(\sqrt{a^2k^2 + b^2l^2}\right)$

Dr.Narendra
Ranjan Malas

LANGUAGE IN INDIA

Strength for Today and Bright Hope for Tomorrow

Volume 23:2 February 2023
ISSN 1930-2940

Editors:
Sam Mohanlal, Ph.D.
B. Mallikarjun, Ph.D.
A. R. Fatihi, Ph.D.
G. Baskaran, Ph.D.
T. Deivasigamani, Ph.D.
Pammi Pavan Kumar, Ph.D.
Soibam Rebika Devi, M.Sc., Ph.D.

Managing Editor & Publisher: M. S. Thirumalai, Ph.D.

Celebrate India!
Unity in Diversity!!

Back Issues of *Language in India* - From 2001

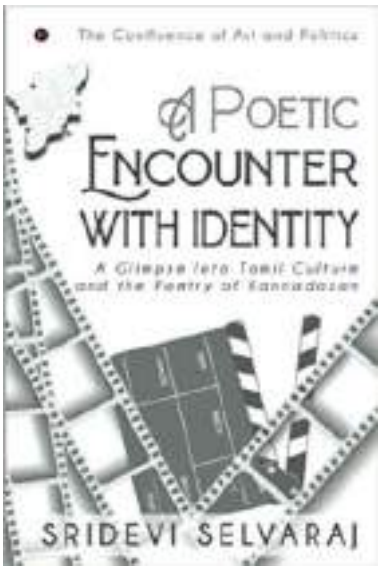

Available in
https://www.amazon.in/dp/B09TT86S4T

Search

IJSSER

Fast Publication within 3

CONTENTS

Language in India ***www.languageinindia.com*** **is an open access journal.** ***Language in India*** ***www.languageinindia.com*** **does not charge readers or their institutions for access.**

We have agreements with database organizations *EBSCOHost database* and *Gale Research/Cengage Learning* for indexing articles and books published in *Language in India*. The journal is included in the *Cabell's Directory*, a leading directory in the USA. It is included also in the *MLA International Bibliography* and the *Directory of Periodicals*

Articles published in *Language in India* are peer-reviewed by one or more members of the Board of Editors or an outside scholar who is a specialist in the related field. Since the dissertations are already reviewed by the University-appointed examiners, dissertations accepted for publication in *Language in India* are not reviewed again.

The next issue (the issue of March 2023) will be uploaded by the fourth week of March 2023 or earlier.

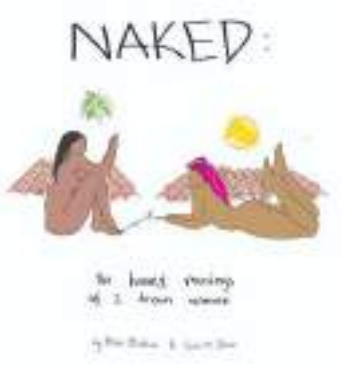

Naked: the honest browsings of two brown women
Available in https://www.amazon.in

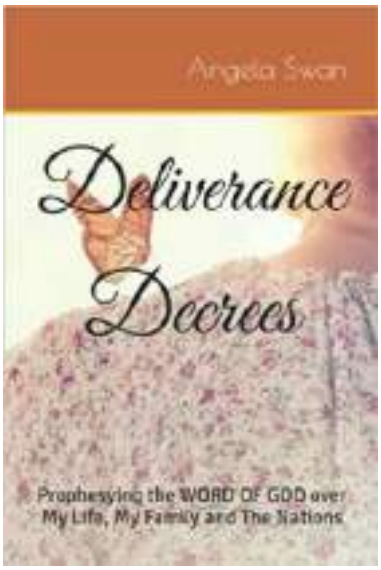

Available in https://www.amazon.com

Click Here for
Weekly Notes on
Practical Ideas for
Research & Better Writing

Click Here to Go to Creative Writing Section

- **Emergence of Englishes and the Issues of Teaching English Pronunciation to Indian Learners** ...
  Dr. Narendra Ranjan Malas, M.A., Ph.D.
- **Linguistic Landscape of a North-East India Town: A Case Study of Sivasagar** ...
  Debraj Gogoi, Ph.D. Scholar and Dr. Sweta Sinha, Ph.D.
- **Classroom Dynamics in EFLL Context: Does It Minimize Learner Anxiety and Develop Learner Autonomy in a Collaborative Learning Environment?** ...
  M. Shajedul Arifeen
- **An Analysis of Class X English Textbook Used in Madhya Pradesh Secondary School Board High Schools** ...
  B. A. Mahalakshmi Prasad, M.A.
- **Journey into the Realm of Mathematics and Language** ...
  B. A. Mahalakshmi Prasad, M.A.
- **The Prose System in the Poetry of Pashto: Scales of Pashto Poetry** ...
  Mohammad Nazir Rohani, Seraj Ahmad Habibi and Said Ghulam Mohammad Hashmi
- **A PRINT VERSION OF ALL THE PAPERS OF FEBRUARY 2023 ISSUE IN BOOK FORMAT**
  This volume is better viewed if you open it online and then save it in your computer. After saving it in your computer, you can easily read and print all the pages from the saved document.
  If you are not connected to a high-speed Internet service provider, you may like to get these downloaded in a "browsing centre" near you and ask them to burn a CD of the entire volume for your personal use and not for distribution.

- **Weekly Notes: Practical Ideas for Research & Better Writing** ...
- **Creative Works** ...
  Various Authors - Vijaya, K.R., Raji Narasimhan; Bala Devi; Selvi Bunce; Tanu Kashyap, Kiran Sikka, Kaneez Fatima Syeda, V. Shoba

---

Search

Get PEER Reviewed, Glol
Quality Research Paper.
Fast Publication within 3

CONTACT EDITOR

Humanities and Social Science

Publish fast Journal

Fast Review. Quick Support Team.World Wide Indexed.Call for Papers-2022.Free eCertificates

iosrjourr

Courtesy: http://www.mapsofindia.com

INSTITUTES & DEPARTMENTS OF LINGUISTICS, INDIAN LANGUAGES, SPEECH AND HEARING, AND ENGLISH LITERATURE! SEND YOUR ANNOUNCEMENTS TO APPEAR IN THIS PLACE!!

HOME PAGE

BOOKS FOR YOU TO READ AND DOWNLOAD FREE!

- *WordNet and its dimensions* -- A Textbook in Tamil ...
  Prof. Rajendran Sankaravelayuthan and Dr. S. Arulmozi
- GENERAL LINGUISTICS -- Tamil Textbook ...
  Prof. Rajendran Sankaravelayuthan
- *Silent Talk Nonverbal Communication* ...
  M. S. Thirumalai, Ph.D.
- Jayampu krishna kathalu – parisilana
  A dissertation submitted to the University of Madras for the partial fulfillment of the award of the M.Phil. Degree in Telugu ...
  Thulluru Ravi
- *Corpus Linguistics* -- A Monograph in Tamil ... **Prof. Rajendran Sankaravelayuthan**

Board of Editors

- Sam Mohanlal, Ph.D.
  Professor-cum-Deputy Director, CIIL (Retired)
- B. Mallikarjun, Former Director
  Centre for Classical Kannada Central University of Karnataka
- A. R. Fatihi, Ph.D., Professor and Head
  Department of Linguistics, Aligarh Muslim University, Aligarh (Retired)
- G. Baskaran, Ph.D. Professor of English, Department of English, Gandhigram Deemed University
- T. Deivasigamani, Ph.D. Associate Professor, Department of English, Annamalai University
- Pammi Pavan Kumar, Ph.D. Associate Professor, Department of Telugu, University of Hyderabad
- Soibam Rebika Devi, M.Sc., Ph.D., National Translation Mission, CIIL, Tibeto-Burman Studies
- **Managing Editor & Publisher:** M. S. Thirumalai, Ph.D.
  Professor-cum-Deputy Director, CIIL (Retired)

GUIDELINES FOR THE SUBMISSION OF ARTICLES, ETC. FOR PUBLICATION IN LANGUAGE IN INDIA www.languageinindia.com

- **A TRANSFER GRAMMAR FOR ENGLISH-TAMIL MACHINE TRANSLATION** ... **Prof. Rajendran Sankaravelayuthan**
  Dr. P. Kumaresan

- ***AN INTRODUCTORY COURSE ON SEMANTICS AND PRAGMATICS*** ...
  Prof. Rajendran Sankaravelayuthan

- ***Nuances of Making Spell and Grammar Checker for Tamil Monograph in Tamil*** ...
  Prof. Rajendran Sankaravelayuthan
  Dr. R. Amutha

- ***COMPUTATIONAL LINGUISTICS A Monograph in Tamil (Tamil)*** ...
  Prof. Rajendran Sankaravelayuthan

- ***Using Theatre To Enhance Learner Language In English Classrooms: A Sri Lankan Experiment – Ph.D. Dissertation*** ...
  Kandiah Shriganeshan, Ph.D.

- ***Acoustic Phonetics and Text to Speech Processing and Speech to Text Processing (Tamil) – Monograph*** ...
  Prof. Rajendran Sankaravelayuthan

- ***Aspects of Vowels Analysis for Speech & Hearing Diagnostics Volume 2*** ...
  Gayathri S G., MSc (Speech& Hearing), PGD Nutrition and Dietetics

- ***Aspects of Vowels Analysis for Speech & Hearing Diagnostics Volume 1*** ...
  Gayathri S G., MSc (Speech& Hearing), PGD Nutrition and Dietetics

- ***Word Sense Disambiguation in Tamil*** ...
  Prof. Rajendran Sankaravelayuthan and Dr. A. Dhanavalli

- ***Semantic Intention and Semantic Relation in Children with Intellectual Disability and Hearing Impairment -- Masters Dissertation*** ...
  Nithina Alice Boban and Satish Kumaraswamy

- ***Paradigms of Marginality in Literature - Exploring the Nuances*** ...
  Prof. Dr. S. Chelliah, M.A., M.Phil., Ph.D., D.Litt., Editor

- ***Ontology of Tamil Vocabulary A Detailed Study of Form and***

Thanks, my dear friend! You are most welcome to send articles for publication in **Language in India www.languageinindia.com.** Our Board of Editors consists of distinguished linguists and literature Professors with many years of contributions to Indian Linguistics, literature, Humanities and Social Sciences. We will evaluate every article before we accept any for publication. We are very happy that you did a good job in your last article.
Please write to us for any further clarification.

Language in India www.languageinindia.com is an international online monthly research journal, and is indexed in four major international databases: EBSCOHost, ProQuest (Linguistics and Language Behavior Abstracts), MLA International Bibliography and Gale Research. The journal is included in the Cabell's Directory, USA. Thus, your research is available in University Libraries all over the world for others to read and cite.

Articles published in Language in India are peer-reviewed by one or more members of the Board of Editors or an outside scholar who is a specialist in the related field. Since the dissertations are already reviewed by the University-appointed examiners, dissertations accepted for publication in Language in India are not reviewed again.

You must do the following:

- Must include your complete address including institutional affiliation and e-mail address on the first page of your article. Please also give your cell phone number (for urgent editorial messages only). It is for the authors to take care of this important part if they want others to correspond with them on the subject.
- You must give the declaration as to the authenticity of the work that you submit. This declaration should state that your article or work submitted for publication in LANGUAGE IN INDIA www.languageinindia.com is an original work by you and that you have duly acknowledged the work or works of others you either cited or used in writing your articles, etc. A model is given below:

  This is to certify that the article ……. submitted for publication in language in India www.languageinindia.comis an original work by me/us based on my/our research, that I/we have duly acknowledged in the said paper the work or works of others I/we used in writing this article, that I/we have duly cited all such work/s in the text as well as in the list of references, and that I/we have presented within quotes all the original sentences and phrases, etc. taken from the sources that I/we have consulted in writing this article.

  I/we further declare that the paper submitted for publication in Language in India www.languageinindia.com has not been previously published, is not currently submitted for review to any other journal, and will not be submitted elsewhere before a decision is made by this journal.

  I/we also declare that I/we will pay the formatting fee for the article/dissertation (specified in the Guidelines) as and when my paper/dissertation is accepted for publication in Language in India www.languageinindia.com.

- Authors may kindly review their articles in the light of the required declaration given above, before they submit their work

Function of Tamil Vocabulary ...
Prof. Rajendran Sankaravelayuthan and K. Anithaa, Ph.D.

- ***A Historical Linguistic Study of Tamil Nouns*** ...
  Prof. Rajendran Sankaravelayuthan and Dr. S. Tamilselvam

- ***Semantic Change and Semantic Extension of Tamil Verbs***
  A Research Monograph (in Tamil) ...
  Prof. Rajendran Sankaravelayuthan Dr. K. Bakkiyaraj

- ***Greening the Young Mind: Eco-consciousness in Contemporary English Language Fiction for Children and Young Adults in India*** ...
  Dr. Shobha Ramaswamy, M.A., B.Ed., DCE, M.Phil., Ph.D.

- ***English To Tamil Machine Translation System Using Parallel Corpus*** ...
  Prof. Rajendran Sankaravelayuthan Dr. G. Vasuki

- **Bharathiar University**
  Coimbatore 641046, Tamilnadu, India
  Department of English and Foreign Languages

  Dr. V. David Arputha Raj, M.A., M.Phil., Ph.D., Editor
  Trends in Select Sahitya Akademi Award-winning Tamil Novels

- ***Word Order Typology and Its Implication in Translation*** ...
  Prof. Rajendran Sankaravelayuthan Dr. N. Gejeswari

- **Select Papers from International Conference on Contemporary Issues in Language and Literature,**
  Thanthai Hans Roever College (Autonomous)
  Elambalur, Perambalur - 621 220 Tamilnadu, India ...
  Editor: K. Nesapriya, Editor

- **Select Papers of the National Conference on Effective Strategies, Innovative Methods & Integrated Pedagogical Approaches to Learning and Teaching English in Heterogenous Classrooms,**
  SRM Valliammai Engineering College, Kattankulathur 603 303, Tamilnadu, India ...
  Editors: Prof N.Lakshmana Perumal, Sheeba Manodh and M.Chithra

- ***Insight into Select Literary Works*** ...
  Editor: Dr. S. Jayanthi, M.A.,

for publication in Language in India www.languageinindia.com. They are wholly responsible for any plagiarism identified in their works. Language in India www.languageinindia.com will not and does not assume any responsibility for the acts of plagiarism committed by the authors.

- If any complaint is received with evidence that your paper is plagiarized or that your paper does not cite sources but gives the impression that the ideas and the sentences you've used from other sources are your own, we will immediately delete the paper and then it is up to the author to make changes suitably and add a certificate of original work. As such retraction is done because of plagiarism, authors may be asked to pay a formatting fee to reinstate their article after corrections are made.
- Kindly view the above as positive directions so that your scholarship is well recognized.
- Kindly note that you are not permitted to add any new author/s or delete the names of authors from the paper/s, once you've submitted your article/s for publication.
- Remember that by maintaining academic integrity we not only do the right thing but also help the growth, development and recognition of Indian scholarship. This applies also to all who submit their articles for publication from other nations as well.
- You must not paginate your article submitted in the Word or pdf formats. www.languageinindia.com will paginate it.
- If your article involves a lot of diacritic marks and is a complex presentation that is difficult to reproduce, you may like to submit your article in PDF format. While doing so, please do not paginate it.
- The title page will be somewhat like this in pdf. Title of the paper in bold, Times New Roman in 16 point, immediately followed by the name/s of the author/s, with each author's name followed by their educational qualification such as Ph.D., M.Phil., or M.A., etc., in 14 point, and then after one line space, a line in bold. After this, give one line space and begin your article. It is better to check how pdf files are formatted in Language in India www.languageinindia.com and proceed accordingly. While in doubt, please send an e-mail to languageinindiaUSA@gmail.com.
- Please include your educational qualifications such as M.Phil., immediately after your name in the first page of the article.
- Give complete details of your address, with full postal number (pin or zip code).Include the e-mail addresses and postal addresses of all the authors of the article. It will be useful to add your cell phone number/s for any urgent contact.
- Please tell all your friends, colleagues, supervisors, and relatives that your article is published in Language in India www.languageinindia.com so that they will log in and see it. You do not become known easily unless your work is publicized first in your circles of friends and relatives!
- Encourage your co-workers also to write articles for Language in India www.languageinindia.com.
- If you can support this publication by donations, you are most welcome to do so, and we will receive the gifts with gratitude and appreciation. Remember, it does cost a lot of money and time, even to perform good works! However, donations will not influence the decision to accept or not accept any submission for publication in www.languageinindia.com.
- Language in India www.languageinindia.com charges a formatting fee of Indian rupees 1400 only for the publication of each article (not exceeding 20 pages) submitted by authors from South Asia and other less affluent countries. Authors from affluent countries are charged a fee of Indian rupees 2800 only. Note that those authors of South Asian origin who work or study in affluent countries are also charged Indian rupees 2800 for each article. This fee covers the editing and formatting of articles, etc. for

M.Phil., Ph.D.

- **Periyar University**
  Department of English, Salem, Tamilnadu, India
  Papers presented in the National Seminar
  Food is not just a Curry: Raison de'tre of Food in Literature - FDLT 2019 ...
  Editors: Dr. V. Sangeetha, Dr. B. J. Geetha,
  Dr. K. Sindhu, Dr. S. Boopathi and Ms. S. Snekha Sri

- **Sri S. Ramasamy Naidu Memorial College**
  Sattur 626203, Tamilnadu, India
  Select Papers of the International Conference on *Translation*: *Exploring the Nuances and Possibilities of Mediating Intercultural Texts* ...
  Dr. S. Jayanthi, M.A., M.Phil., Ph.D., Editor

- **St. Joseph's College for Women, Tirupur, Tamilnadu**
  Select Papers from the Conference *Reading the Nation – The Global Perspective* ...
  R. Rajalakshmi, Editor

- **From Leadership Competencies To Leaderful Practices At Mahatma Gandhi Institute (MGI) – Ph.D. Dissertation, Leeds Metropolitan University** ...
  Dr. Veedotma D. Koonjal

- **Select Papers from the National Conference on Challenges and Opportunities for Teaching and Research in English Language and Literature, March 23, 2018**

  Vellore Institute of Technology, Chennai Campus
  Division of Social Sciences and Languages, Department of English ...
  Dr. V. Rajasekaran, Editor

- ***NEW PERSPECTIVES IN ELT 2018***
  Selected Papers from the National Seminar on New Perspectives in ELT Conducted by the Department of English
  Theni Kammavar Sangam College of Technology, Theni 625534
  Tamilnadu, India ...
  Editors: D. Nagarathinam, Ph.D., and R. Vani, M.A., M.Phil.

- **Annamalai University**
  Department of English

HTML presentation, uploading it to the Internet, maintaining it in the Internet and for doing repairs when necessary.

- When we do the formatting, if we find that the paper has grammar, spelling, word choice, capitalization, phrase and sentence coherence and cogency errors, we'll edit it suitably correcting the errors mentioned above and improve the stylistic presentation. Our copy editor/s will go through the article line by line and edit the paper removing the errors. For this extra work we will charge some extra fee based on the quantum and quality of work done. Kindly note that even with this editing and formatting fee, publication of the article is heavily subsidized considering the actual costs of labor and time involved in editing, formatting, uploading, maintaining it in the Internet and doing repairs when necessary. Many journals with less indexing privileges charge Euro 100 (Indian rupees 6900 or more) per paper.
- The maximum length of an article is set at 20 pages in 1.5 line space and this includes all appendices, etc. which form part of the article. Editing and formatting fee varies with the length of the materials submitted for publication. This editing and formatting fee meets only partially the costs of editing formatting, uploading, maintaining the article in the Internet and for doing repairs when necessary. The decision to publish or not publish depends solely on the merit and relevance of the article accepted.
- Every university-approved Ph.D. dissertation is charged Indian Rupees 4500 (Indian rupees 5500 for scholars from South Asia and others working in non-South Asian countries) and M.Phil. Dissertation is charged Indian Rupees 3000 only (Indian rupees 4000 for scholars from South Asia and others working in non-South Asian countries). Masters dissertations are charged Indian rupees 2200 only (Indian rupees 3200 for scholars from South Asia and others working in non-South Asian countries). University-approved dissertations are not normally reviewed as these have already been approved after review by examiners by the universities. However, minor adjustments may be suggested for easy readability.
- Every monograph (about 150-200 pages) accepted for publication in Language in India www.languageinindia.com will be charged Indian rupees 6000 only (Indian rupees 7000 for scholars from South Asia and others working in non-South Asian countries). For fees to publish the Proceedings of the Seminars and Conferences, please contact the Managing Editor. Services offered include editorial help, formatting and academic suggestions. High Quality and relevance of research and appropriate research methodology, total avoidance of plagiarism are some of our major concerns.

Remember that Language in India www.languageinindia.com is interested in publishing articles that bring out the application of concepts and principles to Indian languages and South Asian social sciences and adjacent sciences, including English language teaching and writing in India and other South Asian nations. We also welcome papers on other languages from other nations as well, following the age-old Indian tradition of welcoming knowledge from everywhere and to serve all. If you've used any one particular concept, idea, or theory, etc., please write about your experience in using these concepts, ideas, or theories, etc., and bring out how you, your co-workers, and your students have either benefited or not. Also include how you modified and/or used these concepts in your classrooms, etc. If what I say is difficult to follow, please see some of the recent articles in Language in India www.languageinindia.com that apply concepts to Indian and South Asian contexts, etc. We are not interested in publishing a mere compendium of ideas from various sources. We are interested in publishing articles on all aspects of language structure and use.

Language in India www.languageinindia.com is an inter-disciplinary online monthly journal. So, we also seek to publish materials on all

Select Papers from the National Seminar on Subaltern Literature: Resistance and Reconstruction

Indian Writing in English: A Subaltern Perspective ...
Editor: Dr. T. Deivasigamani

Black Writings: A Subaltern Perspective ...
Editor: Dr. T. Deivasigamani

- ***English Language, Literature & Culture***
  Select Papers of the Second National Conference on English Language, Literature & Culture
  Kongunadu College of Engineering & Technology, Thottiyam, Tamilnadu, India ...
  Editor: Ms. T. Vembu, M.A., M.Phil., B.Ed., (Ph.D.)

- ***Teaching of Language and Literature*** **... Dr. Dr. S. Jayanthi, M.A., M.Phil., Ph.D., Editor**

- ***Language Learning and Teaching*** **... Dr. S. D. Sasi Kiran and Dr. A. Sharada, Editors**

- ***Building A Global Village (GV) Through Inter Dialogue*** **... Dr. S. D. Sasi Kiran and Dr. A. Sharada, Editors**

- ***Contemporary Literary Perspectives*** **... Dr. A. Sharada and Dr. S. D. Sasi Kiran, Editors**

- ***The Superhuman Character of Nature Playing Superlative Role in William Wordsworth's Poems***
  M.A. Dissertation
  Rajshahi Science and Technology University, Natore **... Mohammad Sultan Ferdous Bahar, M.A.**

- ***PROBLEMS IN TEACHING ENGLISH IN SECONDARY SCHOOLS IN NORTH TRIPURA DISTRICT***
  M.Phil. Dissertation
  SAVITRIBAI PHULE PUNE UNIVERSITY **... MALAY NATH, M.A., M.Phil.**

- ***The Speech Act of Compliment Response as Realized by Yemeni Arabic Speakers***
  Masters Dissertation
  University of Kerala **... Ameen Ali Mohammed Al-Gamal**

aspects of society and culture, research from adjacent sciences and related issues from around the world.

Kindly note that once the article or dissertation etc. is published in Language in India www.languageinindia.com, copyright rests with Language in India and any publication of the same material in outside source in print or in electronic format can be done only with the permission of Language in India www.languageinindia.com.

No new materials can be added once the article is published. Please ensure that when submitting your work, names of all authors are included. No addition of author/s after formatting of the article is done and sent to the author/s is allowed. Please avoid including Bibliography. Instead, please include only a List of References of all works cited within the text, including Internet sources. We generally follow the style sheets of APA, MLA, Indian Linguistics, IJDL and Language. But you need to restrict yourself to one style within your article. Standardization has become very difficult because Indian universities are still in the process of evolving a common style for their research publications. Readability and easy cross reference for future research should guide our authors in choosing an appropriate style in a consistent manner.

GUIDELINES FOR THE SUBMISSION OF ARTICLES IN MAJOR INDIAN LANGUAGES

Language in India www.languageinindia.com publishes articles in major Indian languages. These articles in Indian languages will be published in the PDF format for easy accessibility.

For further guidelines or clarification, please contact the Managing Editor: M. S. Thirumalai, Ph.D. via e-mail languageinindiaUSA@gmail.com.

Authors of articles using Indian scripts are advised to send their articles also in the PDF format (in addition to the Word copy) to languageinindiaUSA@gmail.com.

Language In India is a monthly online journal devoted not only to the study of the languages spoken in the Indian sub-continent, but also to the study of society (history, sociology, politics, economics, etc.) in general around the world. We wish to present the scholarly research findings on the society and related subjects including study of languages in popular language. Our focus is on language use in mass media, education and administration, speech and hearing, sociolinguistic and political aspects relating to these languages and the society in the Indian subcontinent and elsewhere. We wish to present the linguistic descriptions, interdisciplinary research, and current issues of importance relating to Indian languages. **Following the age-old tradition of Indian scholarship, the pages of this journal are open to scholarly articles on any language and society. We believe in co-operation and mutual help to foster amity between all peoples and their languages.** This online journal publishes not only articles, but also book-length reports and studies. We want to be a blessing to Indian and other languages, praying for "strength for today and bright hope for tomorrow." We sincerely believe that every language deserves our whole-hearted support for growth and that every one can find its place in a mosaic of unity and understanding, serving each other and singing the glory of God.

- ***CHALLENGES FACED BY STUDENTS IN LEARNING ENGLISH IN GRADES 11 AND 12 IN BANGLADESHI MADRASAHS***
  Masters Dissertation
  London Metropolitan University **...**
  Muhammad Nazmul Huda Azad

- ***Gender Conflicts as Evident in Contemporary English Literature o*** **...**
  Editor: Dr. R. Anuja

- ***English: Literature and Social Issues***
  ... Editor: T. Vembu, M.A., M.Phil., B.Ed., (Ph.D.)

- ***From financial literacy to financial well being;***
  a study of the level of financial literacy of women teaching faculty in educational institutions in Coimbatore region
  Doctoral Dissertation **... S. Hephzibah Priyadharshini, Ph.D.**

- ***Language Development Strategies in the Era of Globalization: Telugu***
  National Seminar Proceedings
  University of Hyderabad **... Editor: Dr. Pammi Pavan Kumar**

- ***Using English Literature in Higher Secondary EFL Classrooms in Rural Bangladesh: Bridging the Cultures to Facilitate EFL Learning***
  M.A. Dissertation ... Mossa. Sohana Khatun, M.A.

- ***Washback of the Public Examination on Teaching and Learning English as a Foreign Language (EFL) at the Higher Secondary Level in Bangladesh***
  Ph.D. Dissertation ... Md. Enamul Hoque, Ph.D.

- ***Investigating Students' Listening and Speaking Communication and Perceptions through the Implementation of Chinese Culture Content-Based Course***
  Masters Dissertation ... Xingchun Wang

- ***NEW PERSPECTIVES IN ELT***
  Selected Papers from the National Seminar on New Perspectives in ELT Conducted by the Department of English
  Theni Kammavar Sangam College of Technology, Theni 625534
  Tamilnadu, India ...
  Editors: D. Nagarathinam, Ph.D., V. Ramkumar, Ph.D. and R. Vani, M.A., M.Phil.

- **Causes for the Failure of Students in Developing Writing Skills at the HSC Level in Bangladesh Masters Dissertation ... Sukanto Roy, M.A. in ELT**

- **Selected papers from the National Seminar *NEW VISTAS IN ELT: EMPOWERING ENGINEERS FOR EMPLOYMENT* Conducted by the Department of English PSNA College of Engineering and Technology, Dindigul-624622 Tamilnadu, India ... Editors: Dr. Joseph Thomas, Ph.D. G. Vijay, M.A., M.Phil. Mrs. Shabnam Niher, M.A., M.Phil.**

- ***Bubhutsa* Papers on Telugu Language, Literature and Linguistics ... Dr. Pammi Pavan Kumar**

- **An Optimistic Evolution of Existence in *Saffron Dreams* by Shaila Abdullah ... Rabia Ashraf, M.Phil., B.S. (Hons.)**

- ***FICTION FOR CHILDREN AND YOUNG ADULTS IN INDIA: CRITICAL ESSAYS* ... Dr. Shobha Ramaswamy, M.A., B.Ed., DCE, M.Phil., Ph.D.**

- ***Opinion of the High School Teachers about the Cancellation of the SSLC Examination* ... M. Raj Kumar, M.A., M.Ed., PG.D. Ph.D. Research Scholar**

- ***SURVIVAL THROUGH REDEMPTION OF SELF IN THE SELECT NOVELS OF ALICE WALKER* ... N. R. CHARRUMATHI, M.A.., M.Phil., Ph.D.**

- ***Evil, Sin and Suffering in the Select Novels of Graham Greene* ... Suma Aleya John, M.A., M.Phil., Ph.D.**

- **Images of Women in R. K. Narayan's *The Dark Room* ... C. Malathi, M.A., M.Phil., NET, Ph.D.**

- ***Error Analysis and Paragraph Writing* ... Ali Akbar Khansir, Ph.D. Masomeh Ahrami, M.A.**

- ***ENGLISH AS A SECOND LANGUAGE - PROFICIENCY ISSUES OF JAFFNA STUDENTS* (Prescribed as a Text Book for University Undergraduates) ... Dr. V. Suntharesan, Ph.D.**

- ***Snapshot of Elementary School Thai English Teachers' Perceived English Proficiency And Self Reported English Teaching Efficacy*** **... Barbara Best, MA TESOL Candidate**

- ***IMPACT OF BORROWINGS FROM ENGLISH ON JAFFNA TAMIL* (A Text Book For University Students)** **... Dr. V. SUNTHARESAN, Ph.D.**

- ***An Exploratory Study into Factors Affecting Achievement in English among Bangladeshi College Students: An Investigation of Teachers and Students Perceptions*** **... Mohammad Mahbubur Rahman, M.A. in TESOL**

- ***The Role of Motivation in Teaching and Learning English as a Second Language at the Secondary Level*** **... Mosha. Afroza Sultana**

- ***Teaching-Learning English Grammar Papers Presented in the 10th International Conference on English Grammar, Vol. 2*** **... Editor: Dr. Vathana Fenn**

- ***Teaching-Learning English Grammar Papers Presented in the 10th International Conference on English Grammar, Vol. 1*** **... Editor: Dr. Vathana Fenn**

- ***ARCHETYPES IN FANTASY FICTION: A STUDY OF J. R. R.TOLKIEN AND J. K. ROWLING*** **... Dr. Shobha Ramaswamy, M.A., B.Ed., DCE, M.Phil., Ph.D.**

- ***IMPEDIMENTS IN PROMOTING COMMUNICATIVE COMPETENCE AMONG STUDENTS OF ENGLISH AS A SECOND LANGUAGE*** **... V. Suntharesan, Ph.D.**

- ***Writing Problems among the Tertiary Level Students in Bangladesh: A Study in Chittagong Region*** **... Shakila Mustaque, M.A. in English and M.A. in ELT**

- ***A Sociolinguistic Study of Social Stratification in Bangladesh and Its Impact on Academic Performance in English at Secondary Level Education*** **... Md. Abdur Rashid, M.A. in English and M.A. in ELT**

- ***Sri Gidugu Venkata Ramamurti's Life and His Works Papers Read in the National Seminar to Celebrate the 150th Anniversary of***

G. V. Ramamurtigaru ... **Chief Editor Dr. Pammi Pavan Kumar Co-editor Dr. Banala Bhujanga Reddy Honorary Editor Prof. S. Saratjyotsna Rani**

- *The Impact of Teachers' Beliefs on L2 Grammar Teaching* ... **Nayyer Hassan, M.A. TESOL, M.S. TESOL**
- *Tribal Languages of Kerala* ... **Ravi Sankar S. Nair, Ph.D.**
- *Teaching of Adverbials to the Tamil Speaking Learners of English* ... **S. Rajendran**
- *Drama in Indian Writing in English - Tradition and Modernity* ... **Dr. (Mrs.) N. Velmani, Ph.D.**
- *Representation of History in Rahi Masoom Reza's A Village Divided and Amitav Ghosh's The Glass Palace M.Phil. Dissertation* ... **Imran A.K. Surti**
- *Personality Style, Anxiety Sensitivity and Perceived Social Support among the Pregnant Women M.Phil. Dissertation in Clinical Psychology* ... **Mangaleshwari Manjari. N. M.Sc., M.Phil.**
- *Health and Medical Care Services: Claims on National Resources* ... **Editor: C. Subburaman, Ph.D.**
- *An Investigation into Some of the Learning Problems in English Language Writing among Lambada Community Learners in Andhra Pradesh* ... **N. Padmamma, M.Phil.**
- *Teaching Writing Using Picture Stories as Tools at the High School Level: The Movement from Other Regulation to Self Regulation* ... **Y. Nirmala, M.Phil.**
- *Current Perspectives on Education* ... **Editors: P. Udayakumar, M.Sc., M.Phil., M.Ed., M.A., Ph.D. Candidate Dr. M. Lekeshmanaswamy, Ph.D. Dr. K. Dhanalakshmi, Ph.D.**
- *Acoustic Characteristics of Vowels in Telugu* ... **Krishna. Y.**
- *Mother – Daughter Relationships: A Study of The Dark Holds No Terrors,*

Difficult Daughters and Fasting, Feasting ...
Jitender Singh, M.A., M.Phil., NET.

- *Treatment of Violence: A Study of Morrison's The Bluest Eye and Beloved* ...
Shubhanku Kochar, M.Phil., Ph.D. Candidate

- *Dyslexia: A Critical Study of Language Deficiency in Children and Adolescents* ...
Vaishali Narbheram Punjani, M.A., M.Phil. B.Ed.

- *Michael Ondaatje's Anil's Ghost and Vikram Chandra's Sacred Games as Detective Fiction* ...
S. Sridevi, M.A., M.Phil., B.Ed.

- *A Grammar of Malayalam* ...
Ravi Sankar S Nair, Ph.D.

- *The Evolution of Language Laws in Post-Independence India* ...
B. Mallikarjun, Ph.D.

- *Impact of Commercialization on Language with Special Reference to Urdu Lexicon - Doctoral Dissertation* ... ***Somana Fatimah,Ph.D.***

- *Status of English among the Kokborok and Tripura Bangla Learners in Tripura - M.Phil. Dissertation* ...
Swapan Debnath, M.A., M.Phil., Ph.D.

- *Communicative Language Teaching Approach at Higher Secondary Level in Bangladesh – Teachers' Perceptions and Classroom Practice* ... ***Md. Khaled Bin Chowdhury, M.A. (Double)***

- *A Study on Personality Factors Causing Stress among School Teachers - M.Phil. Dissertation* ... ***C. Manjula, M.A., M.Phil., Ph.D.***

- *English Language Teaching Updating the English Classroom with Techniques and Communication Skills A Book on Current ELT* ... ***Chandrika Mohan, M.A., M.A., M.Phil., C.G.T., Ph.D. Candidate***

- *A Song for the Road- Wole Soyinka's Imagery and Tradition* ... ***V. N. Manjula, Ph.D.***

- *A Linguistic Survey of Katta Varadaraju's Dwipada Ramayanam A Ph.D. Dissertation in Telugu* ...
Pammi Pavan Kumar, M.A. (Telugu) M.A. (Linguistics), M. Phil., Ph.D. (Telugu)

- ***Causes of Secondary Students' Failure in Learning English in Bangladesh - Master's Dissertation*** ***... Mian Md. Naushaad Kabir, M.A. ELT, Doctoral Researcher***

- ***Select Speeches of Mrs. Indira Gandhi English to Tamil M.Phil. Dissertation*** ***... J. Abiraami, M.A., M.Phil.***

- ***Linguistics and Literature, Department of Linguistics Silver Jubilee Volume 1*** ***... Editors: C. Sivashanmugam, Ph.D., et al.***

- ***Recent Advances in Linguistics, Department of Linguistics Silver Jubilee Volume 2*** ***... Editors: C. Sivashanmugam, Ph.D., et al.***

- ***Engineering English: A Critical Evaluation - Ph.D. Dissertation*** ***... Albert P'Rayan, Ph.D.***

- ***Kalidasa's Shakuntala and the Doctrine of Rasa*** ***... Tripti Mund, M.A., M.Phil.***

- ***Evolving Strategies for Teaching Basic Vocabulary in L2 through Meaningful Input: An Ethnographic Study with First Generation Learners*** ***... Rajakumar Guduru, M.Phil., Ph.D. Scholar***

- ***Aspects of Autobiography in Indian Writing in English*** ***... Editors: Pauline Das, Ph.D., K. R. Vijaya Murari, Ph.D., and Charu Sheela, M.A., M.Phil., M.B.A.***

- ***Imagery in Donne's Songs and Sonnets*** ***... Fatima Ali al-Khamisi, M.A.***

- ***Parsing in Indian Languages*** ***... Editors: Kommaluri Vijayanand and L. Ramamoorthy***

- ***English Language Teaching (ELT) in Saudi Arabia: A Study of Learners' Needs Analysis with Special Reference to Community College, Najran University*** ***... Dr. Mohd. Mahib ur Rahman, Ph.D.***

- ***Provision for Linguistic Diversity and Linguistic Minorities in India*** ***... Vanishree V.M., MAPL and ELT, M.A., PGDHRM.***

- ***Impact of Students' Attitudes on their Achievement in English: A Study in the Yemeni Context*** ***... Hassan Saeed Awadh Ba-Udhan***

- *A Study of B.ED. Students' Attitude Towards Using Internet in Vellore District, Tamilnadu, India* ... ***T. Pushpanathan, M.A., M.Phil., B.Ed.***
- *Development of a Hindi to Punjabi Machine Translation System, A Doctoral Dissertation* ... ***Vishal Goyal, Ph.D.***
- *A Report on the State of Urdu Literacy in India, 2010* ... ***Omar Khalidi, Ph.D.***
- *English for Medical Students of Hodeidah University, Yemen - A Pre-sessional Course* ... ***Arif Ahmed Mohammed Hassan Al-Ahdal, Ph.D. Scholar***
- *Global Perspective of Teaching English Literature in Higher Education in Pakistan* ... ***Rabiah Rustam, M.S., Ph.D. Candidate***
- *Improving Chemmozhi Learning and Teaching - Descriptive Studies in Classical-Modern Tamil Grammar* ... ***A. Boologa Rambai, Ph.D.***
- *A Phonetic and Phonological Study of the Consonants of English and Arabic* ... ***Abdulghani A. Al-Hattami, Ph.D. Candidate***
- *Some Aspects of Teaching-Learning English as a Second Language* ... ***R. Krishnaveni, M.A., M.Sc., M.Phil., Ph.D. Candidate***
- *The Influence of First Language Grammar (L1) on the English Language (L2) Writing of Tamil School Students: A Case Study from Malaysia* ... ***Mahendran Maniam, Ph.D. (ESL)***
- *Economics of Crime : A Comparative Analysis of the Socio-Economic Conditions of Convicted Female and Male Criminality In Selected Prisons in Tamil Nadu*... ***S. Santhanalakshmi, Ph.D.***
- *Technique as Voyage of Discovery: A Study of the Techniques in Dante's Paradiso* ... ***Raji Narasimhan, M.A.***
- *A Critical Study of The Wasteland - Poetry as Metaphor* ... ***K. R. Vijaya, M.A., M.Phil.***
- *Language and Literature: An Exposition - Papers Presented in the Karunya University National*

Seminar... Editor: J. Sundar Singh, Ph.D.

- *Linguistic Purism and Language Planning in a Multilingual Context ... L. Ramamoorthy, Ph.D.*
- *Papers Presented in the All-India Conference on Multimedia Enhanced Language Teaching - MELT 2009 ... L. Ramamoorthy, Ph.D. and J.R. Nirmala, Ph.D.*
- *A Phonological Study of Variety of English Spoken by Oriya Speakers in Western Orissa - A Doctoral Dissertation ... Arun K. Behera, Ph.D.*
- *Phonological Analysis of English Phonotactics of Syllable Initial and Final Consonant Clusters by Yemeni Speakers of English ... Abdulghani. M. A. Al-Shuaibi, M.A.*
- *Journey of Self-discovery in Anita Nair's Ladies' Coupé ... V. Chandra, M.A.*
- *The Literary Value of the Book of Isaiah ... Helen Unius Backiavathy, M.A., M.Phil., Ph.D. Candidate*
- *A Study of Structural Duplication in Tamil and Telugu - A Doctoral Dissertation ... Parimalagantham, Ph.D.*
- *The Politics of Survival in the Novels of Margaret Atwood ... Pauline Das, Ph.D.*
- *Nonverbal Communication in Tamil Novels - A Book in Tamil... M. S. Thirumalai, Ph.D.*

  Girish Karnad as a Modern Indian Dramatist - A Study... B. Reena, M.A., M.Phil.
- *A Study of English Loan Words in Selected Bahasa Melayu Newspaper Articles... Shamimah Binti Haja Mohideen, M.HSc. (TESL)*
- *The Internal Landscape and the Existential Agony of Women in Anjana Appachana's Novel LISTENING NOW, A Doctoral Dissertation ... M. Poonkodi, Ph.D.*
- *Trade in the Madras Presidency, 1941 - 1947 - A Doctoral Dissertation ... R. Jayasurya, Ph.D.*
- *Trends and Spatial Patterns of Crime in India - A Case Study of a District in*

India...
M. Jayamala, Ph.D.

- *The Trading Community in Early Tamil Society Up To 900 AD* ...
  R. Jeyasurya, M.A., M.Phil., Ph.D.

- *A Study of Auxiliaries in the Old and the Middle Tamil*... ***A.Boologarambai, M.A., Ph.D.***

- *History of Growth and Reforms of British Military Administration in India, 1848-1949* ...
  Hemalatha, M.A., M.Phil.

- *Language of Mass Media: A Study Based on Malayalam Broadcasts - A Doctoral Dissertation*
  ... ***K. Parameswaran, Ph.D.***

- *Form and Function of Disorders in Verbal Narratives - A Doctoral Dissertation* ...
  Kandala Srinivasacharya, Ph.D.

- *Status Marking in Tamil - A Ph.D. Dissertation*
  ... ***P. Perumalsamy, Ph.D.***

- *LANGUAGE AND POWER IN COMMUNICATION*... ***Editors: Jennifer M. Bayer, Ph.D., and Pushpa Pai, Ph.D.***

- *Onomatopoeia in Tamil* ...
  V. Gnanasundaram, Ph.D.

- *Linguistics and Literature* ...
  C.Shunmugom, Ph.D., and C. Sivashanmugam, Ph.D., V. Thayalan, Ph.D. and C. Sivakumar, Ph.D. (Editors)

- *Translation: New Dimensions* ...
  C. Shunmugom, Ph.D., and C. Sivashanmugam, Ph.D., Editors

- *Language of Headlines in Kannada Dailies* ...
  M. N. Leelavathi, Ph.D.

- *Cooperative Learning Incorporating Computer-Mediated Communication: Participation, Perceptions, and Learning Outcomes in a Deaf Education Classroom* ...
  Michelle Pandian, M.S.

- *The Effects of Age on the Ability to Learn English As a Second Language*
  ... ***Mariam Dadabhai, B.A. Hons.***

- *A STUDY OF THE SKILLS OF READING COMPREHENSION IN ENGLISH DEVELOPED BY STUDENTS OF STANDARD IX IN*

THE SCHOOLS IN TUTICORIN DISTRICT, TAMILNADU ...
A. Joycilin Shermila, Ph.D.

- *A Socio-Pragmatic Comparative Study of Ostensible Invitations in English and Farsi* ...
Mohammad Ali Salmani-Nodoushan, Ph.D.

- *TEXT FAMILIARITY, READING TASKS, AND ESP TEST PERFORMANCE: A STUDY ON IRANIAN LEP AND NON-LEP UNIVERSITY STUDENTS - A DOCTORAL DISSERTATION* ...
Mohammad Ali Salmani-Nodoushan, Ph.D.

- *A STUDY ON THE LEARNING PROCESS OF ENGLISH BY HIGHER SECONDARY STUDENTS WITH SPECIAL REFERENCE TO DHARMAPURI DISTRICT IN TAMILNADU*
K. Chidambaram, Ph.D.

- *SPEAKING STRATEGIES TO OVERCOME COMMUNICATION DIFFICULTIES IN THE TARGET LANGUAGE SITUATION - BANGLADESHIS IN NEW ZEALAND* ... ***Harunur Rashid Khan***

- *THE PROBLEMS IN LEARNING MODAL AUXILIARY VERBS IN ENGLISH AT HIGH SCHOOL LEVEL* ...
Chandra Bose, Ph.D. Candidate

- *THE ROLE OF VISION IN LANGUAGE LEARNING in Children with Moderate to Severe Disabilities* ...
Martha Louise Low, Ph.D.

- *SANSKRIT TO ENGLISH TRANSLATOR* ...
S. Aparna, M.Sc.

- *A LINGUISTIC STUDY OF ENGLISH LANGUAGE CURRICULUM AT THE SECONDARY LEVEL IN BANGLADESH - A COMMUNICATIVE APPROACH TO CURRICULUM DEVELOPMENT* ...
Kamrul Hasan, Ph.D.

- *COMMUNICATION VIA EYE AND FACE in Indian Contexts*... ***M. S. Thirumalai, Ph.D.***

- *COMMUNICATION VIA GESTURE - Indian Contexts*... ***M. S. Thirumalai, Ph.D.***

- ***CIEFL Occasional Papers in Linguistics, Vol. 10***

- ***Language Acquisition, Thought and Disorder - Some Classic Positions*...**
  M. S. Thirumalai, Ph.D.

- ***English in India: Loyalty and Attitudes***
  by Annika Hohenthal

- ***Language In Science* ...**
  M. S. Thirumalai, Ph.D.

- ***Vocabulary Education* ...**
  B. Mallikarjun, Ph.D.

- ***A Contrastive Analysis of Hindi and Malayalam* ...**
  V. Geethakumary, Ph.D.

- ***Language of Advertisements in Tamil Mass Media* ...**
  Sandhya Nayak, Ph.D.

- ***An Introduction to TESOL: Teaching English to Speakers of Other Languages* ...**
  M. S. Thirumalai, Ph.D.

- ***Transformation of Natural Language into Indexing Language: Kannada - A Case Study* ...**
  B. A. Sharada, Ph.D.

- ***How to Learn Another Language?*...**
  M.S.Thirumalai, Ph.D.

- ***Verbal Communication with CP Children* ... *Shyamala Chengappa, Ph.D. and M.S.Thirumalai, Ph.D.***

- ***Bringing Order to Linguistic Diversity - Language Planning in the British Raj***
  ...
  Ranjit Singh Rangila,
  M. S. Thirumalai,
  and B. Mallikarjun

REFERENCE MATERIAL

- ***National Education Policy 2020***
  Ministry of HRD, Government of India

- ***Some Inputs for Draft National Education Policy 2016***
  Ministry of Human Resource Development
  Government of India

- ***Tamilnadu State Policy for Children,***
  Government of Tamilnadu

- ***CENSUS OF INDIA 2011 General Data***

- ***CENSUS OF INDIA 2011 DATA ON DISABILITY***
- ***Action Plan of Centre for Classical Kannada***
- ***The Gujral Committee Report on Urdu***
- ***UNIVERSAL DECLARATION OF LINGUISTIC RIGHTS***
- ***Lord Macaulay:***
  The Man Who Started It All and His Minute
- ***Strangers In Their Own Land:***
  Campbell's Defense of Indian Vernaculars
- ***Languages of India, Census of India 1991***
- ***Mother Tongues of India, According to the 1961 Census***
- ***The Constitution of India: Provisions Relating to Languages***
- ***The Official Languages Act, 1963 (As Amended 1967)***

BACK ISSUES

- ***FROM MARCH 2001***

- ***E-mail your articles and book-length reports to languageinindiaUSA@gmail.com.***
- ***Your articles and book-length reports should be written following the MLA, APA, LSA, or IJDL Stylesheet.***
- ***The Editorial Board has the right to accept, reject, or suggest modifications to the articles submitted for publication, and to make suitable stylistic adjustments. High quality, academic integrity, ethics and morals are expected from the authors and discussants.***
- ***Would you like to announce the dates and venues of your conferences, seminars, etc., and also publish the outline proceedings of these programs? Send a report to Language in India.***

Copyright © 2022
M. S. Thirumalai

Publisher: M. S. Thirumalai, Ph.D.
11249 Oregon Circle
Bloomington, MN 55438
USA
languageinindiaUSA@gmail.com

Dr. Chiranjit Pal

BCSIR

Available online at www.banglajol.info

Bangladesh J. Sci. Ind. Res. **57(3)**, 163-172, 2022

BANGLADESH JOURNAL OF SCIENTIFIC AND INDUSTRIAL RESEARCH

E-mail: bjsir07@gmail.com

Effect of substitution of methanatoboron difluoride derivatives on non-covalent interactions with tetraphenylporphyrin

C. Pal

Department of Chemistry, Ramananda College, Bishnupur, Bankura, 722122

Abstract

Tetraphenylporphyrin (TPP) forms non-covalent supra-molecular complexes with methanatoboron difluoride (MBDF) derivatives in dichloromethane. The photo-chemical properties of the association equilibrium of free TPP and MBDFs with the respective supra-molecular complexes were investigated in the ground state. There is formation of isosbestic points which had been taken as proof of the existence of equilibrium between the absorbing species. Monte Carlo simulation and Density functional theory calculation established the experimental results of non-covalent interactions in terms of loss of planarity and frontier molecular orbital calculations defines the electron donor and acceptor. The direction of electron flow is confirmed by the electrochemical indices. The electron rich substituent in MBDF favours the non-covalent binding ability between TPP and MBDF. Both H-bonding and charge transfer interactions are primarily responsible in stabilising these complexes.

Received: 09 June 2022

Revised: 25 July 2022

Accepted: 07 August 2022

DOI: https://doi.org/10.3329/bjsir.v57i3.62018

Keyword: Methanatoboron difluoride; Tetraphenylporphyrin; Density functional theory; Electrochemical indices; Isosbestic point; Non-covalent interaction

Introduction

Porphyrins and their derivatives have been extensively studied for numerous applications due to their exceptional electrochemical and photo-physical properties. The macrocycle of porphyrin is one of the most extravagantly explored because of their importance in photochemistry, photosensitization (Kalyanasundaram *et al.,* 1987), biochemistry, biomedical (Chen *et al.,* 2021) and catalysis (Ni *et al.,* 1987). Synthetic porphyrins also have received substantial attention due to their usefulness in light harvesting materials for the construction of photovoltaic cells (Yeo *et al.,* 2017; Loewe *et al.,* 2002). Though, non-covalent interactions are quite weak but multiple intermolecular interactions cooperate in binding to form stable complexes (Mulder *et al.,* 2004; Badjić *et al.,* 2005; Pal *et al.,* 2016). Supramolecular architectures of porphyrins and their derivatives can be prepared by self-assembly based on non-covalent interaction and molecular recognition (Wu *et al.,* 2021; Villari *et al.,* 2012; Drain *et al.,* 2009; Chaudhuri *et al.,* 2010).

The supramolecular interactions between porphyrin and neutral π-acceptors have been studied for years. In recent times the chemistry of porphyrin-metal complexes is of great interest (Brothers, 2000; Brothers, 2001; Kadish, 2011). The interaction of free base porphyrins with halogen substituted borane has been the topic of attention (Belcher *et al.,* 1994; Mohajer *et al.,* 2004; Brothers, 2008; Pal *et al.,* 2017). It has been revealed that the reaction of free base *meso*-tetraphenylporphyrin (TPP) with $BF_3.Et_2O$ (boron trifluoride diethyl etherate) in wet chlorobenzene yielded a boronated adduct and in this compound two adjacent pyrrole nitrogens are bonded to each B atom with loss of -NH proton (Belcher *et al.,* 1994).

*Corresponding author e-mail: chiranjitpal2010@gmail.com

The H-bond formation between fluorine of BF_3 and -NH protons of porphyrin was also confirmed by Mohajer *et al.*, 2004 in the adduct of BF_3 and free base porphyrin. In the complex of methanatoboron difluoride (MBDF) and Cu-phthalocyanine non-covalent electrostatic interaction was confirmed by our group (Pal *et al.*, 2017).

In this communication the effect of substituents at methanatoboron difluoride moiety on the non-covalent supramolecular interaction between tetraphenylporphyrin and MBDF derivatives (Fig. 1) in ground state have been photo-physically investigated. Spectroscopic investigation of the adducts has been executed and well supported by Monte Carlo simulation and density functional theory (DFT) based computation via reactivity indices and frontier molecular orbital (FMO) descriptors. Our group had previously studied the effect of substituents at porphyrin moiety in TPP and MBDF supramolecular interaction (Pal *et al.*, 2016). The study of the effect of substitution at MBDF moiety enriches the exploration of supramolecular interaction between TPP and MBDF. The trend in equilibrium constant by varying substituent in both the moieties firmly establishes the interaction type viz., charge transfer and H-bonding as well. The need for global minima search among several local minima is accomplished here by Monte Carlo simulation which lacks in our former study. As compared to our previous study the use electrochemical indices plays vital role in establishing the direction of charge flow in this work and may be used as a tool for studying these types of interactions.

Materials and methods

Dichloromethane was used as solvent of spectroscopic grade from Merck, India. According to the reported techniques the three methanatoboron difluorides (Zhang *et al.*, 2006) and tetraphenylporphyrin (Adler *et al.* 1967) used were synthesized. In all the spectral measurements the concentration of MBDFs and TPP were taken in the range 10^{-5} and 10^{-6} M respectively.

Shimadzu UV 1800 series PC spectrophotometer fitted with an electronic temperature controller unit (TCC/240 A) was used for absorption (UV/Vis) spectral measurements. The steady state fluorescence spectra were reported with a temperature controlled Hitachi F-7000 spectrofluorometer. Constant temperature bath (Heto Holten, Denmark) was used to control the temperature within ± 0.1 K.

Using Spartan'14 molecular modelling software of Wavefunction, Inc., USA the computer simulations were executed. Merck molecular force-field calculations were implemented by using the Monte Carlo simulation to search global minima for all the optimized adducts. Gaussian 09 (Linux), Gaussian, Inc. (USA), software was used for the DFT calculations. MPW1PW91/6-31G functional was used to calculate the single point geometries and FMOs for all the free systems and their adducts.

Results and discussion

Ground state interactions

All the MBDF derivatives exhibit a strong one photon absorption ($\varepsilon > 20{,}000\ M^{-1}\ cm^{-1}$) in the 350 nm - 450 nm range in dichloromethane. This corresponding band is due to $\pi \rightarrow \pi^*$ transition and the band is somewhat narrow (50 nm – 75 nm at half-width). Only monomeric species of MBDFs are present in this working concentration range around 15 µM. This is due to the fact that the absorption changes linearly with change in concentration without any variation in spectrum. Interaction of substituted MBDF systems to the electron rich porphyrin (TPP) was examined by visible absorption spectroscopy. Three solutions of the MBDFs (MBDF2, MBDF4 and MBDF5) were titrated separately with a stock solution of TPP in dichloromethane medium. Fig. 2 shows appearance of an isosbestic point for all the MBDF systems and intensity of maximum absorption of MBDFs reduced by addition of the solution of TPP. Table I described the isosbestic points in diverse regions of the spectra on interaction of TPP with MBDF2, MBDF4 and MBDF5 in dichloromethane. Formation of isosbestic point is proof of the existence of equilibrium between two absorbing species (Hemdan *et al.*, 2019). Thus, in the ground state all the MBDFs interacts with TPP and form stable equilibrium with the respective adduct in dichloromethane. In Fig. 2, on the shorter wave length side of all the isosbestic points the peaks are corresponding to the strong S_0 to S_1 absorption of MBDFs and on addition of TPP in the solution of MBDF the intensity of maximum absorption diminishes drastically. And on the other side of the isosbestic point the peaks arises due to the formation of adduct of MBDF and TPP. The electron density could swing from the electron rich TPP to the electron deficient MBDFs and the

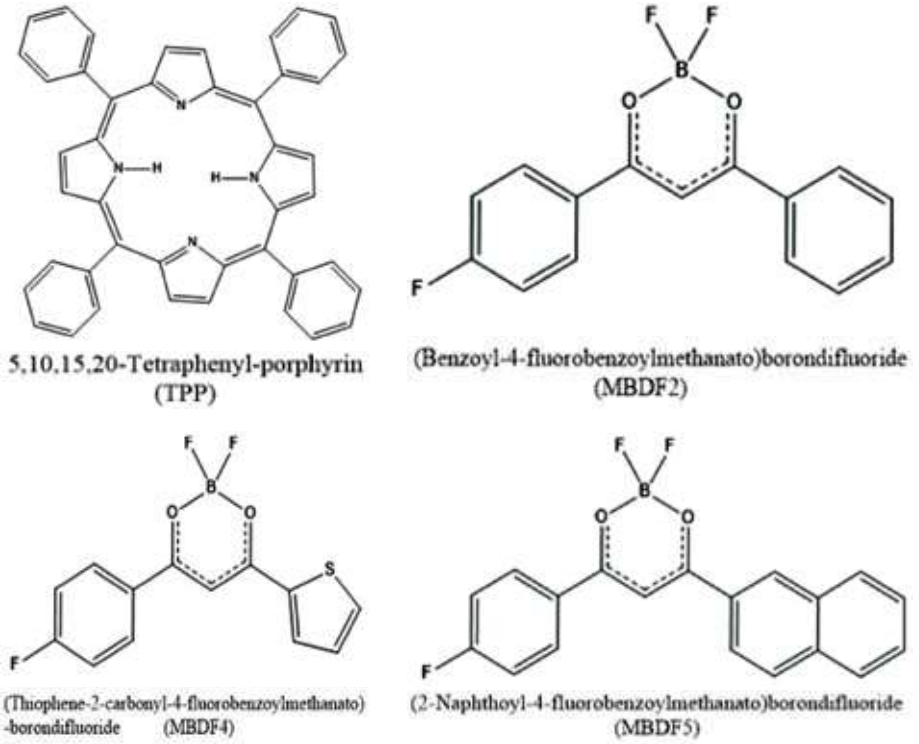

Fig. 1. Structures of the compounds used

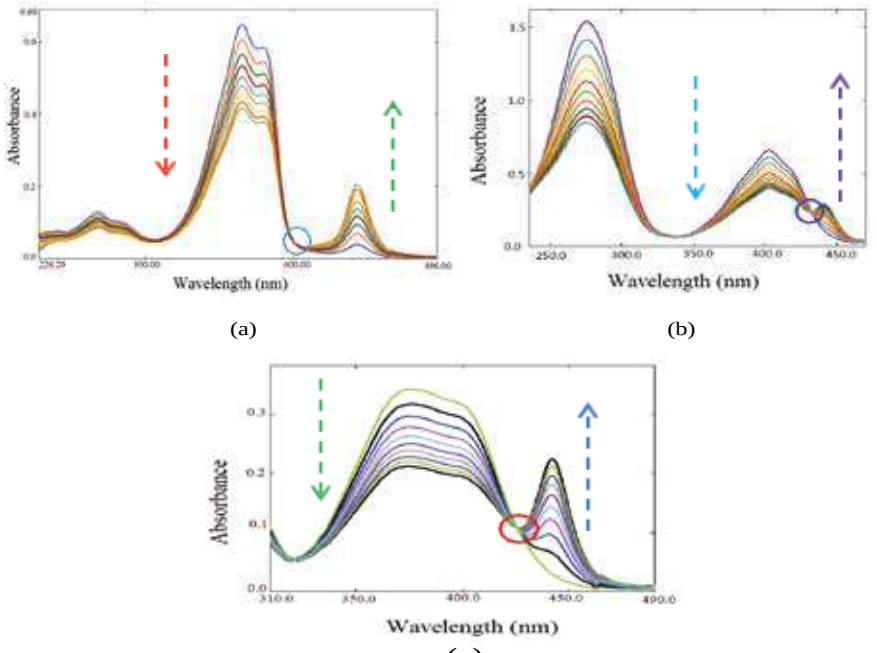

Fig. 2. Absorption spectra due to interaction of (a) MBDF2 (15.9 µM) (b) MBDF4 (15.6 µM) (c) MBDF5 (15.2 µM) with TPP (concentration was varied from 0.0 µM to 1.23 µM) in dichloromethane medium. Isosbestic points are shown within the circle

F-atoms of MBDFs can take part in H-bonding with pyrrolic N-H protons of the porphyrin. Thus, this may be of electron donor-acceptor, π-stacking and H-bonding type interaction. These interactions are well explored and supported by theoretical calculations in theoretical analysis section.

Determination of equilibrium constants

Benesi–Hildebrand equation (Benesi *et al.,* 1949) of the form (eq. 1) was used to determine the equilibrium constant reported in Table I corresponding to TPP/MBDF interaction in ground state

$$\frac{1}{d} = \frac{1}{\varepsilon[MBDF]_0} + \frac{1}{K\{\varepsilon[MBDF]_0\}[TPP]} \qquad (1)$$

where [TPP] is the concentration of the TPP and $[MBDF]_0$ is of the MBDF solution respectively, d is the absorbance of the newly formed complex and $d = [d_{mix} - d^0_{MBDF} - d^0_{TPP}]$, where $d_{mix,}$ d^0_{MBDF} and d^0_{TPP} are the absorbance of the TPP/MBDF mixture, the respective methanatoboron difluoride solution and the TPP solution at the same molar concentration present in the mixture at the same wavelength against solvent as reference. The molar absorptivity ε is that of the complex and K is the equilibrium constant of the complex. The Benesi–Hildebrand (Benesi *et al.,* 1949) method is an adequate approximation and it gives sensible values for equilibrium constant (K), has been exploited many measurements. 1:1 molecular complex formation between the TPP/MBDF was recognized by the linear BH plot at Fig. 3. Pearson's correlation coefficient and coefficient of determination (R-square) are 0.99461 and 0.98772 respectively, indicates a good quality fit. Linear regression was used to get the intercept and the slope.

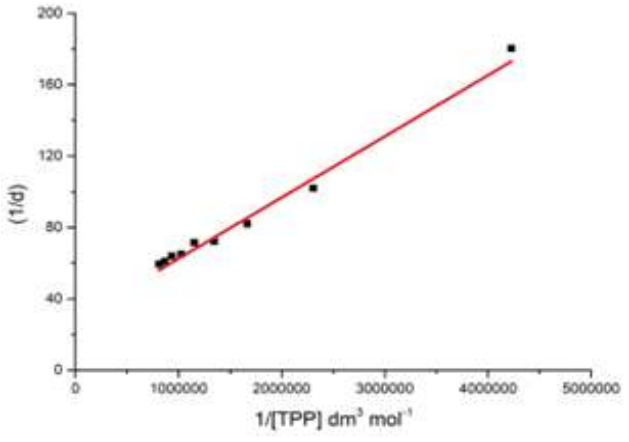

Fig. 3. BH plot of TPP/MBDF2 interacting system in methylene chloride

The complex formation between TPP and MBDF4 is the most proficient as compared to the other interacting systems in the ground state and the equilibrium constant has the order $K_{TPP/MBDF4} > K_{TPP/MBDF2} > K_{TPP/MBDF5}$. The non-covalent H-bonding interaction between the F atom of MBDF and N-H atom of TPP is the strongest in case of TPP/MBDF4 system. The electron density at MBDF ring increases drastically due to the +R effect of the thiophenyl group in MBDF4 which facilities strongest interaction among the others. On the other hand, the naphthyl substituted MBDF5 has the lowest binding constant due to predominant steric effect of the naphthyl group.

Theoretical analysis

Monte Carlo conformational search protocol (Chang *et al.,* 1989; Kong *et al.,* 2000) was used for these complexes. Density based geometry optimization calculations of the adduct structures are mostly used for studying weak intermolecular interactions such as CT, van der Waals, H-bonding, and hydrophobic interactions (Cantrill *et al.,* 2000; Bhasikuttan *et al.,* 2007). It is well known that all the optimization methods employing quantum and semi classical calculations find the local minima or transition structures near to the starting structure. However, DFT based calculations have disadvantages related to the best choice of functional for the system of interest. Many DFT methods provide poor result for weakly-bound intermolecular complexes and hydrogen bonded systems (Sholl and Steckel 2011). The conformational analysis is done for the global minimum among several local minima and energy barriers. Monte Carlo protocol (Chang *et al.,* 1989) is a well-established tool for conformational global minima searching of weakly-bonded adducts and were implemented here based on force-field molecular mechanics (Kong *et al.,* 2000), accessible in the Spartan 14 package. Conformational analysis and structural optimization of these complexes were accomplished by molecular mechanics Monte Carlo simulation and the single point energy calculations were performed by using MPW1PW91/6-31G level of DFT. Fig. 4 presents optimised geometries of the three complexes.

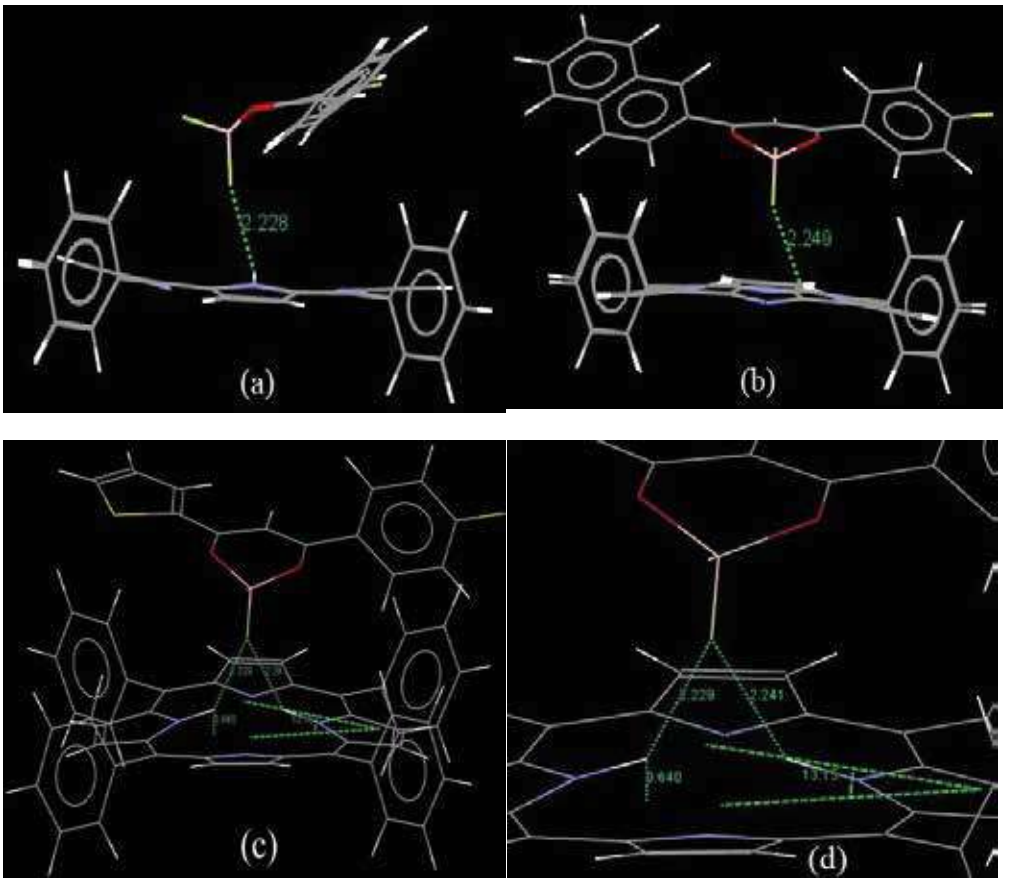

Fig. 4. Orientation of the adduct of (a) TPP/MBDF2 (b) TPP/MBDF5 (c) TPP/MBDF4 (d) TPP/MBDF4 (Zoom in view) interacting systems in optimized ground state geometry showing the interatomic distances in Å

Table I. Isosbestic point appeared on interaction of TPP with MBDFs and the ground state equilibrium constants for the corresponding three complexes

System	Absorption isosbestic point at wavelength (nm)	Ground state equilibrium constant (K) $\times 10^{-5}$
TPP/MBDF2	400.3	8.21
TPP/MBDF4	432.4	27.1
TPP/MBDF5	425.6	3.2

Table II. Parameters of the optimized ground state geometry of the adducts

System	Angles		H bond distance (Å)		distance (Å) of H atom of $N\text{-}H^1$ moiety with the plane of porphyrin ring
	N-H moiety with plane of porphyrin ring	B-F moiety with methanato ring	$N\text{-}H^1$	$N\text{-}H^2$	
TPP/MBDF2	12.51º	33.23 º	2.228	2.237	0.561
TPP/MBDF4	13.15 º	34.19 º	2.229	2.241	0.640
TPP/MBDF5	11.60 º	32.89 º	2.249	2.258	0.554

Table III. HOMO-LUMO energy parameters (electrochemical indices) of the molecules

Moiety	Electronic chemical Potential (μ) (eV)	Global electrophilicity index (ω) (eV)	Global nucleophilicity index (N) (eV)
TPP	-3.56	2.31	4.55
MBDF2	-5.10	3.34	2.44
MBDF4	-5.10	3.54	2.54
MBDF5	-4.83	3.45	2.97

There is a possibility of hydrogen bonding between the N-H protons of porphyrin moiety and B-F fluorine of MBDFs which is in close proximity to each other. In the free State the N-H protons are in a same plane with the porphyrin core. But in the complex the N-H protons go out of plane towards the F-atom of MBDFs which is adjacent to the porphyrin core and is with in H-bonding distance. Whereas the $–O-(BF_2)-O-$ group also goes out of plane towards the pyrrolic proton (Fig. 4a) which was in plane with the methanato group before adduct formation. Table II illustrates the amount of deviation from the planes of the said groups and the deviation if highest in case of MBDF4 due to better H-bonding interaction. All the different substituents of MBDF increases electron density at MBDF ring but the +R effect of thiophenyl group in MBDF4 is most effective than the +I effect of phenyl and naphthyl group. Due to the greater electron density the F-atom of $–O-(BF_2)-O-$ group becomes more negatively charged thus facilitates better electrostatic interaction with the N-H protons of TPP. The H-bonding interaction is not in agreement with the experimental trend of equilibrium constants. The reason for that is not only the hydrogen bonding but the donor to acceptor charge transfer is primarily responsible for stability of these complexes. Thiophenyl group is more electron rich as compared to the phenyl group that facilitates better charge transfer in TPP/MBDF4 complex. The charge transfer is least in case of MBDF5 due the steric effect of naphthyl group. When the donor molecule arranges itself parallel to the π-belt region of the acceptor molecule only then acceptor should interact strongly with the donor molecule. The molecular orbitals of donor and accep-

tor molecules can overlap effectively when they are able to approach quite close to each other without much steric hindrance. Both electron donor acceptor (EDA) charge transfer interaction and the hydrogen bonding contribute amply in the stability of these complexes. TPP/MBDF4 complex is favoured by both these interactions and evidently has the highest observed equilibrium constant.

Electronic chemical potential (μ), electrophilicity index (ω) and nucleophilicity index (N) of the individual isolated molecules has been calculated and displayed in Table III. The electronic chemical potential (μ) is the index to determine the direction of the electronic flux during the charge transfer within the system in its ground state (Pérez *et al.*, 2003). Higher electronic chemical potential (μ) of TPP than MBDF derivatives indicates that charge transfer occurs from TPP to MBDFs. The global electrophilicity index (ω) (Pérez *et al.*, 2003; Chattaraj *et al.*, 2006) measures the stabilization in energy when the system acquires an additional electronic charge (ΔN) from the environment. Those molecules are considered as strong electrophiles for which ω > 1.5 eV. Electrophilicity indexes (ω) of MBDF derivatives are way better than 1.5 eV. Thus, they serve as good acceptor during charge transfer interaction with TPP. The global nucleophilicity (N) index (Domingo *et al.*, 2008) value of TPP is 4.55 eV. N > 3.0 eV are said to be strong nucleophiles and thus TPP acts as a donor during charge transfer.

Frontier molecular orbital interactions

The supramolecular interaction is appropriately understood by analyzing the interaction between the frontier molecular

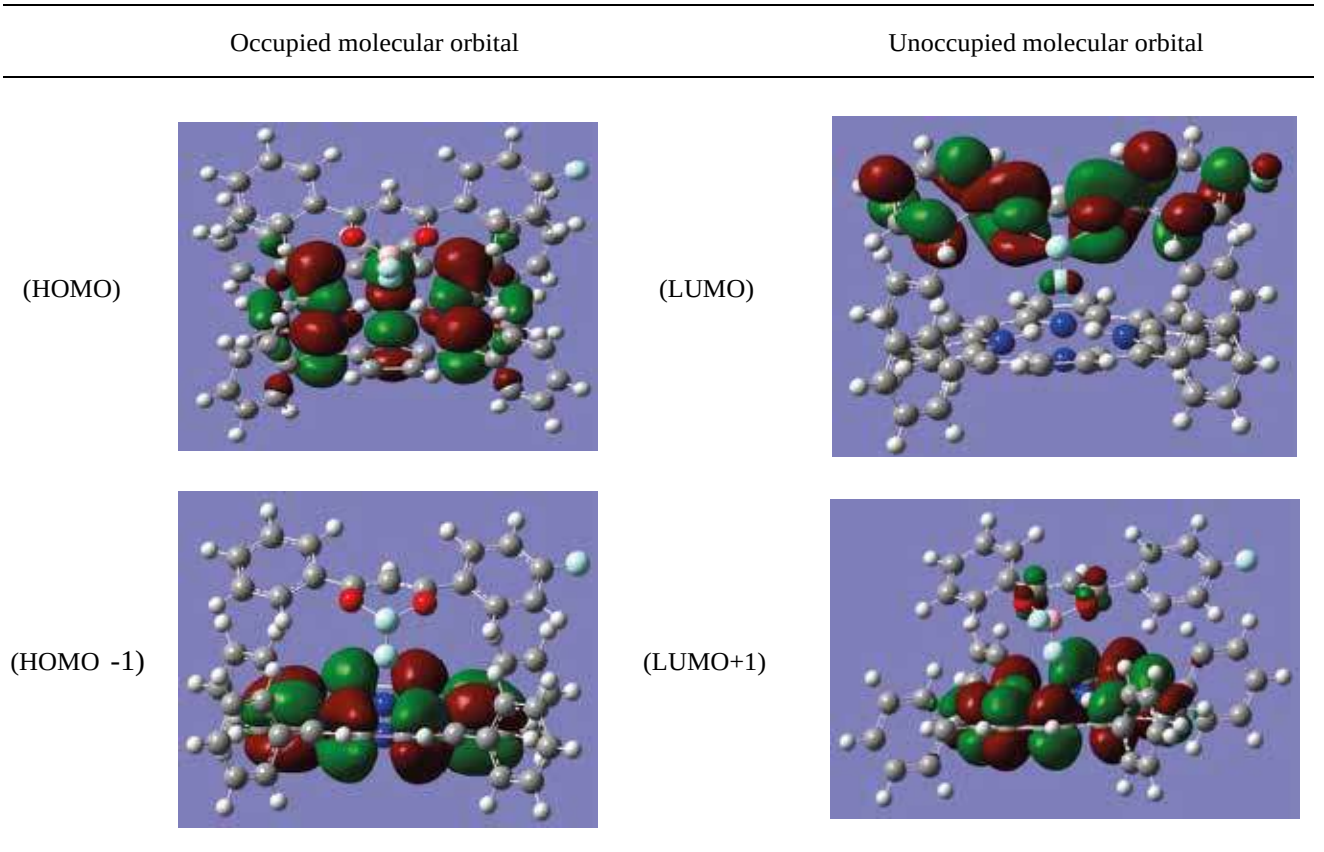

Fig. 5. Frontier molecular orbital pictures of TPP/MBDF2 interacting system

orbitals (HOMO and LUMO) of the two interacting moieties in the adducts such as the donor and the acceptor. MPW1PW91/6-31G level of density functional theory was employed to study the HOMO-LUMO interactions. Fig. 5 illustrates that the HOMO of the complexes resides primarily on TPP while LUMO is located on the acceptor MBDF2 moiety, mostly. This has reasonably substantiated the direction of electron flow in the EDA (electron donor acceptor) complex with the electron rich TPP and electron deficient MBDFs. Hence, the frontier molecular orbital picture illustrates a pictorial description of charge transfer interaction which occurs between haloborane MBDF and free base TPP.

Conclusion

Substitutions in MBDF moiety affect the binding ability with TPP significantly. All the three MBDFs form stable absorption isosbestic on titrating with TPP. DFT based geometry optimization and conformational analysis, frontier molecular orbital calculation and electrochemical indices well justifies the experimental finding of formation of ground state equilibrium. Hydrogen bonding, charge transfer and steric congestion effectively determine the binding ability as evident from the fact that the electron rich substituent in MBDF with less steric congestion favours the binding between TPP and MBDF and has the highest equilibrium constant.

Acknowledgements

The University of Burdwan, WB is acknowledged for giving the opportunity to collect experimental data. Author is very thankful to Dr. Tandrima Chaudhuri for her valuable suggestions in this work.

Declaration of Competing Interest

The author declared no conflict of interests.

References

Adler AD, Longo FR, Finarelli JD, Goldmacher J, Assour J and Korsakoff L (1967), A simplified synthesis for meso-tetraphenylporphine, *J. Org. Chem.* **32**(2): 476-476. DOI:https://doi.org/10.1021/jo01288a053

Badjić JD, Nelson A, Cantrill SJ, Turnbull WB and Stoddart JF (2005), Multivalency and cooperativity in supramolecular chemistry, *Acc. Chem. Res.* **38**(9): 723-732. DOI:https://doi.org/10.1021/ar040223k

Belcher WJ, Boyd PD, Brothers PJ, Liddell MJ and Rickard CE (1994), New coordination mode for the porphyrin ligand in the boron porphyrin complex B_2OF_2 (TTP), *J. Am. Chem. Soc*, **116**(18): 8416-8417. DOI: https://doi.org/10.1021/-ja00097a079

Benesi HA and Hildebrand JH (1949), A spectrophotometric investigation of the interaction of iodine with aromatic hydrocarbons, *J. Am. Chem. Soc.* **71**(8): 2703-2707. DOI:https://doi.org/10.1021/-ja01176a030

Bhasikuttan AC, Mohanty J, Nau WM and Pal H (2007), Efficient Fluorescence Enhancement and Cooperative Binding of an Organic Dye in a Supra-biomolecular Host–Protein Assembly, *Angew. Chem.* **119**(22): 4198-4200. DOI: https:// doi.org /10. 1002/ange. 200604757

Brothers PJ (2000), Organometallic chemistry of transition metal porphyrin complexes, Advances in Organometallic Chemistry, Elesevier **46**: 223-321. DOI: https://doi.org/10.1016/S0065-3055(00)46005-3

Brothers PJ (2001), Organoelement Chemistry of Main Group Porphyrin Complexes, Advances in Organometallic Chemistry, Elesevier **48**: 289-342.

Brothers PJ (2008), Boron complexes of porphyrins and related polypyrrole ligands: unexpected chemistry for both boron and the porphyrin, *Chem. Commun* **(18):** 2090-2102. DOI: https://doi.org/10. 1039/B714894A

Cantrill SJ, Pease AR and Stoddart JF (2000), A molecular meccano kit, *J. Chem. Soc., Dalton trans.* **(21)**: 3715-3734. DOI: https://doi.org/10.1039/B003769I

Chang G, Guida WC and Still WC (1989), An internal-coordinate Monte Carlo method for searching conformational space, *J. Am. Chem. Soc.* **111**(12): 4379-4386. DOI:https://doi.org/10.1021/-ja00194a035

Chattaraj, PK, Sarkar U and Roy DR (2006), Electrophilicity index, *Chem. Rev.* **106**(6): 2065-2091. DOI: https://doi.org/10.1021/cr078014b

Chaudhuri T, Nath S, Chattopadhyay S, Banerjee M and Nayak SK (2010), Supramolecular interactions of meso-tetra-2-chlorophenylporphyrin with fullerenes: A luminescence study, *J. Lumin.* **130**(3): 507-511. DOI: https://doi.org/10.1016/j.jlumin.2009.10.022

Chen J, Zhu Y and Kaskel S (2021), Porphyrin-Based Metal–Organic Frameworks for Biomedical Applications, *Angew. Chem. Int. Ed.* **60**(10): 5010-5035. DOI:https://doi.org/10.1002/anie.201909880

Domingo LR, Chamorro E and Pérez P (2008), Understanding the reactivity of captodative ethylenes in polar cycloaddition reactions: A theoretical study, *J. Org. Chem.* **73**(12): 4615-4624. DOI: https://doi.org/10.1021/jo800572a

Drain CM, Varotto A and Radivojevic I (2009), Self-organized porphyrinic materials, *Chem. Rev.* **109**(5): 1630-1658. DOI: https:// doi.org/ 10.1021/cr8002483

Hemdan S, Mansour A and Ali F (2019). Importance of isosbestic point in spectroscopy: A review. **62:** 1-21. DOI: 10.37376/1571-000-062-004.

Kadish KM, Smith KM and Guilard R (2011), The porphyrin handbook, (Academic Press, USA) 2011, **17**: 1-20.

Kalyanasundaram K, Vlachopoulos N, Krishnan V, Monnier A and Graetzel, M (1987), Sensitization of titanium dioxide in the visible light region using zinc porphyrins, *J. Phys. Chem.* **91**(9): 2342-2347. DOI: https://doi.org/10.1021/j100293a027

Kong J, White CA, Krylov AI, Sherrill D, Adamson RD, Furlani TR, ... and Pople JA (2000), Q-Chem 2.0: a high-performance ab initio electronic structure program package, *J. Comput. Chem.* **21**(16): 1532-1548. DOI: 10.1002/1096987X(200012)21:16%3C1532::AIDJCC10%3E3.0.CO;2-W

Loewe RS, Tomizaki KY, Youngblood WJ, Bo Z and Lindsey, J. S. (2002), Synthesis of perylene–porphyrin building blocks and rod-like oligomers for light-harvesting applications, *J. Mater. Chem.* **12**(12): 3438-3451. DOI: https:// doi.org/ 10.1039/B205680A

Mohajer D, Zakavi S, Rayati S, Zahedi M, Safari N, Khavasi HR and Shahbazian S (2004),Unique 1:2 adduct formation of meso-tetraarylporphyrins and meso-tetraalkylporphyrins with BF_3: a spectroscopic and ab initio study, *New J. Chem.* **28**(12): 1600-1607. DOI: https://doi.org/10.1039/B407529C

Mulder A, Huskens J and Reinhoudt DN (2004), Multivalency in supramolecular chemistry and nanofabrication, *Org. Biomol. Chem. 2*(23): 3409-3424. DOI:https://doi.org/10.1039/B413971B

Ni CL, Abdalmuhdi I, Chang CK and Anson FC (1987), Behavior of four anthracene-linked dimeric metalloporphyrins as electrocatalysts for the reduction of dioxygen, *J. Phys. Chem.* **91**(5): 1158-1166. DOI: https://doi.org/10.1021/j100289a028

Pal C, Chaudhuri T, Chattopdhyay S and Banerjee M (2017), Non-covalent interaction between Cu-phthalocyanine and methanato borondifluoride derivatives in two different medium, *J. Mol. Struct.* **1133**: 95-100. DOI:https://doi.org/10.1016/j.molstruc.2016.11.079

Pal C, Chaudhuri T, Nayak SK and Banerjee M (2016), Chemical physics of non-covalent interaction between tetraphenylporphyrin and (dibenzoylmethanato) borondifluoride in methylene chloride, *J. Indian Chem. Soc.* **93**(9): 1095-1102. DOI:10.5281/zendo.5639437

Pérez P, Domingo LR, Aurell MJ and Contreras R (2003), Quantitative characterization of the global electrophilicity pattern of some reagents involved in 1, 3-dipolar cycloaddition reactions, *Tetrahedron* **59**(17): 3117-3125. DOI: https:// doi.org/10.1016/S0040-4020(03)00374-0

Sholl D and Steckel JA (2011), Density functional theory: a practical introduction, (John Wiley & Sons, Inc., New Jersey) 2009, pp 1-256

Villari V, Mineo P, Scamporrino E and Micali N (2012), Role of the hydrogen-bond in porphyrin J-aggregates, *RSC Adv.* **2**(33): 12989-12998. DOI: https://-doi. org/10. 1039/C2RA22260D

Wu Y, Liu JC, Li RZ and Ci CG (2021), Different Metal Upper Porphyrin Based Self-Assembly Sensitizers

for Application in Efficient Dye-Sensitized Solar Cells, Available at SSRN 3906184. DOI: https://-doi.org/10.1016/j.poly.2021.115573

Yeo H, Tanaka K and Chujo Y (2017), Construction and properties of a light-harvesting antenna system for phosphorescent materials based on oligofluorene-tethered Pt–porphyrins, *RSC adv.* **7**(18): 10869-10874. DOI: https:// doi.org/ 10.1039/ C6RA28735B

Zhang X, Li ZC, Xu N, Li KB, Lin S, Lu FZ and Li FM (2006), β-Diketones bearing electron-donating chromophores and a novel β-triketone: synthesis and reversible fluorescence behaviour, *Tetrahedron lett*. **47**(15): 2623-2626. DOI: https:// doi.org/ 10.1016/-j.tetlet.2006.02.019

R.D.Mukhopadhyay

Chem

CellPress

Article

Out-of-equilibrium chemical logic systems: Light- and sound-controlled programmable spatiotemporal patterns and mechanical functions

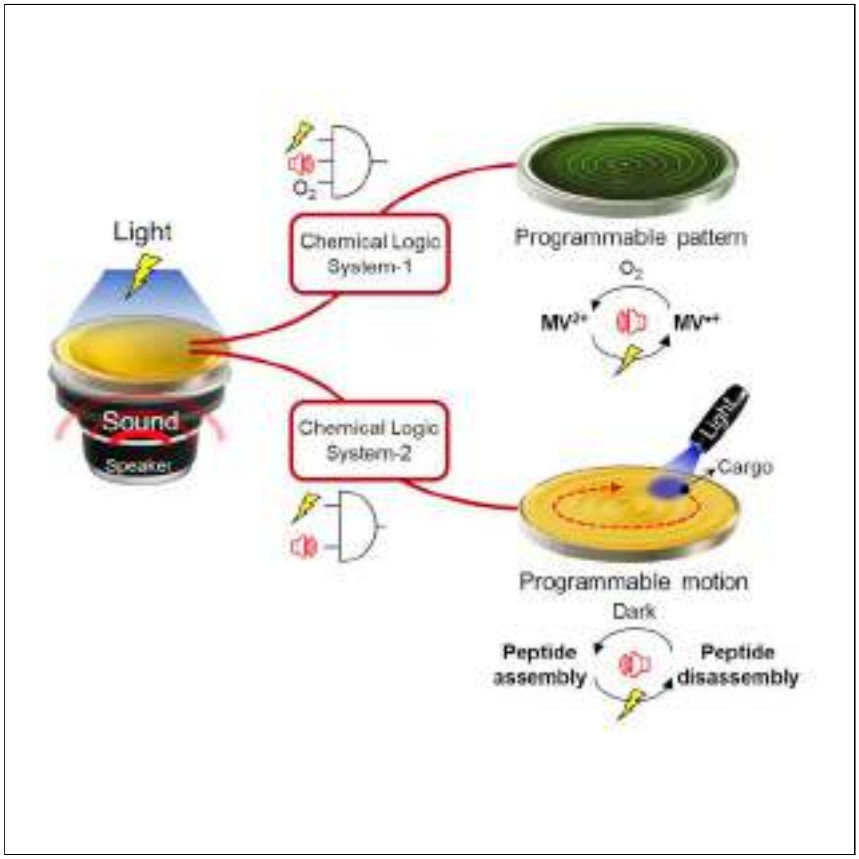

Binary-logic-based information processing in controlling out-of-equilibrium chemical systems to control and execute complex and transient biomimicking functions remains elusive. Herein, we designed out-of-equilibrium chemical systems, which can be controlled through the concerted participation of various physical (light and audible sound) and chemical (oxygen and pH) stimuli. These systems process the information obtained from various external inputs following the rules of Boolean logic, which ultimately leads to a programmed spatiotemporal function such as pattern formation and transporting a cargo through a maze.

Seoyeon Choi, Rahul Dev Mukhopadhyay, Shovan Kumar Sen, Ilha Hwang, Kimoon Kim

rdevmukherjee@gmail.com (R.D.M.)
kkim@postech.ac.kr (K.K.)

Highlights

Controlling out-of-equilibrium systems with light, sound, and chemical inputs

Programming chemical logic systems to execute spatiotemporal functions

Generation of repetitive spatiotemporal patterns

Execution of complex mechanical functions such as guiding a cargo through a maze

Choi et al., Chem 8, 2192–2203
August 11, 2022 © 2022 Elsevier Inc.
https://doi.org/10.1016/j.chempr.2022.04.020

CellPress

Chem

Article

Out-of-equilibrium chemical logic systems: Light- and sound-controlled programmable spatiotemporal patterns and mechanical functions

Seoyeon Choi,[2] Rahul Dev Mukhopadhyay,[1,4,*] Shovan Kumar Sen,[1] Ilha Hwang,[1] and Kimoon Kim[1,2,3,5,*]

SUMMARY

Living systems at different scales function through the sensing of multiple external signal inputs, which are further processed based on binary or more complicated computational models and networks. Inspired by such behavior, here, we show that the information processing in out-of-equilibrium chemical systems utilizing binary Boolean logic can be exploited to obtain transient functions such as spatiotemporally controlled chemical gradients and patterns in response to specific combination of multiple physical or chemical inputs (light, audible sound, and O_2). We further explore systems that are able to execute highly complicated functions such as guiding a cargo through a maze by processing the information from multiple external stimuli. Our approach of integrating and encoding binary Boolean logic within out-of-equilibrium chemical systems for the extraction of mechanical work to execute transient biomimicking functions can expand the realms of systems chemistry and related research and help us design smart materials.

INTRODUCTION

Living systems ranging from the size of a single cell to higher organisms such as animals and human beings obtain specific information (physical or chemical input signals) through their sensory systems, which is thereafter processed based on basic binary logic as well as complex computational algorithms to program much more complicated spatiotemporal functions, e.g., cell division, cell motility, cargo transport, etc. (Figure S1A).[1,2] In the recently passed epoch, the pursuit of making programmable life-like systems in the lab has therefore led to the exploration of complex chemical or biological networks that operate out of equilibrium, where different components interact with each other following a certain logic or program to give rise to a collective emergent behavior.[3–14] However, the possibility of integrating such binary Boolean logic in programming out-of-equilibrium chemical systems (CSs) to obtain transiently functional materials has so far been a daunting task.[3,15–17] If such modules can be created utilizing chemical logic systems (**CLSs**) that encode binary logic and carry out information processing, it may pave the way toward smart systems capable of executing complex biomimicking functions.

Among other physical stimuli, the use of audible sound in controlling chemical processes is still in its infancy.[18–22] Very recently, our group utilized audible sound to control redox-sensitive and pH-sensitive out-of-equilibrium CSs.[23] We anticipated that our approach can offer an alternate strategy to control the spatiotemporal distribution of out-of-equilibrium chemical network systems through the participation

THE BIGGER PICTURE

The complexity of biological processes and their programmability has kindled the imagination of researchers since decades. Exact mimicking of these complex processes to execute life-like functions still remains a distant goal. However, constant efforts are being dedicated to develop artificial life based on the limited knowledge that we have gained on various biological systems and intercellular processes. Among these, the exploration of out-of-equilibrium chemical systems has gained special attention in recent years. Nevertheless, the control over such systems with multiple input signals and programming them using basic Boolean logic for the execution of smart functions remain a challenging task. The present use of light, sound, and chemical inputs in out-of-equilibrium chemical logic systems addresses the aforementioned challenges. The long-term goal in this direction is to increase the complexity of such chemical logic systems and perform more complicated functions.

CellPress

of various chemical (reducing agents, acid, atmospheric gases, etc.) and physical stimuli (sound, light, etc.), maintaining the rules of binary logic to mimic biological processes such as spatiotemporally controlled chemical gradients, patterns, etc. In a seminal work,[24] Hermans and coworkers have demonstrated such features with out-of-equilibrium functional supramolecular polymers.[25,26] We thought of taking this challenge a step ahead by controlling the spatiotemporal location of nanoaggregates of such supramolecular polymers in solution to execute even higher level complex functions under out-of-equilibrium conditions.[27,28] We anticipated that the presence of nanoaggregates having different physical and chemical properties within different locations in a solution can segregate a solution into property-specific spatiotemporal domains, which would be useful in the execution of macroscopic functions such as extraction of mechanical work.[29–32] The topography of liquid surface generated by standing waves has previously been used as a template to assemble floating beads in programmable patterns.[33] We therefore thought of utilizing audible sound generated concentric surface waves as templated tracks for the programmed movement of a floating cargo.

Among the vast examples of mechanical work by systems exhibiting life-like behavior that involves collective intelligence,[32] solving a maze involves locating and reaching a specific target avoiding collisions with physical hurdles encountered along the way.[34] So far, maze solving has been explored using both active (self-propelled) and passive (that needs to be guided) particles through chemotaxis, phototaxis, magnetotaxis, etc.[35–39] Nevertheless, the use of audible sound to guide a passive cargo through a maze is hitherto unknown.

Herein, we demonstrate that the concerted participation of various physical and chemical stimuli, which follows the rules of Boolean math, can be utilized to obtain a programmed spatiotemporal distribution of out-of-equilibrium CSs to program spatiotemporal patterns, chemical gradients, and most importantly, transient mechanical functions (Figure S1B). For instance, the pH-responsive nanoaggregates of a peptide-based gelator can be controlled with light in the presence of a photoacid, leading to a spatiotemporal change in the surface tension of the solution, which further induces motion in a passive floater (cargo) due to the Marangoni effect. The application of audible sound provides specific tracks for cargo movement through the generation of surface waves. An algorithm based on binary logic is further set up to successfully navigate the floating cargo through a maze.

RESULTS AND DISCUSSION

Controlling spatiotemporal pattern formation

Design of multistimuli-responsive redox chemical system for pattern formation: Chemical system 1 (CS1)

As a model multiple stimuli-responsive system, we chose the redox chemistry of methyl viologen ($MV^{2+}/MV^{\bullet+}$), which is known to form spatiotemporal patterns upon dissolution of atmospheric oxygen in solution under normal conditions. Such spatiotemporal patterns can be reproducibly obtained by controlling the dissolution of oxygen in water using audible sound-induced vibration of the air-water interface.[23] MV^{2+} is known to get reduced to its radical cationic ($MV^{\bullet+}$) form through photoinduced electron transfer in the presence of $[Ru(bpy)^3]^{2+}$ (bpy = 2,2′-bipyridine) and triethanolamine (TEOA), which acts as a photosensitizer and sacrificial reductant, respectively (Figure 1A).[40–43] It is therefore possible to control the spatiotemporal chemical distribution in a photoredox-based CS consisting of MV^{2+}, $[Ru(bpy)^3]^{2+}$, and TEOA, which we now call CS1, using a triad of external stimuli, namely light, sound, and oxygen (Figure 1B).

[1]Center for Self-assembly and Complexity (CSC), Institute for Basic Science (IBS), Pohang 37673, Republic of Korea

[2]Division of Advanced Materials Science, Pohang University of Science and Technology (POSTECH), Pohang 37673, Republic of Korea

[3]Department of Chemistry, Pohang University of Science and Technology (POSTECH), Pohang 37673, Republic of Korea

[4]Present address: Department of Chemistry, Ramananda College, Bankura University, Bishnupur 722122, West Bengal, India

[5]Lead contact

*Correspondence: rdevmukherjee@gmail.com (R.D.M.), kkim@postech.ac.kr (K.K.)

https://doi.org/10.1016/j.chempr.2022.04.020

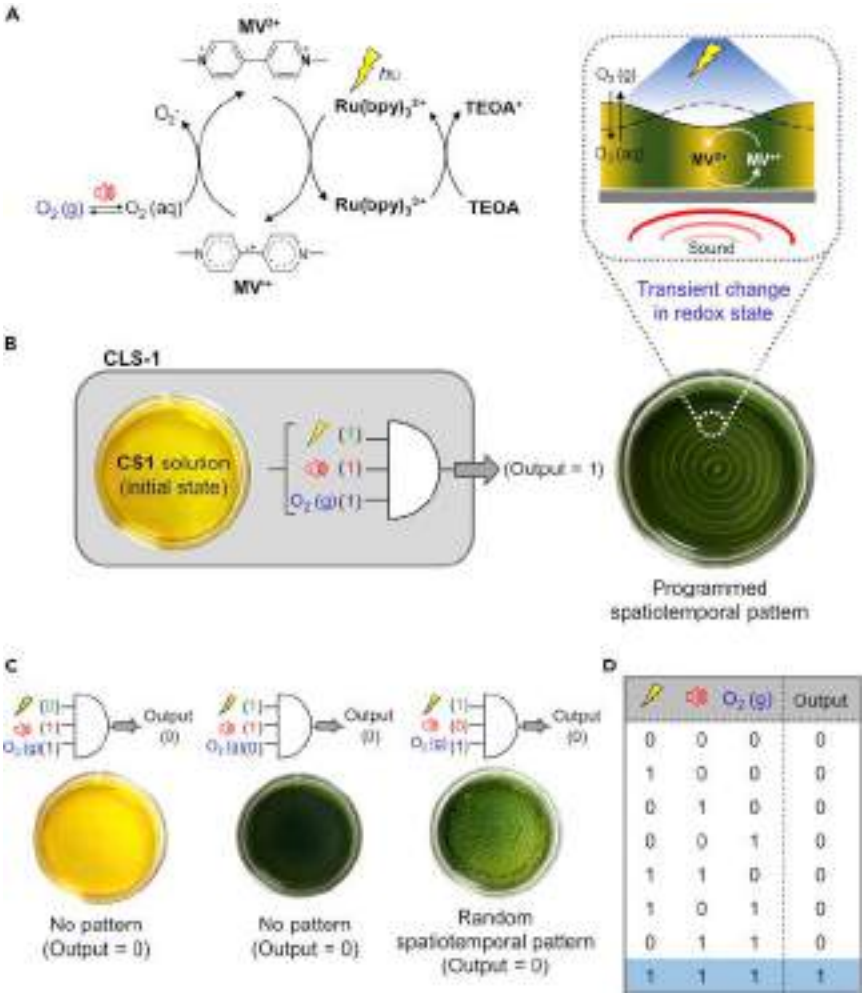

Figure 1. Boolean logic-regulated spatiotemporal pattern formation

(A) CS1 based on the photoreduction of MV^{2+} in the presence of $[Ru(bpy)^3]^{2+}$ and **TEOA**. Here, the redox state of MV^{2+} is regulated by a triad of chemical and physical inputs (e.g., light, audible sound and O_2 [g]). Composition: $[MV^{2+}]$ = 2.0 mM, $[[Ru(bpy)^3]^{2+}]$ = 0.4 mM, [**TEOA**] = 7.0 mM and [glycerol] = 20 wt % in deionized water.

(B) CLS-1 processes the information from three inputs (e.g., light, sound, and O_2 [g]) based on AND logic and produces a spatiotemporal concentric ring pattern as a specific function or output. The inset shows a schematic representation of the cross-sectional view of the **CS1** solution exposed to light irradiation, sound waves, and atmospheric O_2.

(C) Results of pattern experiments in the presence of a combination of two input signals.

(D) Complete truth table obtained from the pattern formation experiments, which correspond to a triple-input AND logic-gate circuit. Audible sound input frequency: 40 Hz.

On irradiating a yellow-colored solution of CS1 placed in a Petri dish (Figure S2) with visible light ($\geq$400 nm, 40 s), a dark green solution was obtained (due to the generation of $MV^{\bullet+}$). When exposed to air, in the absence of any external sound input, a random spatiotemporal pattern was generated (Figure 1C, extreme right). On vibrating the $MV^{\bullet+}$-rich solution with audible sound within a suitable range of frequencies (35–40 Hz) and amplitudes (0.06–0.08 g), it gradually reorganized into a spatiotemporal pattern consisting of dark green and yellow concentric rings (Figure S3; Video S1). To suppress the audible sound-induced lateral flow,[23,44] we increased the viscosity of the solution using glycerol (20 wt%),[45] which resulted in the formation of a concentric ring pattern reproducibly over several cycles. During

the pattern generation process, the nodal regions with minimum vibration show lesser oxygen dissolution and retain the pre-existing green color of the solution, whereas in the antinodal regions, where the vibration is maximum, oxygen dissolves more efficiently into the solution and reoxidizes it back to its yellow state (Figure 1B, right panel-inset).[23] The nodal and antinodal positions are obtained with the same frequencies at the same locations in the solution for all trials (Figure 1B, right panel) making the colored spatiotemporal $MV^{2+}/MV^{\bullet+}$ patterns, the same and predictively reproducible over several cycles.

Boolean logic-regulated pattern formation

The aforementioned **CS1** can process the information from the input signals and produce a specific output in its response. To explain the information processing platform in terms of binary logic, we considered the formation of the concentric ring pattern as the desired output (1) and any other result as an undesired output (0). The desired concentric ring pattern was observed only when the three inputs (light, sound, and O_2) were applied simultaneously (Video S2).[46] As shown in Figure 1, the absence of any one of the three inputs results in an undesired outcome. For instance, under dark conditions, MV^{2+} in **CS1** remains in its inherent state, and the color of the solution remains yellow, whereas under an inert atmosphere, the solution turned green on being irradiated, and MV^{2+} prefers to stay in its reduced state ($MV^{\bullet+}$) for longer periods of time. In the absence of the audible sound, a random maze-like spatiotemporal pattern was observed. It can therefore be inferred that the out-of-equilibrium CLS, which we now call CLS-1, exhibits an AND logic-gate response toward the three inputs: light, sound, and O_2 (Figures 1B and 1C). A truth table summarizing the outputs obtained in all possible combinations of the inputs is provided in Figure 1D.

Repetitive spatiotemporal pattern

In general, a control over spatiotemporal patterns and functions obtained in presence of light irradiation usually involves the use of a photomask.[13,27] However, in the present case, a spatiotemporal pattern is obtained via light irradiation (in presence of sound and O_2) even without using a photomask. We were therefore interested in studying our pattern generation process in the presence of a photomask. Time-dependent changes during the pattern generation process revealed that on continued exposure of a spatiotemporal pattern obtained from **CLS-1** to a sound source (40 Hz) and O_2, the initial state (prominent dark green regions) of the pattern was gradually transformed to a partially decayed state (prominent yellow regions) and ultimately to a completely oxidized state (yellow-colored solution) (Figures 2A and S3). The initial state can however be recovered by irradiating the partially decayed state of the pattern (for 40 s) in the presence of sound and O_2 (Figure 2A). This strategy can be utilized to obtain a repetitive spatiotemporal pattern by refueling **CLS-1** with photoirradiation and draining it under dark conditions for several repeated cycles (Figure S5; Video S3).

We thought it may be possible to control the existing chemical gradients within the pattern by irradiating a selective area of the pattern through a semicircular photomask (Figures 2B and S6; Video S4) in the presence of sound and O_2. Indeed, we observed that the pattern gradually progressed to its partially decayed state under the mask, whereas in the unmasked area, the initial state of the pattern was redeveloped. The chemical gradients that exist in the initial and the partially decayed states of the pattern could be swapped by changing the position of a semicircular photomask over alternate halves in the subsequent cycles (Figure 2B).

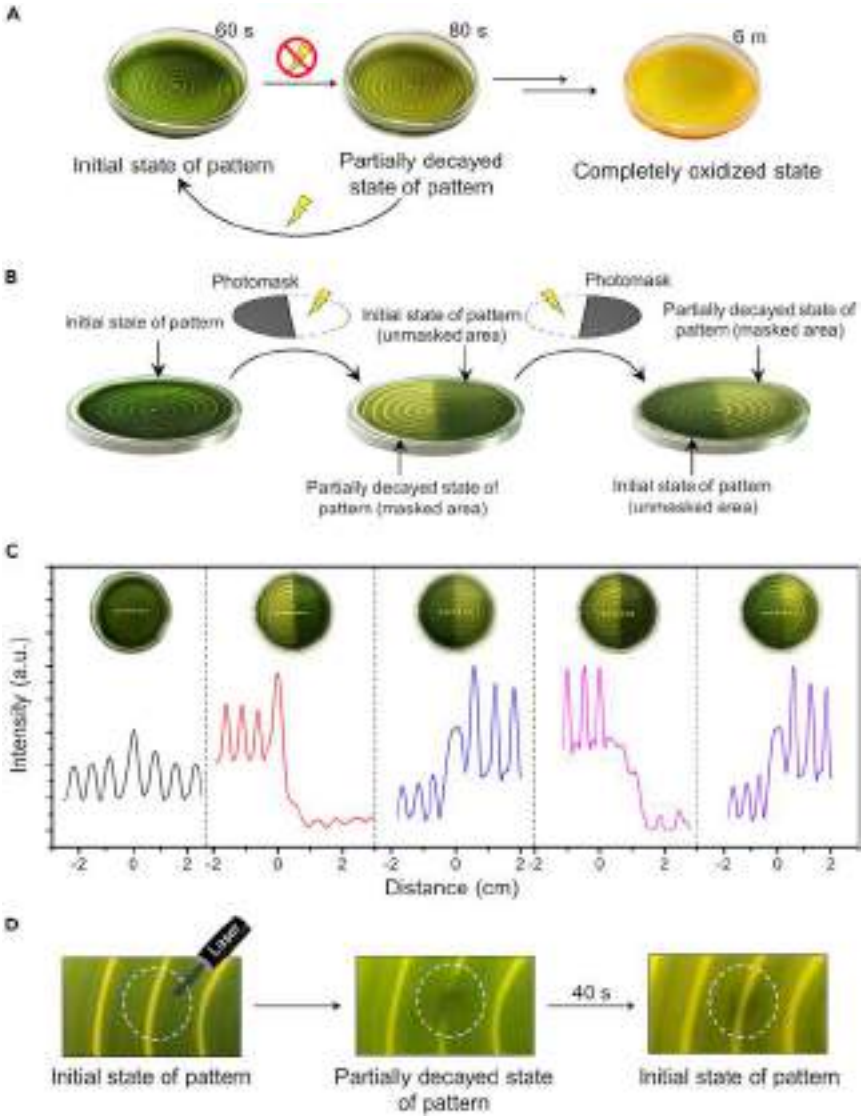

Figure 2. Repetitive spatiotemporal patterns

(A) Time-dependent changes during repetitive pattern generation with irradiated **CLS-1** in presence of sound and O_2. Recovery of the initial state by irradiating the partially decayed state of the pattern (40 s).

(B) Repetitive spatiotemporal patterns generated within the alternate halves of the Petri dish by irradiating it through a semicircular photomask in presence of sound and O_2.

(C) Color intensity profiles extracted from pattern images obtained from the experiment described in Figure 2B.

(D) Chemical composition tweaked at a specific point within the pattern aided by a laser (405 nm) beam in presence of sound and O_2. Audible sound input frequency: 40 Hz.

To further study the changes in the chemical gradients within the pattern, we analyzed the pattern images from different irradiation cycles in Figure 2C. We then compared the color intensities of the individual lines within the concentric ring pattern, which corresponds to the chemical gradients present within the solution (see supplemental information). The color intensity profile was evenly distributed at the beginning (black trace). However, the profiles obtained from the subsequent images clearly suggested the alteration in the chemical gradients in each concentric ring across the two semicircular domains of the spatiotemporal pattern

CellPress

(Figure 2C). Figure S7 and Video S5 show the possibility to obtain different types of repetitive spatiotemporal patterns utilizing different photomasks. The chemical composition at a specific point was further controlled by using a laser pointer (405 nm, 50 mW) (Figure 2D; Video S6). On irradiating a particular point located over a yellow line, we observed the line was erased due to transient generation of $MV^{\bullet+}$. The chemical transformation was however spatiotemporal, and the original pattern was recovered within few seconds due to the sound-assisted expedited oxidation.

Programmed cargo transport and maze solving

Design of out-of-equilibrium self-assembling chemical system for extraction of mechanical work: Chemical system 2 (CS2)

The binary control over the spatiotemporal distribution of out-of-equilibrium supramolecular nanoassemblies imparting different physical properties, e.g., surface tension, viscosity, etc., may be exploited to execute even higher level functions such as extraction of mechanical work.[32,47] We therefore screened a variety of multistimuli-responsive self-assembled systems to explore such applications. Among these, we chose a photocontrolled pH-responsive nanoaggregate system previously studied by Li and coworkers,[48] consisting of diphenylalanine (**FF**) gelator and a protonated merocyanine-based photoacid generator (**MEH**) (CS2). We observed that the system not only exhibited a fast and reversible aggregation behavior but also a reversible change in surface tension of the solution in response to blue light irradiation. Irradiation of blue light causes **MEH** to undergo a ring-closing reaction and convert to its spiropyran (**SP**) form and thereby donate a proton resulting in the disassembly of **FF** nanoaggregates (Figure 3A). This phototriggered transformation between aggregates in combination with sound waves can be used for programmable cargo transport (Figure 3B, right panel). Under dark conditions, the reformation of the nanoaggregates occurs, following the **SP** to **MEH** transformation. The average size of the nanoaggregates dispersed in the CS2 solution estimated by dynamic light scattering (DLS) decreased from 106 to 60 nm after 20 s of photoirradiation (10 W, $\lambda \geq 400$) and recovered after being kept in the dark for 20 s (Figure S8A). A concomitant transient decrease in the light scattering intensity was also observed on the photoinduced dissolution of the nanoaggregates. The morphological transformations between the hierarchical structures formed from these nanoaggregates were further studied by atomic force microscopy (AFM) (Figures S8B and S8C) and scanning electron microscopy (SEM) (Figure S9). Morphological analysis of the **CS2** solution showed the presence of rigid nanofibers (120 nm in height), which were transformed into short rod-shaped aggregates (40–80 nm in height) after 20 s of photoirradiation. Under dark conditions, the rigid nanofiber morphology was recovered (Figure S8). Interestingly, the switching between the out-of-equilibrium nanoaggregates was also accompanied by reversible and transient changes in the surface tension of the solution (Figure 3C).[49,50] We observed a reversible transient decrease in the surface tension of the nanoaggregate dispersion after 5 s of light irradiation (405 nm, 50 mW), where the maximum change in surface tension ($\Delta\gamma$) was ~3 mN/m (Figure S10). The **CS2** solution can be utilized for designing a CLS-2 to execute a Boolean logic-controlled motion of a cargo using light and sound as inputs (Figures 3B and 3D), as described in the next section.

Boolean logic-regulated cargo movement

Having established the conditions required to trigger maximum changes in surface tension upon light irradiation, we placed a styrofoam-based floating cargo on the solution surface of the **CS2** and irradiated it with a laser pointer (405 nm, 50 mW). The spatiotemporal surface tension gradient created by light irradiation led to a

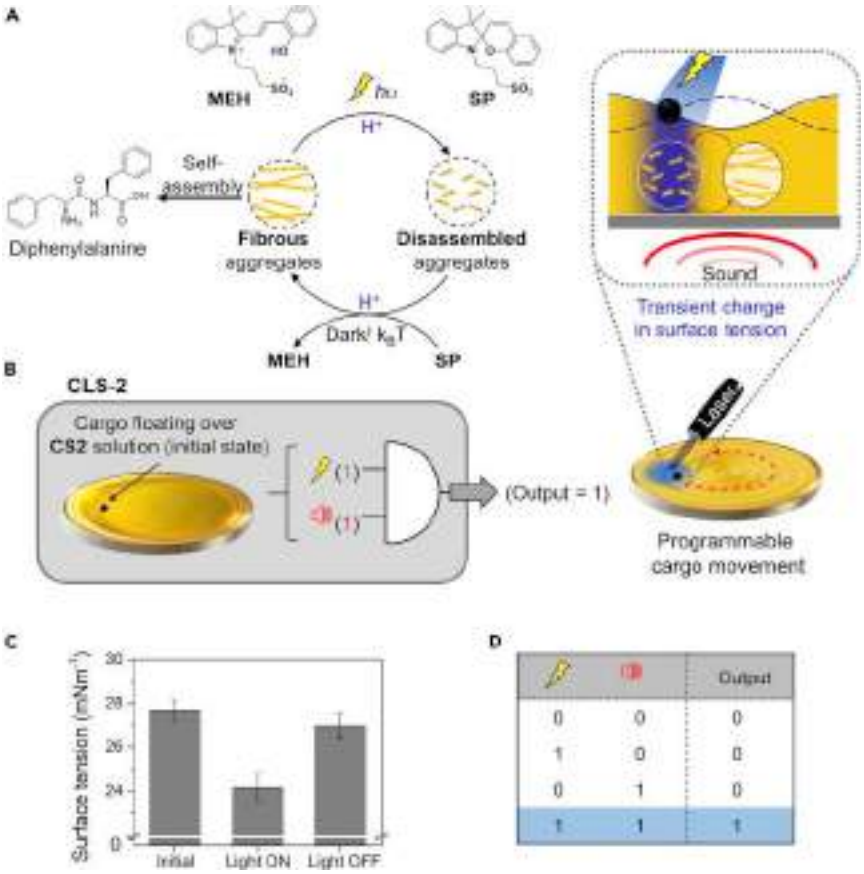

Figure 3. Boolean logic-regulated programmable cargo movement

(A) **CS2** based on light-responsive reversible transition between nanoaggregates of **FF** assembly in the presence of **MEH**. Composition: [**FF**] = 0.5 mM and [**MEH**] = 2.0 mM in toluene.

(B) **CLS-2** processes the information from light and sound inputs based on AND logic and produces programmable cargo movement as a specific output through the combined generation of surface waves and transient changes in surface tension. The inset shows a schematic representation of the cross-sectional view of the **CS2** solution exposed to light irradiation and sound waves.

(C) Reversible changes in surface tension of the **FF**-based nanoaggregate-dispersed solution upon light irradiation (ON) and recovery (OFF).

(D) Complete truth table obtained from the cargo movement experiments, which correspond to a double-input AND logic-gate circuit. Audible sound input frequency: 38 or 42 Hz.

Marangoni effect-induced movement of the cargo away from the irradiated region. However, the trajectory of the cargo could not be specifically controlled (output: 0) in consecutive cycles (Figure S11). Programmable and directional motion of the cargo (output: 1) was however achieved in the combined presence of audible sound generated surface waves and light irradiation (Figures 3B, 3D, and 4). We observed that the parameters of the audible sound input played an important role in determining the type of cargo movement over the solution surface. A sound input of 38 Hz and 0.06 g (audio-I) helped in generating a well-defined route for the orbital motion of the cargo along the nodal regions of the surface waves (Figure 4A; Video S7), where the cargo got practically trapped and exhibited a motion only along this circular track (orbital) (output: 1). On the other hand, with a higher frequency and amplitude sound input (42 Hz and 0.08 g; audio-II), a decrease in the pitch distance of the surface waves was observed, and the cargo could easily escape from the nodal regions on being propelled by light, resulting in a short distance radial motion (output: 1)

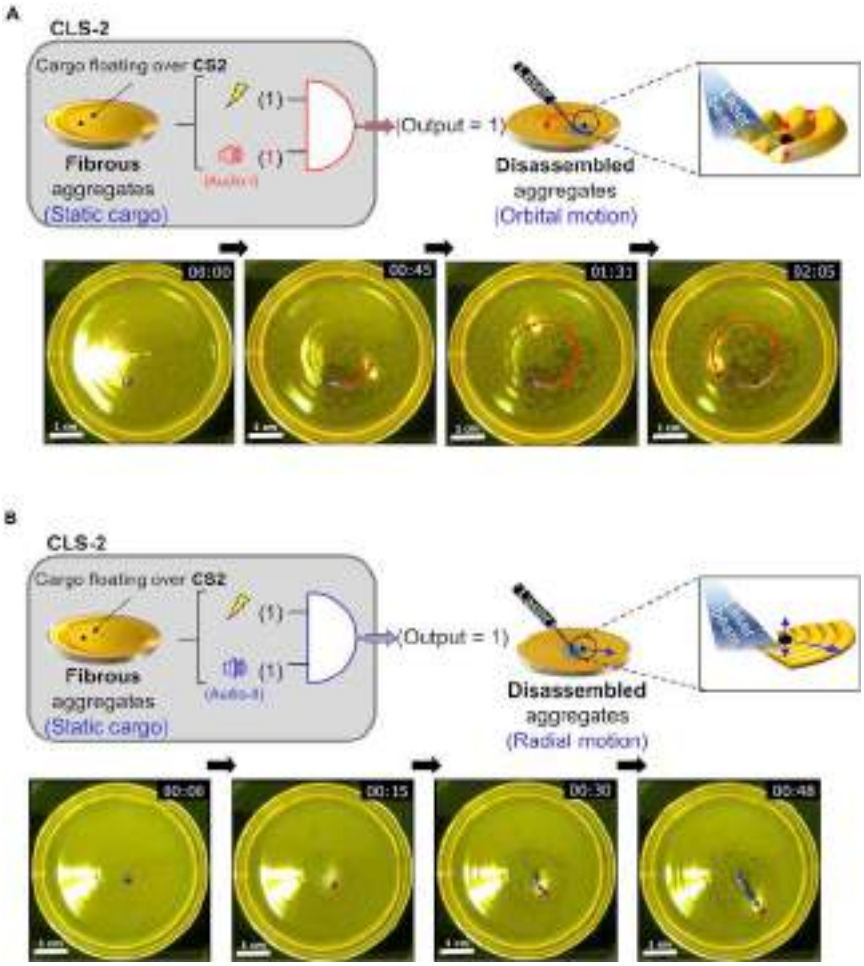

Figure 4. Light and sound controlled programmable cargo movement

(A) Top panel shows that a combined application of light and audible sound (audio-I) on **CLS-2** leads to an orbital motion of the cargo based on AND logic. Schematic representation of the cargo trapped within the nodal regions during orbital motion is shown along with. Bottom panel shows the experimental images of orbital motion taken at 0, 45, 91, and 125 s, respectively (Video S7).

(B) Top panel shows that a combined application of light and audible sound (audio-II) on **CLS-2** leads to a short radial motion of the cargo based on AND logic. Schematic representation of the cargo escaping from the nodal regions during radial motion is shown along with. Bottom panel shows the experimental images of radial motion taken at 0, 15, 30, and 48 s, respectively (Video S8).

In Figures 4A and 4B, initial and final positions of the cargo are marked with blue and red circles.

(Figure 4B; Video S8). In the absence of light irradiation, however, the cargo did not show any movement even in the presence of the sound input audio-II (output: 0). Light irradiation in the absence of audible sound also resulted in an uncontrolled cargo motion (output: 0) as described before. In the absence of both the inputs, the cargo remained static (output: 0) (Figure 3D; Video S9).

Thus, the programmable cargo movement in **CLS-2** exhibited an AND logic-gate response toward the two input stimuli (Figures 3D and 4). The results suggest that the out-of-equilibrium nanoaggregates in the **CS2** solution and their resultant properties e.g., Marangoni effect-induced orbital or radial motion can be programmed through the combined application of light and audible sound. A quantitative understanding of the mechanical work involved in the light and sound controlled

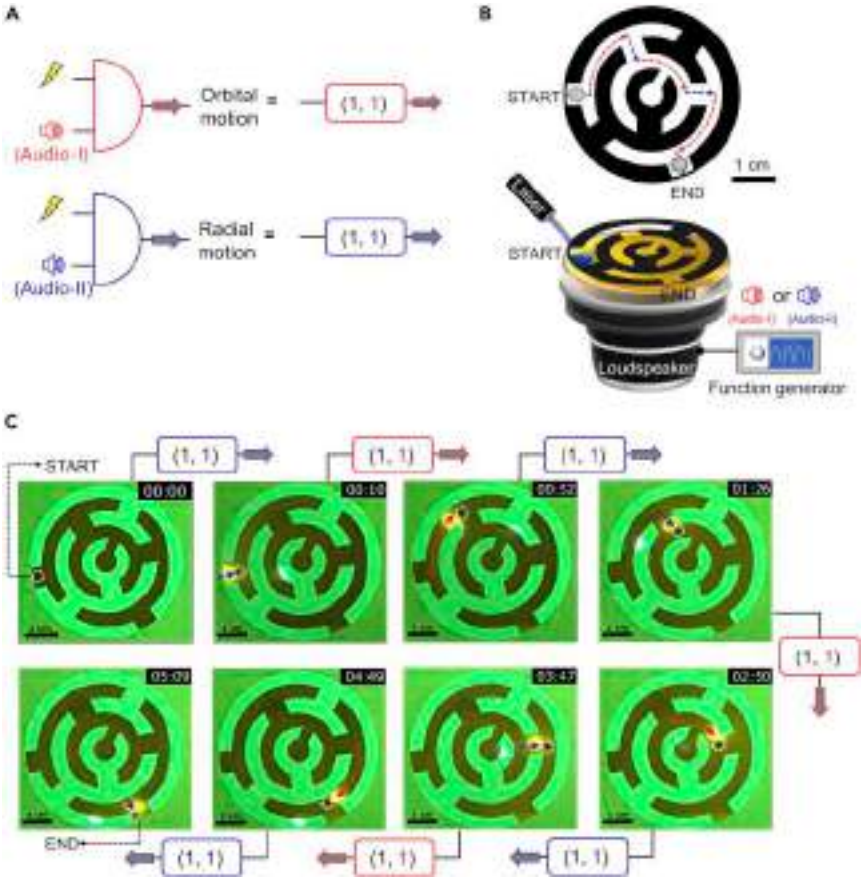

Figure 5. Boolean logic-regulated navigation of a passive cargo through a maze guided by light and audible sound as inputs

(A) AND logic gate with light and audio-I as inputs produces orbital motion. The program is represented by a red box. AND logic gate with light and audio-II as inputs produces short radial motion. The program is represented by a blue box.

(B) Top panel shows the schematic representation of the basic design of the maze structure. The single passageway for maze solving is represented by red- (for orbital motion) and blue-dashed (for short radial motion) lines. Schematic representation of the setup used for the maze experiments is shown at the bottom. The entrance and exit points of the maze are denoted as START and END, respectively.

(C) Photographs at different time intervals showing the successful navigation of a floating passive cargo through the maze aided by a programmed (Figure 5A) sequence of application of inputs (light and audible sound) as chosen by the experimenter.

programmed cargo motion is nontrivial.[51] However, we took advantage of the aforementioned qualitative observation to navigate a cargo over the **CS2** solution through a predetermined path, which is discussed in the next section.

Programmed navigation of a cargo through a maze

The application of the two input signals can be programmed in such a way so as to execute a predetermined sequence of orbital and short radial motion of the cargo over **CLS-2** (Figure 5A), which can be utilized to perform even higher level or complicated functions such as navigating a cargo through a maze (Figure S13). Instead of using a conventional maze with physical barriers, a maze shaped photomask was designed to project over the **CLS-2** solution placed in a Petri dish. Figure 5B shows the basic experimental setup and the maze design, where the entrance and exit points of the maze are denoted as START and END, respectively. In a control experiment, the

cargo was not propelled when the maze passageway was blocked by a photomask (Figure S14; Video S11). The cargo could be moved only along the unmasked curved passageway of the maze, and the photomasked region therefore acted as a bastion or divider (similar to a real physical barrier) for the maze. Since the cargo in this case is "passive,"[36] solving the maze by the cargo requires crucial human intervention. In the absence of sound, the cargo motion could not be specially navigated in the maze passageway due to the phototriggered uncontrolled orbital motion of the cargo (Figure S11; Video S10). This indicates that both light and audible sound inputs are necessary to guide the cargo to successfully solve the maze. The bead was therefore successfully navigated by the experimenter from the start point of the maze to its end through the passageway, remotely regulated by the experimenter who supplied a specific sequence of Boolean logic-based input and output signals (Figure 5C; Video S11). The cargo was propelled only upon light irradiation and remained static when the light source was switched off. Audio-I and light irradiation was utilized to navigate the cargo through the curved passageway. Once the cargo reached near a bottleneck, audio-II and light irradiation were utilized to trigger the short radial motion to navigate the cargo through the bottleneck (Figure S14). The maze was designed in such a way that the distance between two concentric maze passageways through the bottleneck matches well with the short distance in the radial direction (4.8 mm) traversed by the cargo in the aforementioned conditions (Figure S15). In the absence of audible sound, the cargo is propelled through a longer distance and with more velocity, which frequently pushes the cargo under a photomasked area thereby failing to guide the cargo through the maze (Figure S15). The snapshots at different stages during the navigation of the cargo through the maze are shown in Figure 5C.

Conclusions

We have demonstrated that out-of-equilibrium CLSs can be operated by Boolean logic-regulated input processing and can be programmed to exhibit transient changes in their chemical and physical properties to perform specific spatiotemporal functions such as programmed pattern formation exhibiting chemical gradients, cargo transport, and maze solving, etc. The programmed CLSs manifested their ability to sense multiple chemical and physical input signals and process such input information based on binary logic to deliver a desired outcome. Our approach of utilizing programmable out-of-equilibrium **CLSs** to execute transient biomimicking functions such as extraction of mechanical work can be a new paradigm in the research related to systems chemistry. The strategy adopted in the present work may help us in the design and development of smart materials with life-like properties or behavior involving Boolean logic-based out-of-equilibrium CSs of higher complexity.

EXPERIMENTAL PROCEDURES

Resource availability

Lead contact

Further information and requests for resources should be directed to and will be fulfilled by the lead contact Kimoon Kim (kkim@postech.ac.kr).

Materials availability

All unique/stable reagents generated in this study are available from the lead contact with a completed Materials Transfer Agreement.

Data and code availability

The authors declare that all data supporting the findings of this study are available within this article and supplemental information files.

SUPPLEMENTAL INFORMATION

Supplemental information can be found online at https://doi.org/10.1016/j.chempr.2022.04.020.

ACKNOWLEDGMENTS

This work was supported by the Institute for Basic Science (IBS, IBS-R007-D1), Republic of Korea. We thank I.S. Kang (POSTECH) for helpful discussions.

AUTHOR CONTRIBUTIONS

R.D.M. and K.K. conceived the idea. S.C. performed most of the experiments under supervision of R.D.M. S.K.S. and I.H. participated in the pattern experiments. R.D.M., S.C., and K.K. wrote the manuscript and all authors discussed the results, analyzed the data, and commented on the manuscript. K.K. supervised the overall research.

DECLARATION OF INTERESTS

The authors declare no competing interests.

Received: November 20, 2021
Revised: March 12, 2022
Accepted: April 20, 2022
Published: May 13, 2022

REFERENCES

1. Benenson, Y. (2012). Biomolecular computing systems: principles, progress and potential. Nat. Rev. Genet. *13*, 455–468.
2. Kitada, T., DiAndreth, B., Teague, B., and Weiss, R. (2018). Programming gene and engineered-cell therapies with synthetic biology. Science *359*, eaad1067.
3. Wagner, N., and Ashkenasy, G. (2009). Systems chemistry: logic gates, arithmetic units, and network motifs in small networks. Chem. Eur. J. *15*, 1765–1775.
4. Merindol, R., and Walther, A. (2017). Materials learning from life: concepts for active, adaptive and autonomous molecular systems. Chem. Soc. Rev. *46*, 5588–5619.
5. Grzybowski, B.A., Fitzner, K., Paczesny, J., and Granick, S. (2017). From dynamic self-assembly to networked chemical systems. Chem. Soc. Rev. *46*, 5647–5678.
6. Ashkenasy, G., Hermans, T.M., Otto, S., and Taylor, A.F. (2017). Systems chemistry. Chem. Soc. Rev. *46*, 2543–2554.
7. Ragazzon, G., and Prins, L.J. (2018). Energy consumption in chemical fuel-driven self-assembly. Nat. Nanotechnol. *13*, 882–889.
8. Jain, A., Dhiman, S., Dhayani, A., Vemula, P.K., and George, S.J. (2019). Chemical fuel-driven living and transient supramolecular polymerization. Nat. Commun. *10*, 450.
9. Choi, S., Mukhopadhyay, R.D., Kim, Y., Hwang, I.-C., Hwang, W., Ghosh, S.K., Baek, K., and Kim, K. (2019). Fuel-driven transient crystallization of a cucurbit[8]uril-based host-guest complex. Angew. Chem. Int. Ed. Engl. *58*, 16850–16853.
10. Mukhopadhyay, R.D., Choi, S., Sen, S.K., Hwang, I.-C., and Kim, K. (2020). Transient self-assembly processes operated by gaseous fuels under out-of-equilibrium conditions. Chem. Asian J. *15*, 4118–4123.
11. Ikeda, M., Tanida, T., Yoshii, T., Kurotani, K., Onogi, S., Urayama, K., and Hamachi, I. (2014). Installing logic-gate responses to a variety of biological substances in supramolecular hydrogel-enzyme hybrids. Nat. Chem. *6*, 511–518.
12. Komatsu, H., Matsumoto, S., Tamaru, S., Kaneko, K., Ikeda, M., and Hamachi, I. (2009). Supramolecular hydrogel exhibiting four basic logic gate functions to fine-tune substance release. J. Am. Chem. Soc. *131*, 5580–5585.
13. Grzelczak, M., Liz-Marzán, L.M., and Klajn, R. (2019). Stimuli-responsive self-assembly of nanoparticles. Chem. Soc. Rev. *48*, 1342–1361.
14. Moulin, E., Faour, L., Carmona-Vargas, C.C., and Giuseppone, N. (2020). From molecular machines to stimuli-responsive materials. Adv. Mater. *32*, e1906036.
15. Erbas-Cakmak, S., Kolemen, S., Sedgwick, A.C., Gunnlaugsson, T., James, T.D., Yoon, J., and Akkaya, E.U. (2018). Molecular logic gates: the past, present and future. Chem. Soc. Rev. *47*, 2228–2248.
16. Andréasson, J., and Pischel, U. (2015). Molecules with a sense of logic: a progress report. Chem. Soc. Rev. *44*, 1053–1069.
17. Chatterjee, A., Mahato, C., and Das, D. (2021). Complex cascade reaction networks via cross β amyloid nanotubes. Angew. Chem. Int. Ed. Engl. *60*, 202–207.
18. Cravotto, G., and Cintas, P. (2009). Molecular self-assembly and patterning induced by sound waves the case of gelation. Chem. Soc. Rev. *38*, 2684–2697.
19. Tsuda, A., Nagamine, Y., Watanabe, R., Nagatani, Y., Ishii, N., and Aida, T. (2010). Spectroscopic visualization of sound-induced liquid vibrations using a supramolecular nanofiber. Nat. Chem. *2*, 977–983.
20. Miura, R., Ando, Y., Hotta, Y., Nagatani, Y., and Tsuda, A. (2014). Acoustic alignment of a supramolecular nanofiber in harmony with the sound of music. ChemPlusChem *79*, 516–523.
21. Hotta, Y., Fukushima, S., Motoyanagi, J., and Tsuda, A. (2015). Photochromism in sound-induced alignment of a diarylethene supramolecular nanofiber. Chem. Commun. *51*, 2790–2793.
22. Hong, S.-H., Gorce, J.-B., Punzmann, H., Francois, N., Shats, M., and Xia, H. (2020). Surface waves control bacterial attachment and formation of biofilms in thin layers. Sci. Adv. *6*, eaaz9386.
23. Hwang, I., Mukhopadhyay, R.D., Dhasaiyan, P., Choi, S., Kim, S.-Y., Ko, Y.H., Baek, K., and Kim, K. (2020). Audible sound-controlled spatiotemporal patterns in out-of-equilibrium systems. Nat. Chem. *12*, 808–813.
24. Leira-Iglesias, J., Tassoni, A., Adachi, T., Stich, M., and Hermans, T.M. (2018). Oscillations, travelling fronts and patterns in a

supramolecular system. Nat. Nanotechnol. *13*, 1021–1027.

25. Aida, T., Meijer, E.W., and Stupp, S.I. (2012). Functional supramolecular polymers. Science *335*, 813–817.

26. de Greef, T.F.A., and Meijer, E.W. (2008). Supramolecular polymers. Nature *453*, 171–173.

27. Chen, R., Neri, S., and Prins, L.J. (2020). Enhanced catalytic activity under non-equilibrium conditions. Nat. Nanotechnol. *15*, 868–874.

28. Maiti, S., Fortunati, I., Ferrante, C., Scrimin, P., and Prins, L.J. (2016). Dissipative self-assembly of vesicular nanoreactors. Nat. Chem. *8*, 725–731.

29. Ikezoe, Y., Washino, G., Uemura, T., Kitagawa, S., and Matsui, H. (2012). Autonomous motors of a metal-organic framework powered by reorganization of self-assembled peptides at interfaces. Nat. Mater. *11*, 1081–1085.

30. Eelkema, R., Pollard, M.M., Vicario, J., Katsonis, N., Ramon, B.S., Bastiaansen, C.W.M., Broer, D.J., and Feringa, B.L. (2006). Molecular machines: Nanomotor rotates microscale objects. Nature *440*, 163.

31. Kim, Y.S., Liu, M., Ishida, Y., Ebina, Y., Osada, M., Sasaki, T., Hikima, T., Takata, M., and Aida, T. (2015). Thermoresponsive actuation enabled by permittivity switching in an electrostatically anisotropic hydrogel. Nat. Mater. *14*, 1002–1007.

32. Perrot, A., Moulin, E., and Giuseppone, N. (2021). Extraction of mechanical work from stimuli-responsive molecular systems and materials. J. Trends Chem. *3*, 926–942.

33. Chen, P., Luo, Z., Güven, S., Tasoglu, S., Ganesan, A.V., Weng, A., and Demirci, U. (2014). Microscale assembly directed by liquid-based template. Adv. Mater. *26*, 5936–5941.

34. Tweedy, L., Thomason, P.A., Paschke, P.I., Martin, K., Machesky, L.M., Zagnoni, M., and Insall, R.H. (2020). Seeing around corners: cells solve mazes and respond at a distance using attractant breakdown. Science *369*, eaay9792.

35. Lach, S., Yoon, S.M., and Grzybowski, B.A. (2016). Tactic, reactive, and functional droplets outside of equilibrium. Chem. Soc. Rev. *45*, 4766–4796.

36. Cejková, J., Toth, R., Braun, A., Branicki, M., Ueyama, D., and Lagzi, I. (2018). Shortest Path Finding in Mazes by Active and Passive Particles (Springer).

37. Lagzi, I., Soh, S., Wesson, P.J., Browne, K.P., and Grzybowski, B.A. (2010). Maze solving by chemotactic droplets. J. Am. Chem. Soc. *132*, 1198–1199.

38. Chovnik, O., Balgley, R., Goldman, J.R., and Klajn, R. (2012). Dynamically self-assembling carriers enable guiding of diamagnetic particles by weak magnets. J. Am. Chem. Soc. *134*, 19564–19567.

39. Downs, F.G., Lunn, D.J., Booth, M.J., Sauer, J.B., Ramsay, W.J., Klemperer, R.G., Hawker, C.J., and Bayley, H. (2020). Multi-responsive hydrogel structures from patterned droplet networks. Nat. Chem. *12*, 363–371.

40. Jeon, W.S., Kim, H.-J., Lee, C., and Kim, K. (2002). Control of the stoichiometry in host-guest complexation by redox chemistry of guests: inclusion of methylviologen in cucurbit [8]uril. Chem. Commun. *38*, 1828–1829.

41. Trabolsi, A., Khashab, N., Fahrenbach, A.C., Friedman, D.C., Colvin, M.T., Cotí, K.K., Benítez, D., Tkatchouk, E., Olsen, J.-C., Belowich, M.E., et al. (2010). Radically enhanced molecular recognition. Nat. Chem. *2*, 42–49.

42. Ashton, P.R., Ballardini, R., Balzani, V., Credi, A., Dress, K.R., Ishow, E., Kleverlaan, C.J., Kocian, O., Preece, J.A., Spencer, N., et al. (2000). A photochemically driven molecular-level abacus. Chem. Eur. J. *6*, 3558–3574.

43. Jeon, W.S., Ziganshina, A.Y., Lee, J.W., Ko, Y.H., Kang, J.K., Lee, C., and Kim, K. (2003). A [2]pseudorotaxane-based molecular machine: reversible formation of a molecular loop driven by electrochemical and photochemical stimuli. Angew. Chem. Int. Ed. Engl. *42*, 4097–4100.

44. Agrawal, P., Gandhi, P.S., and Neild, A. (2016). Particle manipulation affected by streaming flows in vertically actuated open rectangular chambers. Phys. Fluids *28*, 032001.

45. Segur, J.B., and Oberstar, H.E. (1951). Viscosity of glycerol and its aqueous solutions. Ind. Eng. Chem. *43*, 2117–2120.

46. Light was intentionally switched off after 40 s to avoid the presence of excessive reflected light, which prevented us from recoding the images (read out) of the pattern with its original color and contrasting domains as seen under ambient light. Nevertheless, if we kept the light source switched on to reach a non-equilibrium steady state, the concentric ring pattern was generated and maintained for about a minute before the prolonged irradiation of the solution led to heating and generation of convectional currents at the peripheral regions of the Petri dish (Video S2).

47. Nguindjel, A.-D.C., and Korevaar, P.A. (2021). Self-sustained Marangoni flows driven by chemical reactions. ChemSystemsChem *3*, e2100021.

48. Li, X., Fei, J., Xu, Y., Li, D., Yuan, T., Li, G., Wang, C., and Li, J. (2018). A photoinduced reversible phase transition in a dipeptide supramolecular assembly. Angew. Chem. Int. Ed. Engl. *57*, 1903–1907.

49. Florea, L., Wagner, K., Wagner, P., Wallace, G.G., Benito-Lopez, F., Officer, D.L., and Diamond, D. (2014). Photo-chemopropulsion—light-stimulated movement of microdroplets. Adv. Mater. *26*, 7339–7345.

50. Kausar, A., Nagano, H., Ogata, T., Nonaka, T., and Kurihara, S. (2009). Photocontrolled translational motion of a microscale solid object on azobenzene-doped liquid-crystalline films. Angew. Chem. Int. Ed. Engl. *48*, 2144–2147.

51. Accurate quantification of the mechanical work involved in this process is difficult due to the complex nature of the system. Nevertheless, a back-of-the-envelope calculation (see supplemental information and Figure S12 for details) indicated that ~0.016% of the light energy was converted to the work during orbital motion in presence of the audio-I input.

Chem, Volume *8*

Supplemental information

Out-of-equilibrium chemical logic systems: Light- and sound-controlled programmable spatiotemporal patterns and mechanical functions

Seoyeon Choi, Rahul Dev Mukhopadhyay, Shovan Kumar Sen, Ilha Hwang, and Kimoon Kim

Table of Contents

Supplemental Experimental Procedures

1. Materials and general methods.
All the reagents and solvents used were procured from commercial vendors and used as received without any further purification, unless stated otherwise. Deionized water with a resistivity of 18.2 $M\Omega cm^{-1}$ was used to prepare aqueous solutions. NMR spectra were recorded at 298 K on a Bruker DRX500 spectrometer. Mass spectrum was measured in positive ion mode using a linear ion trap mass spectrometer (LTQ XL, Thermo Scientific, MA, USA) equipped with electrospray ionization source (ESI). Drop-cast and spin-coated samples of peptide nanoaggregates were imaged using a Park NX10 AFM in ambient condition with non-contact mode. SEM analysis of the aforementioned samples were imaged using a JEOL JSM-7401F scanning electron microscope operating at 5 kV. A function generator (AFG-2005, GW Instek) and a speaker (PC83-8, Dayton Audio) were used to generate and control vertical vibrations. Vibrational acceleration was measured by a vibration meter (ST-140, Tenmars). Photos of the experiments were taken by a smartphone or a digital camera. The pending droplet method was used to measure the surface tension of the spiropyran and diphenylalanine nanoaggregate solutions. The contact angle measuring experiments were performed with UNI-CAM/A, GITsoft. The surface tension values were calculated automatically from the instrument using the Young-Laplace equation.

Protocol for light, audible sound and atmospheric oxygen induced programmed spatiotemporal pattern generation experiments. A circular glass Petri dish was mounted on top of a flat acrylic tray placed over a loudspeaker, which was connected to a function generator to generate vertical sinusoidal vibrations (Figure S2). The frequency range and amplitude of vibrations were controlled by the function generator and the amplitude of the vibrations was measured with a vibration meter. For the programmed spatiotemporal pattern generation experiments, frequency in the range of 35-42 Hz with an amplitude of the vibration in the range of 0.06-0.08 g was found to be suitable. For the programmed spatiotemporal pattern experiments, an aqueous solution mixture of $\mathbf{MV^{2+}}$ (2.0 mM), $\mathbf{[Ru(bpy)^3]^{2+}}$ (0.4 mM) (photosensitizer) and TEOA (7.0 mM) (sacrificial reductant) (**CS1**) was prepared. Glycerol (20 wt%) was utilized to prepare the aforementioned solution to suppress the lateral flow thereby generating a concentric ring based pattern.[22,43] The mixture solution was further passed through a Nylon syringe filter (0.2 μm pore size) to totally avoid the presence of any minuscule amount of undissolved residue that may disturb the pattern formation process. The solution was also degassed with argon gas for 30 min prior to each set of experiments. After transferring the mixture solution (5.0 mL) to a 56 mm (inner diameter) glass Petri dish placed on top of a loudspeaker, photochemical reduction of $\mathbf{MV^{2+}}$ was carried out by irradiating the solution with a LED lamp (10 W, $\lambda \geq 400$) placed at a distance of 16 cm above the Petri dish inclined at an angle of ~30° for 40 s to minimize the heating effect. It may also be noted that the pattern images are obtained just after switching off the light source (after 40 s) to avoid excess reflected light while recording the pattern images. Photo induced reduction of $\mathbf{MV^{2+}}$ produces a dark green colored **CS1** solution (considered to be a mixture of blue colored $\mathbf{MV^{\bullet+}}$ and yellow colored $\mathbf{[Ru(bpy)^3]^{2+}}$ solution). The $\mathbf{MV^{\bullet+}}$ absorbs in the range 470 nm-760 nm. Whereas the absorption maximum of $\mathbf{[Ru(bpy)^3]^{2+}}$ is ~450 nm (Figure S16) and therefore the photoreduction works well under the aforementioned experimental conditions. Nevertheless, to avoid the possibility of light rays being unable to penetrate to the bottom of the Petri dish and generate chemical gradients, we gently swirled the Petri dish to start our experiments with a homogeneous solution. In general, the function generator connected to the speaker was also kept switched on during the pattern generation in the dish and the audible sound controlled vertical streaming does the job for us. The pattern images were recorded using a smartphone or a digital camera. In general, the pattern generation started within a few seconds upon applying the sound and light inputs and the developed pattern stayed for a few more minutes (Figure S3 and Video S1). All patterns were optimized at room temperature (25 ± 2 °C). For the Boolean logic related control pattern experiments, the same procedure was followed by switching off/on the individual input stimulus (Figure 1B, C, D). For measuring the height of the surface waves,[1,2] we recorded the surface vibrations in the side direction using a video camera at 960 fps (Figure S4).

Spatiotemporal chemical gradients within a pattern. A solution (5.0 mL) containing $\mathbf{MV^{2+}}$ (2.0 mM), $\mathbf{[Ru(bpy)^3]^{2+}}$ (0.4 mM), TEOA (7.0 mM) and glycerol (20 wt%) in deionized water (**CS1**) was used as described before. When the LED lamp was turned on, the yellow-colored solution of **CS1** turned green

within a few seconds. The light source was then switched off while the function generator (at 40 Hz) connected with the speaker was kept on. The dark green solution changed to a spatiotemporal pattern with typical concentric rings (Figure 1B). In experiments to study the spatiotemporal chemical gradients over the whole pattern area, after a few more seconds of pattern (initial state) development (in presence of the three input stimuli), the light source was switched off and the solution was further exposed to air, keeping the sound source on, the thicker greenish lines in the concentric ring pattern became thinner and the yellowish lines in the concentric ring pattern became more prominent (partially decayed state). The patterned solution was then again exposed to light irradiation to induce the photoreduction of $\mathbf{MV^{2+}}$ (regeneration of the initial state). Reversible changes in chemical composition of the $\mathbf{MV^{\bullet+}}$ rich region and the $\mathbf{MV^{2+}}$ rich region (over the whole area of the pattern) was observed over several repeated cycles by repeated refueling of **CLS-1** with light irradiation (Figure 2A, Figure S5 and Video S3). A photomask was used to specifically control the redox states of the out-of-equilibrium chemical species at predetermined domains within the solution. Photomasks of various designs were prepared with a black paper and attached over a polystyrene based transparent substrate, which acted as a Petri dish cover. After the concentric ring pattern was developed, the photomask was placed over the patterned solution without perturbing the pattern generated in the solution; it was then irradiated with light. $\mathbf{MV^{\bullet+}}$ was regenerated in the illuminated regions of the solution while the chemical species in unexposed regions continued to be oxidized to generate $\mathbf{MV^{2+}}$. Switching the position of the photomask alternately between the two semi-circular halves of the Petri dish, the chemical gradient within the pattern was specifically controlled to give rise to spatiotemporal changes in the chemical gradients (Figure 2B, 2C, Figure S6, S7 Video S4 and S5). In the case of spatiotemporal changes in chemical composition at a point, a hand-held laser (405 nm, 50 mW) pointer was used to trigger the reduction of $\mathbf{MV^{2+}}$ at a specific point of the patterned solution (Figure 2D and Video S6). A magnifying camera lens (12X magnification) was attached to the camera to record clear images or videos of the event. All experiments were performed at room temperature (25 ± 2 ˚C).

Pattern image analyses. The images obtained from the repetitive pattern experiments were analyzed using ImageJ software. Firstly, the RGB color pattern images were converted into grayscale representations, then the gray values were collected using a line profile tool. The brighter regions in yellow color shows more intensity than the darker regions in green color in the line obtained line profile. For each image recorded at a particular instant, line profiles of the image color intensity were measured along a line segment (yellow dashed line shown in Figure 2C, inset) drawn over a particular position on the pattern images.

Protocol for light and sound controlled programmable cargo movements. In a typical experiment, protonated merocyanine (MEH) (for synthesis see supplementary information) and diphenylalanine (FF) were dissolved in 1,1,1,3,3,3-hexafluoro-2-propanol (HFIP) (40 μL), and then toluene (8 mL) was added to achieve the final concentration of FF (2.0 mM) and MEH (8.0 mM) (**CS2**). The mixture was then vortexed vigorously to produce a homogeneous solution and sonicated for 1 h to obtain a yellowish nanoaggregate dispersed solution. After transferring nanoaggregate solution (2 mL) to the Petri dish in a 50 mm (inner diameter), a pure toluene was added to further dilute the mother solution (4 times). The final concentration of the **CS2** solution was 0.5 mM of FF and 2.0 mM of MEH, respectively. After the nanoaggregates were homogeneously dispersed throughout the solution, the function generator connected to the speaker was turned on and cargo movement experiments were carried out and recorded using a smartphone or digital camera. The cargo used was styrofoam-based spherical bead (d = 4-5 mm and m = 2.3 ± 0.24 mg) covered with black Teflon film to circumvent the dissolution of the styrofoam by the solvent. The cargo movement was controlled by a hand-held laser beam (405 nm, 50 mW) pointed towards the solution at a distance of ~6 cm in the presence of audible sound having a suitable range of frequencies (35-42 Hz) and amplitude (0.06-0.08 g) of the vibrations. The light-driven speed of the cargo was measured using ImageJ software.

Characterization of photo responsive nanoaggregates. To demonstrate the morphological changes of the peptide-based nanoaggregates in response to photoirradiation, a **CS2** solution containing FF (0.5 mM), MEH (2.0 mM) and HFIP (10 μL) in toluene (2 mL) was prepared as described before. To prepare samples for morphological analysis by SEM or AFM, an aliquot (10 μL) was removed from the nanoaggregate dispersed solution and spin coated (3000 rpm, 20 s) over silicon wafer substrates. To investigate the dissolution of the nanoaggregates, the nanoaggregate dispersed solution was irradiated with a LED lamp (10 W, λ≥400). Irradiation was continued even during the spin coating process. To confirm the reformation of nanoaggregates, the morphological experiments were carried out after keeping the irradiated

nanoaggregate dispersed solution under dark conditions for 20 s, followed by spin coating. For dynamic light scattering (DLS) measurement, the nanoaggregates dispersed solution (800 μL) was placed in a 1.5 ml disposable cuvette (path length, 10 mm). The average size of nanoaggregates using DLS was measured before/after light irradiation (20 s, 10 W, λ≥400) and after being kept in the dark (20 s) (Figure S8 and S9).

Surface wave pattern dependent cargo movements. To investigate the role of sound input, the cargo movement experiments were carried out in presence of audible sound of different frequencies. A glass Petri dish with the mixture solution containing FF (0.5 mM), MEH (2.0 mM) and HFIP (10 μL) in toluene (8 mL) (**CS2**) was mounted on top of a flat acrylic plate placed over a speaker and the styrofoam-based spherical cargo (*d* = 4-5 mm and 2.3 ± 0.24 mg) was floated on the solution surface without turning on the sound. A black colored acrylic plate was placed over a speaker and a long pass filter (490 nm) was attached behind the mobile camera lens to record clear images or videos of the event avoiding reflected light. In general, while applying a sound input of 38 Hz and 0.06 g (Audio-I) to the mixture solution, an orbital motion of the cargo in the presence of light irradiation was observed (Figure 4A and Video S7). Upon changing the sound input (42 Hz and 0.08 g; Audio-II), we observed a light-propelled short radial motion of the cargo. (Figure 4B and Video S8).

Measurement of transient changes in surface tension upon light irradiation. To understand the reason behind the cargo movements as a result of irradiating the FF and MEH mixture solution (**CS2**), surface tension measurements were carried out by the pending droplet method. A liquid drop (5 μL) was suspended on a dosing 16 G needle and subsequently the analysis of the drop shape was carried out based on the Young-Laplace equation. It indicates that the surface tension (γ) value of the mixture solution before light irradiation is 27.6 ± 0.5 mN m^{-1} (n = 3). When the drop shape was analyzed after 5 s of blue light irradiation (405 nm, 50 mW), a decrease in the surface tension was observed (γ = 24.2 ± 0.6 mN m^{-1} (n = 3)). The original surface tension value (γ = 27.6 ± 0.5 mN m^{-1} (n = 3)) is however recovered under dark conditions. Due to the surface tension gradient generated a Marangoni effect comes into action under these conditions, and the cargo starts moving in a direction away from the point of irradiation of light. The reversible changes in surface tension were reproducible over several cycles. All cargo movement experiments were optimized at room temperature (25 ± 2 ˚C). Similar, control experiments were conducted to measure the photoirradiation dependent changes in the surface tension of the following solutions: (a) A solution of HFIP (10 μl) in toluene (8 mL) and (b) solution containing all the components of **CLS-2** apart from FF (Figure S10).

Estimation of mechanical work. Although it is beyond the scope of the original motivation behind this study, we have tried to estimate the mechanical work during the cargo motion upon the reviewer's request. However, under out-of-equilibrium conditions, it is rather difficult to consider the transient changes in all the experimental factors like solution viscosity, local heating, etc. So, we simplified the situation to come up with a rough estimate of the mechanical work involved. First, we tracked the time dependent displacement and time dependent velocity of the cargo. From these values, we obtained the displacement versus velocity plot for the cargo. The plot shows an increase in the velocity because of the net force acting on the cargo, i.e., the resultant of the gradient in surface tension force that induces the Marangoni effect and the opposing viscous drag. The former force is instantaneously applied on light irradiation. However, the viscous drag continuously acts on the cargo in the opposite direction and ultimately brings the cargo to a rest. Under these conditions the cargo initially accelerates to reach a final velocity (~11 mm/sec in the presence of the sound waves (Audio-I) and then starts retarding under the action of the viscous drag. The differential curve gives us the displacement versus acceleration plot for the cargo. From the known mass of the cargo (2.3 ± 0.2 mg) we estimated the displacement dependent changes in force acting on the cargo. The overall change in the force i.e., the area under the curve gives us an idea about the quantity of mechanical work executed in the process. The input light energy supplied from the laser (110 nW, actual power) was also calculated from the time of photoirradation required to initiate motion in the cargo (2.6 s). It was observed that ~0.016% of the input energy is converted into meaningful mechanical work in the presence of the sound. Although the energy efficiency is substantially low in the presence of sound, probably due to the restricted motion of the cargo in the presence of the surface waves, the motion of the cargo is much more controlled as one can observe from the tracking experiments (Figure S11). It may be noted that these calculations involve

several approximations and therefore only provides us with a fair estimation but not with an accurate value. For details about these calculations please see Figure S12.

Maze experiments. For the maze experiments, a glass Petri dish with a mixture solution containing FF (0.5 mM) MEH (2 mM) in toluene (8 mL) was placed on top of a speaker. A maze shaped photomask was prepared from a black paper and attached over a polystyrene based transparent Petri dish cover. The maze was designed in such a way so that the passageway matches well with the nodal positions of the surface waves. Subsequently, the maze was placed over the mixture solution maintaining a gap of ~5 mm without interfering the formation of the surface waves and the cargo movement upon light irradiation (Figure 5B). The bead was navigated through the maze passageway from the START to the END points, remotely propelled by light and audible sound assisted surface waves (Figure 5C, Figure S13 and Video S11). All experiments were optimized at room temperature (25 ± 2 ˚C) and recorded with a smartphone or digital camera.

2. Synthesis and characterization of MEH

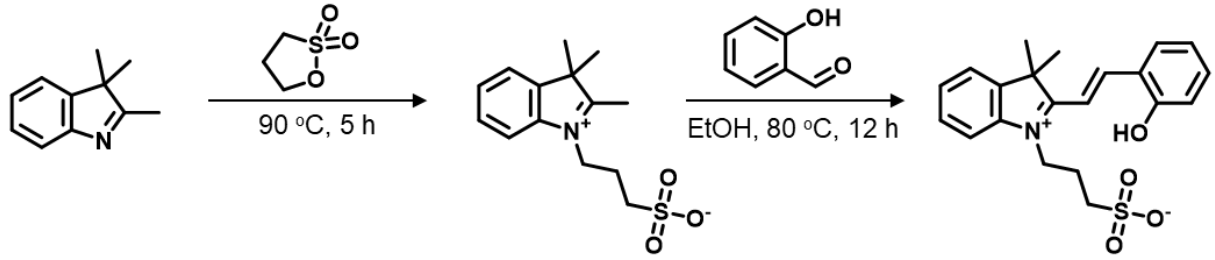

The photoacid generator MEH was synthesized according to the previous reports.[3-5] A mixture of 2,3,3-trimethylindolenine (1.20 g, 7.54 mmol) and propane sultone (1.84 g, 15.07 mmol) was stirred at 90 ˚C for 5 h under argon atmosphere. The obtained purple precipitate of 2,3,3-trimethyl-1-(3-sulfonatepropyl)-3H-indolium was filtered, washed with cold diethyl ether, and finally dried under vacuum. Then, the obtained solid (2.10 g, 7.46 mmol) and 2-hydroxybenzaldehyde (1.38 g, 11.34 mmol) were dissolved in absolute ethanol (10 mL) and refluxed for 12 h. After cooling, the orange product was collected by filtration, washed with ethanol and dried in vacuum (2.3 g, 80%). ^{1}H NMR (850 MHz, DMSO-d_6, TMS): δ = 8.60 (d, 1H), 8.27 (d, 1H), 8.02 (d, 1H), 7.87 (m, 2H), 7.62 (m, 2H), 7.48 (t, 1H), 7.04 (d, 1H), 6. 99 (t, 1H), 4.80 (t, 2H), 2.65 (t, 2H), 2. 18 (m, 2H), 1. 77 (s, 6H). ESI-MS: *m/z* calcd. for $C_{21}H_{23}NO_4S$ 385.13 $[M+Na]^+$: 408.12, found 408.25.

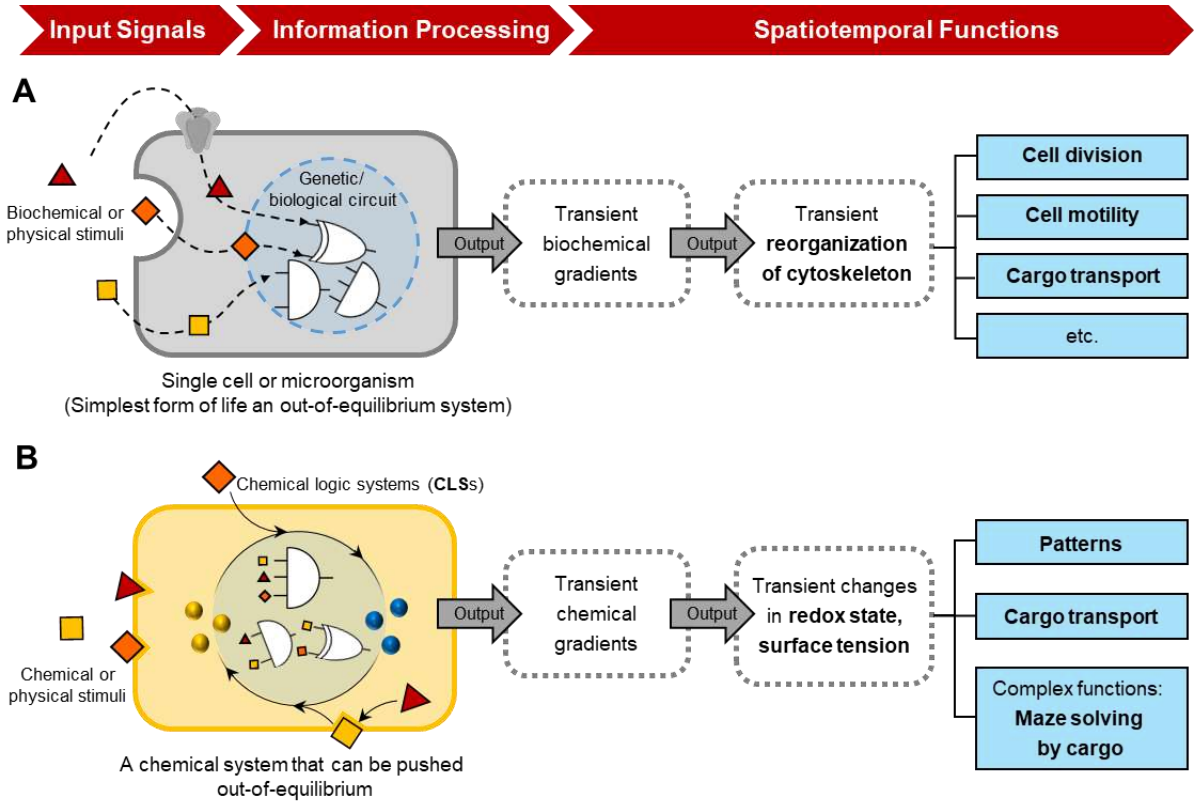

Figure S1. Schematic representation of Boolean logic regulated spatiotemporal functions in out-of-equilibrium natural and artificial systems. (A) Information processing within a single cell or microorganism is operated by a genetic or biological logic circuit to generate transient biochemical gradients that results in the transient reorganization of the cellular cytoskeleton to execute specific biological functions. (B) A conceptual representation of a multi stimuli-responsive out-of-equilibrium chemical system with an ability to process information based on binary logic and generate transient chemical gradients, which can be exploited to execute programmable spatiotemporal functions.

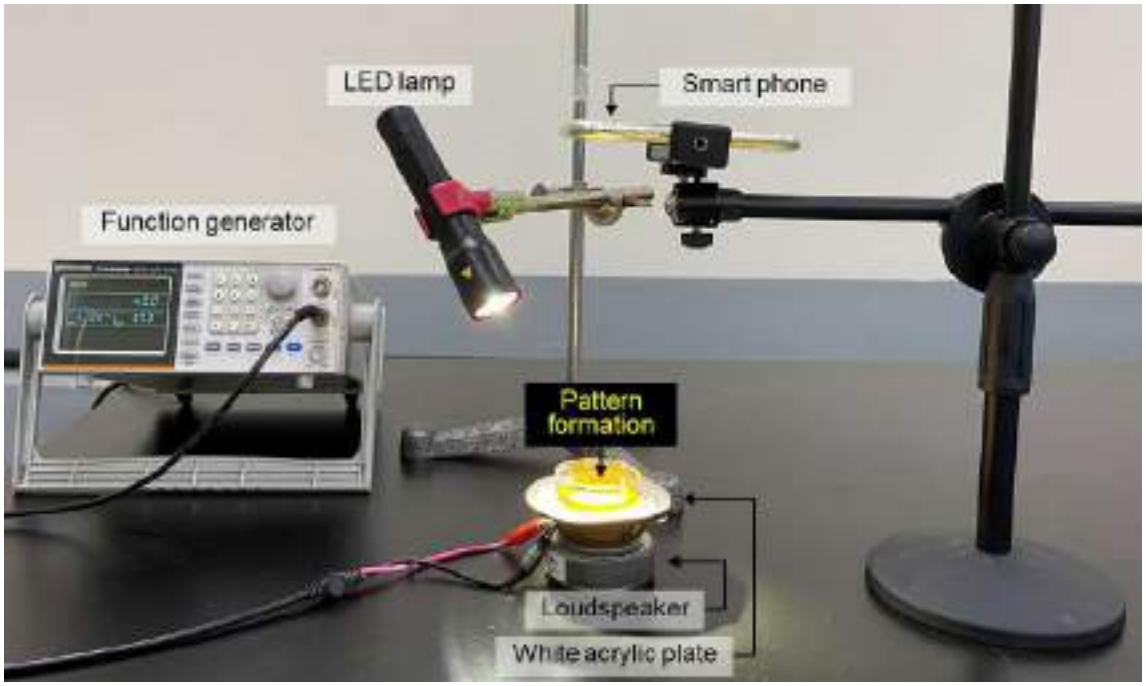

Figure S2. A photograph of the setup used for the spatiotemporal pattern generation experiment using a combination of three external stimuli; light, sound and atmospheric O_2.

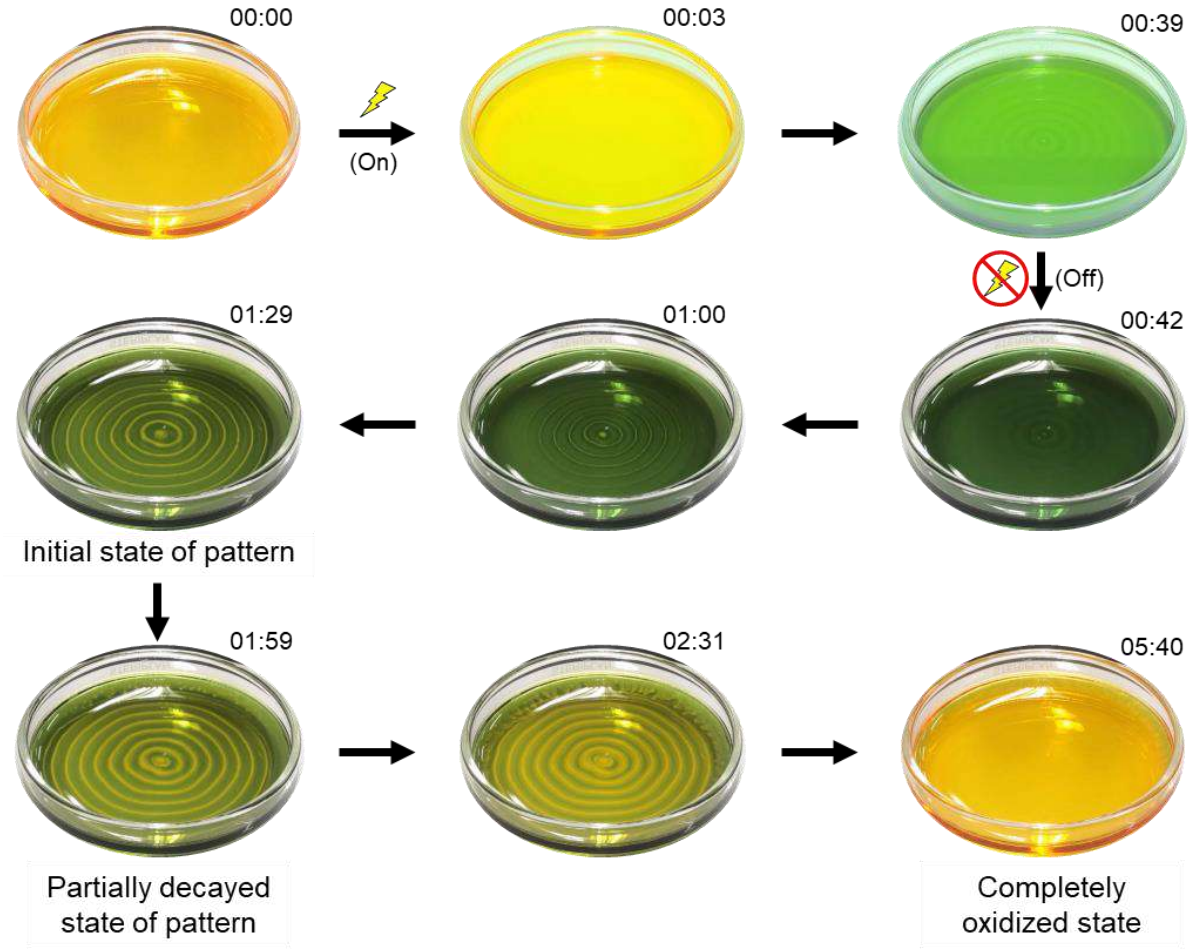

Figure S3. Snapshots obtained from Video S1 showing the time-dependent pattern generation process in **CS1** under the influence of three inputs; light, sound and atmospheric O_2. The photographs show the step-wise process by which an intense green solution is gradually reorganized into a spatiotemporal pattern on vibrating with an audible sound source (40 Hz).

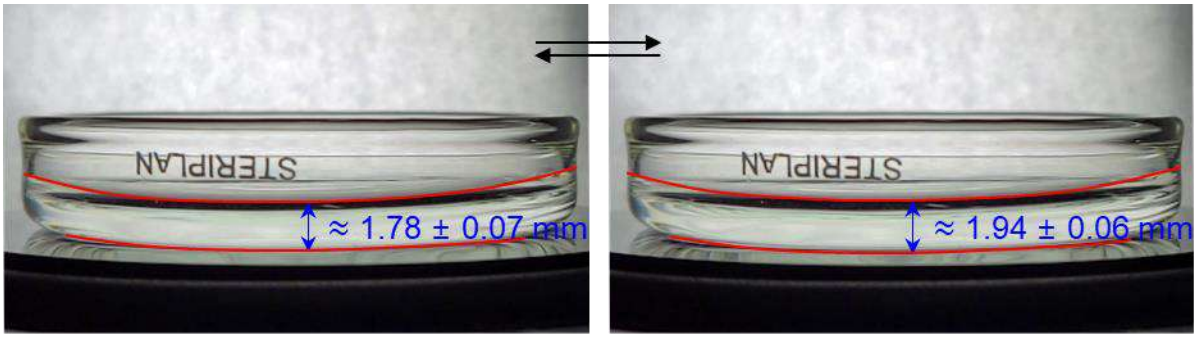

Figure S4. Observation of surface wave height changes of an aqueous solution on application of audible sound. These snapshots were obtained from a video at 960 fps. From our experiments we could observe a maximum displacement of 0.16 ± 0.01 mm of the height of the solution on application of audible sound of frequency 40 Hz.

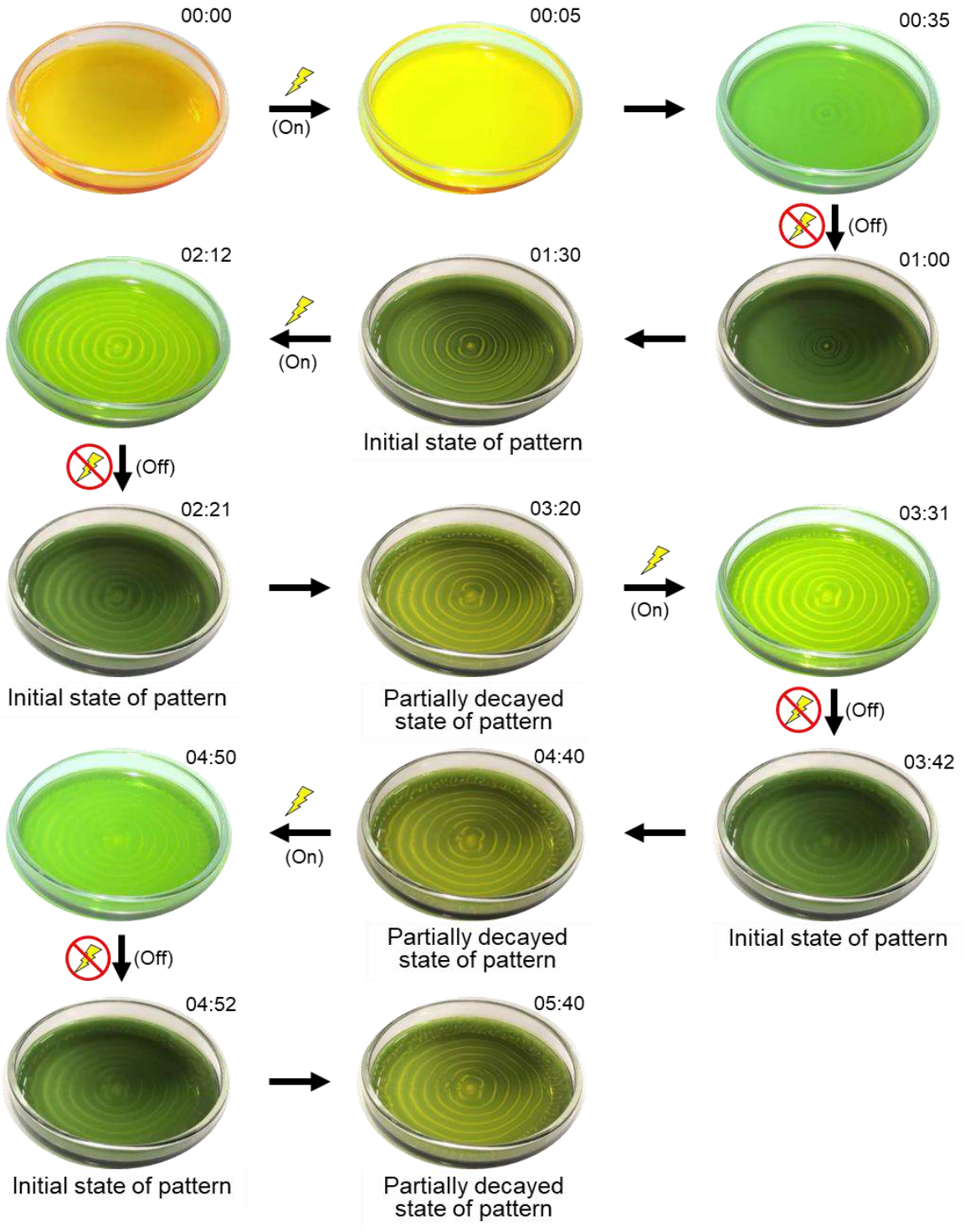

Figure S5. Snapshots obtained from Video S3 showing a reversible spatiotemporal pattern. The initial state of the pattern can be recovered by light irradiation of the partially decayed pattern for repeated cycles.

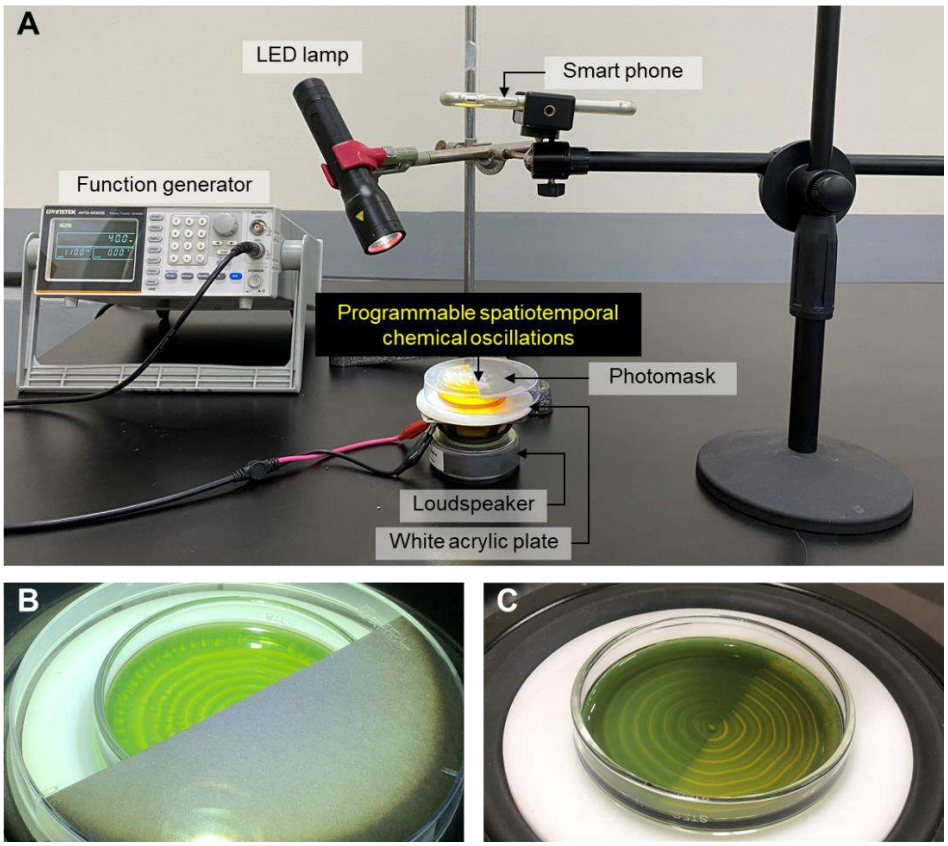

Figure S6. Photographs of repetitive pattern generation experiments. (A) Experimental setup for tuning the chemical gradients present inside a pattern using a photomask. (B) Zoomed image of a Petri dish covered with a semicircular photomask (perspective view). (C) Pattern image obtained after irradiation of the photomask covered Petri dish with a LED lamp (40 s).

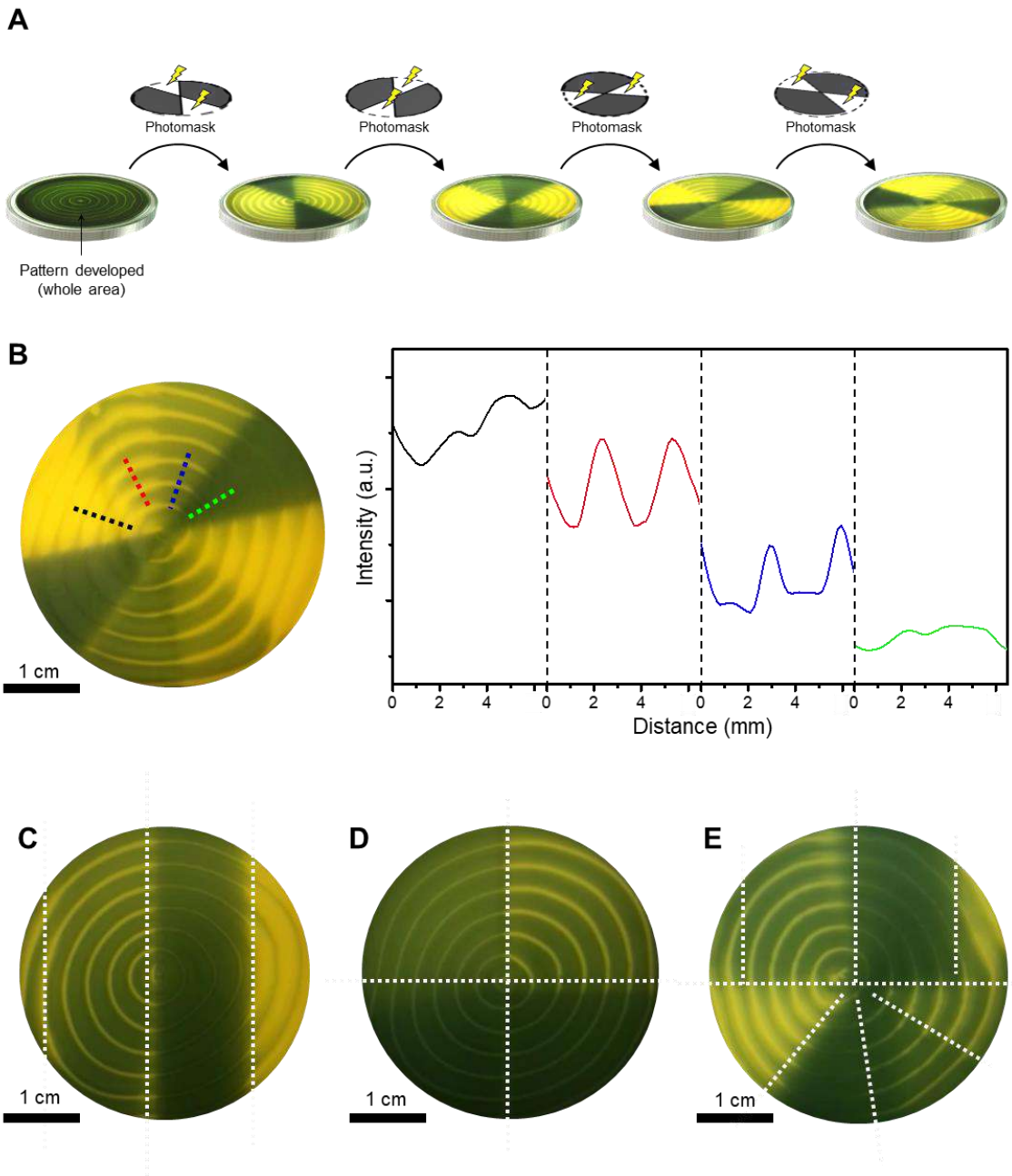

Figure S7. Generation of different types of chemical gradients within a spatiotemporal pattern utilizing differently shaped photomasks. (A) Schematic representation of the experimental procedure to tune the chemical gradients within specific areas inside a pattern regulated by the light in presence of sound and O_2. (B) A pattern image obtained from the experiment described in Figure S7A (left) and color intensity profiles extracted from the pattern image (right). Each dashed line was drawn over a particular position on the pattern image along which the line profile (represented in same color) was calculated. (C), (D), (E) Snapshots obtained from Video S5 showing different types of chemical gradients within the concentric ring pattern.

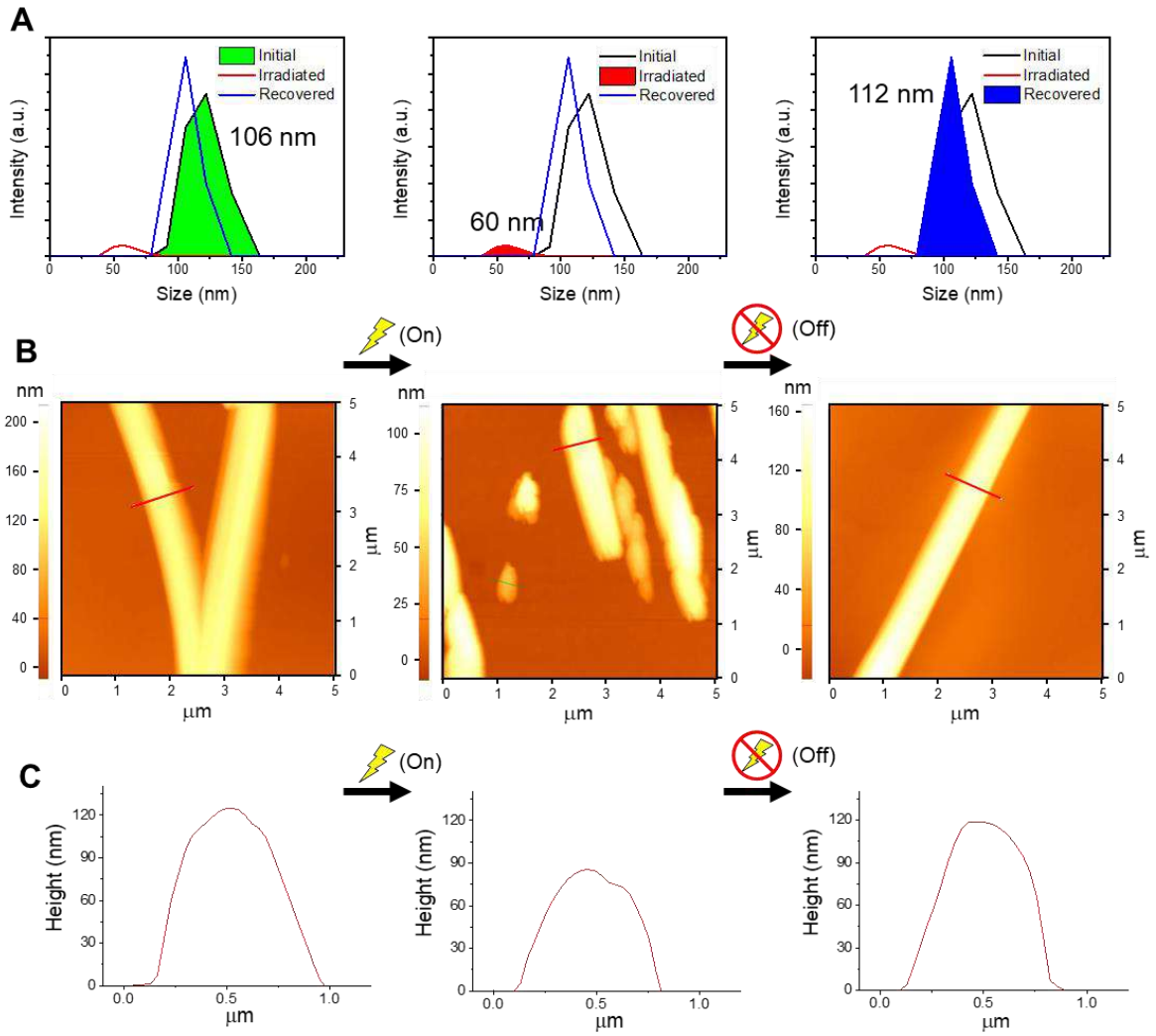

Figure S8. Photo-responsive changes in the size and morphology of FF nanoaggregates. (A) Comparative plots showing the DLS size and scattering intensity measurement of initially formed (left), irradiated (middle) and recovered (right) nanoaggregates of FF. (B) AFM images showing light-induced morphological transformations between FF based rigid nanofibers and short rod-shaped aggregates, obtained after light irradiation and their recovery under dark conditions. The AFM measurement shows the formation of larger aggregates of FF due to the drying of the samples. (C) Corresponding height profiles obtained from AFM images shown in Figure S8B.

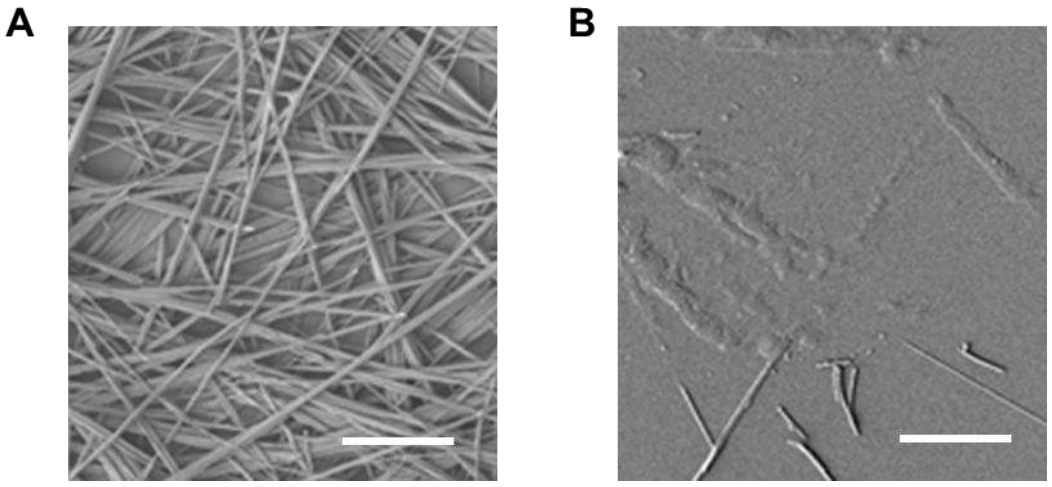

Figure S9. SEM images showing morphological transformations between FF based fibrous (A) and disassembled nanoaggregates (B) obtained after light irradiation (scale bar: 10 μm).

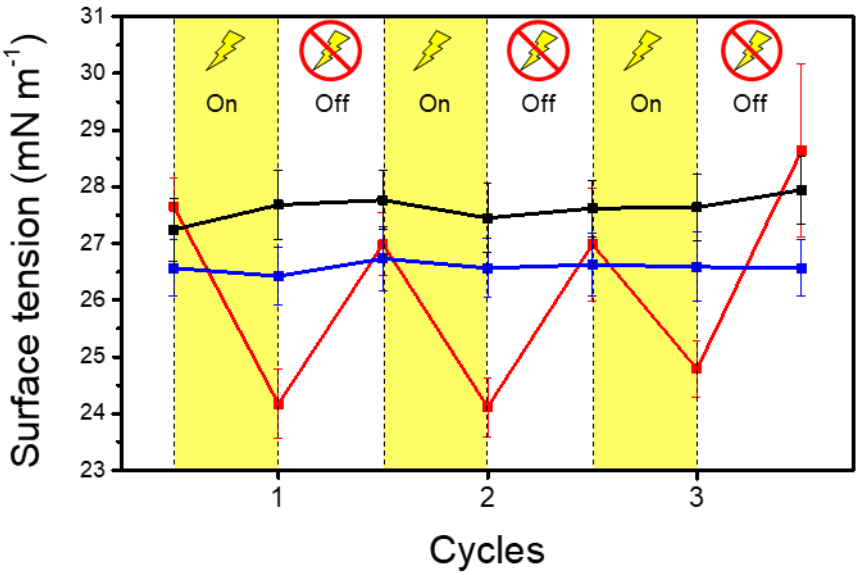

Figure S10. Changes in surface tension of the solution containing FF and MEH (red trace) upon light irradiation (On) and recovery after being kept in the dark (Off). The solution containing only MEH in HFIP and toluene (blue trace) and the solvents alone, i. e., HFIP and toluene (black trace) show no significant changes in surface tension upon light irradiation.

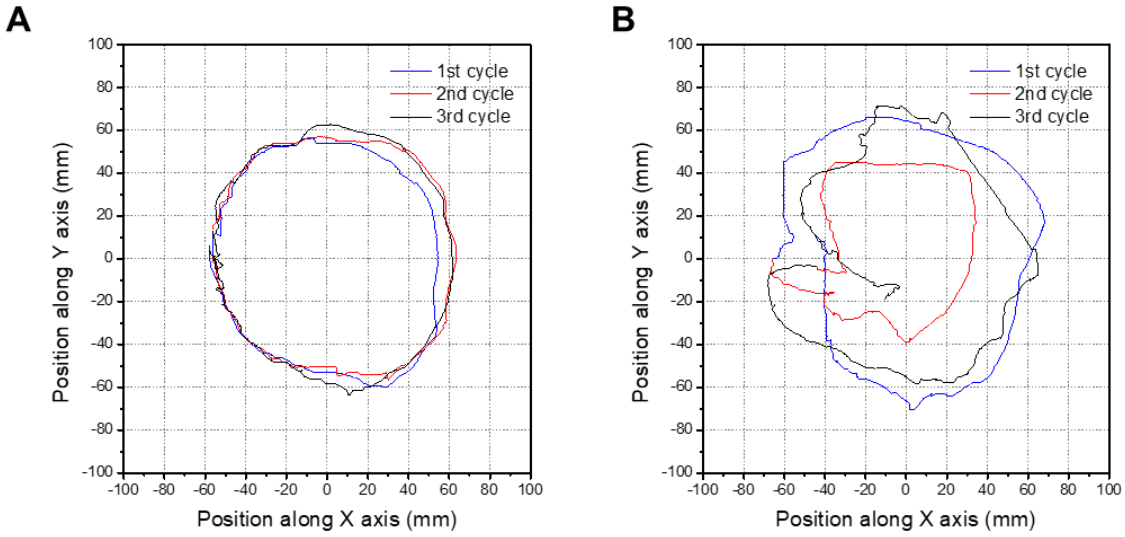

Figure S11. Trajectories of the light controlled orbital motion of the cargo for three cycles (A) in the presence as well as (B) in the absence of audible sound waves (Audio-I) (Video S10). The tracking data confirm that the orbital motion was much more controlled in the presence of sound waves.

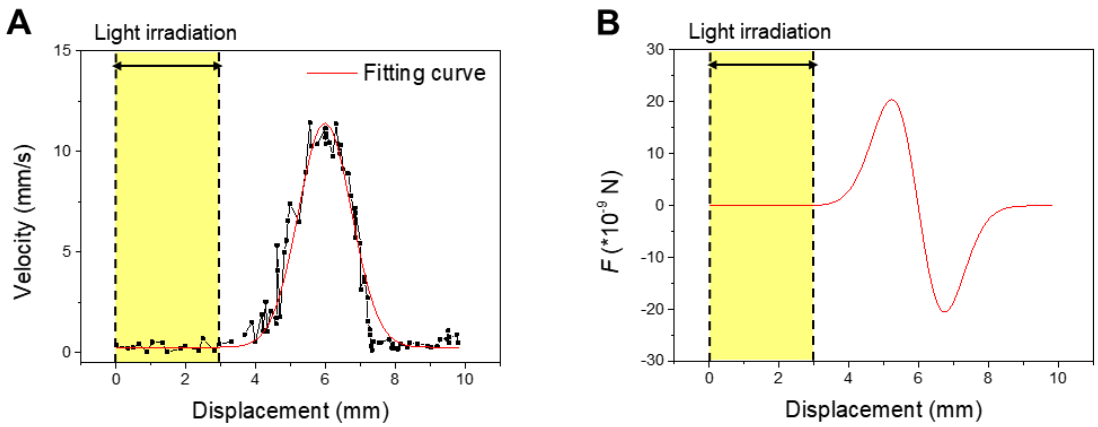

C

Irradiation duration	Input light energy	Work done	Energy conversion
2.6 sec	2.8×10^{-7} J	4.6×10^{-11} J	1.6×10^{-2}%

Figure S12. Estimation of the mechanical energy conversion during light and sound (Audio-I) driven cargo motion along an orbital track. (A) Displacement versus velocity plot and (B) displacement versus force plot. (C) Table shows that 0.016% of input light energy is converted to mechanical work. The experiment was repeated at least 4 times to confirm the reproducibility of the results.

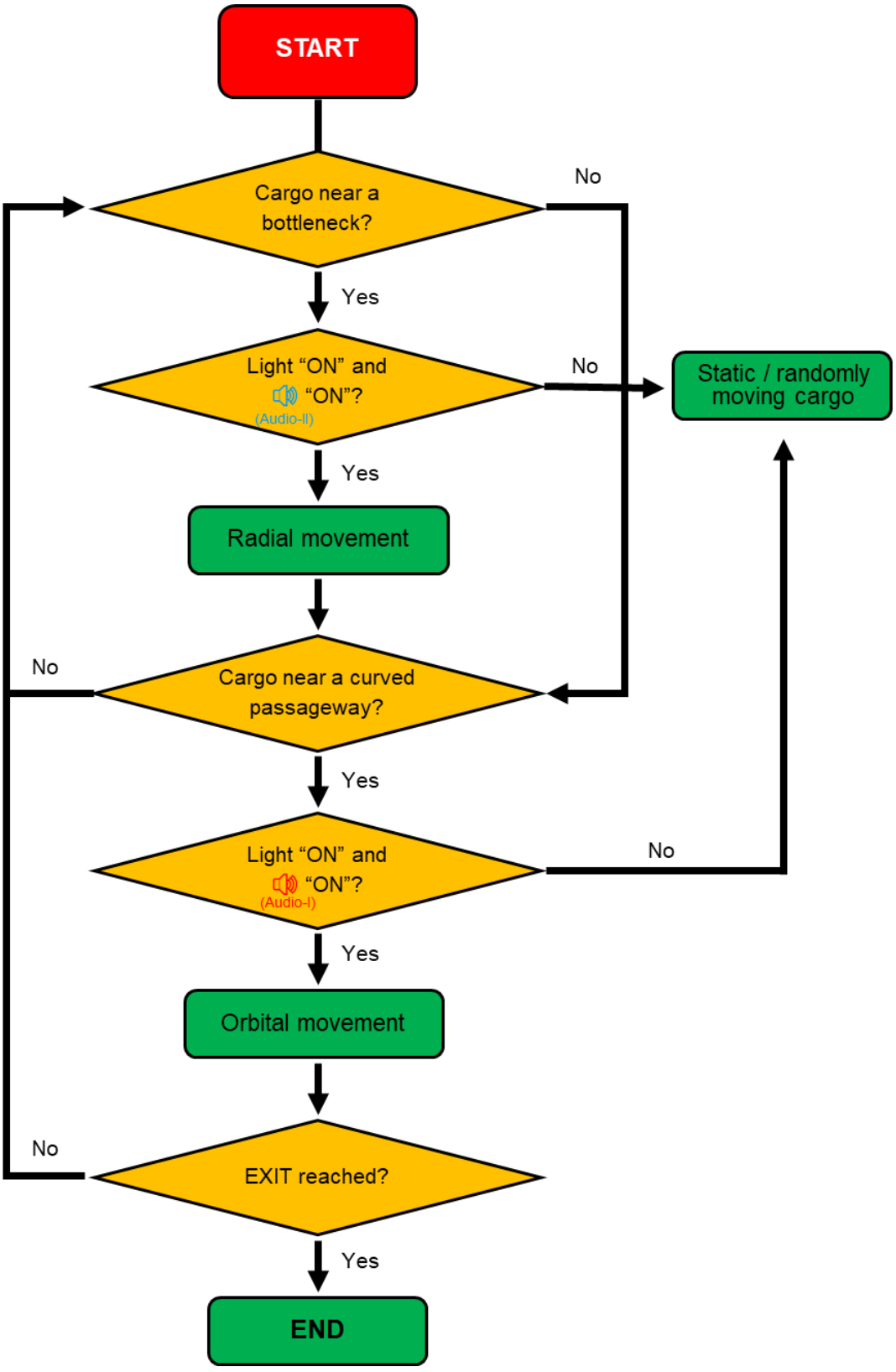

Figure S13. A flow chart showing the overall process that guides a cargo successfully through a maze.

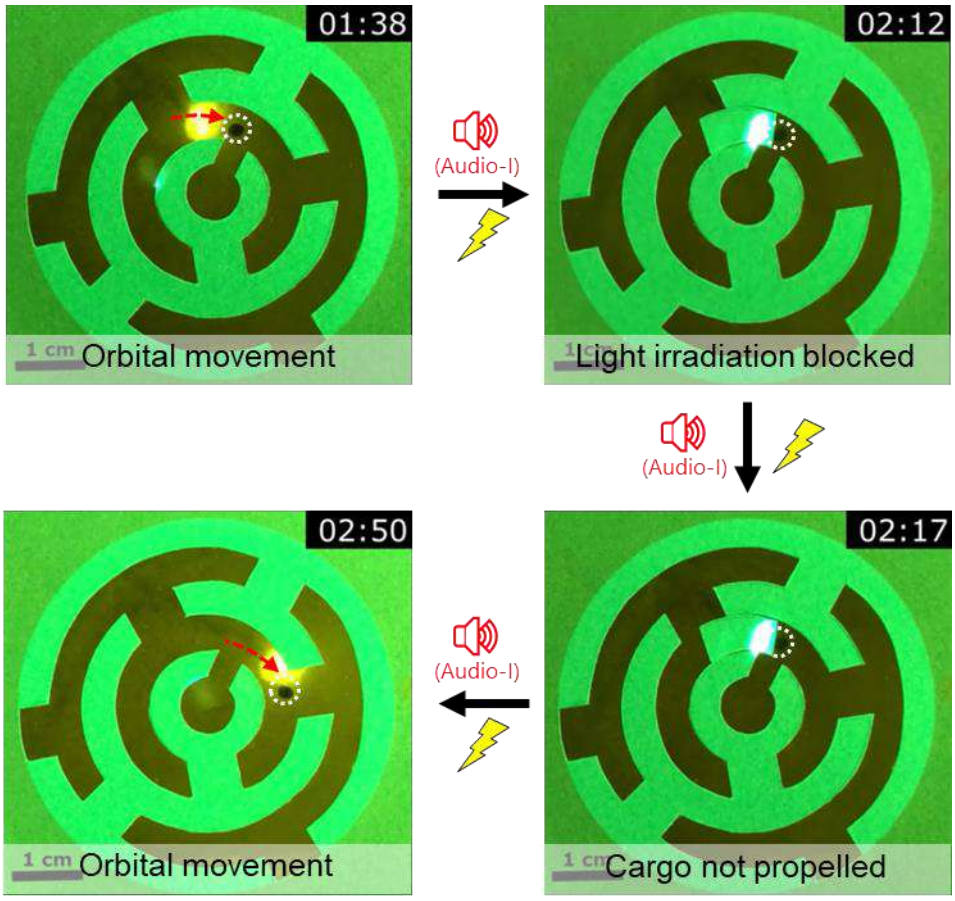

Figure S14. Snapshots of a control experiment performed during the maze solving process (Video S11) shows that the cargo was not propelled when the maze passageway was blocked to inhibit the irradiation of nanoaggregate dispersed solution with blue light.

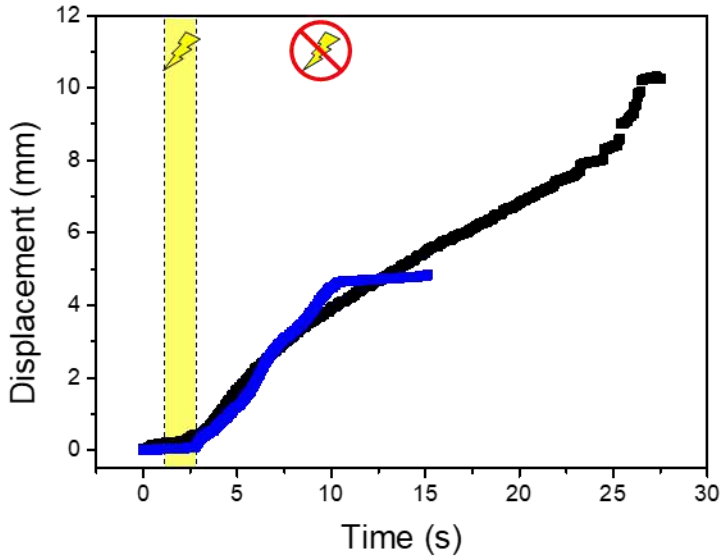

Figure S15. Time dependent displacement changes of a cargo moving in a radial direction in the presence (blue trace) as well as in the absence (black trace) of sound waves (Audio-II). In the absence of audible sound input, the cargo on light irradiation was moved for a comparatively longer distance.

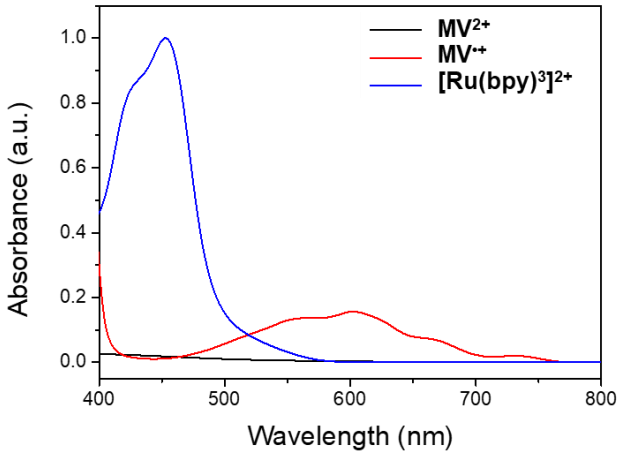

Figure S16. UV-vis absorption spectra of **MV^{2+}** (black trace), **$MV^{\bullet+}$** (red trace) and **$[Ru(bpy)^3]^{2+}$** (blue trace). The **$MV^{\bullet+}$** was generated by chemical reduction using sodium dithionite.

Supplemental References

1. Kalinichenko, V.A., and Sekerzh-Zen'kovich, S.Y. (2007). Experimental investigation of Faraday waves of maximum height. Fluid Dynamics *42*, 959–965.
2. Moisy, F., Rabaud, M., and Salsac, K. (2009). A synthetic Schlieren method for the measurement of the topography of a liquid interface. Exp. Fluids *46*, 1021–1036.
3. Shi, Z., Peng, P., Strohecker, D., and Liao, Y. (2011). Long-lived photoacid based upon a photochromic reaction. J. Am. Chem. Soc. *133*, 14699–14703.
4. Xu, Y., Fei, J., Li, G., Yuan, T., Li, Y., Wang, C., Li, X., and Li, J. (2017). Enhanced photophosphorylation of a chloroplast-entrapping long-lived photoacid. Angew. Chem. Int. Ed. Engl. *56*, 12903–12907.
5. Liao, Y. (2017). Design and applications of metastable-state photoacids. Acc. Chem. Res. *50*, 1956–1964.

Chem

CellPress

Article

Spatiotemporal segregation of chiral supramolecular polymers

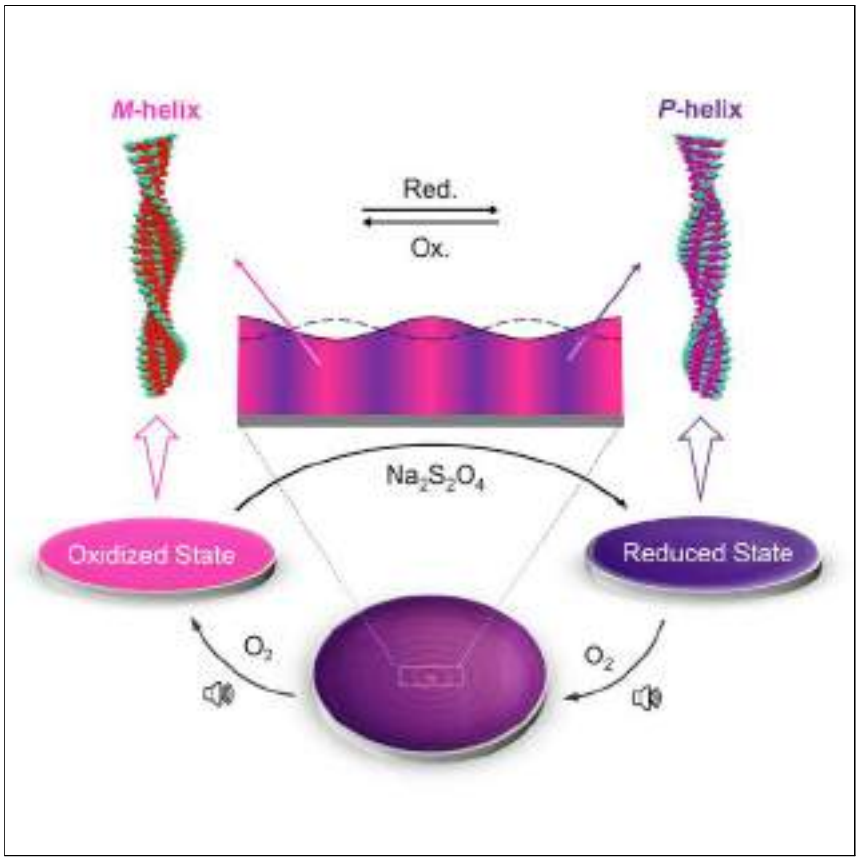

Programmable spatiotemporal control over the segregation of supramolecular polymers of different structures and functions within the same solution is one of the long-standing issues in chemistry. Herein, we achieve this goal by controlling the spatiotemporal distribution of out-of-equilibrium supramolecular polymers in solution, utilizing audible sound-assisted liquid vibrations. This strategy may provide advanced control over the spatiotemporal synthesis of functional supramolecular polymers in the solution state.

Shovan Kumar Sen, Rahul Dev Mukhopadhyay, Seoyeon Choi, Ilha Hwang, Kimoon Kim

rdevmukherjee@gmail.com (R.D.M.)
ihwang1@ibs.re.kr (I.H.)
kkim@postech.ac.kr (K.K.)

Highlights

Chirality switching in out-of-equilibrium supramolecular systems

Spatiotemporally controlled formation of chirally assorted supramolecular polymers

Audible sound-assisted segregation of chiral and achiral supramolecular polymers

Audible sound-assisted segregation of supramolecular polymers of opposite helicity

Sen et al., Chem 9, 1–13
March 9, 2023 © 2022 Elsevier Inc.
https://doi.org/10.1016/j.chempr.2022.10.022

Please cite this article in press as: Sen et al., Spatiotemporal segregation of chiral supramolecular polymers, Chem (2022), https://doi.org/10.1016/j.chempr.2022.10.022

Chem

CellPress

Article

Spatiotemporal segregation of chiral supramolecular polymers

Shovan Kumar Sen,[1] Rahul Dev Mukhopadhyay,[1,4,*] Seoyeon Choi,[2] Ilha Hwang,[1,*] and Kimoon Kim[1,2,3,5,*]

SUMMARY

Programmable spatiotemporal control over the formation of functional supramolecular polymers, which leads to the formation of different morphological forms in solution, is one of the long-standing issues in chemistry. The situation is even more complex especially when dealing with a mixture of species in multicomponent self-assemblies. One way to achieve this goal is by controlling the spatiotemporal distribution of the molecular components in solution, which control the overall aggregation process. Herein, we report the spatiotemporal segregation of different redox-responsive supramolecular assemblies inside spatiotemporal domains generated within the same solution under out-of-equilibrium conditions by using audible sound. Using this approach, we can spatiotemporally control the formation of at least two types of assemblies, which are either both achiral or one of them is chiral, or both are chiral but with opposite helicity. This strategy may provide advanced control over solution-state synthesis of supramolecular polymers, which exhibit morphology-dependent functions.

INTRODUCTION

The manual sorting of crystals of the enantiomeric forms of tartaric acid by Pasteur, using a simple pair of tweezers, can be considered as one of the watershed moments in the field of molecular chirality and stereochemistry. Since then, this field has made tremendous advancements from molecular-level chirality to chiral supramolecular systems. Presently, the advancements in our understanding of supramolecular interactions have made it even possible to program the chirality of supramolecular polymers in solution.[1–4] Controlling the handedness of chiral supramolecular polymers depends largely on the programmability of molecular interactions within the supramolecular assemblies. The most widely adopted strategy to synthesize chiral assemblies is through the aggregation of chiral monomers (chiral homopolymers). Other approaches include, among others, the co-assembly of achiral monomers with chiral inducers (chiral heteropolymers), chiral amplification of supramolecular polymers through the "sergeants-and-soldiers" effect, living polymerization, and specific cases of supramolecular chirality.[5–16] Control over the inversion of helicity of synthesized supramolecular assemblies has also been achieved by application of a variety of external stimuli such as pH, light, redox, temperature, solvents, vortex motion, stirring, introduction of chiral molecules, and so on.[17–42]

Owing to their inherent dynamic nature, several supramolecular polymers, which differ in their chirality, coexist in solution, and manual sorting of a particular type among them is practically impossible due to their small size and random diffusion.

THE BIGGER PICTURE

Achieving programmable control over the formation of chiral supramolecular polymers in solution has gained great interest. Special efforts have been dedicated toward the control of supramolecular helicity with molecular-level manipulation, stimuli-responsive chirality switching, etc. However, spatiotemporal segregation of supramolecular polymers that differ in their chiroptical properties, within the same solution, has been a grueling task. Herein, we demonstrated audible sound-assisted spatiotemporal segregation of chirally different supramolecular polymers in separate domains within the same solution. Specifically, we could spatiotemporally segregate chiral and achiral polymers as well as oppositely chiral polymers with this method. This concept can be further extended to spatiotemporally segregate supramolecular polymers that exhibit distinct functions in order to explore new applications in the research field related to systems chemistry and materials science.

Please cite this article in press as: Sen et al., Spatiotemporal segregation of chiral supramolecular polymers, Chem (2022), https://doi.org/10.1016/j.chempr.2022.10.022

However, if one can create patterned chemical gradients within a solution, where the formation of chiral supramolecular polymers of a particular type can be controlled in a region-specific fashion, it will be possible to arrive at a state where different chiral supramolecular polymers are in principle segregated within the same solution. Chiral supramolecular systems are generally explored under thermodynamically controlled (equilibrium) conditions, and consequently the aforementioned spatial control over supramolecular assemblies exhibiting opposite helicity or that between chiral and achiral assemblies in solution has not been achieved so far. This makes way for out-of-equilibrium supramolecular systems that require a continuous supply of chemical fuel or a physical energy source that can be applied to retain their inherent self-assembled state, thereby providing us with region-specific control over their formation in solution through spatiotemporal pattern formation.[43–47]

In comparison with other physical external stimuli, the use of sound to gain control over the synthesis of chiral assemblies in solution has been rarely explored.[48] Recently, our group showed audible sound can be utilized for region-specific dissolution of atmospheric gases to generate programmable spatiotemporal domains within a solution, in which out-of-equilibrium chemical processes can be executed.[49] We therefore thought of spatiotemporally controlling the formation of redox-responsive chemical systems that form different supramolecular assemblies in their oxidized and reduced states (under out-of-equilibrium conditions) in solution. The audible sound induces surface vibrations and advection currents within the bulk (depth of solution: 2 mm) of a solution placed in a circular vessel (Petri dish). This results in faster dissolution of atmospheric oxygen at the concentric ring-shaped domains, which are located just below the antinodal (maximum vibrating) regions of the surface waves.[49] As a result, the concentration of supramolecular polymers in their oxidized state increases in these regions. The reduced form of the polymers is specifically retained in another set of concentric ring-shaped domains located below the nodal (minimum vibrating) regions of the surface waves. Under normal conditions (without sound), the two different types of polymers are randomly distributed within the solution. However, in the presence of audible sound, concentric ring-shaped domains were generated, and a spatiotemporal pattern consisting of two different types of polymers was obtained (Figure 1A).

Herein, we have exploited multicomponent supramolecular systems that can form different types of achiral or chiral assemblies, depending on the redox state of one of the monomer species present in the assembly (Figure 1B). We spatiotemporally controlled the formation of such redox-responsive assemblies by utilizing audible sound-induced region-specific dissolution of atmospheric oxygen in solution. We first explored the self-assembly of an achiral redox-responsive monomer, where we could spatiotemporally segregate two different achiral assemblies in solution. This was followed by co-assembly studies of the aforementioned achiral redox-responsive monomer with a chiral non-redox-responsive molecule, which dissociated from the assembly resulting in the formation of an achiral assembly when the other partner was reduced. Here, we could specifically achieve spatiotemporal segregation of achiral and chiral supramolecular assemblies through this design. The strategy was further extended with a different chiral partner, which remained associated with the achiral partner irrespective of its redox state. However, the co-assembly obtained through this design exhibited opposite chirality. The spatiotemporal segregation of the two oppositely chiral polymers within the same solution was thereby achieved by utilizing our audible sound-based approach. This technique can be further utilized for the spatiotemporal segregation of other redox-responsive supramolecular polymers with different structures and related properties.

[1]Center for Self-assembly and Complexity (CSC), Institute for Basic Science (IBS), Pohang 37673, Republic of Korea

[2]Division of Advanced Materials Science, Pohang University of Science and Technology (POSTECH), Pohang 37673, Republic of Korea

[3]Department of Chemistry, Pohang University of Science and Technology (POSTECH), Pohang 37673, Republic of Korea

[4]Present address: Department of Chemistry, Ramananda College, Bankura University, Bishnupur, West Bengal 722122, India

[5]Lead contact

*Correspondence: rdevmukherjee@gmail.com (R.D.M.), ihwang1@ibs.re.kr (I.H.), kkim@postech.ac.kr (K.K.)

https://doi.org/10.1016/j.chempr.2022.10.022

Please cite this article in press as: Sen et al., Spatiotemporal segregation of chiral supramolecular polymers, Chem (2022), https://doi.org/10.1016/j.chempr.2022.10.022

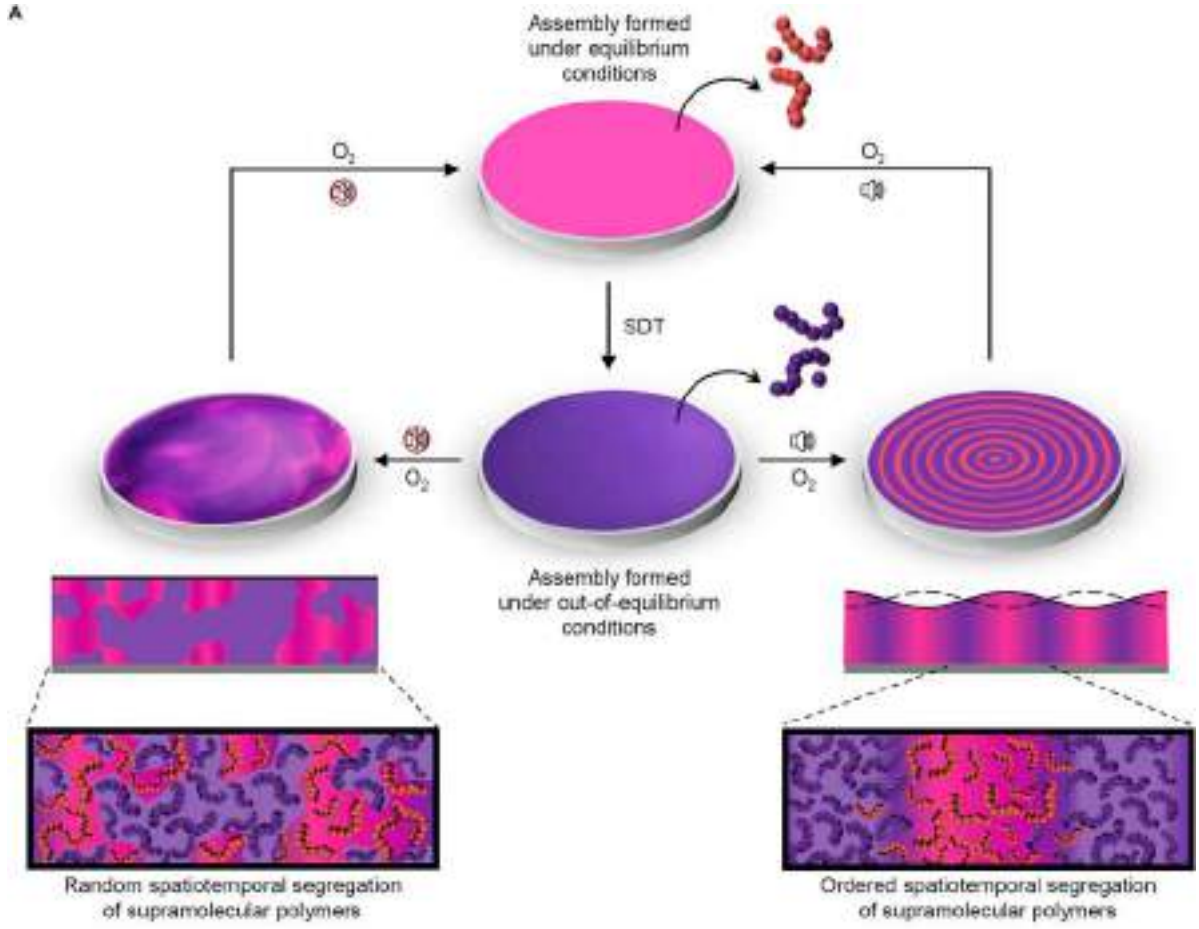

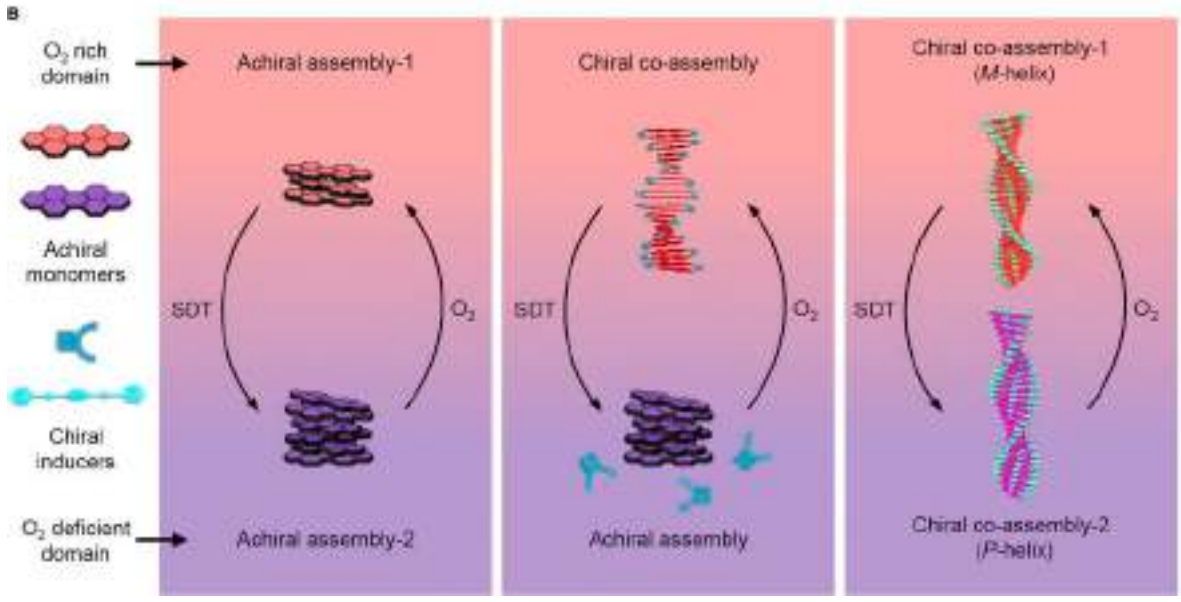

Please cite this article in press as: Sen et al., Spatiotemporal segregation of chiral supramolecular polymers, Chem (2022), https://doi.org/10.1016/j.chempr.2022.10.022

Figure 1. Spatiotemporal segregation of functional supramolecular polymers formed under out-of-equilibrium conditions

(A) Schematic representation of random and ordered spatiotemporal segregation of supramolecular polymers formed under normal (top) and out-of-equilibrium (bottom) conditions, in the absence (left) and presence (right) of audible sound irradiation.

(B) Cartoon showing the design of the chiral multicomponent assemblies. Preferential formation of different types of redox-responsive achiral assemblies and chiral co-assemblies formed under out-of-equilibrium conditions in the O_2-rich and O_2-deficient domains.

Sodium dithionite (SDT) serves as a reducing agent and atmospheric O_2 serves as an oxidizing agent in both (A) and (B).

RESULTS AND DISCUSSION

To study these multicomponent self-assembling systems, we first investigated the redox-responsive self-assembly behavior of the achiral partner to rule out any possibilities of supramolecular chirality in the system. Subsequently, we explored the spatiotemporal segregation of achiral and chiral assemblies within the same solution. This was followed by chiral assemblies exhibiting opposite helicity. A detailed investigation of the spatiotemporal segregation in different self-assembly systems, based on the aforementioned design, is described comprehensively in the following sections.

Spatiotemporal segregation of achiral assemblies

As mentioned before, an integral part of our design is the redox-responsive achiral component. To suit this purpose, we chose a quaternary amine functionalized perylenediimide derivative (PDI),[50] which exhibited strong aggregation behavior in water due to the presence of polar end groups and a hydrophobic polycyclic aromatic core (Figure 2A, left; see supplemental information for synthesis and characterization details of PDI). The formation of PDI assembly was confirmed from temperature-dependent UV-vis spectroscopic investigations (Figure S1). The critical aggregation concentration of PDI was estimated to be 11 μM from emission spectroscopy (Figure S2). Addition of sodium dithionite (SDT, $Na_2S_2O_4$) to the aggregated PDI resulted in a change in color of the solution from red to violet, which corresponded to the formation of dianionic PDI^{2-} (Figure 2A, right). This violet solution, when placed in a Petri dish, reverted to its original red color upon prolonged exposure to atmospheric oxygen; a spatiotemporal pattern consisting of random distribution of violet- and red-colored domains was obtained as an intermediate state under ordinary conditions (Figure S3). We anticipated that in the presence of audible sound, we can achieve a transient intermediate state where the two chemical species (red and violet) will be specifically located along concentric ring-shaped domains (Figure 2A, center). The UV-vis spectrum, corresponding to the neutral PDI assembly in water (red solution), showed a major absorption band at 500 nm. However, upon addition of excess SDT, the absorption spectrum of the violet solution showed a red shift with significant broadening. On oxidation by exposing the solution to air, the original absorption spectrum of PDI was recovered (Figure 2B). These results clearly suggest that in the oxidized state, PDI existed as a neutral PDI assembly in water. However, upon addition of SDT, the dianionic PDI^{2-} exhibited an entirely different assembly behavior. Dynamic light scattering (DLS) further confirmed the redox-responsive transient changes in the size of the aggregates in solution (Figure S4). Circular dichroism (CD) studies indicated that in both cases, the aggregates were achiral in nature (Figure S5). To further investigate this phenomenon, we carried out morphological investigations of the aforementioned assemblies utilizing scanning electron microscopy (SEM). The hierarchical assembly of the formed assemblies in solution resulted in the formation of non-helical nanofibers in both cases. However, the thickness of the fibers was ~80 nm for the neutral PDI assembly, and thicker tape-like fibers (~300 nm) were obtained in the case of the dianionic PDI^{2-} assembly (Figures 2C, 2D, and S7). Both thin and tape-like fibers were observed from a partially oxidized solution of PDI assembly (Figure S8).

Please cite this article in press as: Sen et al., Spatiotemporal segregation of chiral supramolecular polymers, Chem (2022), https://doi.org/10.1016/j.chempr.2022.10.022

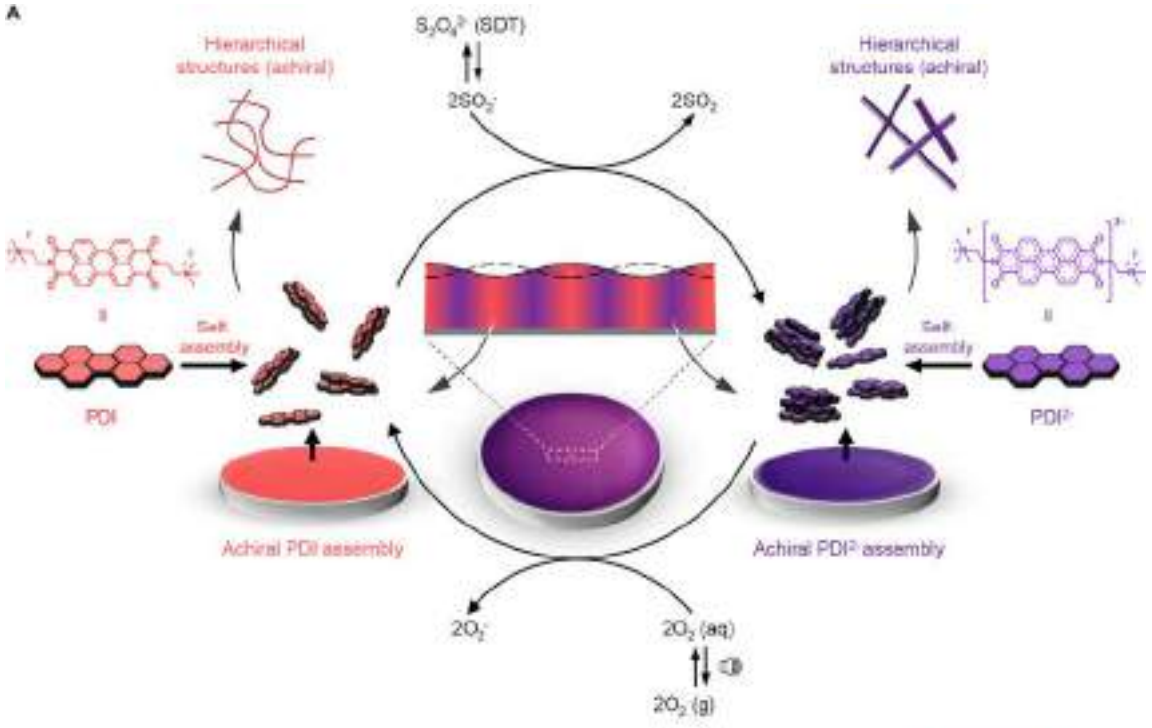

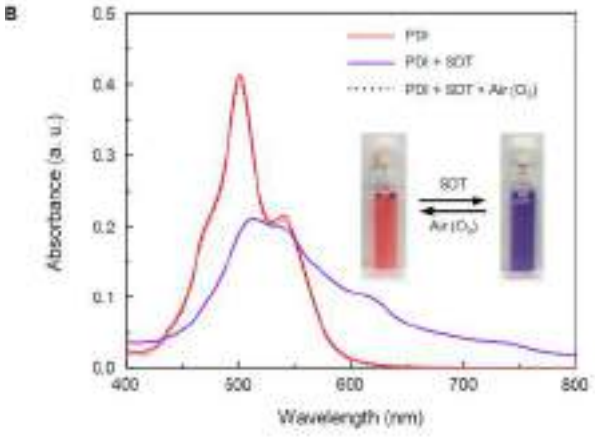

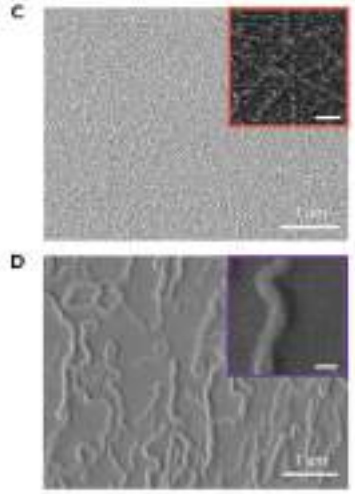

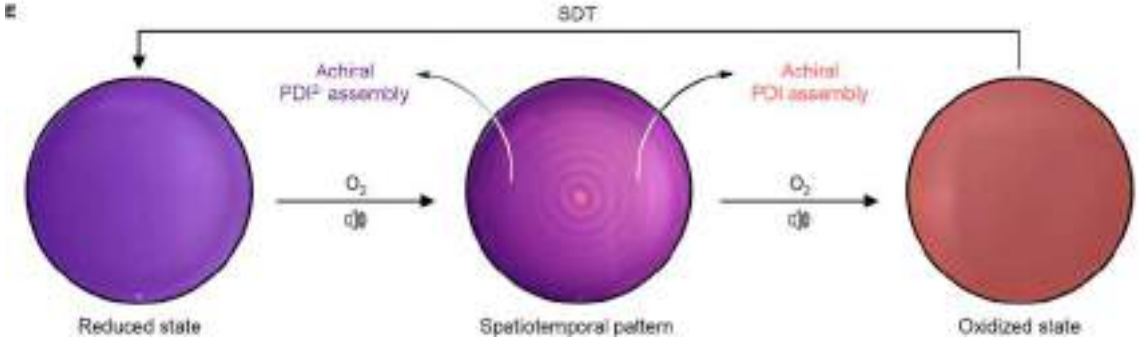

Please cite this article in press as: Sen et al., Spatiotemporal segregation of chiral supramolecular polymers, Chem (2022), https://doi.org/10.1016/j.chempr.2022.10.022

Figure 2. Spatiotemporal segregation of achiral assemblies in redox-responsive PDI self-assembly system

(A) Schematic representation of the redox-responsive spatiotemporal segregation of the achiral PDI and PDI^{2-} assemblies.

(B) UV-vis spectra showing the redox-responsive changes of PDI in water (0.10 mM). Corresponding photographs of the reduced (violet) and oxidized (red) PDI solution (inset).

(C) SEM images of the hierarchical nanofibers formed from the PDI assembly in water (0.20 mM). Inset: magnified image of the nanofibers (scale bars represent 0.3 μm).

(D) SEM images of the hierarchical tape-like nanostructures formed from the PDI^{2-} assembly in water (0.20 mM). Inset: magnified image of the nanofibers (scale bars represent 0.3 μm).

(E) Spatiotemporal segregation of achiral PDI and PDI^{2-} assembly (0.20 mM) in the presence of a 40-Hz sound input.

Having confirmed that the formation of two different types of assemblies could be controlled by controlling the redox state of the PDI, we next explored the spatiotemporal segregation of the aforementioned achiral assemblies by using our audible sound-based strategy (Figure 2E). On vertically vibrating the violet-colored solution containing assembled PDI^{2-} with audible sound operating at an optimized specific frequency of 40 Hz (Figure S9), the solution gradually began to exhibit a spatiotemporal pattern consisting of red- and violet-colored concentric rings. Within this spatiotemporal pattern, the formation of two different types of achiral assemblies of neutral PDI (red) and that of dianionic PDI^{2-} (violet) was observed along the alternately arranged concentric spatiotemporal domains formed in the solution (Figures 2E, center, and S10; Video S1).

Spatiotemporal segregation of supramolecular achiral and chiral assemblies

Having understood the redox-responsive assembly behavior of PDI, we next studied the chiral co-assembly between PDI and adenosine triphosphate (ATP) in water. The positively charged quaternary amine functional groups in the former are expected to interact with the negatively charged phosphate groups of the latter via electrostatic interactions.[51] The resulting chiral co-assembly should in principle exhibit redox-responsive changes in its assembly behavior, and the segregation of such aggregates within concentric ring-shaped domains was therefore expected in the presence of audible sound (Figure 3A). The formation of PDI-ATP co-assembly was confirmed by UV-vis absorption and CD spectroscopic studies (Figure S11).[51] Upon addition of ATP to the PDI solution, the intensities of the absorption band (around 500 nm) decreased, and the new broad shoulder appeared at the longer wavelength (around 580 nm). Due to the presence of ATP, the co-assembly was expected to be chiral, and its formation was therefore characterized by CD spectroscopy (Figure S11). Since PDI is intrinsically achiral, no characteristic CD signal was observed for PDI assembly alone. Interestingly, upon addition of ATP, a positive CD band was observed at 555 nm followed by a negative CD band at 485 nm with a zero crossover point at 507 nm, which suggest the formation of right-handed helical supramolecular co-assembly.[51] The critical aggregation concentration of PDI-ATP co-assembly was estimated to be 13 μM, as determined from CD spectroscopy (Figure S12). The stoichiometry of the constituent monomers in the chiral co-assembly was evaluated to be 1:1 (PDI:ATP), based on CD titrations and a Job plot obtained from CD titration experiments (Figures S13 and S14). Further, changes in zeta potential of PDI-ATP co-assembly were measured at various PDI and ATP ratios; a constant decrease in the zeta potential value upon adding ATP to the PDI aggregate solution verifies the surface co-assembly of ATP (Figure S15). The redox-responsive behavior of PDI-ATP assembly was further studied by CD and UV-vis spectroscopies (Figure 3B). When SDT was added to the PDI-ATP co-assembly, we observed that the aforementioned CD signal disappeared, which suggest the disassembly of the chiral aggregates (Figure 3B). A similar color change of the solution from red to violet was observed on reduction as observed in the case of PDI alone (Figure 2B, inset). The same solution was also studied by UV-vis

Please cite this article in press as: Sen et al., Spatiotemporal segregation of chiral supramolecular polymers, Chem (2022), https://doi.org/10.1016/j.chempr.2022.10.022

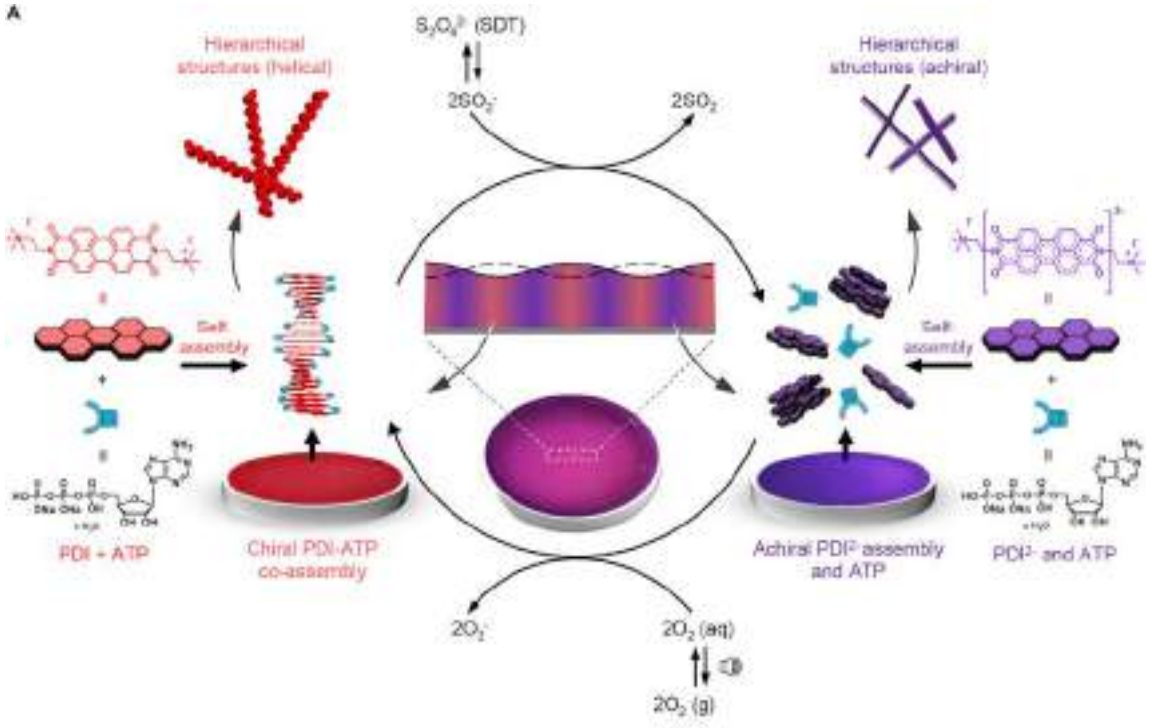

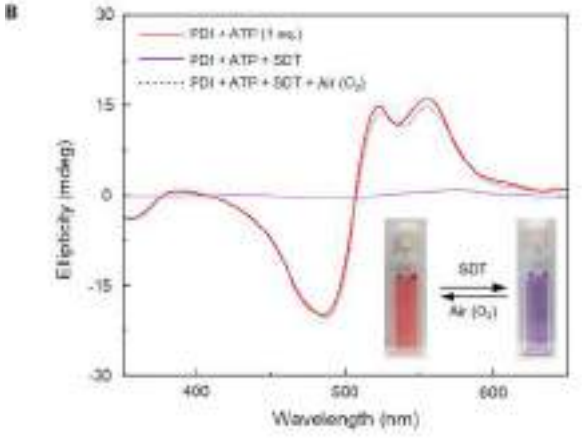

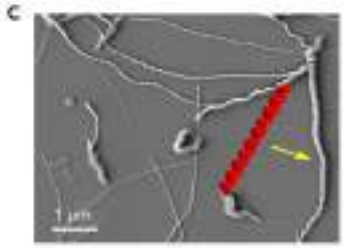

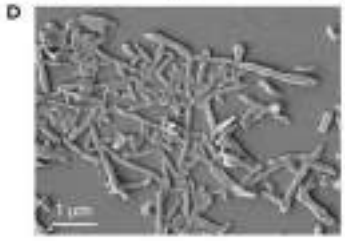

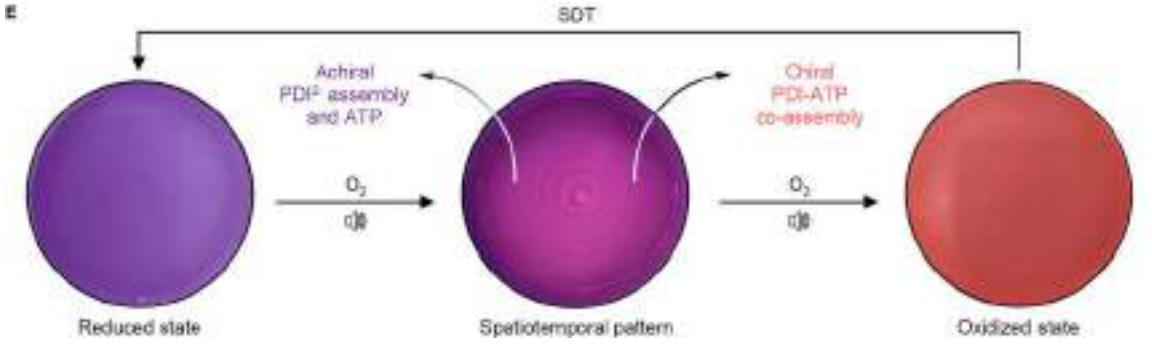

Please cite this article in press as: Sen et al., Spatiotemporal segregation of chiral supramolecular polymers, Chem (2022), https://doi.org/10.1016/j.chempr.2022.10.022

Figure 3. Spatiotemporal segregation of achiral and chiral assemblies in redox-responsive PDI-ATP self-assembly system

(A) Schematic representation of redox-responsive spatiotemporal segregation of achiral PDI^{2-} assembly and chiral PDI-ATP co-assembly.

(B) CD spectra showing the redox-responsive changes of PDI-ATP self-assembly in an aqueous medium (0.30 mM). Inset: corresponding photographs of the reduced (violet) and oxidized (red) PDI-ATP (1:1) solution.

(C) SEM images of the hierarchical right-handed helical nanofibers (*P* helix) formed from the PDI-ATP co-assembly in water (0.20 mM). Inset: cartoon representation of the *P* helix shown as a guide to the eye.

(D) SEM images of the hierarchical tape-like nanofibers formed from PDI^{2-} assembly in water (0.20 mM).

(E) Spatiotemporal segregation of the chiral PDI-ATP co-assembly and achiral PDI^{2-} assembly (0.20 mM) in the presence of a 40-Hz sound input.

spectroscopy, and the broad absorption spectrum matched well with that of the aggregates formed from PDI^{2-} (Figure S16). A plausible reason behind such an observation may be the disassembly of the PDI-ATP aggregates due to the electrostatic repulsion between the negatively charged PDI^{2-} and ATP. This was followed by the reassembly of PDI^{2-} to form an achiral assembly as mentioned in the previous section (Figure 2). On oxidizing the same solution, the CD signal was recovered, suggesting the re-formation of the chiral PDI-ATP co-assembly (Figure 3B).

We next explored the redox-responsive morphological changes of the chiral PDI-ATP co-assembly. SEM investigations confirmed the formation of chiral right-handed helical nanofibers (*P* helix) in the oxidized state (Figure 3C). In the reduced state, however, we observed the formation of ~350-nm-wide tape-like nanofibers (Figures 3D and S18), which matched well with that of the previously observed PDI^{2-} nanofibers (Figure 2D). Both right-handed helical nanofibers and tape-like achiral nanofibers were obtained from a partially oxidized solution of chiral PDI-ATP co-assembly (Figure S19). DLS further confirmed the redox-responsive transient changes in the size of the aggregates in solution (Figure S20). These experiments clearly suggest the formation of chiral co-assembly of PDI-ATP in the oxidized state of the PDI molecule and the formation of achiral assembly of PDI^{2-} under out-of-equilibrium conditions (Figure 3A). The next challenge was therefore to spatiotemporally segregate these chiral and achiral assemblies formed in solution. Thus, we started with a completely reduced solution (violet-colored) (Figure 3E, left), which was obtained by the addition of SDT to a solution of PDI-ATP chiral co-assembly (red-colored). On exposing the aforementioned solution to audible sound operating at a specific frequency (40 Hz), the violet-colored solution (corresponding to PDI^{2-} assembly and ATP) gradually began to exhibit a pattern consisting of red- and violet-colored concentric rings. Audible sound therefore generated a spatiotemporal pattern comprising PDI-ATP (chiral co-assembly) and PDI^{2-} achiral assembly in the same solution (Figures 3E, center, and S21; Video S2). On prolonged exposure to audible sound, the solution reverted to its original red color, corresponding to the formation of chiral PDI-ATP co-assembly (Figure 3E, right). In the absence of audible sound, we observed a random distribution of chiral and achiral assembly domains in solution as an intermediate stage (Figure S22).

Spatiotemporal segregation of assemblies of opposite helicity

Our experiments with the previous self-assembly system suggested that ATP does not prefer to remain associated with PDI^{2-} due to electrostatic repulsion. We therefore needed a chiral partner, which can remain associated with PDI^{2-} and affect the chirality of the assembly in the out-of-equilibrium state (Figure 4A). After screening a number of suitable candidates,[17–25] we chose the enantiomers of a phenylalanine-derived gelator (LPF/DPF), which are known to introduce chirality while forming co-assemblies with achiral molecules,[38,39] as well as to exhibit chemical stimuli-responsive switching in chirality in response to minimal changes in the intermolecular interactions with its achiral partner (see supplemental information for synthesis and characterization details of LPF and DPF molecules).[52] We first studied the

Please cite this article in press as: Sen et al., Spatiotemporal segregation of chiral supramolecular polymers, Chem (2022), https://doi.org/10.1016/j.chempr.2022.10.022

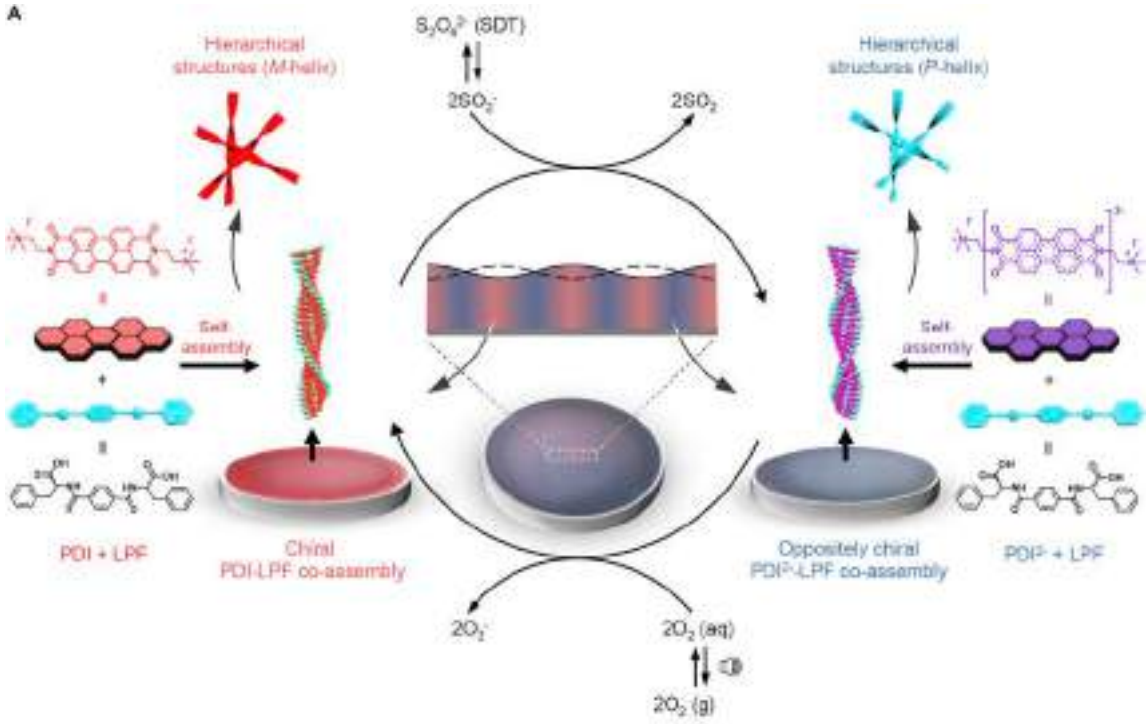

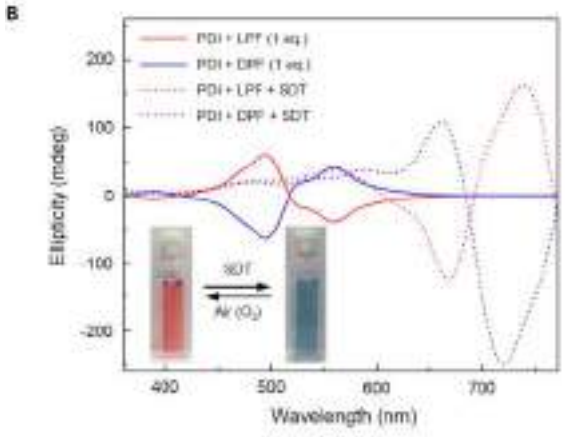

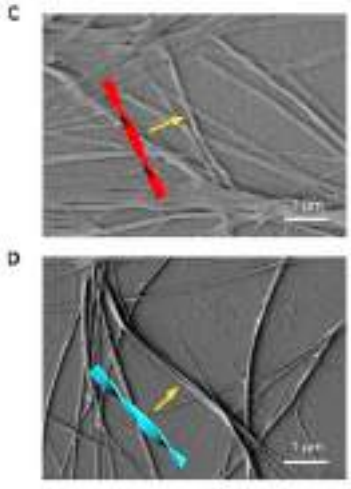

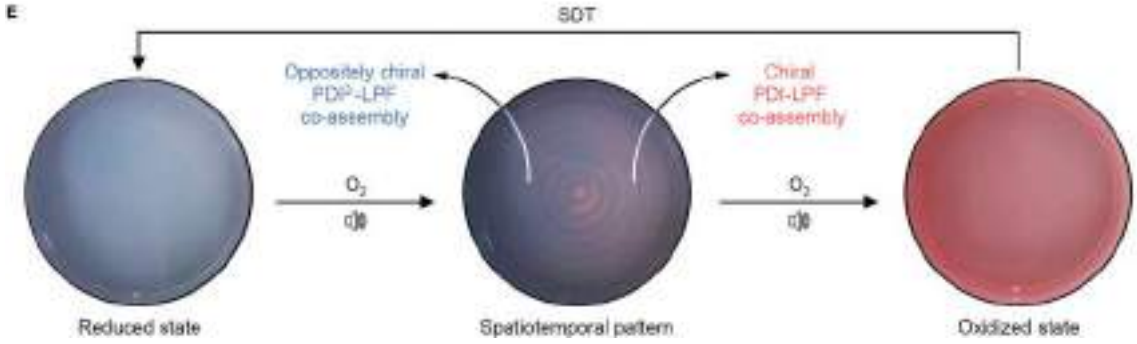

Please cite this article in press as: Sen et al., Spatiotemporal segregation of chiral supramolecular polymers, Chem (2022), https://doi.org/10.1016/j.chempr.2022.10.022

Figure 4. Spatiotemporal segregation of oppositely chiral assemblies in redox-responsive PDI-LPF/PDI-DPF self-assembling systems

(A) Schematic representation of redox-responsive spatiotemporal segregation of PDI-LPF chiral co-assembly and oppositely chiral PDI^{2-}-LPF co-assembly.

(B) CD spectra showing the redox-responsive changes of PDI-LPF self-assembly and PDI-DPF self-assembly in an aqueous medium (0.10 mM). Inset: corresponding photographs of the reduced (blue) and oxidized (red) PDI-LPF (1:1) solution.

(C) SEM images of the hierarchical left-handed helical nanofibers (*M* helix) formed from the PDI-LPF co-assembly in water (0.10 mM). Inset: cartoon representation of the *M* helix shown as a guide to the eye.

(D) SEM images of the hierarchical right-handed helical nanofibers (*P* helix) formed from PDI^{2-}-LPF co-assembly in water (0.10 mM). Inset: cartoon representation of the *P* helix shown as a guide to the eye.

(E) Spatiotemporal segregation of the chiral PDI-LPF co-assembly and oppositely chiral PDI^{2-}-LPF co-assembly (0.10 mM) in the presence of a 40-Hz sound input.

co-assembly between PDI and LPF molecules by using various spectroscopic techniques (Figure S23). CD spectroscopy experiments, upon addition of LPF to the solution of PDI, revealed a negative CD signal at 558 nm followed by a positive CD signal at 493 nm with a zero crossover point at 516 nm. The results suggest the preferential formation of left-handed (*M*-type) helical co-assembly.[39] The critical aggregation concentration of PDI-LPF co-assembly was estimated to be 6 μM, as determined from CD spectroscopy (Figure S24). The stoichiometry of the constituent monomers in the chiral co-assembly was evaluated to be 1:1 (PDI:LPF), based on CD titrations and a Job plot obtained from CD titration experiments (Figures S25 and S26). Interestingly, upon addition of SDT to the PDI-LPF solution, the CD spectrum is switched to a positive CD signal at 738 nm followed by a negative CD signal at 668 nm, suggesting the formation of right-handed helical assembly (*P* helix) (Figures 4B and S27). This is accompanied by a visual change in the color of the solution from red to blue, and the transformation was also reflected in the UV-vis absorption spectrum (Figure S28). The solution reverted to its original state in the presence of atmospheric oxygen after ~20 min.

To gain a better understanding of the system, we synthesized the opposite isomer DPF[20] and studied the PDI-DPF co-assembly by using various spectroscopic techniques as before (Figures S30–S32). We observed that the CD spectrum obtained in the case of PDI-DPF was exactly opposite (mirror image) to that obtained in case of the PDI-LPF co-assembly, both in the neutral and reduced states (Figure 4B). In the absence of irrefutable crystallographic data, it is difficult to comment on the changes in the molecular-level interactions that lead to such chirality switching. Nevertheless, we designed control experiments with three specifically designed chiral molecules consisting of a single amide linkage (BPF), devoid of an aromatic core (LCHF), and another containing two *N*-methylated amide linkages (*N*-methyl-LPF) to understand the role essayed by different types of non-covalent interactions between LPF/DPF and PDI in controlling the helical packing of the co-assemblies both in the oxidized state as well as in the reduced state (see supplemental information for synthesis and characterization details of BPF, LCHF, and *N*-methyl-LPF). Surprisingly, we did not observe any chirality induction through co-assembly formation when each of these three molecules was added to the achiral PDI assembly (figures S33–S35). The results clearly suggest that the co-assembly formation between PDI and LPF/DPF requires amide H-bonding interactions at both ends of the π-aromatic core in case of the chiral partner.

Morphological investigation of the oxidized and reduced states of the PDI-LPF co-assembly was further carried out. SEM images confirmed the formation of chiral left-handed helical nanofibers (*M* helix) in the oxidized state (Figure 4C) and right-handed helical nanofibers (*P* helix) in the reduced state (Figure 4D). We were unable to see oppositely helical fibers within the same frame of the SEM images. A partially oxidized solution of chiral PDI-LPF co-assembly yielded non-helical nanofibers,

Please cite this article in press as: Sen et al., Spatiotemporal segregation of chiral supramolecular polymers, Chem (2022), https://doi.org/10.1016/j.chempr.2022.10.022

which suggests that the switching takes place via an achiral state (Figure S36). DLS further confirmed the redox-responsive transient changes in the size of the two oppositely chiral aggregates in solution (Figure S37). The fibers obtained in the case of PDI-DPF assembly exhibited opposite helicity (Figure S38). As expected, upon exposing a solution consisting of the reduced co-assembly of PDI and LPF to a sound source operating at a specific frequency (40 Hz), the blue-colored solution (Figure 4E, left) gradually began to exhibit a concentric ring pattern comprising blue- and red-colored rings. We were therefore able to spatiotemporally segregate oppositely chiral PDI-LPF and PDI^{2-}—LPF co-assemblies respectively in an aqueous solution using this strategy (Figures 4E, center, and S39; Video S3). We similarly obtained the audible sound-induced patterning of PDI-DPF assembly within spatiotemporal domains in an aqueous solution (Figure S40). In the absence of audible sound-induced vibrations, both PDI-LPF and PDL-DPF co-assemblies led to the development of random spatiotemporal patterns (Figures S41 and S42). In both cases, on continued exposure of the solution to atmospheric oxygen, the aggregate solution reverted to its original state within ~20 min (Figure 4E, right). The next challenge is therefore to obtain a permanent (spatially controlled) pattern consisting of segregated domains of oppositely chiral assemblies and helical superstructures through the simultaneous use of non-covalent and covalent interactions for polymerization.[53]

Conclusions

In conclusion, we have utilized audible sound for the spatiotemporal segregation of different types of functional supramolecular polymers formed as a consequence of multicomponent self-assembly in solution. Determining that assemblies with different molecular packing, morphology, and properties can indeed be segregated within the same solution, we have demonstrated the spatiotemporal patterning of redox-responsive chiral and achiral supramolecular assemblies within an aqueous medium. Further, we have also demonstrated spatiotemporal patterning of two oppositely chiral helical supramolecular assemblies. At present, our audible sound-based approach can be utilized to spatiotemporally segregate at least two different types of redox-responsive supramolecular polymers within the same solution, which is in fact related to the generation of two different types of domains formed in solution depending on the rate of oxygen dissolution. Nevertheless, with the exploration of complex supramolecular systems, the spatiotemporal segregation of multiple functional supramolecular polymers within the same solution confronts us with a new challenge. Efforts in these directions are currently under progress. This concept can be further extended to spatiotemporally segregate supramolecular polymers that exhibit distinct functions in order to explore new applications in the research field related to systems chemistry and materials science.

EXPERIMENTAL PROCEDURES

Resource availability

Lead contact

Further information and requests for resources should be directed to and will be fulfilled by the lead contact Kimoon Kim (kkim@postech.ac.kr).

Materials availability

All unique/stable reagents generated in this study are available from the lead contact with a completed Materials Transfer Agreement.

Data and code availability

The authors declare that all data supporting the findings of this study are available within this article and supplemental information files.

SUPPLEMENTAL INFORMATION

Supplemental information can be found online at https://doi.org/10.1016/j.chempr.2022.10.022.

ACKNOWLEDGMENTS

This work was supported by the Institute for Basic Science (IBS) (IBS-R007-D1).

AUTHOR CONTRIBUTIONS

R.D.M. and K.K. conceived and designed the project. S.K.S. carried out the synthesis, spectroscopic investigations, self-assembly studies, and pattern experiments guided by R.D.M. I.H. provided invaluable inputs and suggestions at the initial stages of this work. S.C. carried out the morphological investigations. R.D.M., S.K.S., I.H., and K.K. wrote the manuscript. All authors discussed the results, analyzed the data, and commented on the manuscript. K.K. supervised all of the research.

DECLARATION OF INTERESTS

The authors declare no competing interests.

Received: May 27, 2022
Revised: September 16, 2022
Accepted: October 20, 2022
Published: November 15, 2022

REFERENCES

1. Eckhardt, C.J., Peachey, N.M., Swanson, D.R., Takacs, J.M., Khan, M.A., Gong, X., Kim, J.-H., Wang, J., and Uphaus, R.A. (1993). Separation of chiral phases in monolayer crystals of racemic amphiphiles. Nature *362*, 614–616.

2. Iavicoli, P., Xu, H., Feldborg, L.N., Linares, M., Paradinas, M., Stafström, S., Ocal, C., Nieto-Ortega, B., Casado, J., López Navarrete, J.T., et al. (2010). Tuning the supramolecular chirality of one- and two-dimensional aggregates with the number of stereogenic centers in the component porphyrins. J. Am. Chem. Soc. *132*, 9350–9362.

3. Besenius, P., Portale, G., Bomans, P.H.H., Janssen, H.M., Palmans, A.R.A., and Meijer, E.W. (2010). Controlling the growth and shape of chiral supramolecular polymers in water. Proc. Natl. Acad. Sci. USA *107*, 17888–17893.

4. Shimomura, K., Ikai, T., Kanoh, S., Yashima, E., and Maeda, K. (2014). Switchable enantioseparation based on macromolecular memory of a helical polyacetylene in the solid state. Nat. Chem. *6*, 429–434.

5. Prins, L.J., Timmerman, P., and Reinhoudt, D.N. (2001). Amplification of chirality: the "sergeants and soldiers" principle applied to dynamic hydrogen-bonded assemblies. J. Am. Chem. Soc. *123*, 10153–10163.

6. Palmans, A.R.A., and Meijer, E.W. (2007). Amplification of chirality in dynamic supramolecular aggregates. Angew. Chem. Int. Ed. Engl. *46*, 8948–8968.

7. Makiguchi, W., Kobayashi, S., Furusho, Y., and Yashima, E. (2013). Formation of a homo double helix of a conjugated polymer with carboxy groups and amplification of the macromolecular helicity by chiral amines sandwiched between the strands. Angew. Chem. Int. Ed. Engl. *52*, 5275–5279.

8. Dorca, Y., Greciano, E.E., Valera, J.S., Gómez, R., and Sánchez, L. (2019). Hierarchy of asymmetry in chiral supramolecular polymers: Toward functional, helical supramolecular structures. Chemistry *25*, 5848–5864.

9. Nakano, T., and Okamoto, Y. (2001). Synthetic helical polymers: conformation and function. Chem. Rev. *101*, 4013–4038.

10. Yashima, E., Maeda, K., Iida, H., Furusho, Y., and Nagai, K. (2009). Helical polymers: synthesis, structures, and functions. Chem. Rev. *109*, 6102–6211.

11. Cornelissen, J.J.L.M., Rowan, A.E., Nolte, R.J.M., and Sommerdijk, N.A.J.M. (2001). Chiral architectures from macromolecular building blocks. Chem. Rev. *101*, 4039–4070.

12. Smulders, M.M.J., Filot, I.A.W., Leenders, J.M.A., van der Schoot, P., Palmans, A.R.A., Schenning, A.P.H.J., and Meijer, E.W. (2010). Tuning the extent of chiral amplification by temperature in a dynamic supramolecular polymer. J. Am. Chem. Soc. *132*, 611–619.

13. Yashima, E., Ousaka, N., Taura, D., Shimomura, K., Ikai, T., and Maeda, K. (2016). Supramolecular helical systems: helical assemblies of small molecules, foldamers, and polymers with chiral amplification and their functions. Chem. Rev. *116*, 13752–13990.

14. Liu, M., Zhang, L., and Wang, T. (2015). Supramolecular chirality in self-assembled systems. Chem. Rev. *115*, 7304–7397.

15. Onogi, S., Shigemitsu, H., Yoshii, T., Tanida, T., Ikeda, M., Kubota, R., and Hamachi, I. (2016). In situ real-time imaging of self-sorted supramolecular nanofibres. Nat. Chem. *8*, 743–752.

16. Mishra, A., Korlepara, D.B., Kumar, M., Jain, A., Jonnalagadda, N., Bejagam, K.K., Balasubramanian, S., and George, S.J. (2018). Biomimetic temporal self-assembly via fuel-driven controlled supramolecular polymerization. Nat. Commun. *9*, 1295.

17. Lin, R., Zhang, H., Li, S., Chen, L., Zhang, W., Wen, T.B., et al. (2011). pH-switchable inversion of the metal-centered chirality of metallabenzenes: opposite stereodynamics in reactions of ruthenabenzene with L- and D-cysteine. Chemistry *17*, 2420–2427.

18. Frisch, H., Unsleber, J.P., Lüdeker, D., Peterlechner, M., Brunklaus, G., Waller, M., and Besenius, P. (2013). pH-Switchable ampholytic supramolecular copolymers. Angew. Chem. Int. Ed. Engl. *52*, 10097–10101.

19. Goskulwad, S., La, D.D., Kobaisi, M.A., Bhosale, S.V., Bansal, V., Vinu, A., Ariga, K., and Bhosale, S.V. (2018). Dynamic multistimuli-responsive reversible chiral transformation in supramolecular helices. Sci. Rep. *8*, 11220.

20. Kousar, A., Liu, J., Mehwish, N., Wang, F., Dang-i, A.Y., and Feng, C. (2019). pH-regulated supramolecular chirality of phenylalanine-based hydrogels. Mater. Today Chem. *11*, 217–224.

Please cite this article in press as: Sen et al., Spatiotemporal segregation of chiral supramolecular polymers, Chem (2022), https://doi.org/10.1016/j.chempr.2022.10.022

21. Kim, Y., Li, H., He, Y., Chen, X., Ma, X., and Lee, M. (2017). Collective helicity switching of a DNA–coat assembly. Nat. Nanotechnol. *12*, 551–556.

22. Pijper, D., Jongejan, M.G.M., Meetsma, A., and Feringa, B.L. (2008). Light-controlled supramolecular helicity of a liquid crystalline phase using a helical polymer functionalized with a single chiroptical molecular switch. J. Am. Chem. Soc. *130*, 4541–4552.

23. Wang, Y., Jiang, Y., Zhu, X., and Liu, M. (2019). Significantly boosted and inversed circularly polarized luminescence from photogenerated radical anions in dipeptide naphthalenediimide assemblies. J. Phys. Chem. Lett. *10*, 5861–5867.

24. Pijper, D., and Feringa, B.L. (2007). Molecular Transmission: controlling the twist sense of a helical polymer with a single light-driven molecular motor. Angew. Chem. Int. Ed. Engl. *46*, 3693–3696.

25. Kim, J., Lee, J., Kim, W.Y., Kim, H., Lee, S., Lee, H.C., Lee, Y.S., Seo, M., and Kim, S.Y. (2015). Induction and control of supramolecular chirality by light in self-assembled helical nanostructures. Nat. Commun. *6*, 6959.

26. Ohta, E., Sato, H., Ando, S., Kosaka, A., Fukushima, T., Hashizume, D., Yamasaki, M., Hasegawa, K., Muraoka, A., Ushiyama, H., et al. (2011). Redox-responsive molecular helices with highly condensed π-clouds. Nat. Chem. *3*, 68–73.

27. Zhang, L., Wang, H.-X., Li, S., and Liu, M. (2020). Supramolecular chiroptical switches. Chem. Soc. Rev. *49*, 9095–9120.

28. Gopal, A., Hifsudheen, M., Furumi, S., Takeuchi, M., and Ajayaghosh, A. (2012). Thermally assisted photonic inversion of supramolecular handedness. Angew. Chem. Int. Ed. Engl. *51*, 10505–10509.

29. Huang, Z., Kang, S.-K., Banno, M., Yamaguchi, T., Lee, D., Seok, C., Yashima, E., and Lee, M. (2012). Pulsating tubules from noncovalent macrocycles. Science *337*, 1521–1526.

30. Ślęczkowski, M.L., Mabesoone, M.F.J., Ślęczkowski, P., Palmans, A.R.A., and Meijer, E.W. (2021). Competition between chiral solvents and chiral monomers in the helical bias of supramolecular polymers. Nat. Chem. *13*, 200–207.

31. Gillissen, M.A.J., Koenigs, M.M.E., Spiering, J.J.H., Vekemans, J.A.J.M., Palmans, A.R.A., Voets, I.K., and Meijer, E.W. (2014). Triple Helix Formation in amphiphilic discotics: demystifying solvent effects in supramolecular self-assembly. J. Am. Chem. Soc. *136*, 336–343.

32. Ribó, J.M., Crusats, J., Sagués, F., Claret, J., and Rubires, R. (2001). Chiral sign induction by vortices during the formation of mesophases in stirred solutions. Science *292*, 2063–2066.

33. Amabilino, D.B. (2007). Supramolecular assembly: Nanofibre whirlpools. Nat. Mater. *6*, 924–925.

34. Yan, Y., Deng, K., Yu, Z., and Wei, Z. (2009). Tuning the supramolecular chirality of polyaniline by methyl substitution. Angew. Chem. Int. Ed. Engl. *48*, 2003–2006.

35. Oda, R., Huc, I., Schmutz, M., Candau, S.J., and MacKintosh, F.C. (1999). Tuning bilayer twist using chiral counterions. Nature *399*, 566–569.

36. Yan, Y., Yu, Z., Huang, Y.W., Yuan, W.X., and Wei, Z.X. (2007). Helical polyaniline nanofibers induced by chiral dopants by a polymerization process. Adv. Mater. *19*, 3353–3357.

37. Huang, Y., Yan, Y., Smarsly, B.M., Wei, Z., and Faul, C.F.J. (2009). Helical supramolecular aggregates, mesoscopic organisation and nanofibers of a perylenebisimide–chiral surfactant complex via ionic self-assembly. J. Mater. Chem. *19*, 2356–2362.

38. Liu, G., Li, X., Sheng, J., Li, P.-Z., Ong, W.K., Phua, S.Z.F., Ågren, H., Zhu, L., and Zhao, Y. (2017). Helicity inversion of supramolecular hydrogels induced by achiral substituents. ACS Nano *11*, 11880–11889.

39. Liu, G., Sheng, J., Wu, H., Yang, C., Yang, G., Li, Y., Ganguly, R., Zhu, L., and Zhao, Y. (2018). Controlling supramolecular chirality of two-component hydrogels by J- and H-aggregation of building blocks. J. Am. Chem. Soc. *140*, 6467–6473.

40. Karunakaran, S.C., Cafferty, B.J., Weigert-Muñoz, A., Schuster, G.B., and Hud, N.V. (2019). Spontaneous symmetry breaking in the formation of supramolecular polymers: implications for the origin of biological homochirality. Angew. Chem. Int. Ed. Engl. *58*, 1453–1457.

41. Noorduin, W.L., Izumi, T., Millemaggi, A., Leeman, M., Meekes, H., Van Enckevort, W.J.P., Kellogg, R.M., Kaptein, B., Vlieg, E., and Blackmond, D.G. (2008). Emergence of a single solid chiral state from a nearly racemic amino acid derivative. J. Am. Chem. Soc. *130*, 1158–1159.

42. Kumar, M., Ing, N.L., Narang, V., Wijerathne, N.K., Hochbaum, A.I., and Ulijn, R.V. (2018). Amino-acid-encoded biocatalytic self-assembly enables the formation of transient conducting nanostructures. Nat. Chem. *10*, 696–703.

43. Mattia, E., and Otto, S. (2015). Supramolecular systems chemistry. Nat. Nanotechnol. *10*, 111–119.

44. Jiao, Y., Qiu, Y., Zhang, L., Liu, W.-G., Mao, H., Chen, H., Feng, Y., Cai, K., Shen, D., Song, B., et al. (2022). Electron-catalysed molecular recognition. Nature *603*, 265–270.

45. Rizzuto, F.J., Platnich, C.M., Luo, X., Shen, Y., Dore, M.D., Lachance-Brais, C., Guarné, A., Cosa, G., and Sleiman, H.F. (2021). A dissipative pathway for the structural evolution of DNA fibres. Nat. Chem. *13*, 843–849.

46. Leira-Iglesias, J., Tassoni, A., Adachi, T., Stich, M., and Hermans, T.M. (2018). Oscillations, travelling fronts and patterns in a supramolecular system. Nat. Nanotechnol. *13*, 1021–1027.

47. Leira-Iglesias, J., Sorrenti, A., Sato, A., Dunne, P.A., and Hermans, T.M. (2016). Supramolecular pathway selection of perylenediimides mediated by chemical fuels. Chem. Commun. *52*, 9009–9012.

48. Kumar, J., Nakashima, T., and Kawai, T. (2014). Inversion of supramolecular chirality in bichromophoric perylene bisimides: influence of temperature and ultrasound. Langmuir *30*, 6030–6037.

49. Hwang, I., Mukhopadhyay, R.D., Dhasaiyan, P., Choi, S., Kim, S.-Y., Ko, Y.H., Baek, K., and Kim, K. (2020). Audible sound-controlled spatiotemporal patterns in out-of-equilibrium systems. Nat. Chem. *12*, 808–813.

50. Huang, Y., Quan, B., Wei, Z., Liu, G., and Sun, L. (2009). Self-assembled organic functional nanotubes and nanorods and their sensory properties. J. Phys. Chem. C *113*, 3929–3933.

51. Ma, T., Li, C., and Shi, G. (2008). Optically active supramolecular complex formed by ionic self-assembly of cationic perylenediimide derivative and adenosine triphosphate. Langmuir *24*, 43–48.

52. Liu, G.-F., Zhu, L.-Y., Ji, W., Feng, C.-L., and Wei, Z.-X. (2016). Inversion of the supramolecular chirality of nanofibrous structures through co-assembly with achiral molecules. Angew. Chem. Int. Ed. Engl. *55*, 2411–2415.

53. Yu, Z., Tantakitti, F., Yu, T., Palmer, L.C., Schatz, G.C., and Stupp, S.I. (2016). Simultaneous covalent and noncovalent hybrid polymerizations. Science *351*, 497–502.

R.D.Mukhopadhyay

https://doi.org/10.1038/s41557-023-01141-0

Cucurbituril curiosities

Check for updates

Rahul Dev Mukhopadhyay and Kimoon Kim consider how cucurbiturils — pumpkin-shaped macrocycles — went from curiosities to compelling cavitands for a host of applications.

One of the most popular traditions during Halloween, is the carving of jack-o'-lanterns, where most commonly the top of a pumpkin is chopped off to make a lid (an open rim), followed by the scooping out of the pulp (to obtain a hollow cavity), carving out a scary face (torus decoration) and then placing a candle (a luminous guest) inside the cavity to greet trick-or-treaters.

For almost half a century, chemists have been involved in synthesizing such pumpkin-shaped structures at the molecular level. Those also feature an intrinsic cavity, which provides an opportunity to explore their host–guest chemistry, and their torus can be decorated by chemical modification. Unlike the aforementioned lanterns though, they possess two open rims, through which guest molecules enter or exit the host cavity. This family of macrocycles has steadily attracted great attention owing to their remarkable molecular recognition properties[1].

In 1905, German chemist Robert Behrend described that the acidic condensation of glycoluril with formaldehyde yielded an insoluble polymeric substance (referred to as Behrend's polymer)[2]. Based on elemental analysis, Behrend suggested that this material contained "at least three molecules of glycoluril" condensed with twice as many formaldehyde molecules. He further noted the exceptional stability of this material in the presence of aggressive reagents as well as its ability to form co-crystals.

Almost 80 years later, in 1981, intrigued by the properties of this material, Mock, Freeman and Shih revisited the original synthesis[3]. Armed with modern structural characterization tools, including X-ray crystallography and nuclear magnetic resonance spectroscopy, they found that the 'polymer' was a macrocycle comprising of six glycoluril units, with a hydrophobic cavity and two hydrophilic rims decorated with six ureido carbonyl units on each side. They named it 'cucurbituril' as it

resembles the shape of a pumpkin, of the *Cucurbitaceae* botanical family.

Today, we refer to this macrocycle as cucurbit[6]uril or simply CB[6]. Mock further reported the formation of 1:1 inclusion complexes of CB[6] with alkylammonium species, rate acceleration of the azide–alkyne click reaction within the CB[6] cavity, and its use as a molecular switch[1]. The 1990s witnessed the synthesis of a variety of intriguing supramolecular assemblies including polyrotaxanes and 'molecular necklaces'.

By 2000, through careful control of the reaction temperature, other members of the family had been isolated — CB[*n*] ($n = 5$, 7 and 8), where *n* is the number of glycoluril units in the macrocycle[4,5]. Although CB[6] still remained the major product of the acid-catalysed formaldehyde glycoluril reaction, chemists now had new pumpkins with new properties to play with. For instance CB[7], which can bind larger guests including fluorescent dyes, was astutely used for the development of label-free continuous enzyme assays (supramolecular tandem assays)[6] and the separation of disubstituted benzene isomers, which are important industrial feedstocks[7]. CB[7] can also form ultrahigh-affinity host–guest complexes with ferrocene and adamantane-based amines, with binding affinities comparable or superior to that of the naturally occurring biotin–streptavidin pair (K_a in the range of 10^{12}–10^{15} versus 10^{13} M^{-1}, respectively)[8].

On the other hand CB[8], with an even larger cavity, facilitates the inclusion of two guest molecules thereby leading to the formation of homo- (same guests) and heteroternary (different guests) complexes. Recently, these have been widely explored for the development of functional supramolecular systems and soft materials exhibiting high mechanical strength. Even larger CB[*n*]s ($n = 10$, 13, 14 and 15) now exist,[1] as well as other analogues such as bambusurils (cavitands with a longer torus whose shape is reminiscent of bamboo stems) and acyclic CB[*n*]-type receptors[1].

An enticing aspect of the chemistry of these host molecules is the introduction of various functional groups at their periphery, by which the scope of their applications has been further expanded[1]. In particular, the ability of functionalized CB[7] to form ultra-stable, yet reversible host–guest complexes with specific guest molecules can be used as a bioorthogonal non-covalent conjugation tool. This behaviour has been termed a 'supramolecular latch'[9] or 'non-covalent click chemistry'[10] and extensively explored for biological applications such as imaging and isolation of proteins[11] as well as supramolecular modification of therapeutic proteins[12].

On the heels of the 2022 Nobel Prize in Chemistry being awarded "for the development of click chemistry and bioorthogonal chemistry", we hope that the 'non-covalent click chemistry' behaviour of CB[7]-based ultrahigh-affinity host–guest complexes can help gain insight into a variety of biological processes.

Rahul Dev Mukhopadhyay[1] & Kimoon Kim[2] ✉
[1]Department of Chemistry, Ramananda College, Bankura University, Bishnupur, West Bengal, India. [2]Department of Chemistry, Pohang University of Science and Technology (POSTECH), Pohang, Republic of Korea.
Twitter: @ProfKimoonKim
✉e-mail: kkim@postech.ac.kr

Published online: 20 February 2023

References

1. *Cucurbiturils and Related Macrocycles* (ed. Kim, K.) (Royal Society of Chemistry, 2019).
2. Behrend, R., Meyer, E. & Rusche, F. *Justus Liebigs Ann. Chem.* **339**, 1–37 (1905).
3. Freeman, W. A., Mock, W. L. & Shih, N. Y. *J. Am. Chem. Soc.* **103**, 7367–7368 (1981).
4. Kim, J. et al. *J. Am. Chem. Soc.* **122**, 540–541 (2000).
5. Day, A., Arnold, A. P., Blanch, R. J. & Snushall, B. *J. Org. Chem.* **66**, 8094–8100 (2000).
6. Hennig, A., Bakirci, H. & Nau, W. M. *Nat. Methods* **4**, 629–632 (2007).
7. Zhang, G. et al. *Chem* **6**, 1082–1096 (2020).
8. Rekharsky, M. V. et al. *Proc. Natl Acad. Sci.* **104**, 20737–20742 (2007).
9. Park, K. M., Murray, J. & Kim, K. *Acc. Chem. Res.* **50**, 644–646 (2017).
10. Schreiber, C. L. & Smith, B. D. *Nat. Rev. Chem.* **3**, 393–400 (2019).
11. Lee, D.-W. et al. *Nat. Chem.* **3**, 154–159 (2011).
12. Webber, M. J. et al. *Proc. Natl Acad. Sci.* **113**, 14189–14194 (2016).

Competing interests

The authors declare no competing interests.

CREDIT: JULIA SUDNITSKAYA/ISTOCK/ GETTY IMAGES PLUS/ GETTY (BACKGROUND PUMPKIN IMAGE)

Saubashya Sur

Acta Biologica Szegediensis

Volume 66(2):192-201, 2022
Acta Biologica Szegediensis
http://abs.bibl.u-szeged.hu/index.php/abs

DOI:10.14232/abs.2022.2.192-201

ARTICLE

The pangenome structure of human pathogen *Mycobacterium kansasii*

Saubashya Sur*

Postgraduate Department of Botany, Life Sciences Block, Ramananda College, Bishnupur-722122, West Bengal, India

ABSTRACT The non-tuberculous *Mycobacterium kansasii*, is the causative agent of destructive pulmonary and extrapulmonary infections in immunocompromised persons. Incessant use of multiple antibiotics and lack of effective vaccines did little to combat *M. kansasii* mediated infections. Here, a bioinformatic analysis has been carried out using PanExplorer, to analyze the pangenome aimed at functional characterization of the bacterium, understanding it's pathogenic lifestyle and recognize the factors shaping evolution and variations amongst strains. *M. kansasii* had a large core genome (60.2%), a small (11.9%) dispensable genome and 27.9% strain-specific genes. The core genome of *M. kansasii* had a high concentration of COGs (Cluster of orthologous genes) linked to energy production and conversion, amino acid transport and metabolism, nucleotide transport and metabolism, coenzyme transport and metabolism, and secondary metabolite biosynthesis, transport and metabolism. Interestingly, numerous genes within the core and dispensable genome were associated with pathogenesis and virulence. Noteworthy among them were type VII secretion, ESX, PP and PPE family proteins. Although, *M. kansasii* genomes revealed overall relatedness and conservation, genomic rearrangements caused variability within the strains. The information from this analysis could assist future microbial genomics research on *M. kansasii*, and further studies, e.g., concerning distinctive gene clusters, and evolution.

Acta Biol Szeged 66(2):192-201 (2022)

KEY WORDS
bioinformatics
non-tuberculous mycobacteria
Mycobacterium kansasii
pangenome
pathogenesis

ARTICLE INFORMATION
Submitted
02 November 2022
Accepted
15 February 2023
***Corresponding author**
E-mail: saubashya@gmail.com

Introduction

Non-tuberculous mycobacteria (NTM) are ubiquitously present mycobacteria, responsible for causing opportunistic infections in humans (Ricketts et al. 2014). Most of the NTMs are environmental bacteria (Luo et al. 2021), incorporating over 170 different species, and are associated with skin and pulmonary diseases in humans (Sur and Pal 2021). The incidence of NTM infections is increasing at a fast pace, and there is evidence of acquired infection from environmental sources and human-to-human transmission (Jia et al. 2021). Additionally, there are instances of the zoonotic potential of NTM-mediated infections (Fukano et al. 2021). Anthropogenic activities, immunocompromisation, antibiotic resistance, and lack of effective vaccines have contributed to the surge of NTM infections (Bryant et al. 2016; Sur 2021).

Mycobacterium kansasii is a NTM responsible for destructive pulmonary infections resembling tuberculosis, in individuals suffering from chronic bronchitis, cystic fibrosis, emphysema, and chronic obstructive pulmonary disease (Banks et al. 1983; Ricketts et al. 2014; Luo et al. 2021). *M. kansasii* is also associated with extrapulmonary infections like septic arthritis, and skin and cervical lymph node diseases (Bernard et al. 1999; Guan et al. 2020). *M. kansasii* is commonly found in immunocompromised individuals (e.g., people suffering from HIV) and is increasingly becoming a matter of concern in the USA, South America, Africa, China, and Japan (DeStefano et al. 2018; Luo et al. 2021). Out of the seven subtypes of *M. kansasii,* type I is the major one with a global presence and greater association with human diseases (Guan et al. 2020; Guo et al. 2022). *M. kansasii*-mediated infections can be controlled using a combination of antibiotics like isoniazid, rifampin, and ethambutol; azithromycin and clarithromycin; as well as amikacin, moxifloxacin, and linezolid (DeStefano et al. 2018; Guo et al. 2022). However, usage of multiple antibiotics, prolonged duration of treatment, and increasing drug resistance became limiting factors (DeStefano et al. 2018).

Over the last 20 years, rapid advancement in microbial sequencing technologies catalyzed the exponential growth of bacterial genomes (Zhao et al. 2012). The massive amount of data necessitated the development of efficient computational tools (Perrin and Rocha 2021).

Saubashya Sur

CRITICAL REVIEWS IN MICROBIOLOGY
2023, VOL. 49, NO. 4, 499–514
https://doi.org/10.1080/1040841X.2022.2082268

Taylor & Francis
Taylor & Francis Group

REVIEW ARTICLE

Check for updates

Mycobacterium abscessus: insights from a bioinformatic perspective

Saubashya Sur, Tanushree Patra, Mistu Karmakar and Anindita Banerjee

Postgraduate Department of Botany, Ramananda College, Bishnupur, India

ABSTRACT

Mycobacterium abscessus is a nontuberculous mycobacterium, associated with broncho-pulmonary infections in individuals suffering from cystic fibrosis, bronchiectasis, and pulmonary diseases. The risk factors for transmission include biofilms, contaminated water resources, fomites, and infected individuals. *M. abscessus* is extensively resistant to antibiotics. To date, there is no vaccine and combination antibiotic therapy is followed. However, drug toxicities, low cure rates, and high cost of treatment make it imperfect. Over the last 20 years, bioinformatic studies on *M. abscessus* have advanced our understanding of the pathogen. This review integrates knowledge from the analysis of genomes, microbiomes, genomic variations, phylogeny, proteome, transcriptome, secretome, antibiotic resistance, and vaccine design to further our understanding. The utility of genome-based studies in comprehending disease progression, surveillance, tracing transmission routes, and epidemiological outbreaks on a global scale has been highlighted. Furthermore, this review underlined the importance of using computational methodologies for pinpointing factors responsible for pathogen survival and resistance. We reiterate the significance of interdisciplinary research to fight *M. abscessus*. In a nutshell, the outcome of computational studies can go a long way in creating novel therapeutic avenues to control *M. abscessus* mediated pulmonary infections.

GRAPHICAL ABSTRACT

ARTICLE HISTORY
Received 8 March 2022
Revised 16 May 2022
Accepted 20 May 2022
Published online 11 June 2022

KEYWORDS
Mycobacterium abscessus; pulmonary infections; nontuberculous mycobacteria (NTM); infectious diseases; bioinformatics

Introduction

Mycobacteria are a diverse group of bacteria characterised by their varying ability to cause diseases. Mycobacteria are categorised into nontuberculous mycobacteria (NTM) and tuberculosis-causing mycobacteria (Johansen et al. 2020). NTM is ubiquitous, heterogeneous (Locatelli et al. 2020), and responsible for pulmonary infections, disseminated infections, cervical lymphadenitis, and infections in the bones and soft tissues (Baldwin et al. 2019). NTM infections are increasing worldwide and have surpassed the incidence of tuberculosis in many countries (Adjemian et al. 2012; Ryan and Byrd 2018; Baldwin et al. 2019). Age, bronchiectasis, exposure to aerosols, indiscriminate use of antibiotics and immunosuppressants, use of showers, and human-pathogen interaction, coupled with improved diagnostic capabilities are the reasons for an increased incidence of NTM induced diseases (Collins 1989; Feazel et al. 2009; Bryant et al. 2016; Johansen et al. 2020; Yoon et al. 2020). The cost of treating NTM is high.

CONTACT Saubashya Sur saubashya@gmail.com Postgraduate Department of Botany, Life Sciences Block, Ramananda College, Bishnupur-722122, India

© 2022 Informa UK Limited, trading as Taylor & Francis Group

Saubashya Sur

Acta Biologica Szegediensis

Volume 67(1):xx-xx, 2023
Acta Biologica Szegediensis
http://abs.bibl.u-szeged.hu/index.php/abs

DOI:10.14232/abs.2023.1.xx-xx

ARTICLE

In silico immunoinformatics based prediction and designing of multi-epitope construct against human rhinovirus C

Saubashya Sur[1]*, Mritunjoy Ghosh[1], Ritu Rai2

[1]Postgraduate Department of Botany, Life Sciences Block, Ramananda College, Bishnupur-722122, West Bengal, India
[2]Department of Botany, Parimal Mitra Smriti Mahavidyalaya, Malbazar-735221, West Bengal, India

ABSTRACT Human rhinovirus C (HRV-C) is an RNA virus infecting human respiratory tract. It is associated with complexities like asthma, chronic obstructive pulmonary disease, and respiratory damage. HRV-C has many serotypes. Till date there is no vaccine. Despite some limitations, corticosteroids, bronchodilators, and common cold medicines are used to treat HRV-C infections. Here, we have used immunoinformatics approach to predict suitable cytotoxic T-cell, helper T-cell and linear B-cell epitopes from the most antigenic protein. VP2 protein of Rhinovirus C53 strain USA/CO/2014-20993 was found to be most antigenic. The multi-epitope construct was designed using the best CTL, HTL and linear B-cell epitopes and attaching them with adjuvant and linkers. Interferon-gamma inducing epitopes and conformational B-cell epitopes were also predicted from the construct. Physicochemical and structural properties of the construct were satisfactory. Binding pockets were identified that could be the targets for designing effective inhibitors. Molecular docking revealed strong binding affinity of the construct with human Toll-like receptors 2 and 4. Normal mode analysis divulged stability of the docked complex. Codon optimization, *in silico* cloning and immune simulation analysis demonstrated suitability of the construct. These findings are likely to aid *in vitro* studies for developing vaccine against HRV-C. **Acta Biol Szeged 67(1):xx-xx (2023)**

KEY WORDS
Human rhinovirus C
immunoinformatics
linker
molecular docking
multi-epitope
toll-like receptors

ARTICLE INFORMATION
Submitted
30 April 2023
Accepted
26 June 2023
***Corresponding author**
E-mail: saubashya@gmail.com

Introduction

Human rhinoviruses (HRVs), first discovered in 1950's, are non-enveloped RNA viruses belonging to the Picornaviridae family (Glanville and Johnston 2015). It infects the upper and lower respiratory tracts in humans (Arruda et al. 1995; Jakiela et al. 2008) and is accountable for acute respiratory complexities in various ethnicities worldwide (Rotbart and Hayden 2000). HRVs are associated with common cold, wheezing, asthma, pneumonia, chronic obstructive pulmonary disease, and flu-like symptoms (Arden and Mackay 2009; Cordey et al. 2010). They have a high rate of mutation assisting adaptability and transmissibility (Cordey et al. 2010). HRVs are categorized into HRV-A, HRV-B, and HRV-C respectively (Hao et al. 2012). Multiple lines of evidence have revealed that HRV-C is more predominant and virulent compared to HRV-A and HRV-B (Hao et al. 2012). The high virulence of rhinovirus C stems from its ability to bind to host cells using cadherin-related family member 3 receptor (Scully et al. 2018). HRV-C is linked to severe symptoms. It is responsible for greater respiratory damage (Palmenberg et al. 2010). HRV-C has been linked to asthma exacerbations worldwide in children (Bizzintino et al. 2011; Mak et al. 2011). Some workers have found a distinct correlation between maternal atopy and asthma in offspring (Miller et al. 2011). HRVs comprise many serotypes whose categorization is based on factors like receptor specificity, predisposition to antiviral responses, similarity in nucleotide sequences, etc. (Lau et al. 2010). The genome of HRVs is made up of a single gene. Nevertheless, its translated product yields structural and non-structural proteins (Jacobs et al. 2013). The capsid contains structural proteins viz. VP1, VP2, VP3, VP4, and VPg whereas non-structural proteins function in replication and assembly (Palmenberg et al. 2010).

Acute airway infections are the major cause of morbidity and mortality worldwide. Although HRV-C is more virulent and linked to the high incidence of asthma, chronic obstructive pulmonary disease in adults, and severe respiratory complexities in children (Bochkov and Gern 2012), little has been achieved in developing a vaccine in the last 70 years. However, the development of effective vaccines is time-consuming and costly. For clinicians, the antigenic diversity of HRVs, the number of serotypes along with lack of good animal models became stumbling blocks for developing vaccines (Papi and Con-